UNIVERSIDADE FEDERAL DE SANTA CATARINA
CENTRO DE CIÊNCIAS FÍSICAS E MATEMÁTICAS
PROGRAMA DE PÓS-GRADUAÇÃO EM FÍSICA

Kauan Dalfovo Marquez

Astrophysical Implications of Exotic Particles and Magnetic Fields in Neutron Stars

Florianópolis
2022

Kauan Dalfovo Marquez

Astrophysical Implications of Exotic Particles and Magnetic Fields in Neutron Stars

Tese submetida ao Programa de Pós-Graduação em Física da Universidade Federal de Santa Catarina para a obtenção do título de doutor em física.
Orientadora: Débora Peres Menezes, D.Phil.

Florianópolis
2022

Ficha de identificação da obra elaborada pelo autor,
através do Programa de Geração Automática da Biblioteca Universitária da UFSC.

Marquez, Kauan Dalfovo
Astrophysical implications of exotic particles and magnetic fields in neutron stars / Kauan Dalfovo Marquez ; orientadora, Débora Peres Menezes, 2022.
157 p.

Tese (doutorado) - Universidade Federal de Santa Catarina, Centro de Ciências Físicas e Matemáticas, Programa de Pós-Graduação em Física, Florianópolis, 2022.

Inclui referências.

1. Física. 2. Modelos Efetivos. 3. Estrelas de Nêutron. 4. Transição de Fases. 5. Magnetares. I. Menezes, Débora Peres . II. Universidade Federal de Santa Catarina. Programa de Pós-Graduação em Física. III. Título.

Kauan Dalfovo Marquez

Astrophysical Implications of Exotic Particles and Magnetic Fields in Neutron Stars

O presente trabalho em nível de doutorado foi avaliado e aprovado por banca examinadora composta pelos seguintes membros:

Prof. Dr. Celso de Camargo Barros Junior
Universidade Federal de Santa Catarina

Profª. Drª. Constança Providência
Universidade de Coimbra

Prof. Dr. Luiz Laércio Lopes
Centro Federal de Educação Tecnológica de Minas Gerais

Certificamos que esta é a **versão original e final** do trabalho de conclusão que foi julgado adequado para obtenção do título de doutor em física.

Documento assinado digitalmente
Paulo Henrique Souto Ribeiro
Data: 15/08/2022 16:24:45-0300
CPF: 730.886.506-10
Verifique as assinaturas em https://v.ufsc.br

Coordenação do Programa de Pós-Graduação

Documento assinado digitalmente
Debora Peres Menezes
Data: 16/08/2022 16:54:02-0300
CPF: 049.032.478-99
Verifique as assinaturas em https://v.ufsc.br

Débora Peres Menezes, D.Phil.
Orientadora

Florianópolis, 2022.

To my mother, for everything.

ACKNOWLEDGEMENTS

To my mother Sionara, who gives me much more than I could ever ask for;

To my sister Júlia, who makes me wish to be better just by being by my side;

To professor Débora who, in addition to being a mentor, shown to be a friend and an example to be followed;

To my cats, Capitu and Escobar, who stayed by my side (or on top of me) during the most part of the writing of this work;

To professors Emmanuel, Marcus, Veronica, Luis Laércio, Debarati and, in special, Constança, who taught me so much with care and dedication;

To my colleagues Bethânia, Mateus, Carline, Helena, Clebson, Clesio and Tulio;

To everyone who contributed to my development as a person or as a scientist, whether teachers, family members, friends or as someone who simply believed in me;

To the coordination and other employees of the PPGFSC, for having welcomed me with affection;

To the entire Brazilian society, for the financial support provided through CNPq;

Thank you, I hope you all remain present in the challenges that lie ahead.

“Ce qui est simple est toujours faux.
Ce qui ne l’est pas est inutilisable.”
Paul Valéry

RESUMO

Embora a classe de remanescentes estelares que não são anãs brancas nem buracos negros seja tradicionalmente chamada de estrelas de nêutrons, esses objetos não são compostos apenas de nêutrons. Mesmo a descrição mais ingênua de tais objetos deve incluir alguma quantidade de prótons e léptons para garantir sua estabilidade. Neste trabalho, pretendemos obter uma descrição de estrelas compactas compostas de matéria densa a partir de modelos relativísticos, com o objetivo de analisar pulsares como estrelas hadrônicas, híbridas e/ou estranhas. Isso é feito dividindo o presente estudo em duas partes: (i) estudar as implicações da inclusão de bárions delta na composição da matéria estelar, e (ii) explorar o diagrama de fases QCD, em especial a possibilidade de desconfinamento hadron-quark no contexto de estrelas compactas. Em ambas as partes, os efeitos de campos magnéticos intensos também são levados em consideração.

Palavras-chave: Modelos Efetivos; Estrelas de Nêutron; Matéria Assimétrica; Transição de Fases; Magnetares.

RESUMO EXPANDIDO

Devido à impossibilidade de se tratar a cromodinâmica quântica (QCD) perturbativamente em regimes de alta densidade, o estudo completo do diagrama de fases da QCD requer abordagens alternativas, e o uso de modelos efetivos relativísticos tem servido como uma valiosa ferramenta para o entendimento conceitual e modelagem de muitos fenômenos relacionados à interação nuclear. Estes modelos, originalmente desenvolvidos tendo em vista suas aplicações no contexto microscópico, i.e., na descrição da matéria nuclear, de colisões de íons pesados ou da subestrutura de hádrons, têm sido extrapolados para o âmbito macroscópico da descrição de matéria densa contínua, como é praxe no estudo de objetos estelares compactos.

Os remanescentes estelares, como são chamadas as estrelas compactas em conjunto com buracos negros, são o estágio final da evolução das estrelas. O estudo destes objetos se situa na intersecção da mecânica quântica, relatividade geral e física estatística, grandes pilares conceituais da física contemporânea. Por isso, os métodos utilizados nesta investigação e os resultados obtidos são de ampla aplicabilidade nos mais diversos campos da física. Por exemplo, as condições extremas de densidade, campo magnético, temperatura e pressão encontradas no interior ou nas imediações desses objetos servem como um 'laboratório natural' para teorias que exigem parâmetros em escalas irreprodutíveis nos laboratórios humanos, beneficiando principalmente a física nuclear e de hádrons, astrofísica e cosmologia.

O caroço das estrelas de nêutrons apresenta a matéria bariônica na situação de mais alta densidade observável atualmente, e é evidente que as partículas apresentam-se em estados de alta energia em relação às suas massas de repouso. É razoável conjecturar que, ao menos em regiões mais centrais, os núcleons tenham sua energia elevada acima da barreira de massa, favorecendo energeticamente a existência de espécies bariônicas mais massivas do que prótons e nêutrons (como os híperons ou as ressonâncias de spin 3/2 do decupleto bariônico).

Outros tipos de matéria exótica também podem ser esperados devido às extremas densidades de energia encontradas em tais objetos, como, por exemplo, matéria estável de quarks desconfinados (chamada na literatura de matéria estranha). Embora a totalidade da experiência física (e cotidiana) ateste que a matéria em seu estado fundamental se apresenta na forma de léptons e quarks confinados, não é possível excluir teoricamente a possibilidade deste ser apenas um estado duradouro metaestável ao invés de o verdadeiro estado fundamental da matéria bariônica. A hipótese de Bodmer-Witten propõe que é possível a existência de matéria estável de quarks desconfinados, desde que haja quarks u, d e s em porções equivalentes. A depender dos modelos efetivos empregados na descrição das matérias hadrônica e estranha, uma transição de fases é esperada no interior da estrela compacta, levando ao aparecimento de um 'caroço' de matéria de quarks livres ou, até mesmo, à total conversão de uma estrela hadrônica metaestável em uma estrela estranha.

Por outro lado, uma classe distinta de estrelas de nêutrons é chamada de magnetares, objetos compactos que possuem o maior campo magnético estável observado na

natureza. Embora a força do campo magnético na região central dessas estrelas permaneça desconhecida, estima-se que elas podem atingir magnitudes da ordem de 10^{18} G. Tais condições extremas certamente desempenham um papel considerável na determinação da composição interna dos magnetares, em especial quando se consideram espécies exóticas de partículas. Ainda, há uma quebra de simetria induzida pela presença do campo magnético levando ao aumento da pressão transversal à direção de B e à diminuição da pressão longitudinal. Para campos magnéticos fortes o suficiente, isso provocará um achatamento nos pólos da estrela de nêutrons. Assim, assumir a simetria esférica na dedução das equações de equilíbrio hidrostático, como feito na obtenção das usuais equações de Tolman-Oppenheimer-Volkoff, não é mais uma boa aproximação. Além disso, deve-se considerar uma dependência do campo magnético com a densidade através de um perfil que não é conhecido de antemão. Portanto, o cálculo numérico deve-se dar a partir das equações de estado levando em consideração as equações de Einstein e de Maxwell para obter as soluções de equilíbrio auto consistentemente.

Fazem parte dos objetivos deste estudo a implementação e refinamento de modelos efetivos para matéria hadrônica, em especial parametrizações de modelos tipo-Walecka como o L3wr, modelos dependentes da densidade como o DDME2, ou extensões do modelo Nambu-Jona-Lasinio (NJL) como o PPM que concordem com grandezas experimentais bem estabelecidas para matéria nuclear, e.g., o "módulo de compressibilidade", a "energia de simetria" e seu slope, tomados no ponto de saturação nuclear. Além destas restrições, observações astronômicas colocam limites nos valores de massas e raios de estrelas compactas. Com o objetivo de permitir a descrição de matéria com híperons ou ressonâncias de spin 3/2 (bárions Δ), que devem estar presentes na modelagem de estrelas compactas, exige-se a busca por melhores esquemas de acoplamentos méson-híperon e méson-delta quando se opta por modelos tipo-Walecka. A inclusão de outras espécies bariônicas no modelo NJL estendido para hádrons é consideravelmente mais complexa, pois esse formalismo exige que se observe a simetria quiral. Tanto a busca por melhores esquemas de acoplamentos para modelos tipo-Walecka quanto a completamente nova extensão do modelo NJL hadrônico para híperons fazem parte do escopo deste trabalho.

A transição de desconfinamento entre matéria hadrônica e de quarks livres é tida como sendo uma transição de fases de primeira ordem para o caso de $T = 0$. A descrição termodinâmica desse tipo de processo pode ser obtida a partir da combinação das equações de estado para as duas fases. A transição pode acontecer após a matéria hadrônica metaestável sobre-pressurizada atingir o ponto de coexistência de fases com a matéria estranha, o que, a depender dos parâmetros de ambos os modelos, pode permitir a construção de uma equação de estado híbrida. O estudo dessas transições de fase também faz parte dos objetivos desse projeto, e relaciona-se intimamente ao objetivo anterior, uma vez que as populações de partículas exóticas na matéria hadrônica (que é uma variável dependente do modelo) têm muita influência na transição para matéria hadrônica.

Além da implementação numérica de modelos efetivos, sejam eles presentes na literatura ou novos desenvolvimentos, pretende-se implementar a descrição de efeitos de campos magnéticos extremos incluindo também momentos magnéticos anômalos das

partículas consideradas. Isso permitirá uma melhor descrição de matéria hadrônica (ou estranha) em magnetares, porém traz as dificuldades adicionais de se ter que considerar a anisotropia introduzida pelo campo magnético e de considerar as equações de Einstein e de Maxwell auto consistentemente na obtenção das soluções de equilíbrio (i.e., diagrama massa-raio, perfis de densidade e de campo magnético nos interiores estelares,etc.).

ABSTRACT

Although the class of stellar remnants that are neither white dwarves nor black holes is traditionally named neutron stars, these objects are not composed solely of neutrons. Even the more naïve description of such objects must include some amount of protons and leptons in order to guarantee their stability. In this work, we intend to obtain a description of compact stars made up of dense matter from relativistic models, with the purpose of analyzing pulsars as hadronic, hybrid and/or strange stars. This is done by dividing the present study into two parts: (i) studying the implications of including delta baryons in the stellar matter composition, and (ii) exploring the QCD phase diagram, in special the possibility of hadron-quark deconfinement in the context of compact stars. In both parts, the effects of intense magnetic fields are also taken into account.

Keywords: Effective Models; Neutron Stars; Asymmetric Matter; Phase Transitions; Magnetars.

LIST OF FIGURES

LIST OF TABLES

CONTENTS

1 INTRODUCTION

The contemporary understanding of all known physical phenomena can be reduced to four fundamental interactions (or forces). While the gravitational force has not yet been described successfully in the form of a *quantum field theory* (QFT), the theories of the other three forces can be pieced together in a single formalism, the so-called *standard model of particle physics*. In this view, the particles of matter (in the most elementar level, *quarks* and *leptons*) do not directly interact with each other, but instead, their interactions are mediated by force fields, consequence of the fact that these particles carry charges. In the perturbative quantum mechanics framework, this process can be understood as the exchange of virtual particles (called *gauge bosons*) between the interacting fermions. The four fundamental forces are presented illustratively in Table 1.

Quarks were proposed as a way to explain the plethora of subatomic particles discovered in accelerators during the 1960s. It was suggested by Gell-Mann and Zweig that *hadrons* (protons, neutrons, pions, lambdas, and many others) were not truly elemental, but rather exhibit a substructure of quarks, with the *baryons* being made of three quarks and the *mesons* of a quark-antiquark pair. This hypothesis was later confirmed by deep inelastic scattering experiments. By the time, three types (or *flavors*) of quarks were employed to successfully explain the properties of all known hadrons and predict some others, but this number counts six in the actual form of the standard model.

In order to properly describe the existence of the *delta* and *omega barions*, that would be constituted by three same-flavor quarks, an extra quantum number had to be proposed to avoid the Pauli exclusion principle. This new quantum number of quarks was called *color charge*, that can take three values (named red, green and blue). As the composite particles do not show any color charge, it is imposed that quarks must be combined in a colorless (or white) way, such as a combination of the three different colors, in barions, or of a color and the respective anticolor, in mesons. Unlike other particles of the standard model, quarks take part in all of the fundamental interactions. They have mass and electric charge, so are subject to gravitational and electromagnetic forces, carry color charge, so can feel the strong force, and can change their flavor in radiative decays, which is explained through the weak interaction.

The quantum field theory that describes the strong interaction is called *quantum chromodynamics* (QCD), and is briefly presented in the following, together with the phase diagram of hadronic matter expected to follow from it. It is still not well understood how some features of the QCD, like the confinement and asymptotic freedom properties, arise from its mathematical structure. So, it is not possible to apply the perturbative methods typical to the particle physics to the low energy region of the QCD

Table 1 – The fundamental forces of nature, corresponding QFT and mediating gauge bosons. "Strength" is taken comparatively to the strong force and "range" represents typical scales where the interaction is relevant [126, 74].

FORCE	QFT	PARTICLE	STRENGTH	RANGE (m)
Strong	Chromodynamics	Gluons	1	10^{-15}
Electromagnetic	Electrodynamics	Photon	$\frac{1}{137}$	∞
Weak	Electroweak Theory[1]	$W^{\pm}$ and Z^0	10^{-20}	10^{-18}
Gravitational	–	"Graviton"	10^{-39}	∞

phase diagram, where many relevant phenomena are expected to occur. An option to deal with this problem is to build effective models that emulate some of the QCD relevant characteristics or symmetries, such as the quark confinement, the dynamic mass production or the resulting nuclear interaction between hadrons.

The QCD Lagrangian density that contains all the dynamics of quarks and gluons subject to the strong force, adopting the Einstein summation and the natural units system
($c = \hbar = k_B = 1$), is given by

$$\mathcal{L} = \bar{\psi}_{qi} i\gamma^{\mu} \left[\delta_{ij}\partial_{\mu} + ig \left(G^{\alpha}_{\mu} t_{\alpha} \right)_{ij} \right] \psi_{qj} - m_q \bar{\psi}_{qi} \psi_{qi} - \frac{1}{4} G^{\alpha}_{\mu\nu} G^{\mu\nu}_{\alpha}, \tag{1}$$

where ψ_{qi} is the Dirac spinor of the quark field of flavor q, color i and mass m_q, G^{α}_{μ} is the four-potential of the gluon gauge fields ($\alpha = 1, \ldots, 8$), and

$$G^{\mu\nu}_{\alpha} = \partial^{\mu} G^{\nu}_{\alpha} - \partial^{\nu} G^{\mu}_{\alpha} - g f^{\alpha\beta\gamma} G^{\mu}_{\beta} G^{\nu}_{\gamma} \tag{2}$$

is the color fields strength tensor, with t_{α} being the *Gell-Mann matrices*, generators of the SU(3) color group that have the structure constants $f^{\alpha\beta\gamma}$, and g being the *color charge*, related to the *strong coupling constant* as $g = \sqrt{4\pi\alpha_s}$ [73].

Unlike photons in the *quantum electrodynamics* (QED), which do not directly interact with each other because are electrically neutral, gluons have a color charge, which makes them subject to chromodynamic interaction with other gluons. As the interactions must conserve the global color charge, gluons must simultaneously carry one color and one anticolor, which implies that the color charge of an individual quark is not preserved by the strong interaction with a gluon, as opposed to the photon-electron interaction. Thus, the gluon field tensor contains the additional term represening interacion between color-charged gluons, making the QCD a non-abelian field theory in contrast to the QED.

[1] Also known as *Glashow-Weinberg-Salam theory*. In fact, it assembles the electromagnetic and weak interactions in the form of an unified *electroweak force*. However, these two forces manifest themselves in very distinct ways for most physical phenomena, what justifies the literature tendency of presenting them as two different interactions [74].

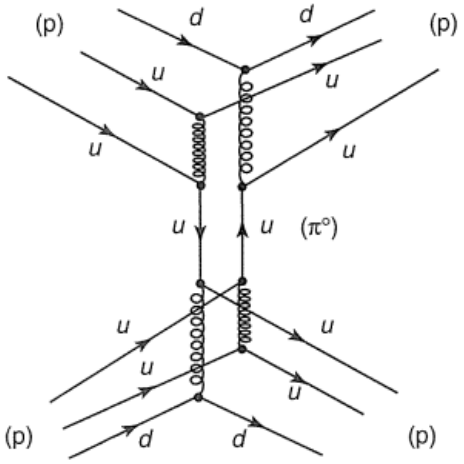

Figure 1 – Feynman diagram describing an Yukawa-type interaction between two protons p (uud) through the exchange of a virtual pion π^0 ($u\bar{u}$ or $d\bar{d}$), in terms of QCD degrees of freedom, adapted from [74].

Therefore, many complex phenomena can emerge from a somewhat simple mathematical structure. For example, it was observed in deep inelastic scatterings that the quarks were practically free inside the hadrons they made up. It can be explained through the gluon-gluon direct interactions allowed by the QCD, which leads to the *antiscreening effect* of color charge. The strong force coupling constant decreases with the four-momentum k^2 approximately as

$$\alpha_s(k^2) = \frac{1}{\beta_0 \ln\left(\frac{k^2}{\Lambda^2_{\text{QCD}}}\right)} \tag{3}$$

where β_0 is a constant [75, 195] and $\Lambda_{\text{QCD}} \approx 220$ MeV is called the *QCD scale*. This renders the QCD interaction stronger at large distances (or low momenta), which leads to the *quark confinement* that forbids quarks to be observed as isolated particles, and implies the other way around in the so-called *assymptotic freedom* that enables the application of perturbative methods in high energy or low density cases (as in heavy ion collisions).

A further example of this complexity is the description of the force acting between two hadrons in terms of QCD degrees of freedom. The so-called *nuclear force*, which initially motivated the study of strong force and was then taken as a fundamental process, is a residual force arising from the non-trivial interaction between six quarks. One of the possible diagrams for this phenomenon is shown in Figure 1, and refers to the pioneering work of Yukawa [203, 202] who, anticipating QCD by nearly 40 years, proposed a theory for the strong force in terms of the exchange of virtual mesons, considering hadrons as elementary particles. Although, as it turned out, this is not the most fundamental nature of the strong force, this approach is very useful in building models for the interaction between hadrons and is still employed in several effective

models.

Although it is possible to apply perturbative methods in high energy and low density events, which complements experimental results obtained in high energy accelerators, most of the theoretical research on strong interactions relies on approximative approaches. Hence, only a few results of the QCD phase diagram are known decisively. The ordinary hadronic matter must be observed for lower temperatures and barionic chemical potentials (or densities), but QGP and a color superconducting phase (named *color-flavor locked*, CFL) are expected at asymptotically large temperatures and densities, respectively.

The only feasible non-perturbative method to explore the regions close to the hadron-quark phase transition is called *lattice quantum chromodynamics* (LQCD), which discretizes the spacetime in grid to search for numerical solutions for the quark dynamics directly from the QCD Lagrangian. Although demanding a high computational cost and still presenting technical difficulties that limit its applicability to the low density regime, the LQCD is an important source of insights to the theoretical study of QCD. The most remarkable result of this approach to the description of the QCD phase diagram is the fact of the transition being of the *crossover* kind at zero chemical potential and occurring around $T = 160$ MeV [171].

Another approach, that allows exploring the non-zero chemical potential regions of the diagram, is the construction of effective models by the suggestion of Lagrangian densities aiming to emulate, at least to some extent, the QCD symmetries and particle dynamics in a system subjected to this type of interaction. Results obtained through this approaches suggest the existence of a first-order phase transition [90]. These two apparently contradictory perspectives can only be reconciled by the existence of a *critical endpoint* (CEP) at the intersection of the transition curve from the LQCD domain, i.e., the crossover at low chemical potentials and high temperatures, and that suggested by the effective models, the phase transition for the high chemical potentials and low temperatures. Nevertheless, the precise location of this critical point and even the order of the phase transition are open questions hard to be dealt by the discussed methods [173].

From experimental and phenomenological results, and information derived from perturbative QCD, LQCD or effective models, it is possible to construct a phase diagram for QCD, as the one shown in Figure 2. The first diagram of this type was proposed by [23] but, due to the fast and constant development of research in the area, there are different proposals for the phase diagram, depending on the theoretical and experimental results considered.

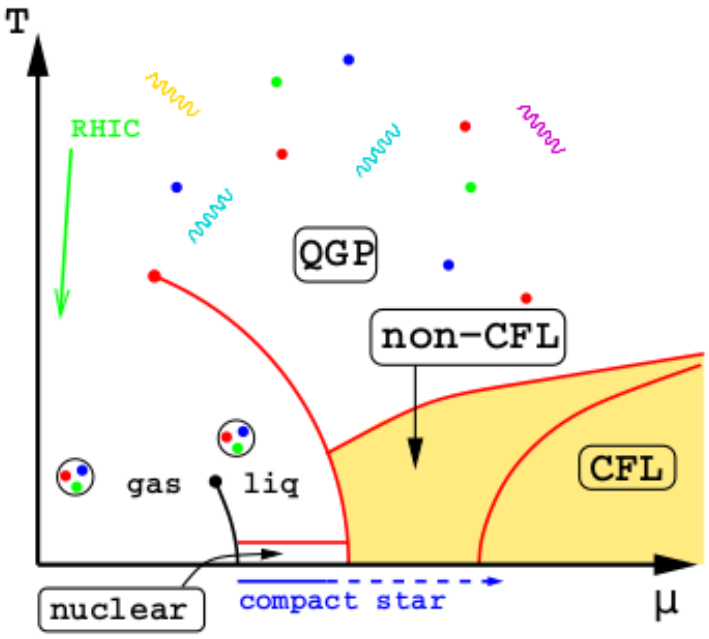

Figure 2 – Conjectured form of the QCD phase diagram [3].

1.1 A BRIEF HISTORIC OVERVIEW

The research on compact stars in its modern form began with the study of white dwarfs. At the end of the 19th century, Friedrich Bessel discovered that Sirius, one of the brightest stars in the night sky, described an elliptical orbit, what suggested that it was part of a binary system whose companion could not be observed. Nearly two decades later, Sirius' companion was identified by Alan Clark, who reported that it had a brightness many orders of magnitude smaller but a mass equivalent to that of Sirius, on the order of the mass of the Sun. In 1914, Walter Adams concluded, through spectroscopy studies, that the surface temperature of the two companions should be equivalent, but the density of one of them much higher than the other. This companion, which came to be classified as a "white dwarf", had its properties explained only in 1926 by Fowler, when he used knowledge of quantum mechanics to take into account the fact that electrons are fermions and, therefore, obey the Fermi-Dirac statistic and the Pauli Exclusion Principle. His hypothesis that the internal constituents of the white dwarf must be degenerate electrons allowed him to state that it was the degeneracy pressure of this electron gas that balanced the gravitational force. This hypothesis allowed the studies of Chandrasekhar and Landau who, in 1930 [28], deduced the limit that bears the name of the first, and that represents the maximum mass of an object so that the gravitational collapse is avoided by the degeneracy pressure of the electrons. This result was obtained by arguments from statistical mechanics, and gives the estimate that the maximum mass of a white dwarf should be 1.44 $M_{\odot}$.

At the same time, Lev Landau proposed the existence of stars made up of degenerate matter with masses above this limit, culminating in the proposal of the existence

of dense stars “similar to giant atomic nuclei”. This can be regarded as an early theoretical prediction of the existence of neutron stars, even before the observation of the existence of the neutron itself [199]. In 1939, Tolman and, independently, Oppenheimer and Volkoff (TOV) [180, 139], obtained the relativistic equation for hydrostatic equilibrium from Einstein’s equations of general relativity. It was already evident at the time that, unlike white dwarfs, where Newtonian gravitation was required, in neutron stars it would be necessary to take into account the effects of relativistic gravitation, which would arise due to the very high densities involved in this type of object.

While Tolman takes a more formal approach, focused on the analytical solution of Einstein’s equations, the work of Oppenheimer and Volkoff is concerned with the solution of the relativistic equation for hydrostatic equilibrium, presenting the ‘physical’ approach still usual for its solution, in addition to bringing the first application of this method in neutron stars. This procedure takes the hydrostatic equilibrium equation together with an equation of state for the matter that constitutes the object, a known relationship between pressure and density *a priori*, in order to allow its numerical solution. In this first study, the authors considered the equation of state of a free fermion (i.e., neutrons) gas as input to the hydrostatic equilibrium equation, and obtained a maximum mass of 0.71 $M_{\odot}$, which was a little disappointing because it was smaller than the Chandrasekhar limit. Quickly, the limitation of this equation of state was realized, and it was concluded that the equation of state for the matter of neutron stars should be obtained by a more adequate effective model, which takes into account interactions between nucleons (protons and neutrons) in order to sustain the higher maximum masses.

The unexpected discovery of the first *pulsars* took place in 1967, by Jocelyn Bell and Antony Hewish, then graduate student and advisor, respectively [83]. The radio pulses perceived by Bell lasted 0.04 s and repeated every precise 1.3373012 s. The lack of a known natural phenomenon that produced radio signals so uniform in their frequency led researchers to consider an artificial origin at first, even suggesting that they had intercepted some form of alien communication (so much so that the signal was named LGM-1, from *Little Green Men*). The subsequent observation of *pulsar* signals in other regions of the sky overturned this working hypothesis, and it was proposed that the captured signals could originate from compact stars. The discovery of *pulsars* was the first observational evidence of neutron stars, which raised the relevance of the discovery far beyond radio astronomy, currently being considered one of the greatest advances of the 20th century in the understanding of the Universe.

Following the guidance of Bell (who was not awarded the 1974 Nobel Prize in Physics with her professor, in a decision that generated much controversy and wide-ranging discussions in the scientific community), many more *pulsars* were discovered in the following years. Today this number exceeds two thousand, appearing dispersed in a

wide range of frequencies and emitting several bands of the electromagnetic spectrum. It was possible to establish, now observationally, that *pulsars* (and, by superposition, neutron stars) are extremely dense objects, exceeding the nuclear saturation density by up to an order of magnitude, so that they have gravitational masses between 1.4 and 2.2 $M_\odot$ and radius from 10 to 12 km.

At the same time, in the 1960s, the hypothesis of compact stars made up of other types of matter besides hadrons came to be considered. In the same way that Chadwick's discovery of the neutron in 1932 was followed almost immediately by the proposal of the existence of astronomical objects made up of neutron matter, Ivanenko and Kurdgelaidze [86, 87] proposed the existence of compact stars made up of quarks, which had just been proposed as fundamental particles by Murray Gell-Mann and George Zweig independently in 1964 [74]. Although the existence of this type of object still lacks observational confirmation, this hypothesis has proved to be an interesting topic of theoretical investigation. The so-called "strange stars" are formed entirely by matter in which the quarks are unconfined, and the "hybrid stars" have a hadronic phase at lower densities and a free quark phase in the stellar core region. The possibility that some *pulsars* are, in fact, compact stars made up of a certain amount of unconfined quark matter is seriously considered today.

Therefore, as briefly explained in this section, the establishment of the field of studies on compact stars, which took place between the 1930s and 1960s, was deeply related to the significant advances in theoretical and experimental physics of the period. The initial works in the area are still relevant today and their methods and results resonate with the current ones. Far from being exhausted, this field still raises an immense number of questions and presents a research program that meets the central points of contemporary physics.

1.2 RELATIVISTIC EFFECTIVE MODELS

Unfortunately, the treatment of the strong force from its fundamental theory is precluded by mathematical difficulties intrinsic to the phenomenology of QCD (Eq. (1)), as discussed in previous sections. One approach to circumvent this problem is to build models that ignore the quark substructure of hadrons, approaching the dynamics in terms of the degrees of freedom of the composite particles as if they were single elementary objects, in order to simplify the complicated chromodynamic interaction through the residual strong force.

The attractive character of this force can be modeled from the exchange of a neutral scalar meson of mass m, which is directly related to the inaugural proposal of Yukawa [203]. At the limit of static sources, this exchange can be translated into the

famous “Yukawa potential”,

$$V(r) = -k\frac{e^{-mr}}{r}, \tag{4}$$

where k is a scale constant, and the range of the interaction is related to the “Compton wavelength” of the mediator, $\lambda_C = 1/m$. As the least massive meson, the meson π (or pion), observed experimentally for the first time by Cesar Lattes [102], must be the main actor in the attractive interaction between baryons[2], and the exchange potential of a pion is exact in the limit $r \to \infty$ [191]. In turn, the characteristic of the nuclear force being repulsive at short distances, which is of central importance in the description and application of hadronic matter, can be qualitatively understood in an analogy with electrodynamics. QED deals with this interaction mediated by photons, which are bosons described by a neutral vector field and by the conservation of electric current. Assuming that the particle mediating the strong interaction is a neutral vector meson ω, related to the conserved baryonic current, it is possible to infer several aspects of the strong force in a parallel to the electromagnetic one. For example, baryonic numbers of like signs repel each other (e.g., p–n or $\bar{n}$–$\bar{n}$) and of opposite signs attract each other (e.g., n–$\bar{n}$ and other mesons), as in the case of electrical interactions. Like $m_\omega \neq 0$, this force has a limited range, unlike the photon, which is non-massive and represents an interaction of infinite range. This confirms the analogy between the two mesons, since, setting $m = 0$, the Yukawa potential ((4)) returns the Coulomb potential [191]. Therefore, the strong interaction between baryons can be, in a first approximation, modeled by the exchange of two mesons (σ and ω).

The construction of models for hadronic matter is of vital importance for understanding the properties of atomic nuclei, nuclear reactions and dense stellar objects, since it is not possible to develop an *ab initio* approach for the description of this type of matter.

The first models that sought to describe this matter in terms of its constituent particles were based on the Skyrme proposal [170]. In this type of approach, we start with a postulated potential in order to model the nuclear force, e.g., Paris or Bonn potentials, conceptually similar to the equation ((4)), and of the Schrödinger Equation. However, this type of model presents some problems, generally due to the fact that the Schrödinger equation is applicable only to non-relativistic particles. The implications of not considering relativistic effects are considerable, both in applying the model to finite nuclei and to unlimited matter [53]. Thus, the construction and use of a relativistic model for hadronic dynamics in the Quantum Field Theory formalism is imperative. The QHD form used hereinafter was initially addressed by [88] and [49], but is usually called “Walecka-type models”, as a result of the relevant work of this author [190].

[2] Feynman’s rules for QCD diagrams allow the mediator of this interaction to be a meson other than π (see Figure 1). However, as all other mesons are more massive than the pion, the term e^{-mr}/r of these vanishes more quickly with distance.

In such models, the interaction among baryons is described through the the exchange of mesons, and here we consider the scalar meson σ, the vector mesons ω and φ (that carries hidden strangeness), isoscalars, and the isovector-vector meson $\vec{\rho}$. In this approach the Lagrangian density reads as

$$\begin{aligned}\mathcal{L} = & \sum_b \bar{\psi}_b \left[\gamma_\mu \left(i\partial^\mu - g_{\omega b}\omega^\mu - g_{\varphi b}\varphi^\mu - \frac{g_{\rho b}}{2}\vec{\tau}\cdot\vec{\rho}^\mu\right) - (m_b - g_{\sigma b}\sigma)\right]\psi_b \\ & + \frac{1}{2}(\partial_\mu\sigma\partial^\mu\sigma - m_\sigma^2\sigma^2) - \frac{\lambda_1}{3}\sigma^3 - \frac{\lambda_2}{4}\sigma^4 \\ & - \frac{1}{4}\Omega_{\mu\nu}\Omega^{\mu\nu} + \frac{1}{2}m_\omega^2\omega_\mu\omega^\mu - \frac{1}{4}\Phi_{\mu\nu}\Phi^{\mu\nu} + \frac{1}{2}m_\varphi^2\varphi_\mu\varphi^\mu \\ & - \frac{1}{4}\vec{R}_{\mu\nu}\cdot\vec{R}^{\mu\nu} + \frac{1}{2}m_\rho^2\vec{\rho}_\mu\cdot\vec{\rho}^\mu + g_{\omega\rho}\,\omega_\mu\omega^\mu\vec{\rho}_\mu\cdot\vec{\rho}^\mu, \end{aligned} \tag{5}$$

where m_i is the mass associated with the $i = \sigma,\omega,\varphi,\rho$ meson field, $\Omega_{\mu\nu} = \partial_\mu\omega_\nu - \partial_\nu\omega_\mu$, $\Phi_{\mu\nu} = \partial_\mu\varphi_\nu - \partial_\nu\varphi_\mu$ $\vec{R}_{\mu\nu} = \partial_\mu\vec{\rho}_\nu - \partial_\nu\vec{\rho}_\mu - g_\rho(\vec{\rho}_\mu\times\vec{\rho}_\nu)$, and $\vec{\tau}$ is the isospin matrix (with vectors in isospin space denoted by arrows). The sum on the index b runs over all the baryonic species considered in the matter composition, described by the field ψ_b with the mass m_b. The scalar self-meson interactions σ^3 and σ^4, together with an additional vector-isovector self-meson $\omega\rho$ interaction, are fitted to improve the value of the compressibility modulus and symmetry energy at saturation density, respectively.

At sufficiently large densities, there will be so many *quanta* (mediating mesons) present in a given volume that it becomes reasonable to approximate the expected values of the quantum fields as classical fields. This procedure is suitable for the scope of hadronic matter applied to the study of compact stars, and is called the relativistic Hartree approximation, mean-field or RMF (from *Relativistic Mean-Field*). It is understood that the system studied is uniform and invariant by translation and rotation. This implies that hadronic matter is free of currents and that, in this approximation, the classical fields must be spatially and temporally constant. Therefore, the RMF approximation consists of the application of substitutions

$$\begin{aligned}\sigma &\to \langle\sigma\rangle = \sigma_0, \\ \omega^\mu &\to \langle\omega^\mu\rangle = \delta_{\mu0}\omega_0, \\ \varphi^\mu &\to \langle\varphi^\mu\rangle = \delta_{\mu0}\varphi_0, \\ \vec{\rho}^{\,\mu} &\to \langle\vec{\rho}^{\,\mu}\rangle = \delta_{\mu0}\tau_3\bar{\rho}_{0(3)},\end{aligned}$$

in the model, where $\delta_{\mu0}$ is the "Kronecker delta", which ensures space-temporal constancy of vector fields, and τ_3 selects only the third component of vectors in isospin space (denoted by the index in parentheses, suppressed henceforth), taking advantage of the fact that isospin is invariant around the third axis.

From the Euler-Lagrange equations, one can obtain the equations of motion for

the fields,

$$\left[\gamma^{\mu}\left(i\partial_{\mu}-g_{\omega b}\omega_0-g_{\varphi b}\varphi_0-\frac{g_{\rho b}}{2}\tau_3\bar{\rho}_0\right)-M_b\right]\psi_b=0, \tag{6}$$

for each baryon b, and

$$m_{\sigma}^2\sigma_0=\sum_b g_{\sigma b}\rho_{sb}-\lambda_1\sigma_0^2-\lambda_2\sigma_0^3 \tag{7}$$

$$m_{\omega}^2\omega_0=\sum_b g_{\omega b}n_b-g_{\omega\rho}\omega_0\bar{\rho}_0^2, \tag{8}$$

$$m_{\varphi}^2\varphi_0=\sum_b g_{\varphi b}n_b \tag{9}$$

$$m_{\rho}^2\bar{\rho}_0=\sum_b g_{\rho b}I_{3b}n_b-g_{\omega\rho}\omega_0^2\bar{\rho}_0, \tag{10}$$

where the effective mass of the baryon b is defined as

$$M_b=m_b-g_{\sigma b}\sigma. \tag{11}$$

The simplification promoted by the RMF considerably reduces the mathematical difficulties of describing nuclear matter. Nevertheless, the variables of interest (i.e., meson fields, densities, and baryon fields) are given as a function of each other, so they still need to be resolved by some method. The equations for the mesonic fields ((7)–(10)) are coupled polynomial equations, which can be easily solved self-consistently by a numerical algorithm. Thus, all mesonic fields were set, requiring only the determination of baryonic fields (ψ) for the complete description of the system and subsequent calculation of the equations of state.

Let a generic operator Γ, we have the expected value of the quantity Γ for a system in the ground state through the expression

$$\langle\bar{\psi}\Gamma\psi\rangle=\frac{\lambda}{(2\pi)^3}\int d\vec{p}\left[\bar{\psi}\left(\vec{p}\right)\Gamma\psi\left(\vec{p}\right)\right]\Theta\left[\mu-E\left(\vec{p}\right)\right], \tag{12}$$

where Θ is the Heaviside function, λ is the degeneracy of the $\psi\left(\vec{p}\right)$ state and μ is the "chemical potential". The following calculations are done in detail by [68], where initially we take $\bar{\psi}\left(\vec{p}\right)\psi\left(\vec{p}\right)=1$ as a scalar density normalization condition and

$$\Gamma=\frac{\partial\mathcal{H}}{\partial M}$$

in ((12)), where $\mathcal{H}$ is Dirac's Hamiltonian operator, $\mathcal{H}\psi=E\psi$, so that it is possible to arrive at the expression for the scalar density,

$$\rho_{sb}=\frac{\lambda_b}{2\pi^2}\int_0^{p_{Fb}}dp\frac{p^2M_b}{\sqrt{p^2+{M_b}^2}}, \tag{13}$$

where λ_b is the spin degeneracy. Similarly, imposing $\psi^\dagger(\vec{p})\,\psi(\vec{p}) = 1$ as a baryonic density normalization condition and making $\Gamma = \gamma_0$, it is possible through this method to arrive at the baryonic (or number) density,

$$n_b = \frac{\lambda_b}{2\pi^2}\int_0^{p_{F\,b}} dp\, p^2 = \frac{\lambda_b}{6\pi^2} p_{F\,b}^3, \tag{14}$$

with p_F denoting the Fermi momentum, i.e., the momentum of the most energetic particle at the last occupied level.

We are aware that spin-3/2 baryons (as the Δs) are in fact described by the Rarita-Schwinger Lagrangian density,

$$\mathcal{L}_{RS} = -\sum_{b=\Delta}\frac{1}{2}\bar{\psi}_{\mu\,b}\left(\varepsilon^{\mu\eta\lambda\nu}\gamma_5\gamma_\eta\partial_\lambda - i m_b\sigma^{\mu\nu}\right)\psi_{\nu\,b}\,, \tag{15}$$

where $\varepsilon^{\mu\eta\lambda\nu}$ is the Levi-Civita symbol, $\sigma^{\mu\nu} = \frac{i}{2}\left[\gamma^\mu,\gamma^\nu\right]$, and $\psi_{\mu\,b}$ is a vector-valued spinor with additional components (when compared to the four component spinor in the Dirac equation), which would demand a discrimination on the Lagrangian of the models for the terms when $b = \{\Delta\}$. Nonetheless, the resulting equation of motion can be written compactly as a Dirac equation $(i\gamma^\nu\partial_\nu - m)\,\psi_\mu = 0$ in the mean-field approximation, allowing us to be less rigorous with the notation, see [144].

The "energy-momentum tensor" $\mathcal{T}_{\mu\nu}$ can be obtained through the expression

$$\mathcal{T}_{\mu\nu} = \sum_j \frac{\partial\mathcal{L}}{\partial\left(\partial^\mu\varphi_j\right)}\partial_\nu\varphi_j - \mathcal{L}g_{\mu\nu}, \tag{16}$$

where the φ_j are the fields of the particles and $g_{\mu\nu}$ represents the tensor of the metric. In addition to being a conserved dynamic quantity, i.e., $\partial_\mu\mathcal{T}^{\mu\nu} = 0$, the energy-momentum tensor is useful in obtaining the EoS from the Lagrangian density, because, for a uniform system in equilibrium, it takes the form

$$\left\langle\mathcal{T}_{\mu\nu}\right\rangle = (\varepsilon + P)\,u_\mu u_\nu - P g_{\mu\nu}, \tag{17}$$

where ε is the energy density, P is the pressure, and u_μ is the four-velocity of the fluid. The *chevrons* $\langle\ \rangle$ represent the expected value, since this formalism is being applied to continuous and unlimited matter [68]. For a perfect fluid in hydrostatic equilibrium, $u_\mu = (1,0,0,0)$, so that

$$u_0{}^2 = 1 \quad \text{e} \quad \left|\vec{u}\right|^2 = 0.$$

Hence,

$$\begin{aligned}\left\langle\mathcal{T}_{00}\right\rangle &= (\varepsilon + P)\,u_0 u_0 - P g_{00}\\ &= \varepsilon + P - P = \varepsilon\end{aligned}$$

and

$$\begin{aligned}\langle \mathcal{T}_{ii} \rangle &= (\varepsilon + P)\, u_i u_i - P g_{ii} \\ &= (\varepsilon + P)\, \left|\vec{u}\right|^2 - P(g_{11} + g_{22} + g_{33}) = 3P.\end{aligned}$$

Therefore, obtaining the energy-momentum tensor from the Lagrangian density (Eq. (16)) and relating it to the expected for a perfect fluid in hydrostatic equilibrium (Eq. (17)), we obtain a prescription for the variables of the equation of state of matter in question,

$$P = \frac{1}{3} \langle \mathcal{T}_{ii} \rangle \,, \tag{18}$$

$$\varepsilon = \langle \mathcal{T}_{00} \rangle \,. \tag{19}$$

The equation of state is obtained from the energy-momentum tensor once the field equations ((7)–(10)) are solved. At $T = 0$, the total energy density ε is given by

$$\begin{aligned}\varepsilon = &\sum_b \frac{\lambda_b}{2\pi^2} \int_0^{p_{F_b}} dp\, p^2 \sqrt{p^2 + M_b^2} + \frac{1}{2} m_\sigma^2 \sigma_0^2 + \frac{\lambda_1}{3} \sigma_0^3 + \frac{\lambda_2}{4} \sigma_0^4 \\ &- \frac{1}{2} m_\omega^2 \omega_0^2 - \frac{1}{2} m_\varphi^2 \varphi_0^2 - \frac{1}{2} m_\rho^2 \rho_0^2 - g_{\omega\rho} \omega_0^2 \rho_0^2,\end{aligned} \tag{20}$$

and the pressure is given by the general thermodynamic expression

$$P = -\varepsilon + \sum_b \mu_b n_b \tag{21}$$

with the index b accounting for the baryon with the chemical potential μ_b. As the baryons are fermions, it is possible to identify the chemical potential with te Fermi energy, i.e., $E_{Fb} = \sqrt{{p_{Fb}}^2 + M_b^2} = \mu_b$, where the Fermi momenta are given by Eq. (14).

It is convenient to define the *asymmetry coefficient* in the terms of the number density of the individual particle species

$$\alpha = \frac{n_n - n_p}{n_n + n_p}, \tag{22}$$

such that

$$p_{Fp} = p_F\, (1 - \alpha)^{1/3} \qquad p_{Fn} = p_F\, (1 + \alpha)^{1/3} \tag{23}$$

and $p_{Fb} = 0$ for other particles, so $n_B = \frac{2p_F^3}{3\pi^2}$. The symmetric matter case is reached simply taking $\alpha = 0$ or, alternatively, $n_p = n_n = n_B/2$.

The *saturation density* n_0 is defined as the density of symmetric nuclear matter where the *binding energy* $\mathcal{E}(n_B,\alpha) = \varepsilon/n_B - M_0$ reaches its minimum, where $M_0 = 939$ MeV is the nucleon mass in vacuum, i.e., when

$$\left.\frac{\partial \mathcal{E}}{\partial n_B}\right|_{n_B = n_0} = 0, \tag{24}$$

with $\alpha = 0$. All the following bulk quantities are, in some degree, known experimentally or constrained theoretically at the saturation density of nuclear matter, or in some band region around n_0 (see, e.g., [52, 163] and references within). Furthermore, the index in $\mathcal{O}_0$ indicates the quantity $\mathcal{O}$ taken at $n_B = n_0$.

From the equations of state, i.e., P and ε, it is possible to calculate the *incompressibility modulus* [174]

$$K = 9 \left.\frac{\partial P}{\partial n_B}\right|_{\alpha=0}. \tag{25}$$

and the *skewness coefficient*

$$Q = 27 n_B^3 \left.\frac{\partial^3(\varepsilon/n_B)}{\partial n_B^3}\right|_{\alpha=0}. \tag{26}$$

Another set of bulk nuclear matter parameters follow from the symmetry energy, which is an important quantity to model nuclear matter and finite nuclei by probing the isospin part of nuclear interactions, given by

$$\mathcal{S} = \frac{1}{2} \left.\frac{\partial^2(\varepsilon/n_B)}{\partial \alpha^2}\right|_{\alpha=0}. \tag{27}$$

One can expand the symmetry energy $\mathcal{S}$ around the saturation density n_0 as

$$\mathcal{S}(n_B) = \mathcal{S}_0 + L_0\eta + \frac{1}{2}K_0^{\rm sym}\eta^2 + \frac{1}{6}Q_0^{\rm sym}\eta^3 + \mathcal{O}(\eta^4), \tag{28}$$

where $\eta(n_B) = (n_B - n_0)/3$ and the coefficients of the expansion are the *slope of the symmetry energy*,

$$L = 3n_B\frac{\partial \mathcal{S}}{\partial n_B}, \tag{29}$$

the *curvature of the symmetry energy*,

$$K^{\rm sym} = 9n_B^2\frac{\partial^2 \mathcal{S}}{\partial n_B^2}, \tag{30}$$

and the *skewness of the symmetry energy*,

$$Q^{\rm sym} = 27n_B^3\frac{\partial^3 \mathcal{S}}{\partial n_B^3}, \tag{31}$$

taken at $n_B = n_0$ [11].

It is also relevant to notice that the EoS of asymmetric nuclear matter, taken as its binding energy per nucleon $\mathcal{E}$, can be expanded around the isospin asymmetry coefficient as

$$\mathcal{E}(n_B,\alpha) = \mathcal{E}(n_B,0) + \mathcal{S}_2(n_B)\alpha^2 + \mathcal{S}_4(n_B)\alpha^4 + \cdots, \tag{32}$$

from where, excluding surface contributions, one can identify the n-th order symmetry energy as

$$\mathcal{S}_n = \frac{1}{n!} \left.\frac{\partial^n(\varepsilon/n_B)}{\partial \alpha^n}\right|_{\alpha=0}. \tag{33}$$

This expression leads to the well-known empirical parabolic law of asymmetric nuclear matter binding energy, from where the symmetry energy can be obtained from the difference between the binding energy of the pure neutron (α = 1) and symmetric matters (α = 0), i.e., as $\mathcal{S} \simeq \mathcal{E}(n_B,1) - \mathcal{E}(n_B,0)$. At normal nuclear matter density, the magnitude of the 4th order coefficient is estimated to be very small (less than 1 MeV). At supra-saturation densities, however, there are very limited data available, making the situation much less clear [24].

Due to the absence of an effective hegemonic model for matter in the QCD regime, the description of dense hadronic matter can be done in several different ways. In the most part of this work, the modeling was restricted to theories of the Walecka type, but even this class of models may present differences in the number and type of interactions considered. Furthermore, each individual modeling is dependent on a set of free parameters, adjustable through empirical data, which allows a large amount of adjustments (and, consequently, of models) for hadronic matter. Ref. [52] analyzed 263 representative models of this class, contrasting their predictions with well-established experimental quantities for nuclear matter, e.g., the "compressibility modulus", the "symmetry energy" and its *slope*, taken at and around the nuclear saturation point (n_0). It was verified that the theoretical results fit the empirical limits in only 35 of these models, contained in two main categories of the non-linear Walecka-type, (i) models in which the coupling constants are dependent on the baryonic density and that include the δ meson (not included in any model discussed in this thesis), and (ii) models that consider terms of cross-interaction of the mesonic fields.

The RMF models employed in this work are described in the following, and Table 2 shows the symmetric nuclear matter properties at saturation density of each one. The parameter values of each individual model can be found in the respective reference. As each author adopt distinct conventions for the Lagrangian terms (e.g., multiplicative constants), we opt to do not show them here.

The fitting of the model free parameters are made by considering ordinary nuclear matter, composed only by nucleons. To account for other baryonic species, we parametrize their couplings in terms of the nucleon-meson couplings. Considering the baryons to include nucleons $N = \{p, n\}$, hyperons $H = \{\Lambda, \Sigma^+, \Sigma^0, \Sigma^-, \Xi^0, \Xi^-\}$ and/or spin 3/2 resonances $\Delta = \{\Delta^{++}, \Delta^+, \Delta^0, \Delta^-\}$ (see Table 3 for the properties of the particles), the interaction coupling between each meson and each hyperon or Δ can be defined in terms of a scaling of the meson-nucleon coupling g_{iN}, defining the coefficient $x_{ib} = g_{ib}/g_{iN}$, with $i = \sigma,\omega,\varphi,\rho$ and $b = \{N\},\{H\},\{\Delta\}$. The hyperon coupling scheme parameters can be determined from fitting the hyperon potential depth for isospin-symmetric matter at saturation, if its value is known, with the remaining relative strength of the coupling constants determined by phenomenological inference, as done by [68], or symmetry group arguments, as proposed by [114].

Table 2 – Symmetric nuclear matter properties at saturation density for the models employed in this work: the nuclear saturation density n_0, the binding energy per particle B/A, the incompressibility K, the symmetry energy $\mathcal{S}$, the slope of the symmetry energy L, and the nucleon effective mass M. All quantities are in MeV, except for n_0 that is given in fm^{-3}, and the effective nucleon mass is normalized to the nucleon mass.

Model	n_0	B/A	K	$\mathcal{S}$	L	M/m
GM1	0.153	16.33	300.5	32.5	94	0.70
GM1$\omega\rho$	0.153	16.33	300.5	30	94	0.70
L3$\omega\rho$	0.156	16.20	256	31.2	74	0.69
DDME2	0.152	16.14	251	32.3	51	0.57
CMF	0.150	16.00	300	30	75	–
Constr. [52, 54]	0.148–0.170	15.8–16.5	220–260	28.6–34.4	36.0–86.8	0.6–0.8

The Δ couplings are treated more freely, as their behavior is not well known and to study their role is one of the main objectives of this work. The scarce information present in the literature, such as transport models and quasi-elastic scattering of electrons off nuclei [36], allows us to infer that the nucleon-Δ potential is slightly more attractive than the nucleon-nucleon one, so that, $U_N - 30$ MeV $\lesssim U_\Delta \lesssim U_N$, which implies $x_{\sigma\Delta}$ is greater than 1. Also, the vector coupling is constrained by LQCD results as respecting the relation

$$0 \leq x_{\sigma\Delta} - x_{\omega\Delta} \leq 0.2, \tag{34}$$

and no constraint is put in the $x_{\rho\Delta}$ value [193, 156, 152]. All of these constraints will be taken with a grain of salt, as we aim to explore the behavior of NS matter according to these parameters in a comprehensive way, not discarding the whole regions of possible values beforehand. Anyway, these constraints will be remembered in the evaluation of the results.

1.2.1 GM1

The first relativistic mean-field (RMF) model we discuss is a version of the hadron-dynamics model (5), in which the strong interaction is emulated by the exchange of scalar-isoscalar meson σ, the vector-isoscalar meson ω, and the vector-isovector meson ρ. Here, we consider the GM1 parametrization [66], which was adjusted to reproduce nuclear saturation properties employing extra scalar self-meson interactions σ^3 and σ^4, together with an additional vector-isovector self-meson $\omega\rho$ interaction, fitted to improve the value reproduced by the symmetry energy at saturation density.

The original GM1 set yields an incompressibility modulus of K = 300.5 MeV and a symmetry energy of S = 32.5 MeV at the saturation density. When the $\omega\rho$ interaction is introduced (called GM1$\omega\rho$ parametrization), the coupling constant $g_{\omega\rho} = 2.015\times10^{-2}$ is numerically obtained so that the symmetry energy is fixed to be the same as the CMF model described next, i.e., S = 30, and the remaining parameters are the same as in

the standard GM1 parametrization. The GM1 parametrization does not satisfy all the nuclear matter and astrophysical constraints [51, 117], however it is still widely employed and it allows comparisons with a large amount of results available in the literature. Recent results indicate that the symmetry energy slope constrained from the neutron skin thickness measurement performed by PREX [155] can be larger that previously accepted, reaching values in the range 106 ± 37 MeV. If this result is confirmed, the GM1 parametrization still holds a good prediction power. The inclusion of the crossed interaction between the mesonic fields, as performed here, reduces the symmetry energy slope from 94 MeV in the original GM1 parametrization to 69 MeV in the GM1$\omega\rho$, a value within the usually acceptable range [31, 81, 51]. There are other proposals in the literature aiming to reconcile the GM1 model with observables, e.g., in Ref. [118] it is suggested a parametrization with the same parameters as GM1, but with a density dependent coupling for the ρ meson field.

1.2.2 L3$\omega\rho$

We also include in our discussions the recently proposed L3$\omega\rho$ parametrization [109], which includes an additional $\omega\rho$ interaction that allows the correct prediction of slope of the symmetry energy, neutron-star radii and tidal deformabilities. It is a non-linear version of the Walecka model, where the baryon interactions are mediated by the σ, ω, ρ and φ mesons, within the mean field approximation, as presented above. The φ meson (with hidden strangeness) couples only to the hyperons, allowing a higher maximum mass to be reproduced for neutron stars, thus circumventing the well-known hyperon puzzle [27], that will be discussed in detail further in this work, with an effect similar to the higher-order ω^4 self interaction, also included. In addition to satisfying standard astrophysical constraints from LIGO/VIRGO and NICER, the model satisfies nuclear ground-state properties of finite nuclei and bulk properties of infinite nuclear matter. It is also consistent with the PREX-2 results for the symmetry energy of $L = 106 \pm 37$ [155], though at the lower end of the error band. The fittings of the self couplings λ and κ, and the couplings between the mesons $i = \{\sigma, \omega, \rho, \varphi\}$ and baryons b, defined in terms of the ratios $x_{ib} = g_{ib}/g_{iN}$, are discussed in detail in [109].

Relevant for this work, the scalar meson couplings are fitted to reproduce the hyperon potential depth $U_\Lambda = -28$ MeV (for isospin-symmetric matter at saturation) and the remaining relative strength of the coupling constants are determined by SU(3) symmetry group arguments, as proposed by [114], determining the complete hyperon-meson coupling scheme from a single free parameter, α_V. Despite the value of α_V, hyperons are always present in the neutron-star matter and the sequence of hyperon thresholds is always the same, with an inversely proportional relationship between α_V and the stiffness of the EoS. In this work, we choose to use $\alpha_V = 0.5$, which results in values for the additional potentials $U_\Sigma = +21.8$ MeV and $U_\Xi = +35.3$ MeV,

and a stiffer EoS with respect to the values $\alpha_V = 0.75$ or 1.0 that are considered in [114]. Though the potential for the Ξ^- mesons is repulsive in the parametrization used, recent observational constraints predict it to be attractive [63], but to reproduce such an attractive potential we would need an extra free parameter in the meson couplings [109].

1.2.3 DDME2

In this study, hadronic matter is also described within a relativistic mean-field approach with density dependent couplings. This class of models is shown to be very consistent in the description of nuclear matter experimental properties [50], and also when astrophysical constraints are imposed [54, 117]. In such models, the interaction is described through the the exchange of mesons, and here we consider the scalar meson σ, the vector mesons ω and φ (that carries hidden strangeness), isoscalars, and the isovector-vector meson $\vec{\rho}$. Differently from the previous models, the density-dependent parameterizations do not include non-linear (self interaction or crossed) meson terms. The density dependent coupling constants $g_{\sigma N}$, $g_{\omega N}$ and $g_{\rho N}$ are adjusted in order to reproduce some of the nuclear matter bulk properties using the following scaling with the baryonic density n_B

$$g_{iN}(n_B) = g_{iN}(n_0)\, a_i \frac{1 + b_i(\eta + d_i)^2}{1 + c_i(\eta + d_i)^2} \tag{35}$$

for $i = \sigma,\omega$ and

$$g_{\rho N}(n_B) = g_{\rho N}(n_0)\, \exp[-a_\rho(\eta - 1)], \tag{36}$$

with $\eta = n_B/n_0$, where n_0 is the nuclear saturation density. The Euler-Lagrange equations are used to calculate the equations of motion for the meson and baryon fields, see for instance [185], and a complete description for the hadronic matter given by this Lagrangian density can be derived from there. The model parameters considered here are obtained from a fitting that considered known experimental constraints on values of nuclear matter binding energy, compressibility modulus, symmetry energy and its slope, as well the ^{208}Pb neutron skin measurements. This parameterization is labeled as DDME2 and its details can be found in [101].

The couplings of the σ meson to the Λ and Ξ hyperons were determined from a fit to hypernuclear binding energies, while for the Σ, it has been fixed by imposing that at saturation the Σ potential in symmetric nuclear matter is +30 MeV, i.e. we have considered a repulsive interaction as seems to be the indication from experimental measurements [64]. The couplings to the σ meson have been taken from [59, 60], as being

$$x_{\sigma\Lambda} = 0.621, \quad x_{\sigma\Sigma} = 0.467, \quad x_{\sigma\Xi} = 0.321.$$

The magnitude of the couplings for the isoscalar-vector mesons are given by the SU(6) symmetry

$$x_{\omega\Lambda} = x_{\omega\Sigma} = \frac{2}{3}, \quad x_{\omega\Xi} = \frac{1}{3}, \quad x_{\varphi\Lambda} = x_{\varphi\Sigma} = -\frac{\sqrt{2}}{3}, \quad x_{\varphi\Xi} = -\frac{2\sqrt{2}}{3}.$$

The coupling of each hyperon to the ρ meson is defined by the product of the hyperon isospin with the ρ meson coupling to the nucleon, i.e., $x_{\rho H} = \tau_H$.

1.2.4 CMF

An extra relativistic mean field model, based on a different formalism of the previously discussed, is also included as a way of having more clarity in the evaluation of the model dependency of the results. The chiral mean-field (CMF) model is based on a nonlinear realization of the SU(3) sigma model. As in all chiral models, the masses of the baryons are generated (and not just modified) by the medium. In this way, at large temperatures and/or densities they decrease allowing chiral symmetry to be restored, in agreement with LQCD results [1]. In this work, we restrict ourselves to the hadronic version of the model (with leptons), which was fit to reproduce hadronic vacuum masses, decay constants, nuclear saturation properties, and to reach ~ 2.1 $M_\odot$ stars containing nucleons and hyperons, developed by [43], and disregard the possibility of phase transitions to quark matter. We add an additional $\omega\rho$ interaction to be in better agreement with data for the slope of the symmetry energy, neutron-star radii, and tidal deformabilities [42, 46]. We also add a higher-order ω^4 interaction to reproduce more massive neutron stars [45].

The mean-field model Lagrangian density has the terms

$$\mathcal{L}_b = \sum_b \bar{\psi}_b[i\gamma_\mu\partial^\mu - \gamma_0(g_{\omega b}\omega + g_{\rho b}I_{3_b}\rho + g_{\varphi b}\varphi) - M_b]\psi_i \,, \tag{37}$$

and

$$\begin{aligned}\mathcal{L}_{\rm m} = {} & \frac{1}{2}\left(m_\omega^2\omega^2 + m_\rho^2\rho^2 + m_\varphi^2\varphi^2\right) + g_4\left(\omega^4 + \frac{\varphi^4}{4} + 3\omega^2\varphi^2 + \frac{4\omega^3\varphi}{\sqrt{2}} + \frac{2\omega\varphi^3}{\sqrt{2}}\right) \\ & - k_0(\sigma^2+\zeta^2+\delta^2) - k_1(\sigma^2+\zeta^2+\delta^2)^2 - k_2\left(\frac{\sigma^4}{2} + \frac{\delta^4}{2} + 3\sigma^2\delta^2 + \zeta^4\right) \\ & - k_3(\sigma^2-\delta^2)\zeta - k_4\ln\frac{(\sigma^2-\delta^2)\zeta}{\sigma^2\zeta} - m_\pi^2 f_\pi\sigma - \left(\sqrt{2}m_k^2 f_k - \frac{1}{\sqrt{2}}m_\pi^2 f_\pi\right)\zeta \,,\end{aligned} \tag{38}$$

where the effective mass of baryons is $M_b = g_{\sigma b}\sigma + g_{\delta b}I_{3\,b}\delta + g_{\zeta b}\zeta + m_b$, including additional corrections given by the scalar-isovector δ and scalar-isoscalar (with hidden strangeness) ζ mesons, and a small bare mass correction m_b. The couplings were fitted to reproduce hadronic vacuum masses, decay constants, nuclear saturation properties, and to reach more than 2.1 $M_\odot$ stars. See [160] for a complete list of coupling constants.

Following the SU(3) and SU(6) coupling schemes for the scalar and vector couplings of the mesons to the baryons, there are only two free parameters left: one fitted to reproduce a reasonable hyperon potential U_Λ and another one ($r_V = g_{N\Delta}/g_{\omega\Delta} = 1.25$) chosen to reproduce the potential $U_\Delta \sim U_N$ for symmetric matter at saturation, resulting additionally in $U_\Lambda \sim$ –27 MeV, U_Σ = 6 MeV, U_Ξ = –17 MeV, and U_Δ = –64 MeV (in the presence of the additional interaction ω^4). A much larger r_V would suppress all Δ's, while a much lower value would suppress all hyperons.

This model was already used to investigate the influence of heavier resonances [167] and magnetic fields [41, 61] in neutron stars. See Ref. [41] and references therein for a complete list of coupling constants.

1.3 COMPACT STAR DESCRIPTION

The models presented above were originally developed for their applications in the microscopic context, i.e., in the description of nuclear matter or heavy ion collisions. In this work, these models will be extrapolated to the macroscopic scope of the description of dense continuous matter, as is customary in the study of compact stellar objects. The procedure for moving from microphysics, in the form of effective relativistic models, to macrophysics, in the form of observational variables of compact stellar objects, will be discussed in this section.

Atomic nuclei are held together by the attraction arising from the strong residual force between nucleons, which is the initial motivation for studying this interaction. However, even in the case of nuclear matter, the strong force cannot sustain nuclei of atomic number A greater than approximately 200, certainly much lower than that found in neutron stars. Furthermore, as already discussed, the repulsive character of this force is of central importance for the case of dense stellar matter, which also makes it difficult for this force to guarantee the unity of the star. Therefore, it is noted that neutron stars must be "gravitationally bound", i.e., the degeneracy pressure of the hadrons is counterbalanced by the gravitational force.

However, as the Coulomb repulsion force is much stronger than the gravitational attraction, the condition is imposed

$$\frac{Z_{ef}e^2}{R^2} < \frac{GAm^2}{R^2} \quad \Rightarrow \quad Z_{ef} < 10^{-36}A, \tag{39}$$

where Z_{ef} is the net charge number of the particles contained in the star [68]. As this condition is quite strong, compact stars are considered to be electrically neutral objects, so stellar matter must be made up of several particles, whether leptons or other baryonic species, negatively and positively charged. This implies that hadronic matter, in this context, can be severely asymmetrical with respect to isospin (or the relative amounts of baryonic species), while nuclear matter is, in general, nearly symmetrical.

Free neutrons are unstable particles to the so-called β decay, with a half-life of about 10 minutes [74]. It is expected, however, that this process is somehow counterbalanced within neutron stars that are made up largely (although not entirely) of free neutrons. This process, in which free leptons contained in matter 'collide' with a proton and form a neutron and its neutrino, is called inverse β decay. This cycle of forward and reverse β decays is the so-called Urca process, which plays a central role in the cooling of neutron stars. Generalizing this type of process to other baryons, we have the Urca process defined as

$$B_1 \rightarrow B_2 + \beta + \bar{\nu}_\beta \quad \rightleftharpoons \quad B_2 + \beta \rightarrow B_1 + \nu_\beta, \tag{40}$$

where B_i can represent any baryons, as long as they are suitable for energy and charge conservation, and β is a negatively charged lepton, associated with the respective neutrino (antineutrino) ν_β ($\bar{\nu}_\beta$). Baryons are understood to be degenerate inside neutron stars, and this argument extends to lepton gas. This feature is important in the process of defining the populations of particles inside the star, since the equilibrium state of matter will be reached when the two reactions of the Urca process reach equilibrium. This will occur when there are no more energy levels accessible to the leptons produced in the direct β decay, since it imposes

$$E_{FB_1} = E_{FB_2} + E_{F\beta}, \tag{41}$$

so that when all energy levels less than the Fermi energy are occupied, the process will cease. Identifying that $E_F = \mu$ for matter in the ground state, one can deduce the state in which this stability is reached, in the so-called "chemical equilibrium" (or "β"). For the fraction of matter consisting of baryons of type B, with charge q_B, it is possible to show that

$$\mu_B = \mu_n - q_B \mu_{e^-}, \tag{42}$$

from which it can be seen that the baryonic chemical potentials can be written directly in terms of the independent neutron and electron potentials, respectively μ_n and μ_{e^-} [169].

Moving from micro to macrophysics requires submitting the EoS that describes dense matter to conditions of mechanical (or hydrostatic) equilibrium, since compact stars are understood to be sufficiently stable objects in their internal structure. It is therefore necessary to determine the relationship between gravitational force and degeneracy pressure of matter inside the star in the equilibrium situation. Compact stars are bodies whose gravitational field is extremely intense, so the equilibrium relationship must be established within the framework of general relativity. In this context, the way in which spacetime geometry and its matter-energy content correlate is dictated by Einstein's Field Equation,

$$R_{\mu\nu} - \frac{1}{2} R g_{\mu\nu} = 8\pi \mathcal{T}_{\mu\nu}, \tag{43}$$

where $R_{\mu\nu}$ is the "Ricci curvature tensor", R is the "scalar curvature", $g_{\mu\nu}$ is the metric tensor and $\mathcal{T}_{\mu\nu}$ is the energy-momentum tensor, which is, in this case, the energy-momentum tensor for an ideal fluid in equilibrium, because space-time is flat in the distance scale of the interaction between the particles.

Thus, the relativistic hydrostatic equilibrium condition arises from the solution of ((43)) for the interior of a static spherical object, which employs the so-called "Schwarzschild metric", defined by the line element

$$ds^2 = -e^{2\varphi(r)}dt^2 + \left[1 - \frac{2\,m(r)}{r}\right]^{-1} dr^2 + r^2 d\Omega^2, \tag{44}$$

where $m(r)$ is the "gravitational mass" inside the sphere of radius r [128]. One can determine $\varphi(r)$ taking advantage of the symmetries of the problem, which also allow, together with the energy-momentum tensor for an ideal fluid, to rewrite ((44)) in the form of the differential equation

$$\frac{dP}{dr} = -\frac{[\varepsilon(r) + P(r)]\left[m(r) + 4\pi r^3 P(r)\right]}{r\,[r - 2m(r)]}, \tag{45}$$

where the gravitational mass is

$$m(r) = \int_0^r dr' 4\pi r'^2 \varepsilon\left(r'\right), \tag{46}$$

and $\varepsilon(r)$ and $P(r)$ are the energy density and pressure in the spherical shell of radius r. The equation for relativistic hydrostatic equilibrium ((45)) is called the Tolman-Oppenheimer-Volkoff (TOV) equation.

Comparing the TOV with its classical analogue, the Newtonian hydrostatic equilibrium equation,

$$\frac{dP}{dr} = -\frac{\varepsilon(r)\,m(r)}{r^2}, \tag{47}$$

it is noted that the pressure decreases much more rapidly in the relativistic case, i.e., general relativity predicts that stationary spherical objects are subject to more intense gravitational forces than predicted by Newtonian gravitation, which suggests that situations taken as stable by the classical description can collapse if relativistic effects are taken into account [128].

This object will be perceived by a distant observer as having a radius $r = R$, defined from the boundary condition $P(R) = 0$, and a gravitational mass $M = m(R)$, given by ((46)). Other boundary conditions are also important, such as $m(0) = 0$ and the definitions of central pressure and central energy density,

$$P(0) = P_c \qquad \text{e} \qquad \varepsilon(0) = \varepsilon_c. \tag{48}$$

It can be identified that the equation ((45)) will diverge for the radius $R_S = 2M$, called the "Schwarzschild radius", which represents the minimum radius that the star can

have, given its mass, so that its internal pressure is able to counterbalance gravity and prevent the object's gravitational collapse into a black hole.

The TOV solution starts from the equations of state, which dictate the behavior of P and ε for the constituent matter of the star, but the equation ((45)) is exactly solvable for a few cases of EoS . Numerically, the solution is made from a central energy density ε_c and obtaining of the pressure gradient and, consequently, of the following values of $\varepsilon(r)$. This procedure is repeated iteratively until the surface of the star, where the pressure is zero, in the radius that corresponds to the radius of the star, $P(R) = 0$. Solving the TOV for different values of central energy density ε_c, we arrive at the results corresponding to a family of possible stars for the given EoS, which is illustrated through a diagram of the gravitational mass *versus* the star radius.

Determining hydrostatic equilibrium solutions for the TOV does not in itself ensure the stability of the compact star. It is important for the correct interpretation of mass-radius diagrams to understand under what conditions equilibrium can be reestablished after the stars are removed from this situation. Analyzing the expected behavior for the TOV solutions for a star of mass M and central energy ε_c, it is noted that (i) if the star is compressed, its central density increases to a value $\varepsilon'_c > \varepsilon_c$, so the pressure in the new configuration must be sufficient to overcome gravity, returning the star to its initial equilibrium state, which will only happen if the mass M', which the star must have in order for it to be in equilibrium in the configuration ε'_c, is greater than the initial mass M, and (ii) if the star undergoes an expansion, its central density decreases to a value $\varepsilon'_c < \varepsilon_c$, so the gravitational attraction of the star must overcome the pressure, causing the star to contract and return to the initial configuration, which demands that the mass M', which the star would have in the new configuration if it were in equilibrium, is less than the initial mass M. From these two situations, it can be seen that

$$\frac{dM}{d\varepsilon_c} > 0 \tag{49}$$

is a necessary condition for stable solutions of TOV [138]. Unstable solutions can be seen in mass-radius diagrams from the point at which mass and radius begin to decrease with increasing central energy density.

1.4 OBJECTIVES OF THE WORK

Starting from the topics exposed above, we intend to obtain a description of compact stars made up of dense matter from relativistic models, with the purpose of analyzing pulsars as hadronic, hybrid and/or strange stars. This is done by dividing the present study into two parts. In a first moment, the implications of including delta baryons in the stellar matter composition. In Chapter 2, results published in [123] are discussed. We analyse the properties of two different matter compositions: nucleonic

matter with delta baryons and nucleonic matter with hyperons and delta baryons, by applying a relativistic mean-field description of neutron star matter with density dependent couplings. The delta-meson couplings are allowed to vary within a wide range of values obtained by experimental data, while the hyperon-meson couplings are fitted to hypernuclear properties. Neutron star properties with no deconfinement phase transition are studied. In Chapter 3, we expand this investigation to magnetars, studying dense matter with hyperons and deltas under the influence of strong magnetic fields considering the effects of Landau levels, with and without taking into account the anomalous magnetic moment, as published in [47] and [122].

The second part of this work is dedicated to the study of the QCD phase diagram, in special to explore the possibility of hadron-quark deconfinement in the context of compact stars. In Chapter 4, an extended version of the Nambu–Jona-Lasinio model is developed for the description of hadronic matter, for the cases of nucleonic (protons and neutrons only) and hyperonic (protons, neutrons and lambdas) matter. The latter case was not previously discussed within the NJL model theoretical framework, and it is a novel and relevant contribution to the exploration of the QCD phase diagram, as describing matter with strangeness content is important to the study of the hadron-quark phase transition. Different extensions of the Nambu-Jona-Lasinio model are used to investigate a possible hadron-quark phase transition at zero temperature in Chapter 5, in order to check the possibility of a hadron-quark phase transition to occur in the interior of compact stars, as published in [72]. Yet, we reproduce a comparison of the phase diagram obtained in this framework with the vectorial MIT model one, as published in [112]. Finally, in Chapter 6, we investigate the effects of strong magnetic fields on the hadron-quark phase transition point at zero temperature, and compare them with the results obtained with non-magnetised matter [121]. An investigation of the phase transitions that could sustain hybrid stars is also performed, as published in [9]. The conclusions are drawn in Chapter 7.

Part I

Delta Baryons in Neutron Star Matter

2 DELTA BARYONS IN NEUTRON STARS

The starting point for determining the macroscopic structure of compact stars is the assumption of a specific microscopic model, which leads to the calculation of an equation of state (EoS) for dense matter. The EoS encodes the particle population of baryons and leptons and how they interact through the strong interactions, constrained by equilibrium conditions, such as β-stability and charge neutrality, as discussed in the previous Chapter.

Although the class of stellar remnants that are neither white dwarves nor black holes is traditionally named *neutron stars* (NS), these objects are not composed solely of neutrons. Even the more naïve description of such objects must include some amount of protons in order to guarantee the stability of the nuclear matter, and this fact was already pointed out in the first proposals of the existence of NS by Landau, Baade and Zwicky in the early 1930s. The extremely high energies estimated to occur in the core of neutron stars are more than sufficient to create heavier particle species, beyond the traditional proton-neutron-electron admixture.

Almost forty years ago, Glendenning [65] discussed in his seminal paper different scenarios considering non-nucleonic degrees of freedom in NS matter, including hyperons, delta baryons, pions and kaons, within a relativistic mean field approach. It has since become common in the literature to consider the entire spin-1/2 baryon octet, e.g. [67, 148, 10, 14, 135, 187, 121, 161, 168, 130]. In this work, Glendenning found that the delta baryons do not nucleate inside the NS core. This result was due to the coupling parameters chosen, as it was shown later that, with a convenient choice of the couplings minimally constrained by the existing experimental measurements, delta baryons may indeed occur inside neutron stars [198, 167], so recently the role of the spin-3/2 decuplet has been slowly gaining attention, e.g. [104, 200, 129, 156, 118, 162, 153, 9, 179, 45, 119]. The lightest spin-3/2 baryons (the Δs) are only $\sim$ 30% heavier than the nucleons (protons and neutrons) and are even lighter than the heaviest spin-1/2 baryons of the octet (the Ξs). Thus, unless the Δs are subject to a very repulsive coupling, they are expected to appear at the same density range as the hyperons (around 2 or 3 times the nuclear saturation density).

The knowledge of the NS composition and the signatures of this composition is presently a field of intense investigation. To consider the entire spin-1/2 baryon octet as part of the NS matter composition is almost the standard in the nuclear astrophysics community but, more recently, there is a strong interest in understanding how the presence of the delta baryons specifically may influence the properties of NS and their evolution.

Not much is known about how Δ baryons couple in dense matter, but their potential for isospin-symmetric matter at saturation density is expected to be attractive and in

Table 3 – Vacuum mass, electric charge, isospin 3rd component, spin, normalized magnetic moment, and normalized anomalous magnetic moment of baryons considered in this work. Electric charge is shown in units of the electron charge and μ_N is the nuclear magneton.

	M_b (MeV)	$q_b(e)$	$I_{3\,b}$	S_b	μ_b/μ_N	κ_b/μ_N
p	939	+1	$+\frac{1}{2}$	1/2	2.79	1.79
n	939	0	$-\frac{1}{2}$	1/2	–1.91	–1.91
Λ	1116	0	0	1/2	–0.61	–0.61
Σ^+	1193	+1	+1	1/2	2.46	1.67
Σ^0	1193	0	0	1/2	1.61	1.61
Σ^-	1193	–1	–1	1/2	–1.16	–0.37
Ξ^0	1315	0	$+\frac{1}{2}$	1/2	–1.25	–1.25
Ξ^-	1315	–1	$-\frac{1}{2}$	1/2	–0.65	0.06
Δ^{++}	1232	+2	$+\frac{3}{2}$	3/2	4.99	3.47
Δ^+	1232	+1	$+\frac{1}{2}$	3/2	2.49	1.73
Δ^0	1232	0	$-\frac{1}{2}$	3/2	0.06	0.06
Δ^-	1232	–1	$-\frac{3}{2}$	3/2	–2.45	–1.69

a range of 2/3 to 1 times the potential of the nucleons, which is of order –80 MeV [48, 152]. Different properties of baryons considered in this study are shown in Tab. 3.

In [37], the authors have studied the effect of heavy baryons on the constitution of hot non-homogeneous matter, in particular their effects on the light clusters abundance and dissolution, using two relativistic mean-field nuclear models (FSU2H [181], a model with non-linear mesonic terms, and DD2 [186], a model with density dependent couplings). For the delta baryon, the couplings were restricted to values compatible with experimental observations as discussed in [48, 156]. It was found that the model FSU2H was much more restrictive, because most of the couplings would not be acceptable to describe neutron stars since the effective nucleon mass would become zero at densities below the maximum mass configuration. On the other hand, the DD2 model seemed to show much more flexibility and allowed a wider range of acceptable couplings. In [156], the FSU2H model has been fully investigated, but there was no reference to the implications of the fact that the effective nucleon mass may become null at still low densities. In [99], this problem was also encountered, but the authors have modified their model in order to avoid this issue.

In this section of the work, we will explore in depth the effects of the delta baryon couplings considering a the DDME2 model, that describes adequately nuclear matter properties and NS observations, considering the Δ admixture, in both pure nucleonic and hyperonic NS matters. For both matter competitions, we will study the behavior of the nucleon effective mass, the speed of sound, the Δ and hyperonic fraction and the electron chemical potential, and also discuss the star properties such as mass and radius. We will pay special attention to some interesting aspects, as the possible increase

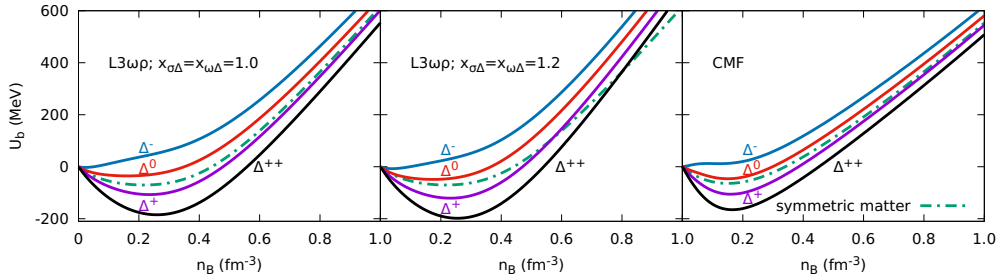

Figure 3 – Single-particle potentials of Δ baryons as a function of baryon number density in isospin-symmetric nuclear matter (dashed-dotted line) and pure neutron matter (solid lines) for the L3$\omega\rho$ model using two different Δ scalar interaction strengths (left and middle panels) and for the CMF model (right panel).

of the NS maximum mass as compared to hyperonic only stars, or the possibility of the formation of stars with more than 80% of Δ-baryons at the core center. Also, special compact stars may exist in some hyperon-free delta-dominated composition, the ones we have named *deltic stars*.

We start our discussion with the single-particle interaction potential for the Δ baryons in dense nuclear matter, which is a measure of the energy cost of adding one particle b in a b-less matter with the given condition. For the L3$\omega\rho$ model, it can be written as

$$U_b = -g_{\sigma b}\sigma + g_{\omega b}\omega + g_{\rho b}I_{3b}\rho + g_{\varphi b}\varphi \ , \tag{50}$$

and, for the CMF model,

$$U_b = g_{\sigma b}\sigma + g_{\delta b}I_{3_b}\delta + g_{\zeta b}\zeta - m_{b,vac} + g_{\omega b}\omega + g_{\rho b}I_{3b}\rho + g_{\varphi b}\varphi \ . \tag{51}$$

In isospin-symmetric nuclear matter, all families of baryons experience the same potential, since the meson field ρ (and δ) are null in this situation. In neutron rich matter, particles with positive isospin projections (as the positively charged Δs) are more bound than their zero- and negative-isospin counterparts, with the largest difference occurring for pure neutron matter, that can be taken as an extrapolation of neutron-star matter in β-equilibrium. The first two panels of Fig. 3 show how the L3$\omega\rho$ model scalar and vector interactions affect the Δ potentials. In all cases, the particle potentials eventually become positive as the density increases, corresponding to unbound states, but they stay negative in the relevant interval of densities around nuclear saturation, where their depth determines how much they are bound.

For the L3$\omega\rho$ model, the larger the scalar coupling value (i.e., the parameter $x_{\sigma\Delta}$), the lower the potentials are in the low density regions. Complementary to that, the larger the vector coupling (i.e., the parameter $x_{\omega\Delta}$), the more repulsive the potentials for Δs are, which reflect in more positive curves in the high density region, where the repulsive channel dominates. Also, it can be seen that the potential depends less on

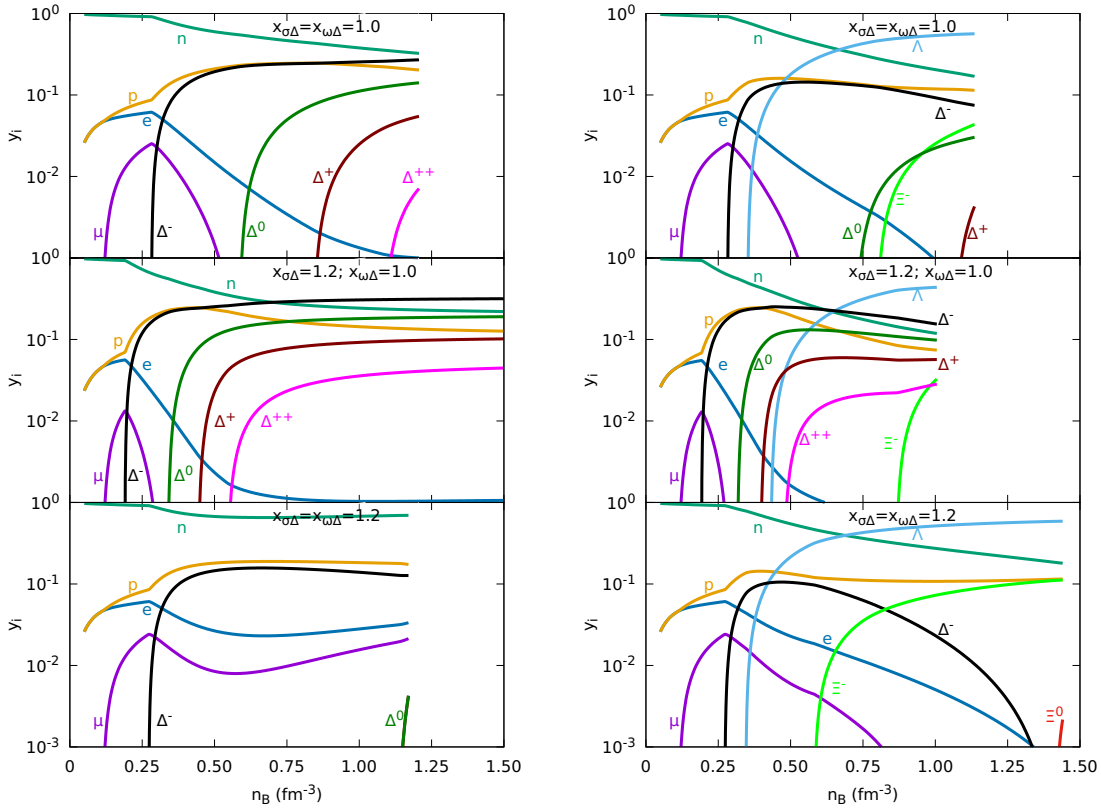

Figure 4 – Particle relative populations as a function of the density for the DDME2 model, fixing $x_{\rho\Delta} = 1.0$, for the NΔ (left) and NHΔ (right) matter compositions.

the species of Δ in the CMF model. Magnetic-field effects are not included, but it was verified that fields up to $B = 3 \times 10^{18}$ G do not affect the results shown in Fig. 3.

We now discuss the composition and expected onset of the different heavy baryons in β-stable, charge-neutral NS matter, as described by the DDME2 model formalism exposed in the previous section. Fig. 4 shows the particle fractions when the baryonic composition considered is the hyperon-free matter, i.e., composed by nucleons and delta baryons (labeled NΔ), and delta-admixed hypernuclear matter, i.e., composed by nucleons, hyperons and deltas (labeled NHΔ). The negatively charged spin-3/2 baryons are favored when charge neutrality is enforced, while the positively charged ones are suppressed, in the same way as what usually takes place with the hyperons. Being negatively charged, the Δ^- can replace a neutron-electron pair at the top of their Fermi seas, being favored over the lighter Λ and Σ baryons because of the fact that their potential is more attractive, to a proportion which the mass difference is counterbalanced. When allowed, the first hyperon to appear is the Λ, as it is the lighter one and neutrally charged.

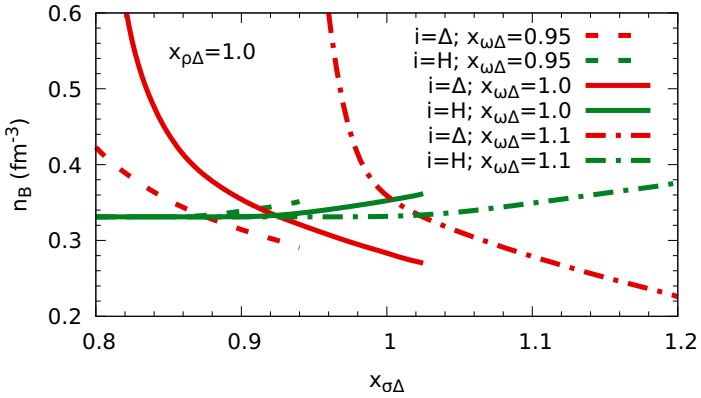

Figure 5 – Onset density of the hyperons and deltas in the NHΔ matter composition for the DDME2 model, varying the $x_{\sigma\Delta}$ and $x_{\omega\Delta}$ couplings.

Analysing Fig. 4, we conclude that if the coupling fractions are lager than one, in hyperon free (NΔ) matter, having $x_{\sigma\Delta} > x_{\omega\Delta}$ favors the appearance of all Δ species, even the one with charge +2; if $x_{\sigma\Delta} = x_{\omega\Delta}$, the larger the coupling the less favored the Δ-baryons are, due to the ω-dominance at large densities that occurs because the σ field saturates; also, the electrons are efficiently replaced by Δ^--baryons if the $x_{\omega\Delta}$ is not too large. When hyperons are included in the (NHΔ) matter, the Λ-hyperon sets after the Δ^- and is pushed to quite high densities if $x_{\sigma\Delta} > x_{\omega\Delta}$; if $x_{\sigma\Delta} = x_{\omega\Delta}$ the larger $x_{\omega\Delta}$ the more important is the contribution of the Ξ^--hyperon, and the smaller Δ^- because the larger the $x_{\omega\Delta}$, the more repulsive the Δ^- interaction at high densities, see [156]. The presence of hyperons strongly disfavors the increase of Δ fractions at high densities because hyperons feel a much weaker repulsion since the coupling to the ω-meson is smaller. This fact is exemplified by the competition between the Δ^- and the Ξ^-, as one can notice in the bottom-right panel of Fig. 4, whith the former suppressing the first as it is lighter and subject to a less repulsive coupling.

In Fig. 5, we show the onset of hyperons and deltas as function of the coupling parameters. As expected, a large (attractive) $x_{\sigma\Delta}$ coupling favors the onset of the resonances, while a large (repulsive) $x_{\omega\Delta}$ postpones it. For a fixed $x_{\omega\Delta}$, there will always be a $x_{\sigma\Delta}$ where the Δ^- and the Λ appear at the same density, beyond which the resonances are favored. If we impose the constraint given by Eq. (34), Δ^- will always appear first, further delaying the appearance of hyperons from the delta-free threshold of the model.

The families of stars that result from the input of the obtained equations of state (EoS) in the Tolman-Oppenheimer-Volkoff (TOV) equations of relativistic hydrostatic equilibrium are shown in Fig. 6 for hyperon-free matter and Fig. 7 for Δ-admixed matter including hyperons. In each figure we show results for three values of the coupling-fractions $x_{\omega\Delta}$ (0.95, 1.0 and 1.1) and $x_{\rho\Delta}$ (0.5, 1.0 and 1.5). The colorbar indicates the $x_{\sigma\Delta}$ value which we vary between 0.8 to 1.2. In the following figures, the full black line represents the results obtained with the pure nucleonic (N) EoS, and the black dash-

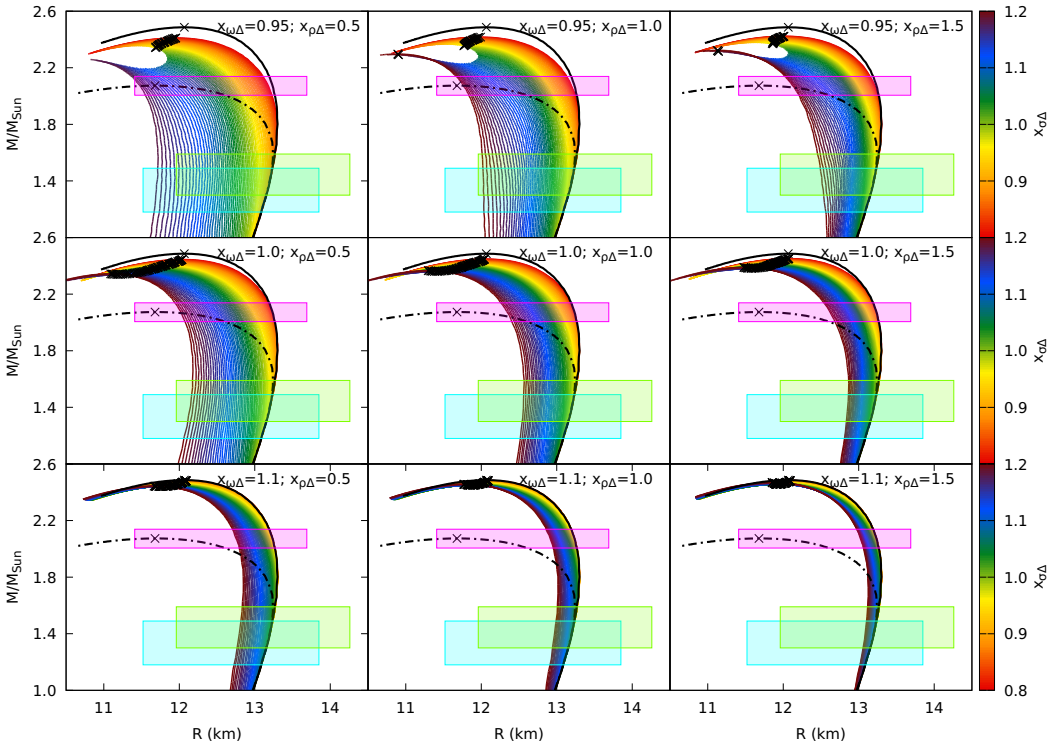

Figure 6 – Mass-radius diagrams for the DDME2 model, for some choices of $x_{\rho\Delta}$ and $x_{\omega\Delta}$, varying the $x_{\sigma\Delta}$ parameter for the NΔ matter composition (color scale). The solid and dot-dashed black lines represent the N and NH compositions, respectively, and the black crosses indicate the maximum mass star if this configuration is reached. The squares represent NICER constraints (see text).

dotted line has been calculated for a hyperonic (NH) EoS. In these figures the crosses indicate the maximum mass configuration. The top panels in both figures, and middle panels of Fig. 7, show some EoS that do not reach the maximum mass star. In the presence of hyperons, this happens for for $x_{\sigma\Delta}$–$x_{\omega\Delta} \gtrsim 0.1$. Formally, the maximum mass star is obtained when the TOV stability conditions of having a positive derivative of the star mass with respect to its central density ($\partial M/\partial \varepsilon_c \geq 0$) reaches a zero value. Black crosses indicate the maximum mass star for each EoS if this criteria is attained. As we will discuss later some mass-radius curves to not reach the maximum configuration because the effective mass of the nucleon becomes zero at a too low density. This problem was identified in other works [99, 105, 153, 37], but its consequences were not fully explored until now. In [99], the authors have modified the model in order to avoid negative effective masses for the nucleon.

The shaded squares in the figures represent observational constraints obtained from NICER measurements, the blue and green squares are independent analysis of

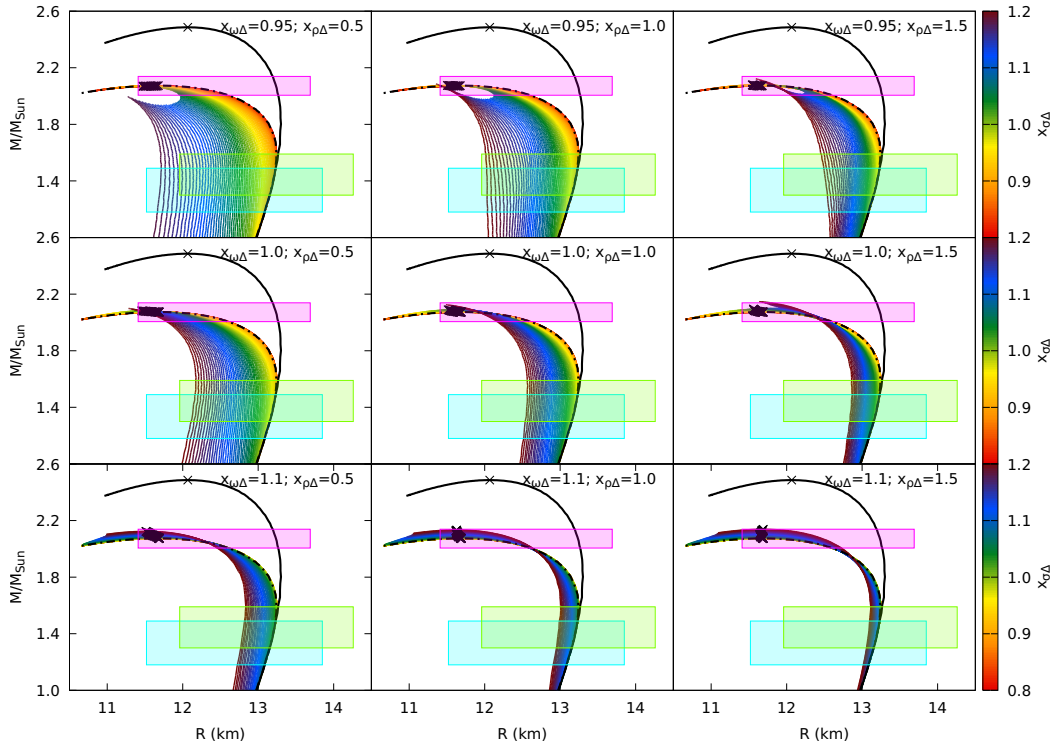

Figure 7 – Same as Fig. 6, but for NHΔ matter composition.

the pulsar PSR J0030+0451, that resulted in $M = 1.34^{+0.15}_{-0.16}$ M_{Sun} and $R = 12.71^{+1.14}_{-1.19}$ km according to Ref. [157], and in $M = 1.44^{+0.15}_{-0.14}$ M_{Sun} and $R = 13.02^{+1.24}_{-1.06}$ km according to Ref. [127], respectively. The magenta square represents the recent measurement of the pulsar PSR J0740+6620 [58] of $M = 2.072^{+0.067}_{-0.066}$ M_{Sun} and $R = 12.39^{+1.30}_{-0.98}$ km, at a confidence interval of 68% [158]. The uncertainties associated with the observations are not small enough to put strong constraints on the coupling parameters we are investigating. All models that reach the maximum mass configuration are compatible with the observational constraints for the several scenarios of matter composition considered, either with nucleons and deltas or including hyperons as well.

From the figures, we see that $x_{\sigma\Delta}$ competes with $x_{\omega\Delta}$ and $x_{\rho\Delta}$, with greater values of the first making the stellar radius decrease when compared with the delta-free matter composition. Larger values of $x_{\sigma\Delta}$ are associated with a larger attraction, and therefore a softer EoS at intermediate densities when the effect of the σ-meson dominates. A similar effect occurs when smaller values of $x_{\rho\Delta}$ are taken: the smaller the $x_{\rho\Delta}$, the smaller the radii obtained for a given pair $x_{\sigma\Delta}$- $x_{\omega\Delta}$. This can be understood because a smaller $x_{\rho\Delta}$ decreases the repulsion associated with the proton-neutron asymmetry. Another interesting effect is the fact that the simultaneous presence of hyperons and deltas increases the maximum mass above the hyperonic matter maximum mass limit

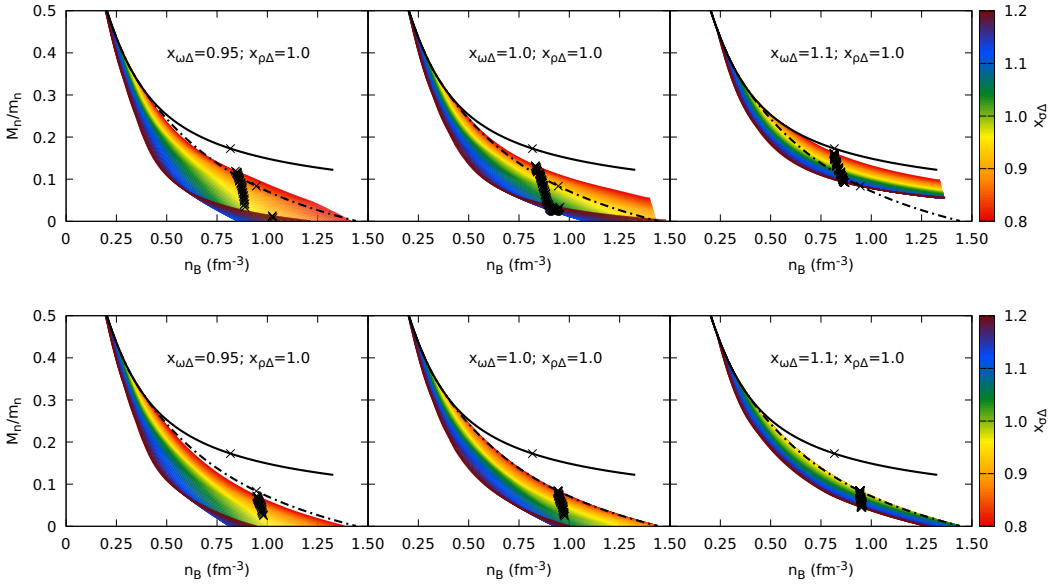

Figure 8 – Nucleon effective mass as a function of the density for the DDME2 model, taking $x_{\rho\Delta} = 1.0$, for some choices of $x_{\omega\Delta}$ and varying the $x_{\sigma\Delta}$ parameter for the NΔ matter composition (top panels) and for NHΔ matter composition (bottom panels). The solid and dotted-dashed black lines represent the N and NH compositions, respectively, and black crosses indicate the central values of the maximum mass star if this configuration is reached.

if $x_{\omega\Delta} \geq 1$. This is due to the fact that at high densities the effect of the vector meson dominates over the sigma meson and the delta coupling to the ω-meson is larger than the coupling of the nucleons or hyperons to the ω-meson. The role of the couplings in the maximum mass is quite complex, and will be better understood later in the discussion.

In Fig. 8 we plot the nucleon effective mass,

$$M_n = m_n - g_{\sigma N}\sigma, \tag{52}$$

as a function of the density. When we consider the nucleon-only neutron star matter composition, M_n decreases asymptotically with n_B. When other baryon species are included in the matter composition (either hyperons, deltas, or both), we see a much faster decrease of the nucleon effective mass. This behavior is understood from the fact that each new particle present adds (through the scalar density dependence of the σ field) to the negatively contributing term of Eq. (52). The greater the multiplicity of baryons in the matter, the faster is the drop of M_n, as we can see from comparing top and bottom panels of Fig. 8 or even comparing the delta admixed with the N or NH compositions inside each panel, noting that the higher values of $x_{\sigma\Delta}$ produce higher fractions of deltas. For some configurations, the drop is so fast that the nucleon effective mass becomes too small and reaches zero before attaining the maximum densities expected to occur in the maximum mass configuration. This behavior was

already well-known for the hypernuclear star matter [165], but the inclusion of deltas makes it even more pronounced.

These EoS do not describe neutron stars properly, and therefore must be discarded from our analysis. We argue that these EoS would be valid if a phase transition to deconfined quark matter could occur at a density below the one at which the nucleon effective mass becomes zero. This scenario will be explored in a future work. For the models with a non-vanishing effective nucleon mass, the EoS are computed while the thermodynamic stability condition $dP/d\varepsilon \geq 0$ holds true. A liquid-gas type of phase transition is expected to occur when the thermodynamic stability is lost but, as the EoS can be computed to densities far beyond the ones present in stellar interiors (reaching at least $n_B = 1.25$ fm^{-3}), and disregarding some unrealistic choices of very negative values of the relation $x_{\sigma\Delta} - x_{\omega\Delta}$, this behavior would not be prevalent in any physically reasonable scenario. We will just consider unfitting the models that are not able to attain the maximum mass configuration when their EoS is applied to the TOV equations, as here we assume a scenario that does not allow for a hadron-quark deconfinement phase transition. The delta couplings are also constrained by some unphysical behavior such as the effective nucleon mass becoming zero at too low densities, or the EoS predicting a thermodynamic instability really near the saturation density that does not seem to be observed, but no constraint can be implied from the astrophysical observations.

In Fig. 8, the results are shown considering the whole computed EoS, and black crosses indicate maximum mass star if this configuration is reached for the scenario in question. The maximum central density is around $n_B = 0.85$ fm^{-3} for the NΔ composition, and around $n_B = 1.00$ fm^{-3} for the NHΔ composition. When deltas are favored to a point of suppressing all other species (higher values of $x_{\sigma\Delta}$ and/or lower values of $x_{\omega\Delta}$), the situation reverts back to the N matter composition asymptotic behavior, leading to the diminishing of the negatively contributing terms in Eq. (52), but now the Δ baryons are the most abundant particles. In this extreme limit, the EoS reaches the maximum mass star configuration once again, e.g., the indigo blue curve in Fig. 8 top left panel (this configuration is composed by a fraction of 80% of deltas, see Fig. 10).

The derivative of the pressure with respect to the energy density is the speed of sound, a quantity that provides information about shear viscosity, tidal deformability and gravitational waves signatures [109]. At zero temperature, its square is simply defined as

$$v_s^2 = \frac{\partial P}{\partial \varepsilon} \, . \tag{53}$$

It can be interpreted also as a measure of the EoS stiffness, with a higher speed generating a higher pressure at given energy density and, therefore, sustaining a bigger star mass for a given radius. Results for the speed of sound are shown in Fig. 9, where one can notice the kinks due the different particle onsets. If only nucleonic matter is allowed in the N composition, quite high Fermi levels must be occupied. With the

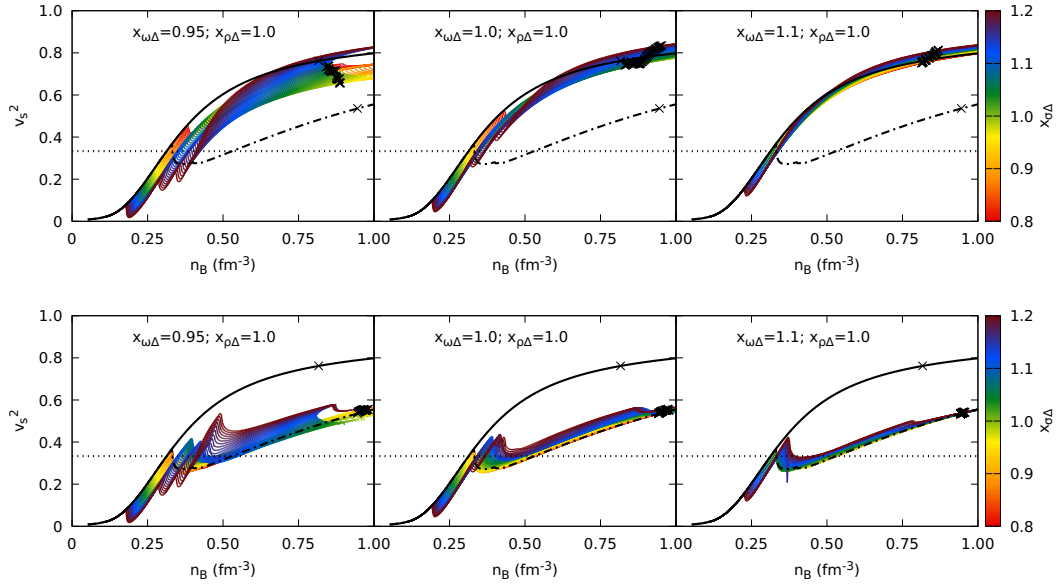

Figure 9 – Speed of sound squared as a function of the density for the DDME2 model, taking $x_{\rho\Delta} = 1.0$, for some choices of $x_{\omega\Delta}$ and varying the $x_{\sigma\Delta}$ parameter for the NΔ matter composition (top panels) and NHΔ matter composition (bottom panels). The solid and dotted-dashed black lines represent the N and NH compositions, respectively, and black crosses indicate the central values of the maximum mass star if this configuration is reached. The dotted line represents the conformal limit $v_s^2 = 1/3$.

inclusion of new particles, the presence of more degrees of freedom, distributes the Fermi pressure among the different particles and softnens the EoS. It holds true in the intermediate densities (for $n_B < 0.50$ fm^{-3}) for the NΔ composition, and always after the hyperon onset in the NH and NHΔ compositions. The behavior of hyperonic neutron-star matter, however, is affected in a more complicated way by the inclusion of delta baryons. The NHΔ composition is softer than the NH case at lower densities, but this situation is reversed at the middle regions. This is due to the strong coupling of the deltas to the ω-meson. For the same reason at high densities NΔ matter has a larger speed of sound that N matter. This difference then is reduced in the higher densities once again.

Perturbative QCD results for very high densities (more than 40 times the nuclear saturation density) predict an upper limit of $v_s^2 = 1/3$ [5]. In such high densities, far beyond the ones reached in the neutron star interiors, the baryonic matter is expected to be deconfined in quark matter. However, several authors have discussed that the two solar mass constraint requires a speed of sound well above the conformal limit, indicating that matter inside NS is a strongly interacting system [4, 131, 177, 154]. Nevertheless, within the description undertaken in [5], it was shown that the size of the quark core in hybrid stars is related to the speed of the sound of the quark matter, and very massive quark matter cores are expected in the NS interiors if the conformal limit

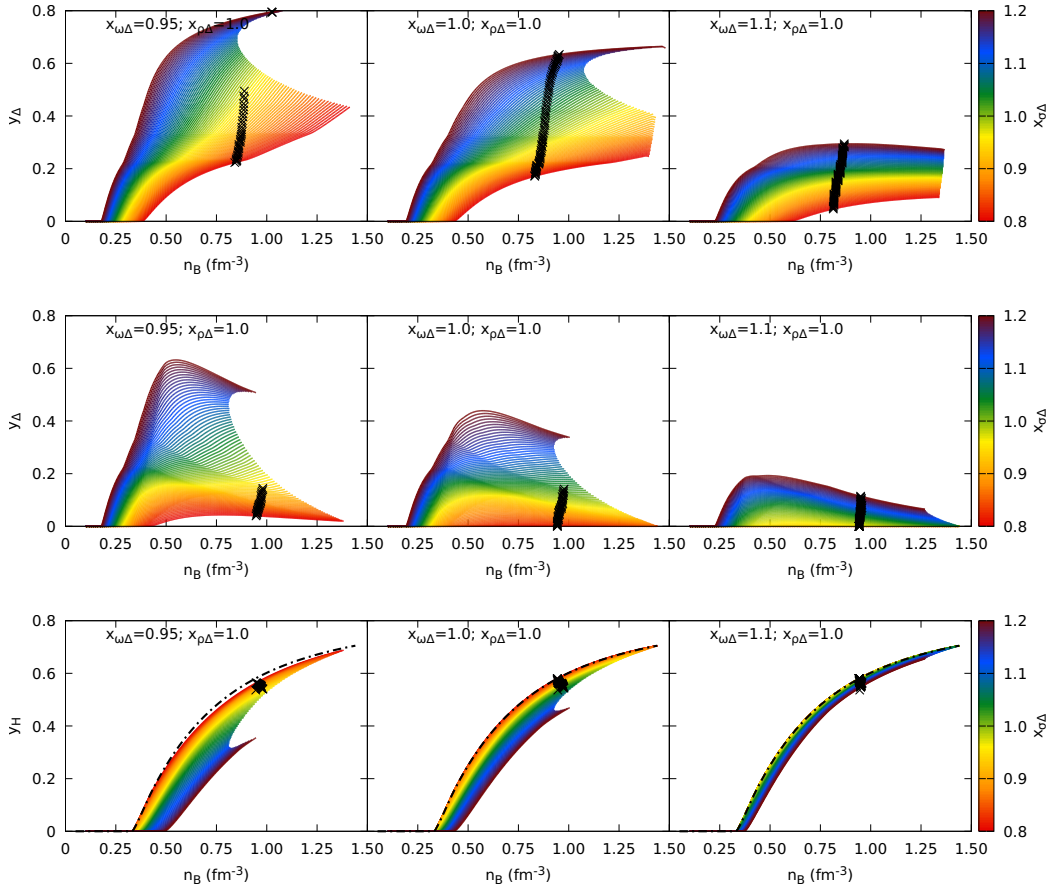

Figure 10 – Delta fraction for the DDME2 model, for the NΔ matter composition (top panels) and for NHΔ matter composition (middle panels), and hyperon fraction for NHΔ matter (bottom panels) as a function of the density, taking $x_{\rho\Delta} = 1.0$, for some choices of $x_{\omega\Delta}$ and varying the $x_{\sigma\Delta}$ parameter . Black crosses indicate the central values of the maximum mass star if this configuration is reached.

is not strongly violated. As shown in Fig. 9, the onset of hyperons and deltas breaks the monotonic behaviour of v_s^2, reducing the speed of sound, but the conformal limit is always violated due to the fact that we are describing hadronic (and not deconfined quark) matter. The speed of sound behavior, showing a sudden decrease, is similar to the one found in other works when new degrees of freedom set in, such as the onset of hyperons in [110] or of *s*-quarks in [56].

The relative populations of each kind of baryon are shown in Fig. 10, where we have defined the particle fractions as $y_i = \sum_b n_b/n_B$, with $i = \{H,\Delta\}$ meaning that the summation runs only over the hyperons or deltas, respectively. Very large delta fractions are expected for the larger values of $x_{\sigma\Delta}$, the effect being quite drastic if the $x_{\omega\Delta} < 1$. In this case many EoS do no attain the maximum star mass and are considered invalid. In the presence of hyperons the condition of attaining the maximum mass configuration is stronger, because the nucleon effective mass goes to zero too soon. Taking $x_{\omega\Delta} > 1$ these difficulties cease to occur. The hyperon fractions are also shown in Fig. 10 bottom

panels. As expected larger $x_{\sigma\Delta}$ couplings, which favor the appearance of deltas will disfavor the appearance of hyperons. This completes the conclusion drawn from Fig. 10 middle panels where it is seen that for stars with both deltas and hyperons, large delta contents do not reach the maximum mass configuration. We also conclude that for models that are able to attain the maximum mass configuration identified by the cross, the hyperon fraction at the center of the star is of the order of 50% and the delta fraction is below 20%. In the presence of hyperons, the maximum delta fraction is attained for densities between $2\rho_0$ and $3\rho_0$ and takes values below 30%. Although the delta baryons set in first, they are replaced by hyperons at high densities because the coupling of the delta baryons to the *omega*-meson is stronger.

Looking for, e.g., the upper-mid panel of Fig. 6, we identify an isolated configuration where the EoS reaches the maximum mass with a very large $x_{\sigma\Delta}$. From the respective left panel of Fig. 10, is it possible to see that this configuration is composed of around 80% of delta baryons, considering all isospin projections together. It explains why the nucleon effective mass reverts to the asymptotic behavior in order to allow the description or higher densities (see the left panel of Fig. 8). These results suggest that compact stars might exist in some hyperon free delta-dominated composition, that we label *deltic stars*.

The bottom row of Fig. 6 allows us to see a rather unexpected behavior. For these choices of $x_{\omega\Delta}$ and $x_{\rho\Delta}$, the maximum masses increase with $x_{\sigma\Delta}$, i.e., with a greater fraction of deltas (see Fig. 10). It may be considered counter intuitive since, taking as example the hyperon puzzle [27], the inclusion of more particles involves more degrees of freedom, lowers the Fermi levels. Following this reasoning, it is expected that the admixture of deltas in hypernuclear matter would make the EoS softer, but it is not always the case. In Walecka-type relativistic models (a category in which we include the DDME2 and other density-dependent parameterizations in), the attractive σ field grows rapidly until about 3 times the saturation density, but then shows a softer dependence on n_B at higher densities. On the other hand, the repulsive ω field grows indefinitely in a linear fashion and, then, becomes dominant in the denser regions. There are more deltas in the matter composition for larger σ-delta couplings, and, since the ω-delta coupling is always taken to be much greater than the ω-hyperon coupling (that is not greater than $\sim 2/3 g_\omega$), configurations where deltas are more abundant will have a stronger repulsion than scenarios that only consider the NH composition, resulting in a stiffer EoS and a higher maximum mass.

The effect of the meson-delta couplings on the maximum stellar mass is illustrated in Fig. 11. We note that, for a fixed $x_{\omega\Delta}$, increasing the parameter $x_{\sigma\Delta}$ will always produce a more massive star. When the parameter $x_{\sigma\Delta}$ is fixed, the maximum mass will reduce slightly for greater $x_{\omega\Delta}$. The main factor in play here is the balance between the relative fractions of hyperons and deltas: a larger $x_{\sigma\Delta}$ favors larger delta fractions. The

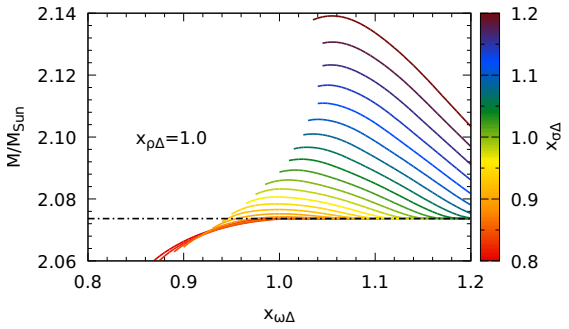

Figure 11 – Maximum stellar mass as a function of the $x_{\omega\Delta}$ coupling for the DDME2 model, taking $x_{\rho\Delta}$ = 1.0, varying the $x_{\sigma\Delta}$ parameter for the NHΔ matter composition. The dotted-dashed black horizontal line represents NH composition maximum mass (M = 2.07 M_{Sun}), and the curves are plotted only for values where the maximum mass star configuration is reached.

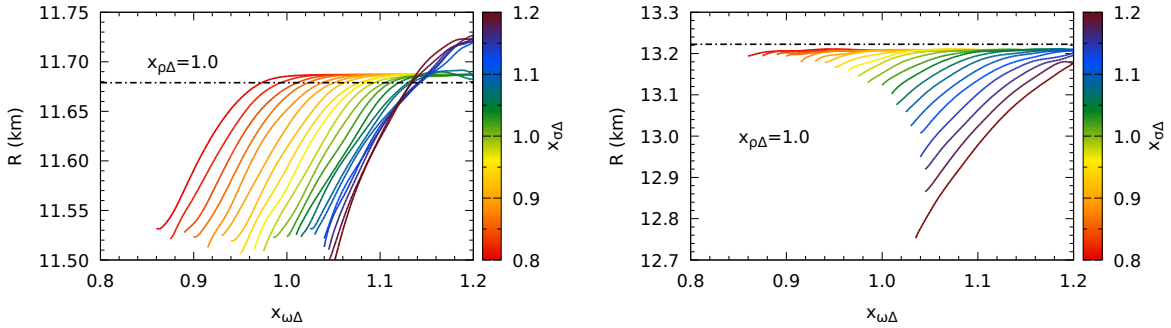

Figure 12 – Radii of the maximum mass (left) and canonical (right) stars as a function of the $x_{\omega\Delta}$ coupling for the DDME2 model, taking $x_{\rho\Delta}$ = 1.0, varying the $x_{\sigma\Delta}$ parameter for the NHΔ matter composition. The dotted-dashed black horizontal line represents NH composition radius (R = 11.67 km and R = 13.22 km, respectively), and the curves are plotted only for values where the maximum mass star configuration is reached.

deltas couple more strongly to the omega fields. Even though, stronger sigma-meson couplings are involved, the omega field dominance at large densities results in a stiffening of the EoS, and, therefore, larger masses. In [104], a similar conclusion was drawn, although the maximum mass was obtained for $1.1 < x_{\omega\Delta} < 1.2$, and smaller maximum masses are obtained. This difference is probably occurring because a different hyperon interaction was considered. Notice, however, that we do not consider $x_{\omega\Delta} > 1.2$ and that with our parametrization we do not get maximum mass configurations for $x_{\sigma\Delta} - x_{\omega\Delta} \gtrsim 0.1$.

In Fig. 12, we perform a similar study for the radius of the maximum mass star (left panel) and radius of the 1.4 $M_\odot$ star (right panel). For $x_{\rho\Delta}$ = 1.0, the presence of Δs may reduce the maximum mass radius in 100-150 m, 11.5 km being the minimum, and the 1.4 $M_\odot$ star radius in 20-500 m, with a minimum of 12.7 km. Only models that attain maximum mass configurations are represented in Fig. 11 and 12. In [104] smaller

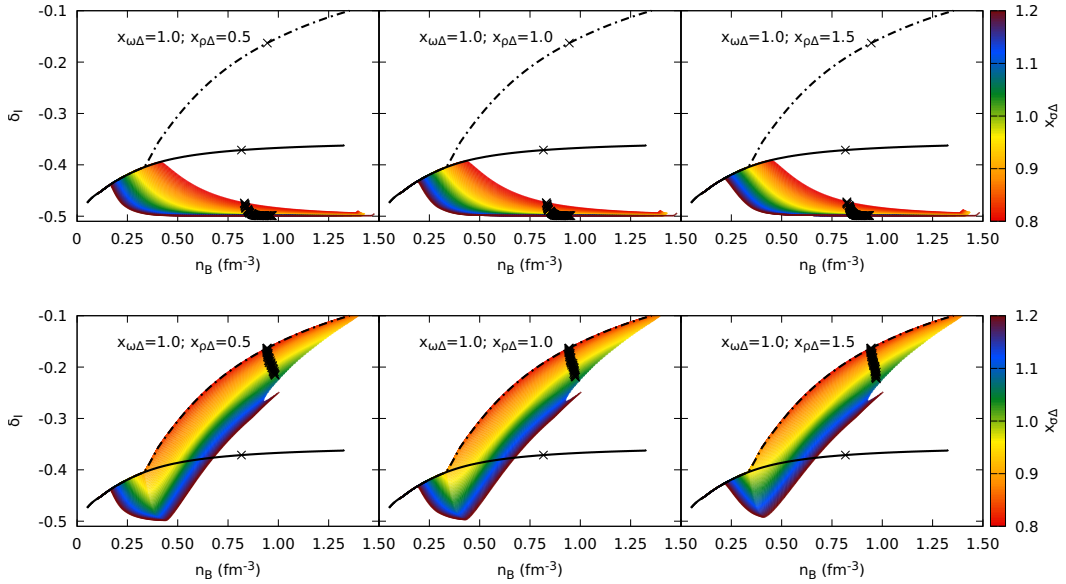

Figure 13 – Isospin asymmetry coefficient Eq. (54) as a function of the density for the DDME2 model, taking $x_{\rho\Delta} = 1.0$, for some choices of $x_{\omega\Delta}$ and varying the $x_{\sigma\Delta}$ parameter for the NΔ matter composition (top panels) and for NHΔ matter composition (bottom panels). The solid and dotted-dashed black lines represent the N and NH compositions, respectively.

radii are obtained, and the presence of Δs may give rise to a reduction of the radius of the canonical star of up to $\approx$ 2 km. However, it is not clear if the authors exclude models that do not attain the maximum mass. In [156], the authors have obtained, with FSU2H, effects of the order of the ones discussed in the present work with DDME2. From Fig. 6 and 12, it is seen that the presence of Δs (induced by larger values of $x_{\sigma\Delta}$) cause a significant decrease in the radius of the stars with intermediate masses. This is explained by the fact that the appearance of the deltas softens the EoS in the intermediate density region, as clearly seen in the top panels of Fig. 9, the star matter is further compressed and consequently its radius reduces [156].

The stiffening of the EoS due to the delta admixture, was also noticed in Ref. [45], where it was suggested that it occurs due to the isospin asymmetry. At high densities, however, the delta admixture makes the EoS stiffer, despite the fact that the new degrees of freedom tend to soften the EoS. This was first noticed in Ref. [45], where it was suggested that it occurs due to the isospin asymmetry. We define the coefficient

$$\delta_I = \frac{\sum_b I_{3\,b} n_b}{\sum_b n_b} \,, \tag{54}$$

that represents the average 3$^{\text{rd}}$ isospin component of a given matter composition, weighted by each particle relative density, as shown in Fig. 13. The density at which the curves with and without Δs split marks the appearance of the Δ^- baryon, which turns the isospin asymmetry more negative and, consequently, makes the EoS stiffer. It happens

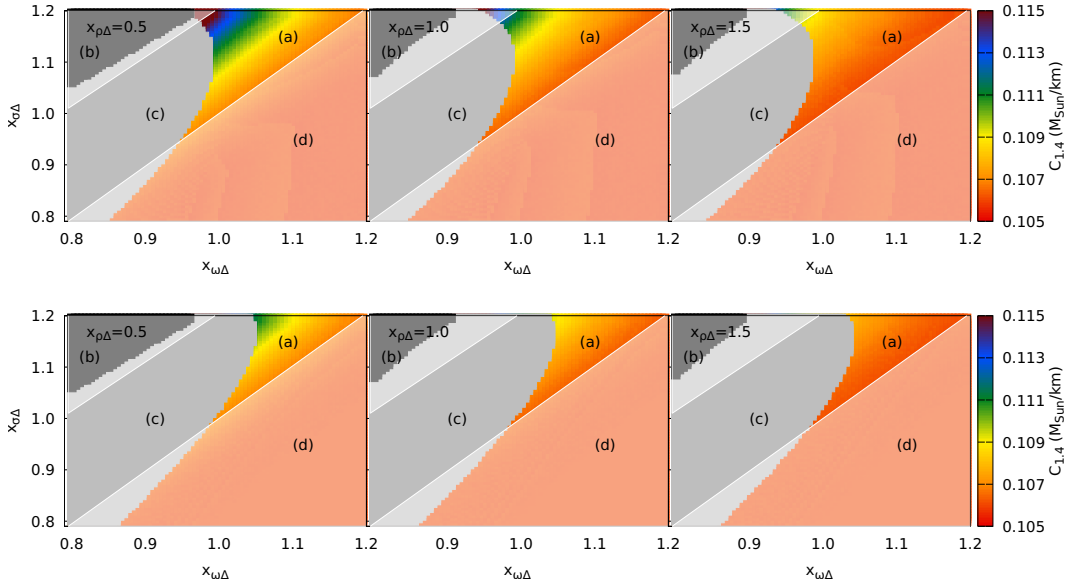

Figure 14 – Constraints on meson-delta couplings for the DDME2 model, for the NΔ matter composition (top panels) and for the NHΔ matter composition (bottom panels). The color gradient (a) indicates the compactness of the canonical star. The black region (b) represents values for which $\frac{dP}{d\varepsilon} < 0$ before $n_B = 0.2$ fm^{-3}. The gray region (c) represents values where the maximum mass star configuration is not reached when inputting the EoS in the TOV equations. The white-shaded region (d) indicates the combinations of parameters that do not fulfill the constraint given by Eq. (34) [193].

earlier for larger $x_{\sigma\Delta}$ couplings, as this is the determinant parameter to favor the onset of the deltas. For the NΔ composition (top panels of Fig. 13), the isospin asymmetry coefficient tends to more negative values as the density increase, because the matter turns to be dominated by the Δ^-. This tendency is stronger for smaller $x_{\omega\Delta}$ couplings, as a strong ω coupling does not favor delta populations at higher densities. However, when the NHΔ composition is considered (bottom panels of Fig. 13), the isospin asymmetry coefficient becomes less negative once the hyperon threshold is reached and follows the NH composition behavior after that, becoming less negative as the matter is more dominated by the hyperons. Nevertheless, the configurations with relatively more deltas present (i.e., bigger $x_{\sigma\Delta}$, drawn in indigo blue in the plots) show more negative values of δ_I.

In Fig. 14, we summarize the constraints on the values of the couplings that ensure the existence of neutron stars compatible with the stability criteria and with the observational results. For three values of the coupling $x_{\rho\Delta}$ (0.5, 1 and 1.5), the compactness of a 1.4 $M_\odot$ star is plotted versus the $x_{\sigma\Delta}$ and $x_{\omega\Delta}$. The color gradient indicates the compactness, defined as $C_M = M/R$, of the canonical ($M = 1.4$ $M_\odot$) star. The compactness of the isolated neutron star RX J0720.4-3125 is inferred to be $C = 0.105 \pm 0.002$ M_{Sun}/km [78], which gives us an additional parameter for analysis,

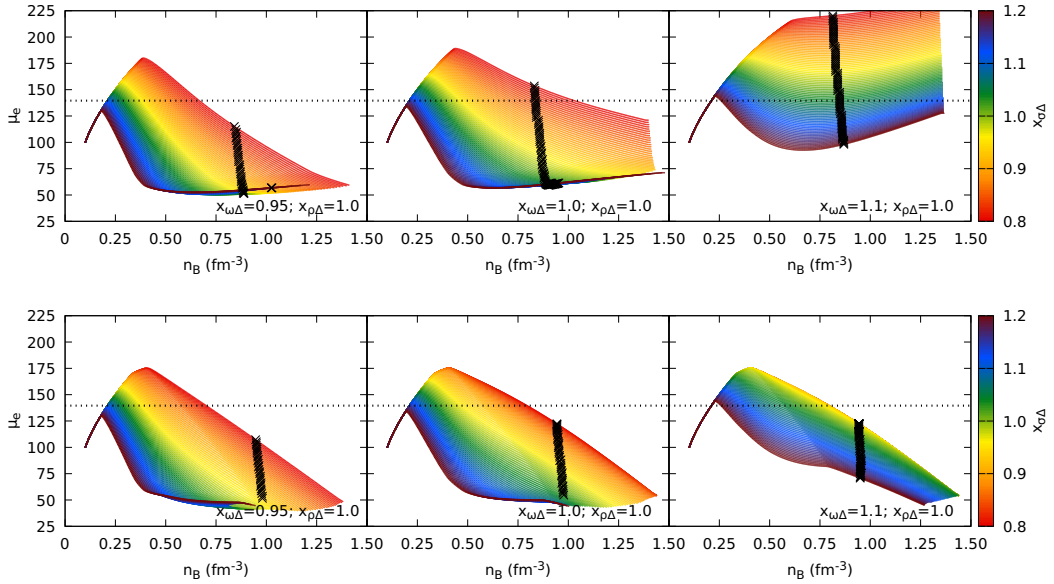

Figure 15 – Difference between the delta and the neutron chemical potentials as a function of the density for the DDME2 model, for NΔ (top pannels) or NHΔ (bottom panels) matter composition. The dashed line represents the vacuum π-meson mass.

specially focused on the less massive star radii. From the figures, we see the effect of $x_{\rho\Delta}$ in making the canonical star less compact as the parameter increases, improving the agreement with this constraint. The black region on the upper-left corner represents values for which $dP/d\varepsilon < 0$ before $n_B = 0.2$ fm^{-3}, meaning that the thermodynamic stability condition is not satisfied at quite low densities, when it would not be expected. The gray region represents values where the maximum mass star configuration is not reached because the effective nucleon mass goes to zero. Note that all configurations approved by these two criteria fulfill the observational constraints shown in Fig. 6. The white-shaded region indicates the combinations of parameters that do not fulfill the constraint given by Eq. (34) [193]. The remaining points correspond to meson-delta couplings that satisfy all constraints. Comparing with the coupling domain obtained in [156], a larger domain was obtained, indicating that solutions with $x_{\omega\Delta>1.0}$ and $x_{\sigma\Delta} > 1.0$ are possible. The difference are essentially connected with the model: DDME2 allows for a larger parameter domain for which the effective mass does no go to zero before the maximum mass configuration is attained. For a large enough $x_{\rho\Delta}$, the constraint $C = 0.105 \pm 0.002$ M$_{\rm Sun}$/km is satisfied for $x_{\sigma\Delta}$ and $x_{\omega\Delta}$ larger than one. A smaller value of $x_{\rho\Delta}$, e.g. 0.5 in the left panel, is more constraining with respect to the combination $x_{\sigma\Delta}$-$x_{\omega\Delta}$ and does not allow for large values of $x_{\sigma\Delta}$.

In the present work, we have considered that the delta baryons are stable in stellar matter as done in many other works. This may be justified because the possible final states for the decay of the delta to occur are blocked. The stability of this matter must be checked, because the relatively low nucleon fractions could imply that their

higher Fermi levels may not be occupied to block the delta decay. Generally, in vacuum the delta $\Delta = \{\Delta^{++},\Delta^{+},\Delta^{0},\Delta^{-}\}$ quickly decay via the strong force into a nucleon $N = \{p,n\}$ and a pion of appropriate charge,

$$\Delta \longrightarrow N + \pi,$$

so the difference between the delta and the nucleon (effective) chemical potentials should be less than the pion energy in the medium. Just for reference, we show in Fig. 15 the electron chemical potential (i.e., the difference between the Δ and the nucleon (effective) chemical potentials), and indicate the vacuum pion mass with a dotted line, m_{π} = 139.5 MeV. If final states are not Pauli blocked, the Δ^{-} could decay into a neutron and a π^{-}, which in beta equilibrium would have a chemical potential equal to the electron chemical potential. In several scenarios the electron chemical potential is larger than the pion vacuum mass. This would indicate that indeed the pion condensate would be favorable. However, in Refs. [65, 136], the authors showed that the repulsive s-wave pion-nucleon interaction does not favor pion condensation because, in the medium, the pion energy is above its vacuum mass.

3 DELTA BARYONS IN MAGNETARS

Magnetars are a class of compact objects that possess the largest stable magnetic fields observed in nature, with surface magnitudes inferred for the poloidal component in the range of $10^{11} - 10^{15}$ G at the surface [77] and values more than one order of magnitude larger in the interior [38]. Although the strength of the magnetic field in the central region of these stars remains unknown, they could reach $\sim 10^{18}$ G according to the scalar virial theorem [100], and simultaneous solutions of Einstein and Maxwells equations for poloidal and also toroidal configurations [183]. Such extreme conditions certainly play a considerable role when determining the internal composition and macroscopic structure of magnetars.

Additionally, it is of special interest to investigate how spin-3/2 baryons are affected by the presence of strong magnetic fields due to the possibility of them having large electric charge and additional spin and isospin projections. The effects of Landau levels in dense stellar matter containing Δ baryons was first discussed in the context of neutron-star matter by [178] and later by [45]. In this work we study for the first time the effects of strong magnetic fields in Δ-admixed hypernuclear stellar matter, accounting also for effects due to their anomalous magnetic moments (AMMs).

For magnetic fields larger than $\sim 10^{16}$ G, the deformation of the stellar geometry away from spherical symmetry is above 2% [69]. Therefore, the usual relativistic hydrostatic equations usually employed when describing non-magnetised stars, i.e., the Tolman-Oppenheimer-Volkoff equations, which assume spherical symmetry as part of their derivation from the general relativity equations, cease to be adequate. For this reason, we then make use of anisotropic solutions from the Einstein and Maxwell equations to explore for the first time the macroscopic structure of magnetars with strong internal magnetic fields and containing Δ-admixed hypernuclear matter.

3.1 MATTER COMPOSITION UNDER EXTREME MAGNECTIC FIELDS

To consider the effects of an external magnetic field B on fermions, we modify the calculation of thermodynamic quantities of each particle species with non-zero electric charge q, at zero temperature, according to the rule

$$\int d^3k \rightarrow \frac{|q|B}{(2\pi)^2} \sum_{\nu} \int dk_z, \tag{55}$$

where k is the momentum, z is the direction of the magnetic field and the sum in ν, the discretized orbital angular momentum that the charged particle acquires in the plane transverse to B, goes until a maximum (integer) corresponding Landau level for which its momentum is still real, i.e.,

$$\nu \leq \nu_{\max} = \left\lfloor \frac{\bar{E}^2 - \bar{m}^2}{2|q|B} \right\rfloor, \tag{56}$$

where the relation

$$\nu = n + \frac{1}{2} - \frac{s}{2}\frac{q_b}{|q_b|} , \tag{57}$$

depends on spin and electric charge. The number of Landau levels occupied by particles increases with density and temperature, but decreases with the magnetic field strength, as seen in Ref. [6]. In the cases we study in this work, the number of Landau levels goes from zero or 1 at low densities to a number ≤ 5 (for the proton) at large densities, corresponding to the center of the neutron stars.

The anomalous magnetic moment (AMM) of a particle is a deviation from the magnetic moment of that particle, as predicted by the "classical" tree-level prediction. Historically, the term *anomalous* was used to describe the deviation from the Dirac equation prediction for a system of fermions under the influence of a magnetic field, the magnetic moment, and thus, refers to fundamental particles. *Dipole* moment, on the other hand, is used for composite particles, such as baryons, since their value depends on the configuration of quarks and gluons inside it, and thus, are not *anomalous* in the strict sense. As commonly used in the literature and for simplicity, in this work we use the term AMM in all cases.

The energy spectrum of baryons with an AMM can be empirically determined, but a theoretical derivation of their values from first principles is yet an unaccomplished task. The AMMs of nucleons are measured to a very high precision, with errors of the order of 10^{-9} [166], but the same does not apply to heavier baryons. Measurements of the hyperon AMMs are precise to an order of 10^{-2} [82], while Δs are experimentally determined only for the positively charged Δ^{++} and Δ^{+}. For the Δ^{+}, there is a single measurement of $\mu_{\Delta^+}/\mu_N = 2.7^{+1.0}_{-1.3} \pm 1.5$ that comes from the $\gamma p \to p\pi\gamma'$ reaction, while for the Δ^{++} there are several measurements coming from the $\pi^+ p \to \pi^+ p\gamma$ bremsstrahlung cross section, with values in the range $\mu_{\Delta^{++}}/\mu_N = 3.7 - 7.5$ [115]. These measurements include systematic uncertainties, but additional theoretical uncertainties lead to errors $\sim \pm 3$. Complementary to experimental results, lattice quantum chromodynamics (LQCD) has been able to extract AMM values for Δ baryons. The values utilized in this paper are based on the predictions from LQCD provided in [33] that lie within the experimental uncertainties of the experimentally measured AMMs.

Different properties of baryons considered in this study are shown in Tab. 3. The AMM strength coefficients κ_b are related to the magnetic moments μ_b through the relation

$$\kappa_b = \mu_b - q_b \mu_N \frac{M_p}{M_b} , \tag{58}$$

which depends on the baryon charge q_b, the nuclear magneton $\mu_N = e/2M_p$, with e being the electron charge, and the ratio of the proton mass M_p to the baryon mass M_b. Although the expression (58) is derived for spin-1/2 fermions in the non-relativistic regime, it is still commonly employed to the description of the spin-3/2 particles [115, 116]. This

subject is controversial, as the Rarita-Schwinger equation with minimal coupling predicts a gyromagnetic ratio of 2/3, while low energy/optical theorems predict a value of 2. For a more in-depth discussion we refer to [39], which studies a generic non-minimal electromagnetic coupling in the Rarita-Schwinger formalism. In this work, we also account for the leptons (electron and muon) AMMs, given by $\kappa_e/\mu_{B_e} = 1.15965 \times 10^{-3}$ and $\kappa_\mu/\mu_{B_\mu} = 1.16592 \times 10^{-3}$, respectively, with $\mu_{B_l} = e/2M_l$, for $l = \{e,\mu\}$.

The equations of motion for the mesonic fields are obtained from the model Lagrangian densities via the Euler-Lagrange equations. When the AMM is considered, the Fermi momentum (squared) can be calculated, in the presence of a magnetic field, from the difference between the Fermi energy (squared) and

1. the square of the effective mass modified by the AMM for particles that are not electrically charged ($q_b = 0$),

$$k_{F,b}^2(s) = {E_{F\,b}^*}^2 - \left(M_b^* - s\kappa_b B\right)^2 ; \tag{59}$$

2. the square of the effective mass modified by Landau quantization and AMM for particles that are electrically charged ($q_b \neq 0$),

$$k_{F,b}^2(\nu, s) = {E_{F\,b}^*}^2 - \left(\sqrt{M_b^{*2} + 2\nu|q_b|B} - s\kappa_b B\right)^2 . \tag{60}$$

For the momentum of leptons, M^* is simply M. In the latter case, the Fermi momentum refers to the local direction of the magnetic field, hereafter defined as the z-axis. In the transverse direction to the local magnetic field, the Fermi momentum is restricted to discrete values $2\nu|q_b|B$, where the Landau levels ν relate to the orbital angular momentum n via the relation (57).

The degeneracy of each particle λ_ν at $B = 0$ takes into account spin and/or number of colors ($\lambda_\nu = 2$ for the spin-1/2 baryons and leptons, $\lambda_\nu = 4$ for the spin-3/2 baryons, and $\lambda_\nu = 6$ for quarks; note that $\lambda_{\nu=0}$, the degeneracy of the zeroth Landau level, is always half of the usual value), but the presence of a magnetic field breaks the spin degeneracy. For particles with spin 1/2, the first Landau level ($\nu = 0$) is occupied by a single spin projection: $s = +1$ for $q_b > 0$ and $s = -1$ for $q_b < 0$. The second level ($\nu = 1$) and above are occupied by both spin projections $s = \{\pm 1\}$. For the spin-3/2 positively charged Δs, the first level ($\nu = 0$) is occupied by the spin projections s= {+3, +1}, the second level ($\nu = 1$) by $s = \{+3, \pm 1\}$, and hereafter all spin states are occupied. For the negatively charged Δ^- spin projection, signs are reversed for the lowest levels.

When the AMMs are considered, the number density for each baryon is also

defined separately for electrically charged and uncharged particles, respectively,

$$n_b^{(q_b\neq 0)} = \frac{|q_b|B}{2\pi^2}\sum_{\nu,s} k_{Fb}(\nu,s)\ ; \tag{61}$$

$$n_b^{(q_b=0)} = \bar{\psi}_b\psi_b = \frac{1}{2\pi^2}\sum_s \left\{ \frac{k_{Fb}^3(s)}{3} - \frac{s\kappa_b B}{2}\left[\left(M_b^* - s\kappa_b B\right) k_{Fb}(s) + E_{Fb}^{*2}\left(\arcsin\left(\frac{M_b^* - s\kappa_b B}{E_{Fb}^*}\right) - \frac{\pi}{2}\right)\right]\right\}\ , \tag{62}$$

as well as the scalar densities,

$$n_{sb}^{(q_b\neq 0)} = \bar{\psi}_b\gamma_0\psi_b = \frac{|q_b|BM_b^*}{2\pi^2}\sum_{s,\nu}\frac{\sqrt{M_b^{*2}+2\nu|q_b|B}-s\kappa_b B}{\sqrt{M_b^{*2}+2\nu|q_b|B}} \times \ln\left|\frac{k_{Fb}(\nu,s)+E_{Fb}^*}{\sqrt{M_b^{*2}+2\nu|q_b|B}-s\kappa_b B}\right|\ ; \tag{63}$$

$$n_{sb}^{(q_b=0)} = \frac{M_b^*}{4\pi^2}\sum_s\left[E_{Fb}^* k_{Fb}(s) - \left(M_b^* - s\kappa_b B\right)^2 \ln\left|\frac{k_{Fb}(s)+E_{Fb}^*}{M_b^* - s\kappa_b B}\right|\right]. \tag{64}$$

A complete list of thermodynamic quantities for magnetized fermions at both finite and zero temperature is given in Ref. [40]. For non-charged particle, the pressure and energy density expressions take the usual form. In what follows, we consider that the strength of the magnetic field B is a fixed quantity in the equation of state (EoS). We refer to Refs. [148] for a more detailed discussion of the formalism involved in the description of strong magnetic field effects on the equation of state of models with interactions.

In a first moment, we disregard the AMM effects in order to study the effects of the Δ coupling scheme in magnetized neutron star matter. Here we define the notation $\beta = x_{\sigma\Delta}$. The effects of the scalar-Δ coupling are shown in Figs. 16 and 17, when comparing the top ($\beta = 1.0$) and bottom ($\beta = 1.1$) panels. The increase of this interaction changes the overall Δ-particle threshold to lower densities, while it pushes the hyperon threshold to higher densities. This effect is more pronounced when the $\omega\rho$ interaction and $\beta = 1.1$ are used (bottom panel of Fig. 17). In this case, the Λ's are the only hyperons present, while the four Δ species appear at relatively low densities. The amount of leptons is reduced significantly. For comparison, see Fig. 18 for a more extreme scenario in which the hyperons were artificially suppressed. In this case, as expected, there is an even larger amount of different Δ species at a given density.

Concerning our choice of values for the parameter β, they cover the meaningful range that switches from having many hyperons to having many spin 3/2 baryons. While lower values would completely exclude the Δ's from our density range, a larger value would completely exclude the hyperons. As seen when comparing both panels of Fig.

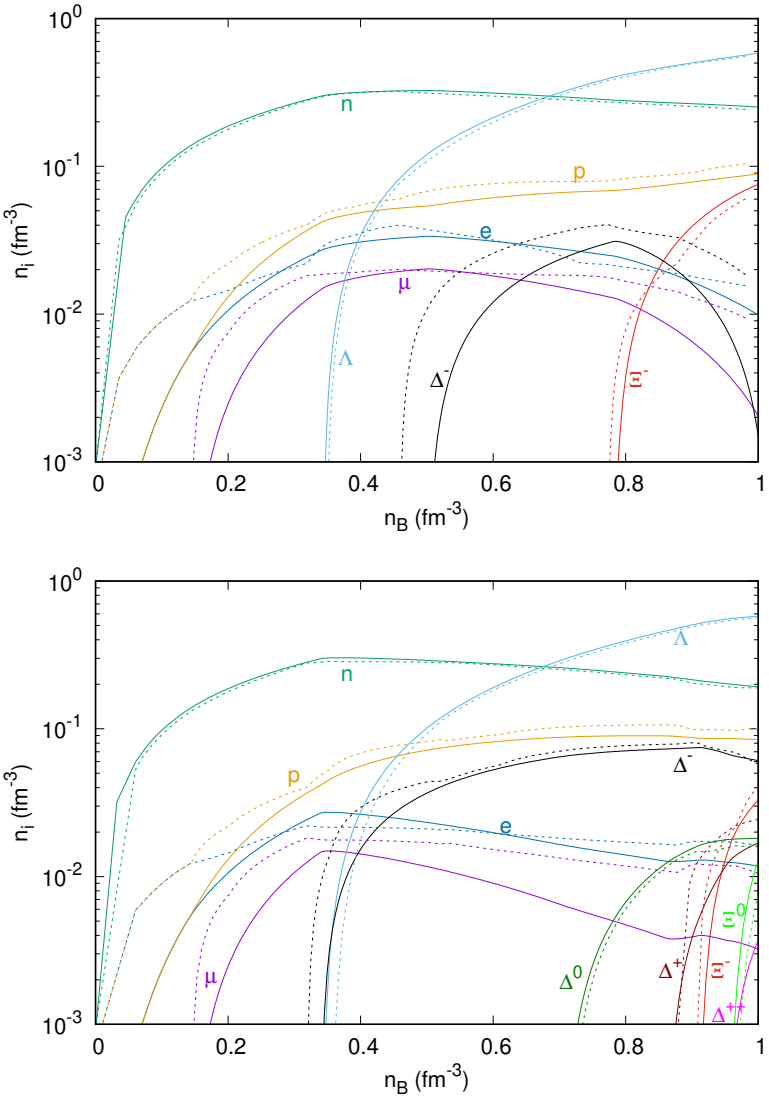

Figure 16 – Particle population for the RMF model with GM1, β = 1.0 parametrization (top panel) and β = 1.1 parametrization (bottom panel) as a function of the baryon number density. Full lines show results without magnetic fields, while dashed lines show results including a magnetic field strength of $B = 3 \times 10^{18}$ G.

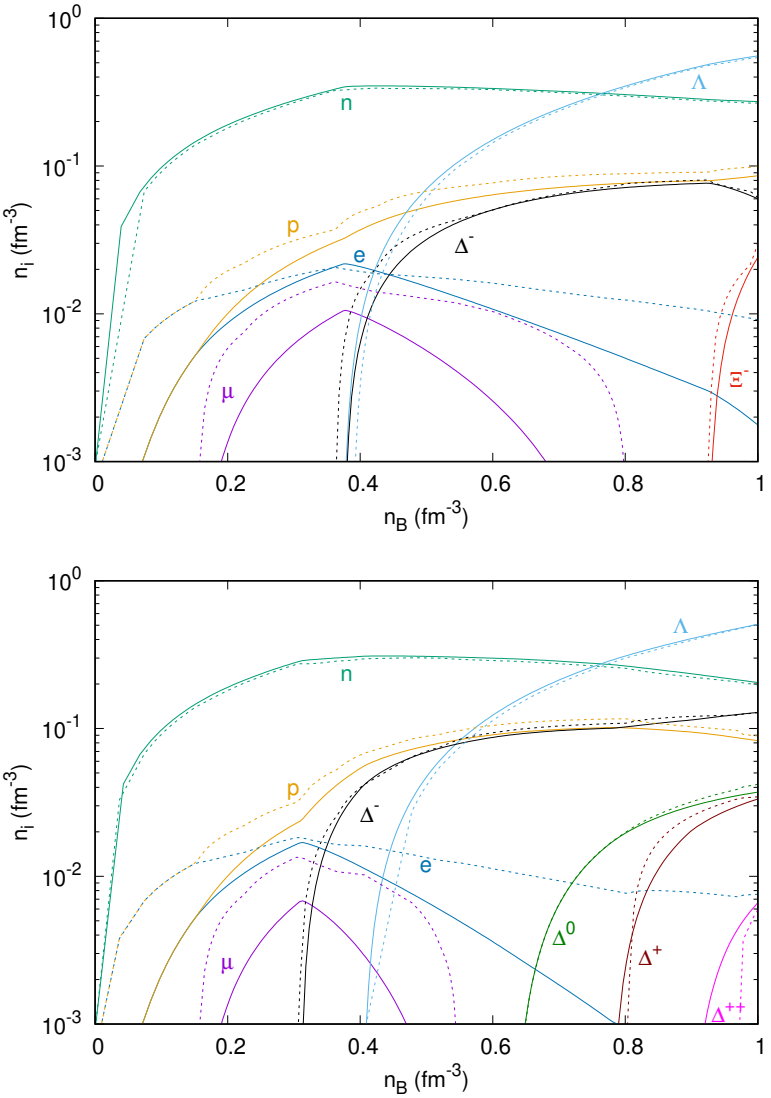

Figure 17 – The same as in Fig. 16, but using the new GM1$\omega\rho$ parametrization.

16, our choices of β are already very close to these extreme cases, in such a way that increasing or decreasing β further would not alter significantly our results. On the other hand, in the presence of the $\omega\rho$ coupling, as seen in the top panel of Fig. 17, a lower β could decrease further the amount of Δ's, producing different results.

Another interesting feature is the interplay between the Ξ^- and Δ^- relative populations. In the top panel of Fig. 16, one can see that Δ^-'s start to appear at $n_B \approx 0.5$ fm^{-3} (when the magnetic field is not considered), and their population keeps growing with density until it represents 3% of the total baryon number density $n_B \approx 0.8$ fm^{-3}. At this point, the (lighter) Ξ^-'s appear and rapidly suppress the other negative particles, dominating over the Δ^-'s soon afterwards. This dynamics is delayed in scenarios where the hyperons are not preferred, e.g., in the scenario shown at the bottom panel of Fig. 17, where the Δ's show a fast uninterrupted increase with density. This characteristic fast increase occurs for all Δ baryons when the hyperons are fully suppressed (see Fig. 18).

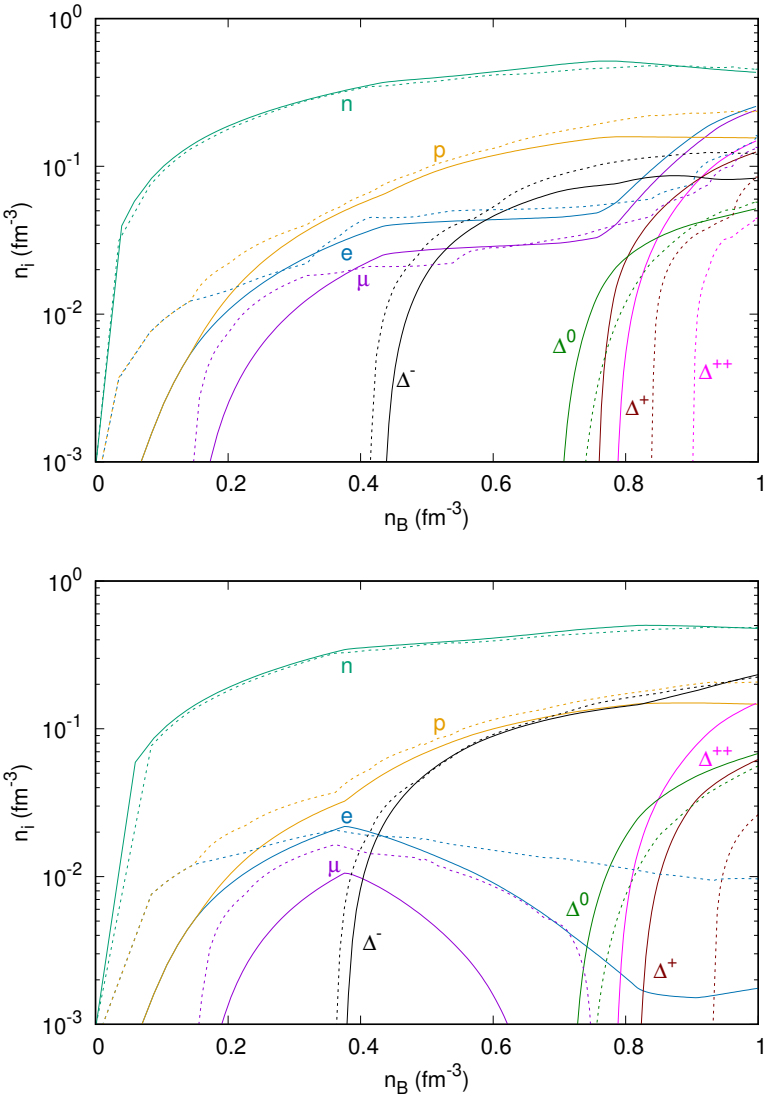

Figure 18 – Particle population for the RMF model with GM1 parametrization (top panel) and GM1$\omega\rho$ parametrization (bottom panel), suppressing the hyperons and taking $\beta = 1.0$. Once more, full lines show results without magnetic fields, while dashed lines show results including a magnetic field strength of $B = 3 \times 10^{18}$ G.

Magnetic field effects on the particle populations are shown using dashed lines in Figs. 16-18. We find that the magnetic field produces a significant enhancement in the amount of most charged particles, including protons, electrons, muons, Σ^-'s, and Δ^-'s, but an overall suppression of Δ^+'s and Δ^{++}'s when they are present. The latter is related to the increased amount of protons. In the cases in which hyperons are not present, the magnetic field induces a more significant change in the Δ population, as shown in Fig. 18. The cusps in the dashed curves correspond to threshold crossings for the maximum Landau levels, known as van Alphen oscillations [76]. In these figures, a constant magnetic field of magnitude $B = 3 \times 10^{18}$ G was chosen. This corresponds to about the largest magnetic field strength that can be reached in the center of magnetars, as predicted by numerical calculations that solve Einstein's and Maxwell's equations for a pure poloidal configuration. In reality, the magnetic field is not constant within neutron stars, but was found to increase with density by less than one order of magnitude when solving Einstein's and Maxwell's equations for a pure poloidal configuration [46].

In order to enrich and generalize our results, we repeat some of our analysis for a second relativistic hadronic model, the CMF, already presented in the previous chapter. In Fig. 19, we show for the first time the introduction of the ω^4 interaction in the population of pure hadronic matter (with coupling constant –4.7), and with additional baryons from the decuplet Δ's, Σ^*'s, Ξ^*'s, and Ω's. Note that in Ref. [45] a phase transition to quark matter suppressed most of the hyperons. Here, although we include the whole baryon decuplet, only the Δ's appear in the relevant regime.

The difference between the two panels in Fig. 19 is only due to the addition of the $\omega\rho$ interaction (with normalized coupling constant 0 on the left panel and 62 in the right panel). This interaction generates matter with a more soft symmetry energy beyond saturation (lower value for slope), meaning a lower energy cost to produce isospin and, therefore, a larger neutron-to-proton ratio, more Σ^-'s and Δ^-'s, but less leptons and Λ's. As a result, the Δ^-'s appear before any hyperon species. The very slow increase of Σ^-'s with density (for zero magnetic field) barely affects the Δ^- population.

Continuing our discussion with only configurations that include the $\omega\rho$ interaction, the top panel of Fig. 20 illustrates the case in which hyperons are suppressed. Note that not even in this case the other baryons from the decuplet appear in the density regime relevant for neutron stars, although a larger amount of Δ^-'s appear at large densities. As shown by the dashed lines of the figures, the magnetic field further enhances the amount of negatively charged Δ's.

For $B = 0$, the matter EoS (namely, P vs. ε) shows a simple monotonically increasing behavior, however its derivatives show interesting features generated, e.g., by changes in particle composition. Next, we discuss the incompressibility modulus

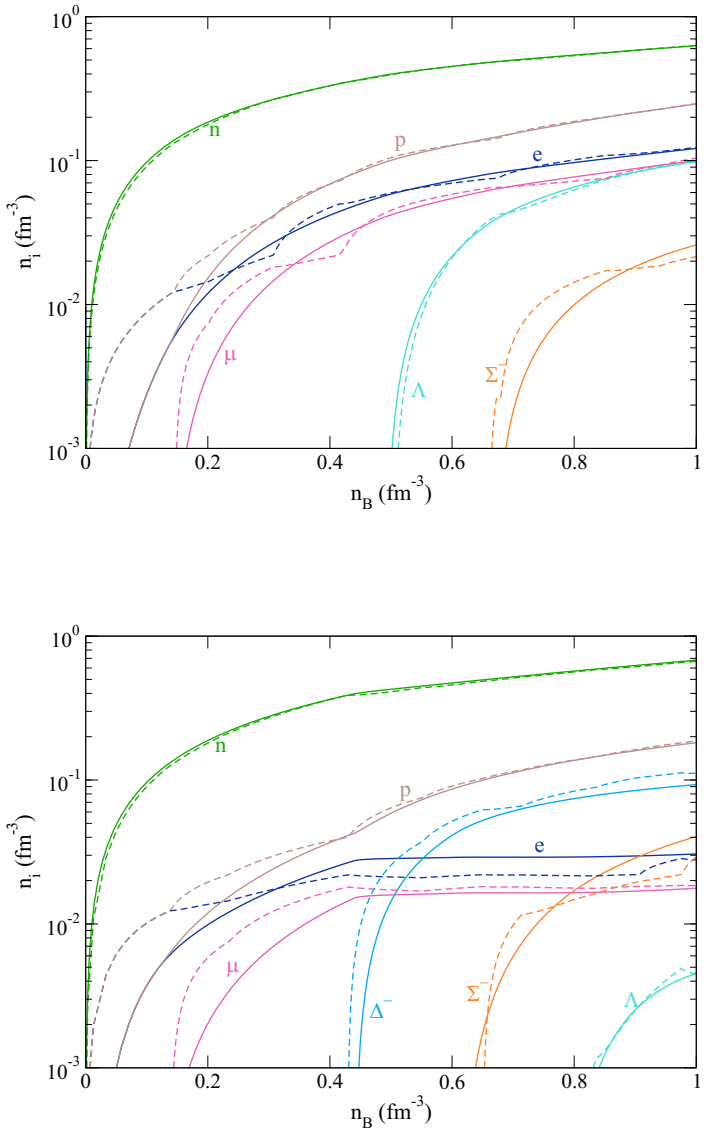

Figure 19 – Particle population for the CMF model without (top panel) and with (bottom panel) the $\omega\rho$ interaction as a function of the baryon number density. Full lines show results without magnetic fields, while dashed lines show results including a magnetic field strength of $B = 3 \times 10^{18}$ G.

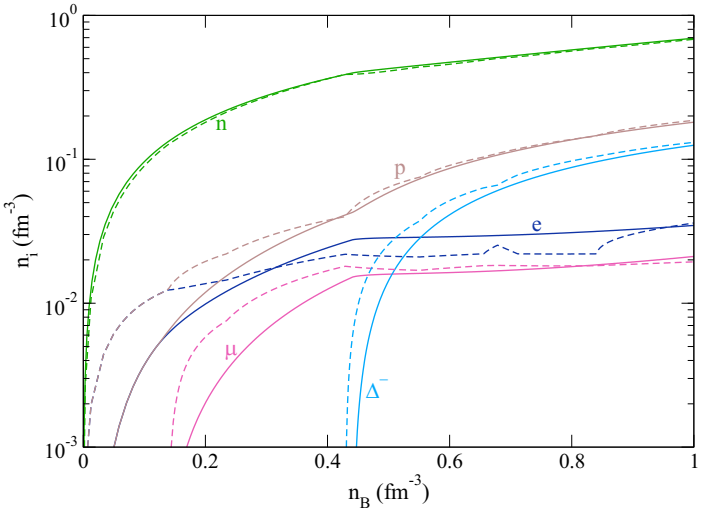

Figure 20 – Same as the bottom panel of Fig. 19, but suppressing the hyperons.

(usually referred to simply as compressibility), given by

$$K = 9\frac{\partial P}{\partial n_B} \,. \tag{65}$$

At saturation density, compressibility values for isospin-symmetric matter can be compared with laboratory data. We find values of 256 MeV and 300 MeV for the L3$\omega\rho$ and CMF models, respectively. Laboratory values range between 220 < K < 260 MeV [51, 109] and 250 < K < 315 MeV [175].

The top panel of Fig. 21 shows the effect of the inclusion of different particle species in the compressibility for the L3$\omega\rho$ model, in the absence of an external magnetic field. The kinks in the curves are consequence of the onset of new particle species, which are shifted to lower densities by the inclusion of both Δs and respective stronger scalar interactions. For $x_{\sigma\Delta} = 1$, the effective mass of nucleons becomes zero at $n_B \sim 0.85$ fm^{-3} and, for this reason we lack solutions at higher densities. The bottom panel of Fig. 21 shows that in the CMF model the kinks are much smaller than in the L3$\omega\rho$ model, with the only displacement of the curve occurring at the onset of the first non-nucleon baryon. As a consequence, the different CMF EoS behave more similarly as the density increases.

The stiffer EoS are formally the ones with larger values of the speed of sound v_s, but here we discuss stiffness with respect to K, related to v_s through $v_s^2 = K/(9\mu)$ [43]. Isospin symmetric matter is softer at low densities, but becomes stiffer at large densities due to the Pauli exclusion principle because, as only nucleonic matter is considered, higher Fermi levels must be occupied. The behavior of neutron-star matter (charge neutral and in chemical equilibrium) depends on the composition, but it is always softer than the symmetric matter case after the hyperon or Δ onsets, as the

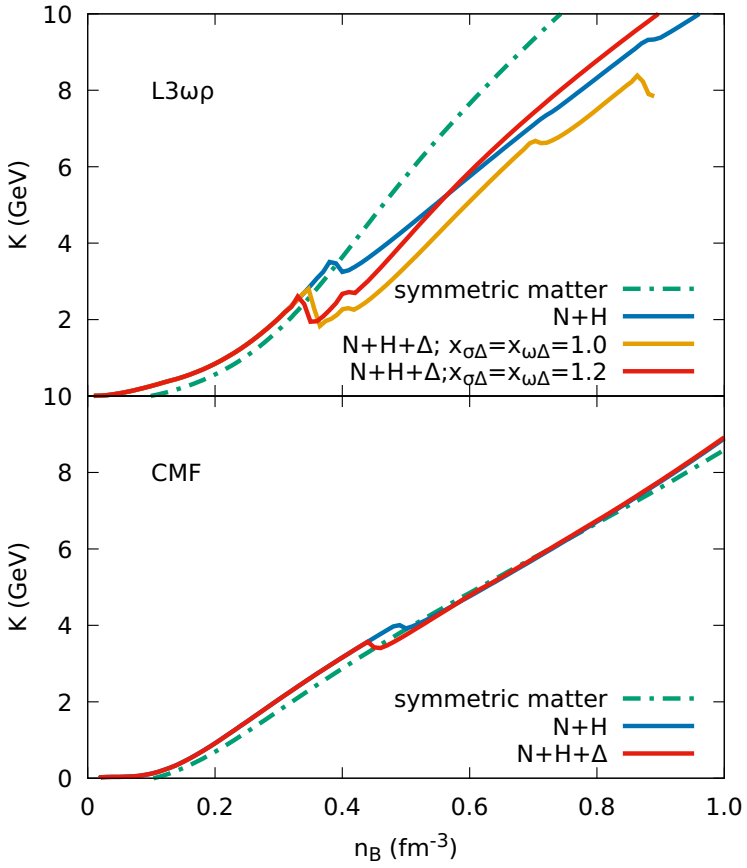

Figure 21 – Compressibility as a function of baryon number density in isospin-symmetric matter with only nucleons (dashed-dotted line) and neutron-star matter (full lines) shown for different compositions and interaction strengths for the L3$\omega\rho$ (top panel) and for the CMF model (bottom panel). $B = 0$.

presence of new Fermi levels turns the EoS softer. Matter with hyperons but no Δs is stiffer at intermediate densities (than matter with Δs), however it is softer at large densities, especially in the case of strong scalar interaction (for the L3$\omega\rho$ model). This trend was noticed previously by [45], where we showed that the inclusion of Δs could turn the EoS stiffer (than the cases where they were absent), despite the fact that the new degrees of freedom soften the EoS. This is related to isospin asymmetry, which we discuss in the following.

We define the isospin fraction as the average 3$^{\text{rd}}$ isospin component of a given matter composition, weighted by the relative densities, i.e.,

$$Y_{I_3} = \frac{\sum_b I_{3\,b} n_b}{\sum_b n_b} \,, \tag{66}$$

as shown in Fig. 22. For nucleonic matter only, $Y_{I_3} = 0$ means matter with the same amount of protons and neutrons, while $Y_{I_3} = -0.5$ means pure neutron matter. The density at which the curves with and without Δs split marks the appearance of the

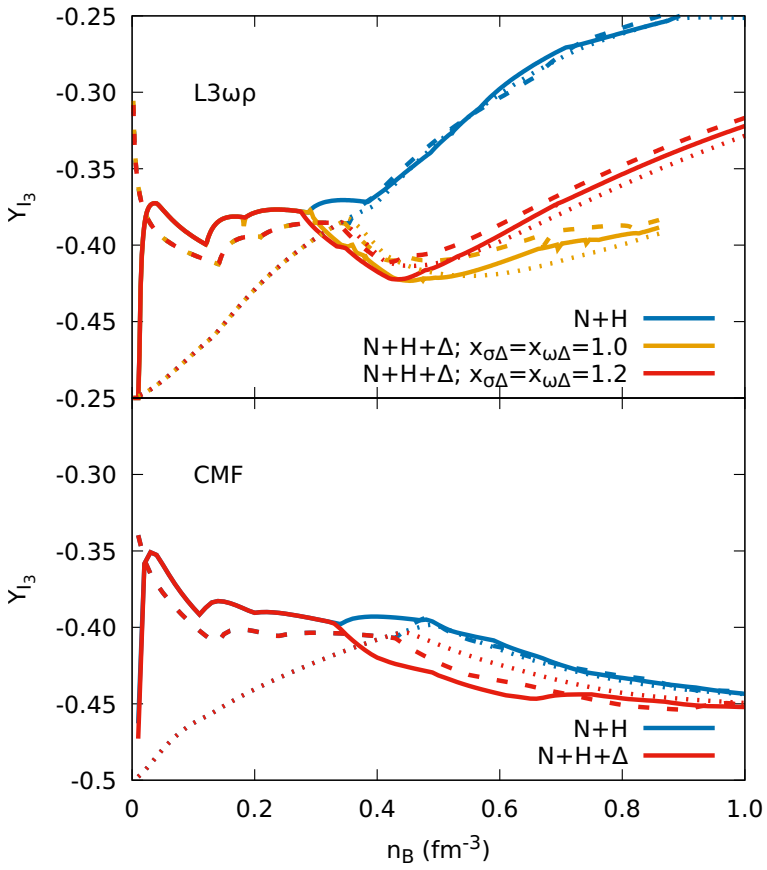

Figure 22 – Isospin fraction as a function of baryon number density for neutron-star matter with $B = 0$ (dotted lines) and with magnetic field $B = 3 \times 10^{18}$ G when considering (solid lines) or disregarding (dashed lines) the effects of the anomalous magnetic moments and shown for different compositions and interaction strengths. The top and bottom panels show results for the L3$\omega\rho$ and CMF models, respectively.

Δ^-s, which increase the isospin asymmetry (turn the isospin fraction more negative). The effect is much larger for the L3$\omega\rho$ model (top panel) than the CMF model (bottom panel), which hints that the amount of Δs reproduced in each model is different. Both effects generated by the magnetic fields, i.e. Landau quantization and AMM, decrease the isospin asymmetry (less negative Y_{I_3}) at low and intermediate densities.

A better understanding on the effects of the inclusion of Δ baryons, magnetic fields, and AMM in neutron-star matter subject to strong magnetic fields can be obtained from Fig. 23. Comparing the top row ($B = 0$) with the lower one ($B = 3 \times 10^{18}$ G), we can see that some of the charged particles are favored when magnetic field effects without AMMs are considered, an effect that is more pronounced for protons, whose onset density is pulled to very low densities for both models. As a consequence, their population becomes more similar to the neutron one in densities below ~ 0.05 fm^{-3}, turning Y_{I_3} less negative. The inclusion of AMM enhances this effect. This explains

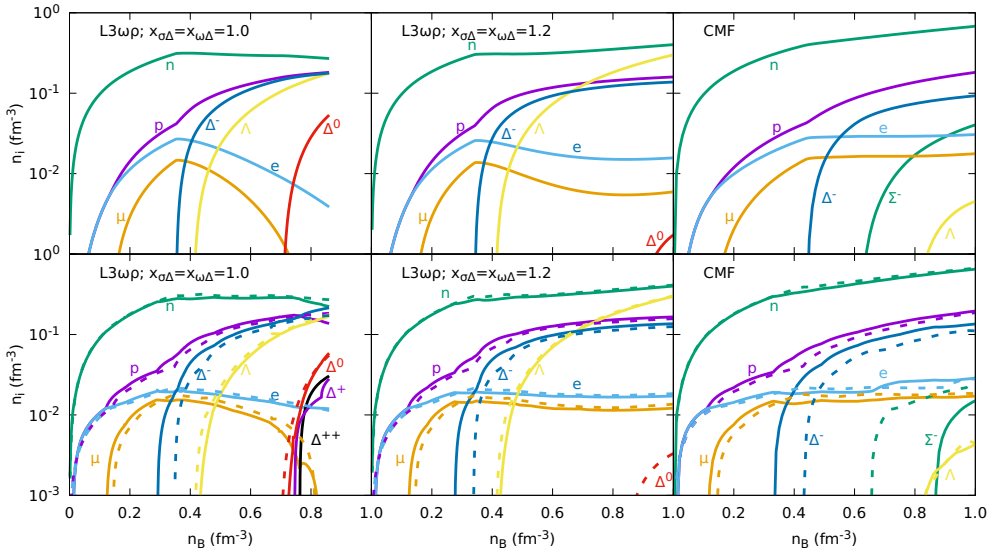

Figure 23 – Particle composition of neutron-star matter with Δs, with $B = 0$ (top panels) and magnetic field $B = 3 \times 10^{18}$ G (bottom panels), when considering (solid lines) or disregarding (dashed lines) the effects of the anomalous magnetic moment. The left and middle panels show results for the L3$\omega\rho$ model with different interactions, while the right panel shows results for the CMF model.

why the isospin asymmetry depends both on the magnetic field and on the AMM in the lower density region, as shown in Fig. 22. The Δ^- threshold (at densities around 0.3 fm^{-3}) coincides with the region at intermediate densities beyond which the N+H+Δ EoS are softer than the respective N+H EoS. The Λ (and the Σ in the CMF model) hyperons appear at larger densities than the Δ^-s. The remaining Δs appear at much larger densities and in amounts that depend on the interactions in the L3$\omega\rho$ model.

To discriminate AMM effects on the particle composition is not trivial, as they depend on the AMM coupling strength and sign, on the particle mass, charge, and density. Additionally, different spin projections are separately enhanced or suppressed, but this cannot be clearly seen in Fig. 23, as it follows the usual convention and shows the sum of all spin projections for each particle. For this reason, we make use of a quantity that reveals the degree of spin polarization, more suited to discuss spin projection asymmetry of fermions.

We define the total spin polarization of a given matter composition, weighted by the relative densities, in analogy to Eq. (66), i.e.,

$$Y_{\rm spin} = \frac{\sum_{b,s} s n_b(s)}{\sum_{b,s} n_b(s)} \,, \tag{67}$$

and shown the results in Fig. 24. For a fixed magnetic field strength, all charged particles are fully spin polarized at low densities: only spin projection 1/2 for protons and spin projection 3/2 for positive Δs, only spin projection -1/2 for leptons and negative Σs, and

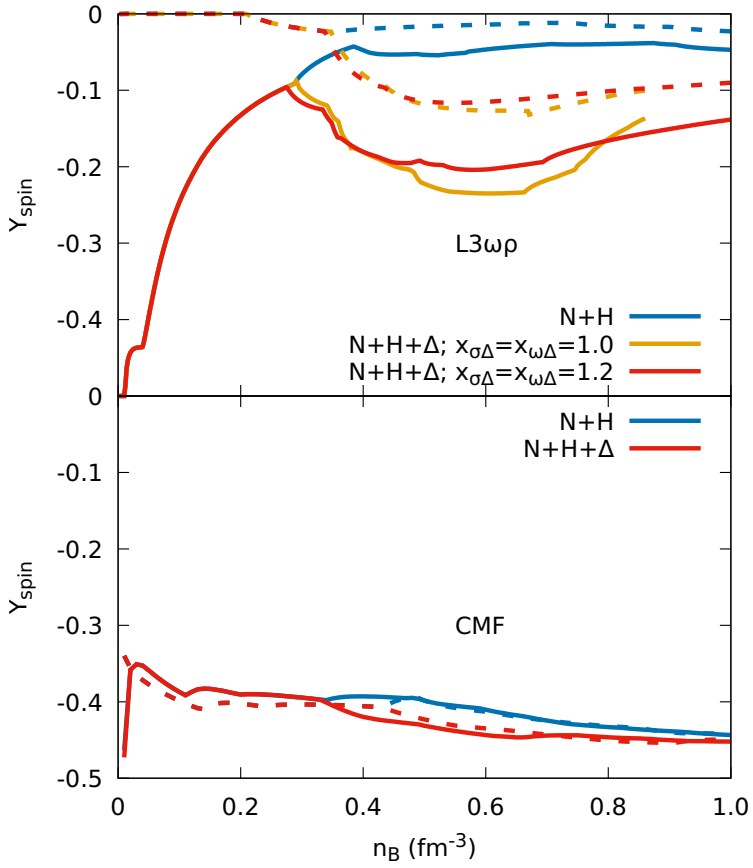

Figure 24 – Spin polarization fraction as a function of baryon number density for neutron-star matter with magnetic field $B = 3 \times 10^{18}$ G, when considering (solid lines) or disregarding (dashed lines) the effects of the anomalous magnetic moments and shown for different compositions and interaction strengths. The top and bottom panels show results for the L3$\omega\rho$ and CMF models, respectively.

spin projection -3/2 for negative Δs. When AMMs are considered, neutral particles obey the same logic, presenting only positive (negative) spin projections according to their positive (negative) sign of κ_b. At intermediate densities, full polarization is broken for more massive particles, but not for leptons and Λs. But, regardless, the polarization never goes to zero, meaning that partial spin projection imbalance remains at high densities. Overall, spin polarization fraction is much stronger for the CMF model (bottom panel) than for the L3$\omega\rho$ model (top panel). Full polarization can be understood from Eqs. (59), (60), and (57), which explains why particles with different isospin projections present different momenta and why particles occupying the first Landau level ($\nu = 0$) are more abundant when only a few levels are occupied. This happens for strong magnetic fields and low particle densities, or simply less massive particles.

It is a well-established concept that the magnetic field is not constant within neutron stars, but increases towards their centers where the density is larger. But,

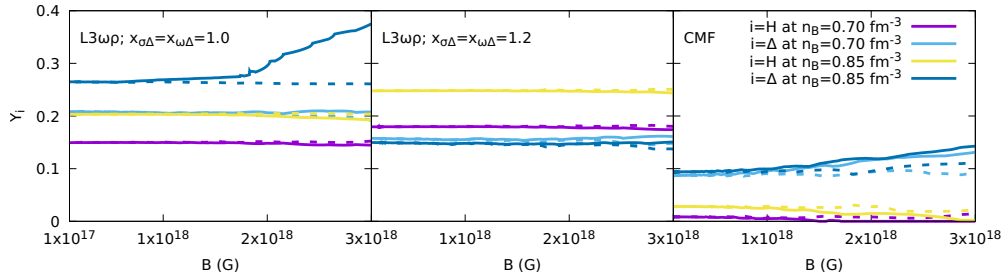

Figure 25 – Exotic particle (hyperon and Δ) fraction as a function of magnetic field strength when considering (solid lines) or disregarding (dashed lines) the effects of the anomalous magnetic moment, shown for two given densities. The left and right panels show results for the L3$\omega\rho$ with different interactions and CMF models, respectively.

before we discuss stellar configurations with macroscopic magnetic fields in detail, we study how one more relevant quantity changes as a function of magnetic field strength. The fraction of exotic particles can be defined as the following quantity

$$Y_i = \frac{\sum_{b\in i} n_b}{\sum_b n_b} , \tag{68}$$

for $i = H$ or Δ, shown in Fig. 25. On the left panel for the L3$\omega\rho$ model, the amount of Δs is slightly reduced at a given density but then increases tremendously at the larger density when the AMM is included, a behaviour quantitatively not reproduced with larger coupling constants, as seen on the middle panel. The amount of hyperons, on the other hand, is not significantly modified by the magnetic field, only slightly decreases in the presence of AMM and is affected by the small fluctuations related to the De Haas-Van Alphen oscillations [76]. The right panel shows the same qualitative behavior for the CMF model, which has a more clear substitution of hyperons in favor of deltas for higher values of B, independently of the density or accounting for the AMM.

3.2 MACROSCOPIC STRUCTURE

For spherically symmetric neutron stars, given an EoS $P(\varepsilon)$, the global structure can be obtained by solving the Tolman-Oppenheimer-Volkoff (TOV) equations of hydrostatic equilibrium. For the crust, we use the BPS EoS [12]. As an startiing point, we only analyze mass-radius curves produced from EoS without magnetic field effects, with the purpose of comparing different cases and parametrizations with observational data. We leave the study of mass-radius relations for magnetic neutron stars to a further section, as this requires the solution of a more complicated system of equations in general relativity [62, 147].

In Fig. 26, we show RMF model results without (left panel) and with (right panel) the $\omega\rho$ interaction. In both cases, the pure nucleonic stars are more massive, and the

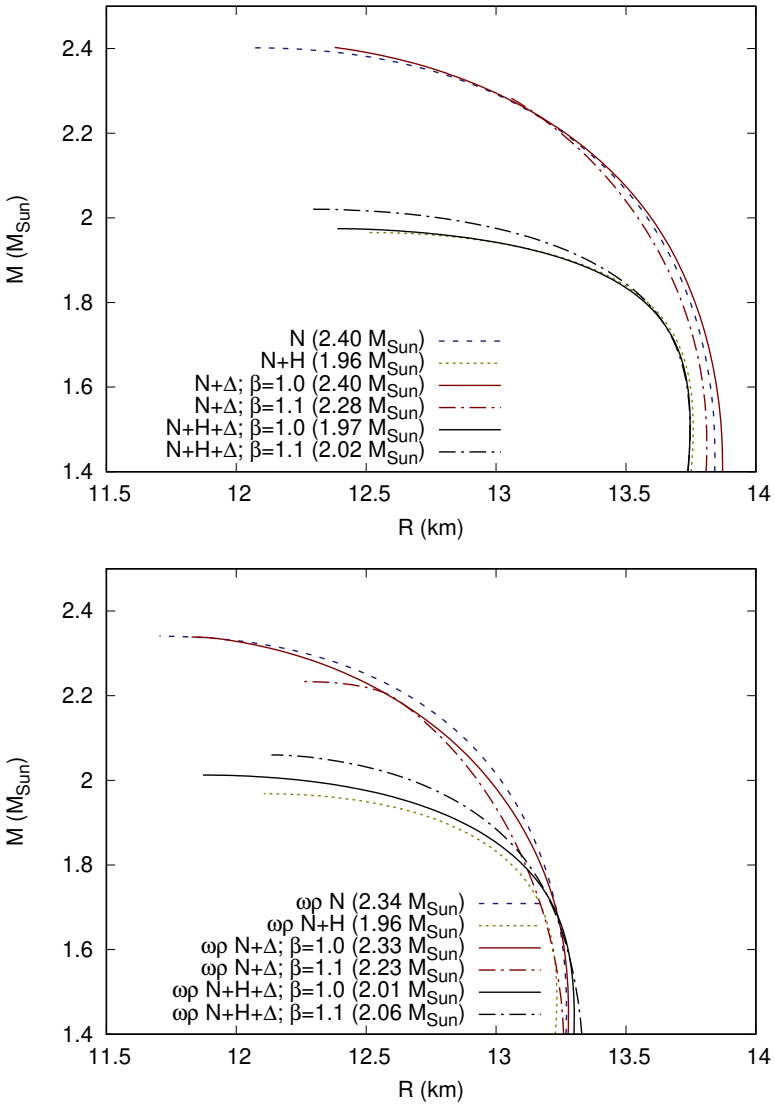

Figure 26 – Mass-radius diagram for the RMF model with GM1 parametrization (top panel) and GM1$\omega\rho$ parametrization (bottom panel), showing results without magnetic field effects. The maximum stellar masses are indicated for all cases.

ones that contain hyperons less massive. But, more interestingly, stars that include all degrees of freedom are more massive than the ones that include only nucleons and hyperons, and this effect is more obvious for the case with $\omega\rho$ interaction and β = 1.1. When the hyperons are suppressed, the stellar masses increase even more, in some cases surpassing the nucleonic star masses.

This discussion is related to the well-known hyperon puzzle [27], but with a twist. As shown in Fig. 27, going from dashed lines to solid or dot-dashed, the addition of Δ's decreases the fraction of nucleons (some neutrons) and hyperons (Λ's) to create Δ's and some protons. The overall increase in isospin asymmetry makes the EoS stiffer, even when more degrees of freedom are present. The larger population change caused by the $\omega\rho$, β = 1.1 parametrization only enhances this effect. See Ref. [106] for a detailed

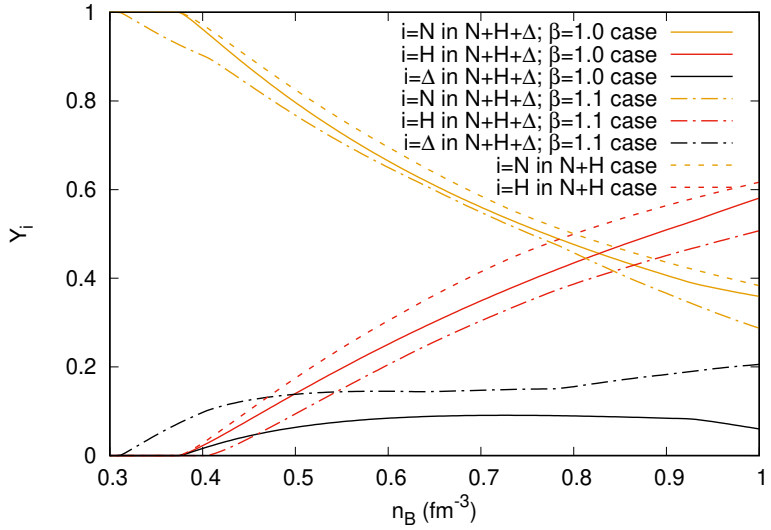

Figure 27 – Fraction of nucleons, hyperons and Δ's for the RMF model with GM1$\omega\rho$ parametrization when considering a N+H (dashed lines) or a N+H+Δ population, with β = 1.0 (solid lines) or β = 1.1 (dashed-dotted lines). Magnetic field effects are not included.

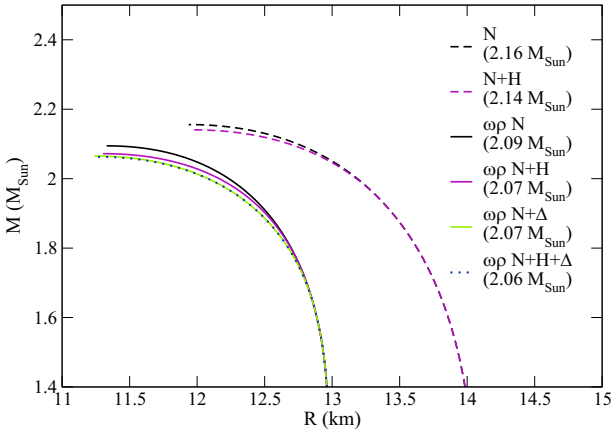

Figure 28 – Mass-radius diagram for the CMF model showing results without magnetic field effects. The maximum stellar masses are indicated for all cases.

study of the effect of the symmetry energy at larger densities on the properties of neutron stars with Δ baryons. Concerning stellar radius modifications, the intermediate density EoS softening caused by the $\omega\rho$ interaction turns stars smaller in all cases. Lower radii for $\sim 1.4\ M_{\rm Sun}$ stars improves the agreement of this model with NICER and LIGO data [127, 157, 2].

In Fig. 28, the dashed curves show results without the $\omega\rho$ interaction for the CMF model. In this case, for our selected parametrization, the Δ's are never present. We show results for nucleons only, and also including hyperons, when the maximum mass decreases. The remaining curves show results with the $\omega\rho$ interaction. In this

case, the radii of the $\sim 1.4\ M_{\rm Sun}$ stars and respective tidal deformabilities are again in much better agreement with NICER and LIGO data. The pure nucleonic stars are more massive, followed by the stars also including hyperons, also including Δ's and, finally, including all degrees of freedom, when the maximum allowed mass decreases still by only a small amount. The difference when compared to the RMF model discussion in the previous paragraph is that not many hyperons appear in the CMF model in any case, so the suppression (mainly of Σ^-'s) caused by the appearance of Δ's is small, and does not change significantly the isospin amount. From the right panel of Fig. 5 it can be seen that the overall number of exotic baryons i) H's+Δ's in the N+H+Δ case, then ii) Δ's in the N+Δ case, then the iii) H's in the N+H case, correspond inversely to the maximum masses of neutron stars for each case. This dynamics works in the same ways as the hyperon puzzle, but extended to include Δ's.

The TOV equations cannot be applied to describe the structure of the magnetars we study in this work because the spherical symmetries assumed in the Schwarzschild line element will not hold. This is due to the strong magnetic fields we infer for such objects, which produce highly deformed stellar shapes. Instead, the stellar structure must be determined by solving equations in General Relativity describing the stationary configuration for the fluid, coupled with Einstein field equations. The energy-momentum tensor, which contains the information on the matter properties of stars, enters the stellar structure equations as the source of the Einstein equations. Neglecting the coupling to the electromagnetic field, one generally assumes a perfect fluid and the energy-momentum tensor takes the form

$$T_f^{\mu\nu} = (\varepsilon + P)\ u^\mu u^\nu + P\ g^{\mu\nu}\ , \tag{69}$$

where ε denotes the (matter) energy density, P the pressure, and u^μ the fluid four-velocity.

The EoS then relates pressure and energy density to the relevant thermodynamic quantities. In [30], the general expression for the energy-momentum tensor in the presence of an electromagnetic field was derived, starting from a microscopic Lagrangian including interactions between matter and the electromagnetic field

$$\begin{aligned} T^{\mu\nu} = T_f^{\mu\nu} &+ \frac{1}{\mu_0}\left(-B^\mu B^\nu + (B\cdot B)u^\mu u^\nu + \frac{1}{2}g^{\mu\nu}(B\cdot B)\right) \\ &+ \frac{x}{\mu_0}\left(B^\mu B^\nu - (B\cdot B)(u^\mu u^\nu + g^{\mu\nu})\right)\ , \end{aligned} \tag{70}$$

where μ_0 is the vacuum permeability, $g^{\mu\nu}$ the metric tensor, and x is the magnetisation. The electromagnetic field tensor has been expressed as $F_{\mu\nu} = \varepsilon_{\alpha\beta\mu\nu}u^\beta B^\alpha$, with $\varepsilon_{\alpha\beta\mu\nu}$ being the four-dimensional Levi-Civita symbol [71]. Assuming an isotropic medium and a magnetisation parallel to the magnetic field, the magnetisation tensor $M_{\mu\nu}$ can be written as

$$M_{\mu\nu} = \varepsilon_{\alpha\beta\mu\nu}u^\beta a^\alpha\ , \tag{71}$$

Table 4 – Central baryon (n_c) and energy (ε_c) densities as a function of magnetic field strength for neutron stars of radius 12 km with L3$\omega\rho$ model for $x_{\sigma\Delta} = x_{\omega\Delta} =$ 1.0(1.2) in the top panel and CMF model in the bottom panel

	n_c (fm^{-3})		ε_c (MeV/fm^3)	
B (G)	N+H	N+H+Δ	N+H	N+H+Δ
0	0.672	0.618 (0.614)	742	658 (657)
5×10^{17}	0.701	0.659 (0.653)	783	712 (708)
1×10^{18}	0.747	0.714 (0.707)	850	786 (783)
0	0.629	0.625	678	672
5×10^{17}	0.680	0.677	747	741
1×10^{18}	0.749	0.746	843	837

with the magnetization four-vector defined as $a_\mu = \frac{x}{\mu_0} B_\mu$. In the absence of magnetisation, i.e. for $x = 0$, this expression reduces to the standard magnetohydrodynamics form for the energy-momentum tensor [71].

Strong magnetic fields result in an anisotropy of the energy momentum tensor and break spherical symmetry, such that with increasing strength of the magnetic field, the shape of a magnetar departs more and more from a spherical shape. Interpreting the spatial elements of the fluid rest frame energy-momentum tensor as pressures, then there is a difference induced by the orientation of the magnetic field, commonly referred to as "parallel" and "perpendicular" pressures. Several earlier works tried to compute the mass-radius relations of strongly magnetised neutron stars through a first approach using isotropic TOV equations [151, 57, 42]. In these works, the components of the macroscopic energy-momentum tensor in the fluid rest frame are used to obtain the energy density ε, parallel ($P_{\parallel}$) and perpendicular ($P_{\perp}$) pressures. In Heaviside-Lorentz natural units, the pure electromagnetic contribution to the energy-momentum tensor, which is anisotropic, has values of $B^2/2$ and $-B^2/2$ in the perpendicular and parallel directions to the local magnetic field, respectively. However, this approach can drastically overestimate the mass of neutron stars, as shown in Fig. 3 of [69].

Several works obtained the global structure models of magnetars by solving coupled Einstein-Maxwell equations, taking into account the anisotropy of the stress-energy tensor [140, 84, 93, 201, 62, 178, 183]. In these studies either a perfect fluid, a polytropic EoS, or a realistic EoS was assumed, but do not take into account the magnetic field modifications due to its quantisation.

Ideally, to explore magnetic field effects such as Landau quantisation and AMM on the global properties of the star, one must solve the coupled Einstein-Maxwell equations, along with a magnetic field dependent EoS. In [30] and [61], global numerical models for magnetars were obtained by consistently solving Einstein-Maxwell equations with magnetic field dependent quark EoS. It was however explicitly demonstrated by [30, 29] that the maximum mass of a neutron star is minimally modified due to the

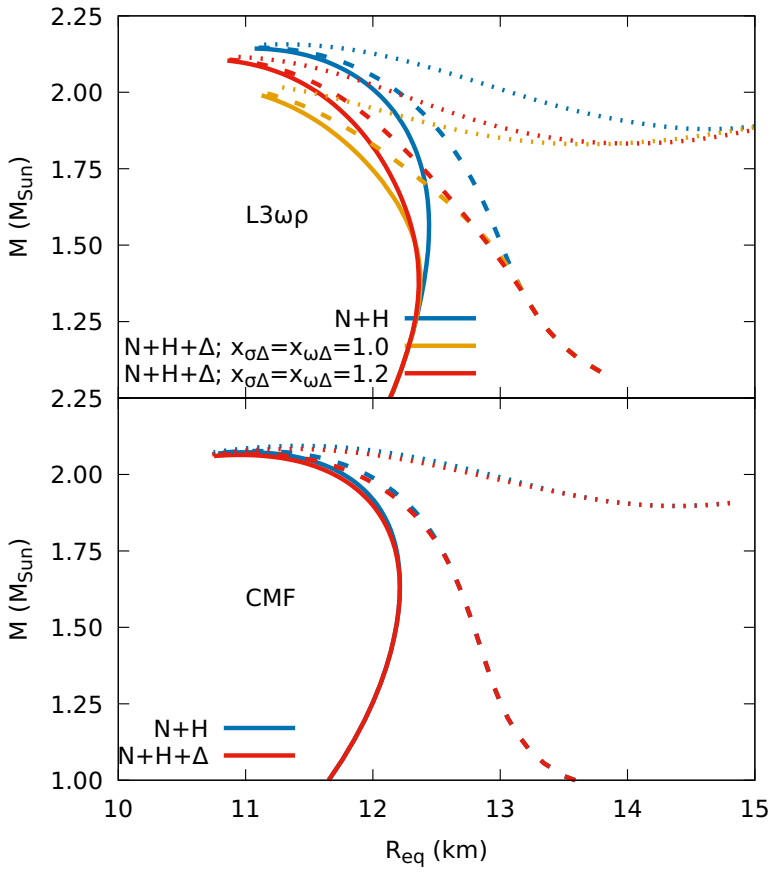

Figure 29 – Stellar mass as a function of equatorial radius for different compositions and interaction strengths, for central magnetic fields $B = 0$ (solid lines), $B = 5 \times 10^{17}$ G (dashed lines), and $B = 10^{18}$ G (dotted lines). The top and bottom panels show results for the L3$\omega\rho$ and CMF models, respectively.

magnetic field dependence of the microscopic EoS, even for the highest magnetic fields. Therefore in this work, we assume a non-magnetic ($B = 0$) matter contribution to the EoS to compute global neutron-star models and the magnetic field enters structure calculations only through the dominant pure electromagnetic field contribution. Although it remains to be checked explicitly in future work, the effects of Landau quantisation and AMMs are not expected to sensibly affect the results of this study. Note however, that this is not the case for microscopic properties of matter, as discussed in the following.

As described here, to compute the effect of the strong magnetic fields on the structure of the magnetars, one must solve the coupled Einstein–Maxwell equations with the equations of state. For the chosen poloidal field geometry, we solve the Einstein–Maxwell equations within the numerical library LORENE[1] using a multi-domain spectral method. In Fig 29, we show the mass radius relations for the *L*3$\omega\rho$ and the CMF models, with and without Δs, as a function of equatorial radius for sequences of

[1] `http://www.lorene.obspm.fr`

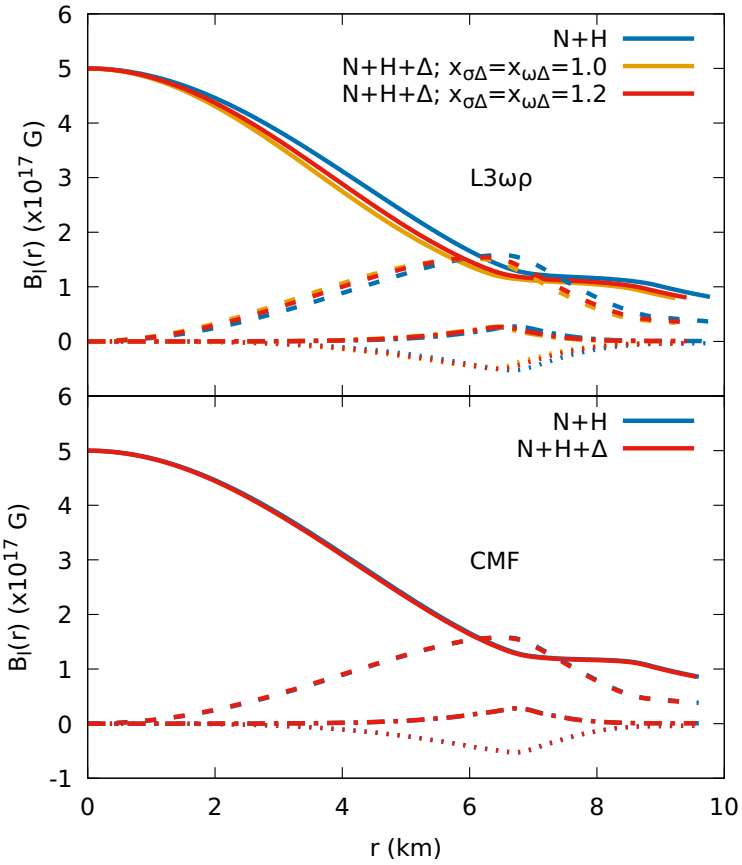

Figure 30 – Magnetic field distribution inside a neutron star of mass $1.8M_{\odot}$ and central magnetic field of $B = 5 \times 10^{17}$ G for different compositions and interaction strengths. Solid, dashed, dashed-dotted and dotted are, respectively, the first four even multipoles of the magnetic field norm (l = 0,2,4,6), shown as functions of the coordinate radius. The top and bottom panels show results for the L3$\omega\rho$ and CMF models, respectively.

constant stellar central magnetic field. Despite the fact that, for the choices discussed here for $x_{\sigma\Delta}$ and $x_{\omega\Delta}$ parameters in the $L3\omega\rho$ model, the masses of N+H+Δ stars never surpass the respective N+H configurations, we still observe that the the maximum mass (shown in Fig. 29) follows the same ordering of a large (and most relevant) portion of Fig. 22 for the compressibility.

In Fig. 29, any differences between the mass-radius curves for the $B = 0$ case (solid lines) arise from the differences in the (non-magnetic) EoS, while the differences with magnetic field come from the pure electromagnetic field contribution. We know that the Lorentz force originating from the pure electromagnetic field affects the low density part of the EoS. This is why the maximum mass of very massive stars does not change with increasing magnetic field strength, but the mass and radius of less massive stars increase significantly. For the $L3\omega\rho$ model, the inclusion of Δs decreases modestly the maximum stellar mass, especially for the larger coupling. However, for the CMF model,

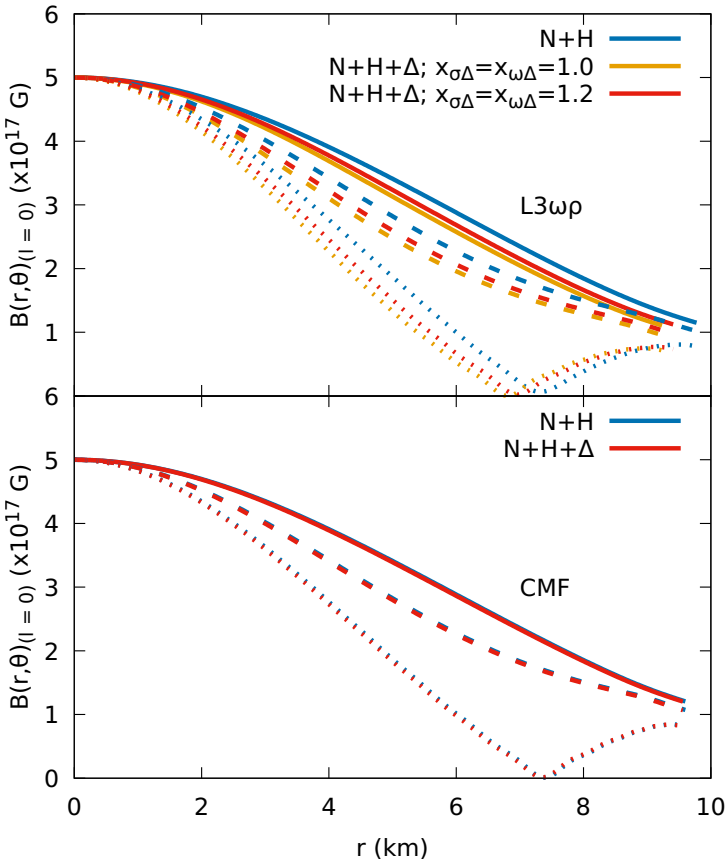

Figure 31 – Magnetic field distribution inside a neutron star of mass $1.8M_{\odot}$ and central magnetic field of $B = 5 \times 10^{17}$ G for different compositions and interaction strengths. Solid, dashed and dotted are the dominant monopolar ($l = 0$) term at the polar ($\theta = 0$), intermediate ($\theta = \pi/4$) and equatorial ($\theta = \pi/2$) orientations, respectively, shown as functions of the coordinate radius. The top and bottom panels show results for the L3$\omega\rho$ and CMF models, respectively.

we do not see meaningful changes on the mass-radius diagram with the inclusion of Δs. From Table 4 we see that, keeping the radius of the neutron star fixed (going up vertically in Fig. 29), the increase in the strength of the central magnetic field increases both the central baryon and energy densities, as a larger matter pressure is necessary to balance the Lorentz force. The addition of Δs decreases both quantities, as these stars are naturally (at B=0) smaller.

At this point, we note that the maximum mass value of the stellar family described by the $L3\omega\rho$ model with Δs and $x_{\sigma\Delta} = 1.0$ (the yellow curve) has not been attained because, as explained earlier, the EoS numerical code stops converging at large densities due to reaching zero nucleon masses. Such behavior indicates that hadronic matter is no longer stable at this point and deconfinement to quark matter must be considered. We leave such analysis to a future work. But, since the trend of the yellow curve is quite

obvious, we can conclude that its maximum mass is lower when compared to the other coupling and composition.

Using the full numerical solution, we also study the effect of the EoS on the magnetic field configurations inside a given star. We decompose the magnetic field norm in terms of spherical harmonics

$$B(r,\theta) \approx \sum_{i=0}^{l_{max}} B_l(r)\, Y_l^0(\theta)\ , \tag{72}$$

and plot the first four even multipoles (l = 0,2,4,6) as function of coordinate radius for both the EoS models and coupling strengths in Fig 30. We also plot the profile of the dominant monopolar, spherically symmetric, term (l = 0) inside the star in Fig 31. For $L3\omega\rho$ model, specially if we include Δs, the magnetic field norm decreases slightly inside the star but, for CMF model, we do not see any considerable changes.

The macroscopic properties of magnetars for the above choice of EoS models were obtained by solving Einstein-Maxwell equations within the LORENE library. It was found that maximum masses as high as 2 $M_\odot$ can be attained even on inclusion of Δ particles. This is due to isospin readjustment at large densities, which turns the EoS stiffer. The Δs also respond more strongly to the AMM, which is expected due to the fact that they present additional electric charges and isospin projections. As a consequence, Δ-admixed hypernuclear stellar matter possesses larger spin polarization. The latter effect is more dramatic for the L3$\omega\rho$ model, which presents a larger number of exotic particles than the CMF model. Considering strong magnetic fields, heavy stars tend to contain more deltas in their interiors. They are not necessarily more massive than their B = 0 counterparts, but are larger and, for a given radius, present larger central number density and energy density. While Δs modify the magnetic field distribution very little inside stars, they decrease their radii, improving the agreement with modern observational data of neutron-star radii and tidal deformability.

Part II

The Hadron-Quark Phase Transition

4 NAMBU–JONA-LASINIO DESCRIPTION OF HADRONIC MATTER

In confining theories as QCD, it is admitted that only gauge invariant objects should be observable. So, as the QCD Lagrangian is invariant under local transformations in color space $SU(3)_c$, only color singlet (white) objects are observable, i.e., hadrons (quark-antiquark and three-quark bound states). Equation ((1)) also exhibits an approximate flavor symmetry in the light quarks sector (u, d, s), arising from the fact of the mass differences between the flavors being much smaller than the QCD scale, that leads to many relations for masses of hadrons within a specific multiplet, e.g., the *Gell-Mann–Okubo mass formula* [164].

One more important feature of the QCD Lagrangian is the *chiral symmetry*, meaning that left-handed and right-handed components of the quark fields can be transformed independently by symmetry operations such that they make no difference to the theory, i.e., by projecting $\psi = \psi_L + \psi_R$ where

$$\psi_{L,R} = \left(\frac{1 \mp \gamma^5}{2}\right)\psi. \tag{73}$$

Taking as an example the two-flavor QCD Lagrangian in the *chiral limit* (i.e., with massless quarks since the term $m\bar{\psi}\psi$ breaks chiral symmetry explicitly), the equation ((1)) can be written as

$$\mathcal{L} = \bar{q}_L i\not{D} q_L + \bar{q}_R i\not{D} q_R + \mathcal{L}_{\text{gluons}}, \tag{74}$$

with $q = \begin{bmatrix}\psi_u & \psi_d\end{bmatrix}^T$ and $\not{D}$ being the covariant derivative, which makes straightforward to show this Lagrangian remains unchanged by any unitary transformations, independently if acting on q_L or q_R in different ways. The group of this so-called *flavor chiral symmetry* is denoted as $U(2)_L \times U(2)_R$ and decomposes into

$$SU(2)_L \times SU(2)_R \times U(1)_V \times U(1)_A.$$

The *singlet vector group* $U(1)_V$ represents a true symmetry of the theory and, as so, corresponds to the baryon number conservation, while the *singlet axial group* $U(1)_A$ is explicitly violated by a quantum anomaly arising from the gluon sector of the QCD Lagrangian. The remaining $SU(2)_L \times SU(2)_R$ group is spontaneously broken by non-vanishing *quark condensates* $\left\langle \bar{q}_R^a q_L^b \right\rangle = v\delta^{ab}$, that occurs due to the non-perturbative nature of the QCD vacuum state, amounting to the *isospin symmetry group* $SU(2)_V$. The three broken generators correspond to three *Goldstone bosons*, and quark masses can be considered as being dynamically generated by the spontaneous chiral symmetry breaking, since they were taken as massless particles in the initial QCD Lagrangian. As the quarks do have a finite mass, the chiral symmetry of QCD is broken explicitly by this terms. However, as quark masses are small compared to the interaction scale, the chiral symmetry can still be seen as an approximate symmetry of the theory, which renders,

through spontaneous breaking, light but not massless *pseudo-Goldstone bosons* that can be identified as the three pions. This mechanism provides an explanation to the huge difference between bound states observed masses and the sum of the masses of their forming particles, e.g., the valence quarks bare masses in a proton contribute to only 9.4 MeV of the barion total mass ($m_p \approx 938$ MeV). The same argument can be traced for the light quarks sector (u, d, s) of the QCD Lagrangian, resulting in the final unbroken group being the *eightfold way group* $SU(3)_V$ and the respective eight broken generators corresponding to the meson octet [146].

The first theoretical approach to the chiral symmetry breaking in a fermionic quantum field theory was performed by [134], anteceding the proposal of quarks and the QCD formulation. The original *Nambu–Jona-Lasinio* (NJL) model aimed to describe interacting nucleons, motivated by the fact that this interaction holds a partially conserved *axial vector current*, associated to the approximate chiral symmetry. Since it imposes the nucleon mass to be small in the Lagrangian level, the spontaneous symmetry breaking, in analogy to the BCS theory of superconductors, provides a mechanism which generates dynamically the large nucleon mass.

The NJL Lagrangian can be written for one species of particles as

$$\mathcal{L} = \bar{\psi}\left(i\partial\!\!\!/ - m\right)\psi + G\left[(\bar{\psi}\psi)^2 + \left(\bar{\psi}i\gamma^5\psi\right)^2\right]. \tag{75}$$

It describes a four-fermions point-like interaction proportional to the dimensional coupling constant G. It is relevant to notice that, while the axial term (that with γ_5) vanishes in the mean-field approximation, it is still required to keep the Lagrangian chirally symmetric and, in this sense, should be considered to be part of the model Lagrangian even without having impact on the further derivation of the mean-field thermodynamics [95].

Supposing the vacuum expectation $\langle 0|\bar{\psi}\psi|0\rangle$ being non-zero, thus responsible for the breakdown of the chiral symmetry, the movement equation of the spinor field can be obtained through the so-called *Hubbard-Stratonovich transformation*, i.e., the bosonization of the model by auxiliary fields given by the non-vanishing condensates. Only expectation values that are bilinear in the quark fields are allowed, which preserves all original symmetries of the Lagrangian, apart from chiral symmetry (spontaneously broken by the condensates) and Lorentz invariance (explicitly broken by the chemical potential). So, neglecting quadratic terms in the fluctuations, the Lagrangian can be linearized from taking

$$(\bar{\psi}\psi)^2 = 2\rho_s(\bar{\psi}\psi) - \rho_s^2 \quad \text{and} \quad (\bar{\psi}\gamma^\mu\psi)^2 = 2n_B(\psi^\dagger\psi) - n_B^2, \tag{76}$$

where the scalar and vector condensates are $\rho_s = \langle\bar{\psi}\psi\rangle$ and $n_B = \left\langle\psi^\dagger\psi\right\rangle$, also called *scalar density* and *barionic density*, respectively. In particular terms in channels without condensate or the space components in the vector vertex drop out. From the variational

Figure 32 – Non-perturbative correction to the fermion propagator. The bare and dressed propagator are denoted by the thin and bold line, respectively [20].

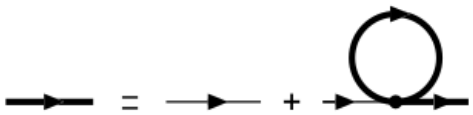

principle, one can write

$$(i\partial\!\!\!/ - m)\,\psi + 2G\,\langle\bar{\psi}\psi\rangle\,\psi - 2G\left\langle\bar{\psi}\gamma^5\psi\right\rangle\gamma^5\psi = 0, \tag{77}$$

that can be identified as the *Dirac equation*

$$(i\partial\!\!\!/ - M)\,\psi = 0, \tag{78}$$

where the *constituent mass* is given by the *gap equation*

$$M = m - 2G\langle\bar{\psi}\psi\rangle. \tag{79}$$

This shift in the mass can be understood as a non-perturbative correction to the self-energy, i.e., to consider the fermion propagator *dressed* by the one-loop correction as depicted in Figure 32.

Also, the fermion condensate can be evaluated from the dressed fermion propagator
$S(p) = (p\!\!\!/ - M + i\varepsilon)^{-1}$ as

$$\langle\bar{\psi}\psi\rangle = -i\int\frac{d^4p}{(2\pi)^4}\mathrm{Tr}S(p) = -4i\int\frac{d^4p}{(2\pi)^4}\frac{M}{p^2 - M^2 + i\varepsilon}, \tag{80}$$

with the trace to be taken in color, flavor, and Dirac space (only the latter contributes in this example). As a consequence of the dimensionality of the coupling constant G, the NJL model is not renormalizable, thus a regularization scheme must be employed to the divergent integrals. Here, it is done by applying a sharp cutoff in the three-momentum ultraviolet region of the above integration limits, often denoted as Λ.

Applying standard techniques of thermal field theory, as presented in Appendix A, it is possible to evaluate the fermionic loop which enters the gap equation at non-vanishing temperature or chemical potential. In this situation, the gap equation finally reads

$$M = m + 4G\int\frac{d^3p}{(2\pi)^3}\frac{M}{\sqrt{p^2 + M^2}}\left[1 - n_p(T,\mu) - \bar{n}_p(T,\mu)\right], \tag{81}$$

where, since quarks (or hadrons) are fermions, n_p and $\bar{n}_p$ are the *Fermi-Dirac distribution functions* for the particles and antiparticles with momentum p, respectively given by

$$n_p(T,\mu) = \frac{1}{1 + e^{(E_p - \mu)/T}} \quad \text{and} \quad \bar{n}(T,\mu) = \frac{1}{1 + e^{(E_p + \mu)/T}}, \tag{82}$$

Figure 33 – Solution of equation ((81)) to the constituent mass for zero density and non-zero temperatures (left panel) and for zero temperature and non-zero densities (right panel). Dashed lines indicate the chiral limit ($m = 0$) of the parameter choice indicated by solid lines [adapted from 20].

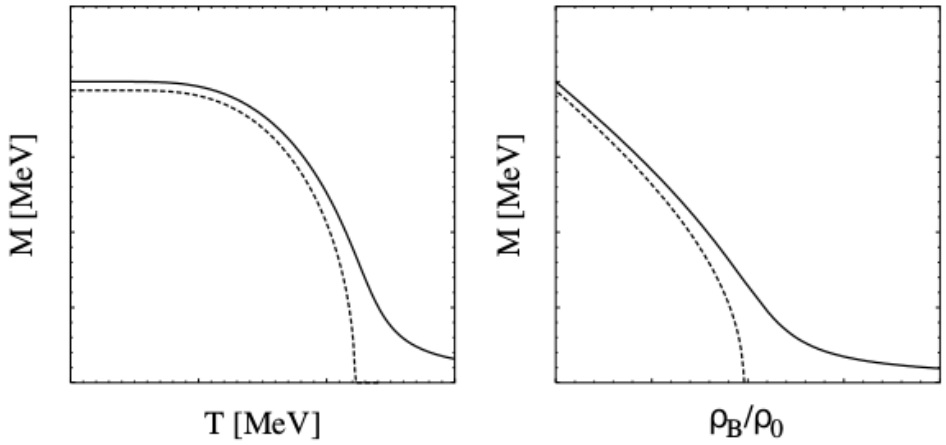

with $E_p = \sqrt{p^2 + M^2}$ such that, e.g., the total *number density* is

$$n_B = 2 \int \frac{d^3p}{(2\pi)^3} \left[n(T,\mu) - \bar{n}(T,\mu) \right] . \tag{83}$$

In general, the gap equation has more than one solution, e.g., in the chiral limit, the trivial configuration $M = 0$ is always a valid solution, but non-trivial solutions $M = \pm M_0 \neq 0$ can occur as well. It is possible to show that the vacuum energy is always minimized by the solution with the largest value of M [188]. Figure 33 illustrates the behavior of the gap equation (Eq. (81)) solutions at non-vanishing temperature and density. In this situation, where there is a medium, the occupation numbers are non-zero and reduce the value of the constituent mass for low temperatures and densities. As the temperature or the density increase, the particle distribution factor tends to zero, and the constituent mass M approaches the value of the current mass m. This mechanism is called *chiral symmetry restoration*, as the ground state solution goes back to the light particle case.

This model has three free parameters to be fitted (m, G and Λ). When using the NJL as a model of QCD, these parameters are usually fixed by fitting the pion mass m_π and the pion decay constant f_π, that must satisfy the *Gell-Mann–Oakes–Renner relation*

$$f_\pi^2 m_\pi^2 = -m \langle \bar{\psi}\psi \rangle + \mathcal{O}(m^2). \tag{84}$$

In the following, the NJL formalism briefly described above will be extended to more complete approaches, better suited to describe both free quark and hadronic matter, through the mean-field calculation of the *grand-canonical thermodynamic potential*.

Even though the original NJL model was proposed considering nucleonic degrees of freedom, the lack of confinement soon became a problem within the QCD

theoretical framework, which made it to be reinterpreted as a schematic quark model [96]. The fact that the NJL Lagrangian does not confine the fermion fields also implies that it is unable to describe the saturation properties of the nuclear matter. However, it can be easily fixed by the inclusion of an extra channel representing a scalar-vector interaction. The same logic can be applied to many other channels of interaction, aiming to improve the description of other important bulk properties, which give origin to the so-called *extended Nambu–Jona-Lasinio* (eNJL) models family [98]. One version of these eNJL models, partially developed in this work, is discussed ahead, where a hadronic eNJL model is presented for the cases of nucleonic (protons and neutrons only) and hyperonic (protons, neutrons and lambdas) matter. The latter case was not previously discussed within the NJL model theoretical framework, and it is a novel and relevant contribution to the exploration of the QCD phase diagram, as describing matter with strangeness content (i.e., strange quark matter and hyperonic hadron matter) is important to the study of the hadron-quark phase transition.

4.1 NUCLEONIC MATTER

The extended NJL Lagrangian density that models hadronic matter is given, generically, by

$$\mathcal{L}_{\text{eNJL}} = \bar{\psi}\left(i\partial\!\!\!/ - \hat{m}\right)\psi + \mathcal{L}_I. \tag{85}$$

A rather broadened eNJL model able to describe hadronic matter constituted by protons and neutrons, named here as PPM NJL model, was proposed in a first version by [142] and it is reobtained in the following including the treatment of non-zero temperature to the authors original deductions. This model is constructed from ((85)), taking $\psi = \begin{bmatrix}\psi_p & \psi_n\end{bmatrix}^T$ to represent the nucleon fields of masses $\hat{m} = \text{diag}(m_p, m_n)$, again assuming isospin symmetry in the Lagrangian level, and the interaction part $\mathcal{L}_I$ given by several four-point and crossed eight-point interactions compatible with the SU(2) flavor symmetry. Hence, the PPM NJL model is given by the Lagrangian density

$$\begin{aligned}\mathcal{L}_{\text{PPM}} = {} & \bar{\psi}\left(i\partial\!\!\!/ - \hat{m}\right)\psi + G_s[(\bar{\psi}\psi)^2 + (\bar{\psi}i\gamma_5\vec{\tau}\psi)^2] - G_v(\bar{\psi}\gamma^\mu\psi)^2 \\ & + G_\rho[(\bar{\psi}\gamma^\mu\vec{\tau}\psi)^2 + (\bar{\psi}\gamma_5\gamma^\mu\vec{\tau}\psi)^2] - \chi_{sv}G_sG_v[(\bar{\psi}\psi)^2 + (\bar{\psi}i\gamma_5\vec{\tau}\psi)^2](\bar{\psi}\gamma^\mu\psi)^2 \\ & + \chi_{s\rho}G_sG_\rho[(\bar{\psi}\psi)^2 + (\bar{\psi}i\gamma_5\vec{\tau}\psi)^2][(\bar{\psi}\gamma^\mu\vec{\tau}\psi)^2 + (\bar{\psi}\gamma_5\gamma^\mu\vec{\tau}\psi)^2] \\ & - \chi_{v\rho}G_vG_\rho(\bar{\psi}\gamma^\mu\psi)^2[(\bar{\psi}\gamma^\mu\vec{\tau}\psi)^2 + (\bar{\psi}\gamma_5\gamma^\mu\vec{\tau}\psi)^2],\end{aligned} \tag{86}$$

with G_a standing for the coupling constants for the different channels, the crossed interactions between channels a and b weighted by the coefficient $\chi_{ab} = G_{ab}/G_aG_b$, and where $\vec{\tau}$ is the Pauli isospin matrix. For nuclear matter, the simpler versions of the NJL model does not lead to binding, the introduction of the term in G_{sv} copes with this unwanted feature. Yet, the G_v term simulates a chiral-invariant short-range repulsion between the nucleons, the G_ρ term allows for the description of isospin asymmetric

matter, the G_{sv} term accounts for the density dependence of the scalar coupling, and the $G_{s\rho}$ and $G_{v\rho}$ terms make the density dependence of the symmetry energy softer. As in the quark case, the theory is renormalized via a three momenta cutoff Λ.

So, the thermodynamic potential that follows from ((86)) reads

$$\Omega(T,\mu;M,\tilde{\mu}) = \sum_{i=p,n}\Omega_{M_i}(T,\tilde{\mu}_i) + G_s\rho_s^2 - G_v n_B^2 + G_\rho\rho_3^2 + \chi_{sv}G_sG_v\rho_s^2n_B^2 \\ -\chi_{s\rho}G_sG_\rho\rho_s^2\rho_3^2 + \chi_{v\rho}G_vG_\rho n_B^2\rho_3^2, \quad (87)$$

where the displaced free Fermi gas contribution Ω_{M_i} is given by ((108)), taking $N_c = 1$, as hadrons do not show color degeneracy, and the gap equations

$$M = m - 2G_s\rho_s - 2G_{sv}\rho_s\rho^2 + 2G_{s\rho}\rho_s\rho_3^2 \quad (88)$$

$$\tilde{\mu}_i = \mu_i - 2G_v\rho \pm 2G_\rho\rho_3 + 2G_{sv}\rho\rho_s^2 \mp 2G_{s\rho}\rho_3\rho_s^2 + 2G_{v\rho}\rho\rho_3(\rho_3 \pm \rho), \quad (89)$$

with the upper (lower) signs taken for $i = p$ ($i = n$). The scalar and number total densities are given by $\rho_S = \rho_{s_p} + \rho_{s_n}$ and $n_B = n_p + n_n$, with ρ_{s_i} and n_i defined by equations ((111)) and ((112)), as usual, and the *isospin density* defined as $\rho_3 = n_p - n_n$. The procedure of determining the free parameters of the theory, as applied in this work, is discussed in the following, and the suitable sets found are shown in Table 5.

4.2 HYPERONIC MATTER

When describing hadronic matter at very high densities, the appearance of *hyperons*, i.e., baryons containing one or more strange quarks, is expected. The hyperon formation process is a consequence of the fermionic nature of nucleons, which makes their chemical potentials very rapidly increasing functions of the density. So, as, e.g., the chemical potential of the nucleons becomes sufficiently large, the most energetic particles can decay via weak processes into Λ hyperons, creating a new Fermi sea for this hadronic species and lowering the system total energy [16]. Such process could take significant role in high baryonic density environments, as the expected to occur in the core of compact stars or during heavy-ion collisions. In the first case, the presence of hyperons turns the stellar matter equation of state *softer* and, as a consequence, decreases the maximum gravitational mass sustained by this matter. The difficulty in reconciling the high observed masses of neutron stars with the description of these objects when there are hyperons in their interior is known as *the hyperon puzzle*. Also, being able to describe hadronic matter with an initial content of strangeness is relevant to study the QGP formation and to explore the QCD phase diagram, since the free quark matter can be stable if containing *s* quarks, if so, and many processes of deconfinement preserve the flavor fractions during the hadron-quark phase transition [137, 121].

Starting from ((85)), a novel extended version of the NJL model suited to describe hadronic matter constituted by protons, neutrons and Λ hyperons is proposed, in analogy to the PPM NJL model. This $SU(3)$ eNJL model for hadrons, named PPMM NJL model, is built assuming three species of barions, $\psi = [p \quad n \quad \Lambda]^T$ with current masses $\hat{m} = \text{diag}(m_p, m_n, m_\Lambda)$. Similarly to the $SU(3)$ quark matter description, the $SU(3)$ symmetry is explicitly broken, even assuming the isospin symmetry ($m_p = m_n$) in the Lagrangian level, because m_Λ cannot be confidently chosen equal to the nucleon mass. Hence, the PPMM NJL model is given by the Lagrangian density

$$\begin{aligned}
\mathcal{L}_{\text{PPMM}} &= \bar{\psi}\left(i\partial\!\!\!/ - \hat{m}\right)\psi + G_s\sum_{a=0}^{8}[(\bar{\psi}\lambda_a\psi)^2 + (\bar{\psi}i\gamma_5\lambda_a\psi)^2] - G_v(\bar{\psi}\gamma^\mu\lambda_0\psi)^2 \\
&+ G_\rho\sum_{a=1}^{8}[\left(\bar{\psi}\gamma^\mu\lambda_a\psi\right)^2 + \left(\bar{\psi}\gamma_5\gamma^\mu\lambda_a\psi\right)^2] - \chi_{sv}G_sG_v\sum_{a=0}^{8}[(\bar{\psi}\lambda_a\psi)^2 + (\bar{\psi}i\gamma_5\lambda_a\psi)^2](\bar{\psi}\gamma^\mu\lambda_0\psi)^2 \\
&+ \chi_{s\rho}G_sG_\rho\sum_{a=0}^{8}[(\bar{\psi}\lambda_a\psi)^2 + (\bar{\psi}i\gamma_5\lambda_a\psi)^2]\sum_{a=1}^{8}[\left(\bar{\psi}\gamma^\mu\lambda_a\psi\right)^2 + \left(\bar{\psi}\gamma_5\gamma^\mu\lambda_a\psi\right)^2] \\
&- \chi_{v\rho}G_vG_\rho(\bar{\psi}\gamma^\mu\lambda_0\psi)^2\sum_{a=1}^{8}[\left(\bar{\psi}\gamma^\mu\lambda_a\psi\right)^2 + \left(\bar{\psi}\gamma_5\gamma^\mu\lambda_a\psi\right)^2], \qquad (90)
\end{aligned}$$

where $\lambda_0 = \sqrt{2/3}\,\mathbb{I}$ and $\lambda_1, \ldots, \lambda_8$ are the Gell-Mann matrices. The interaction terms in ((90)) do not represent the more general $SU(3)$-symmetric Lagrangian possible, but are chosen this way in analogy to the form of ((86)). As in the PPM case, this model is a generalization of ((113)), and the equations below should recall the results for three-flavor quark matter presented in the following when assumed $G_\rho = \chi_{ab} = K = 0$ [159, 97, 189].

The mean-field thermodynamic potential can be obtained from this Lagrangian in the same way as presented before, through the bosonization of the model by the auxiliary fields given by the non-vanishing condensates. In particular terms in channels without condensate or the space components in the vector vertex drop out, and only the Gell-Mann matrices with non-zero diagonals contribute, i.e., λ_0, λ_3 and λ_8, as exchange terms do not play a role ($\psi_i\psi_j = 0$ for $i \neq j$). Thus, the thermodynamic potential is given by

$$\begin{aligned}
\Omega = &\sum_{i=p,n,\Lambda}\Omega_{M_i}(T,\mu_i) + 2G_s(\rho_{s_p}^2 + \rho_{s_n}^2 + \rho_{s_\Lambda}^2) - \frac{2}{3}G_v n_B^2 + G_\rho\left(\rho_3^2 + \frac{1}{3}\rho_8^2\right) \\
&+ \frac{4}{3}\chi_{sv}G_sG_v(\rho_{s_p}^2 + \rho_{s_n}^2 + \rho_{s_\Lambda}^2)n_B^2 - 2\chi_{s\rho}G_sG_\rho(\rho_{s_p}^2 + \rho_{s_n}^2 + \rho_{s_\Lambda}^2)\left(\rho_3^2 + \frac{1}{3}\rho_8^2\right) \\
&+ \frac{2}{3}\chi_{v\rho}G_vG_\rho n_B^2\left(\rho_3^2 + \frac{1}{3}\rho_8^2\right), \qquad (91)
\end{aligned}$$

where $\Omega_{M_i}(T,\mu_i)$ is the same as given in equation ((108)) with $N_c = 1$. The total number density is given by $\rho_s = \rho_{s_p} + \rho_{s_n} + \rho_{s_\Lambda}$, with ρ_{s_i} and n_i defined by equations ((111))

Table 5 – Parameter sets for the PPM Lagrangian density ((86)). The units of G_a are fm^2, and of χ_{ab} are fm^4. Λ and m are in MeV.

Set	Λ	G_s	G_v	G_ρ	χ_{sv}	$\chi_{s\rho}$	$\chi_{v\rho}$	m
PPM-1	407.89	3.60	3.450	-0.20	0.15	0.05	0	135
PPM-2	407.89	3.60	3.450	-0.20	0.15	0.05	0.05	135
PPM-3	417.60	3.30	3.15	-0.20	0.15	0.10	0	150
PPM-4	411.24	3.45	3.30	-0.20	0.15	0	0.10	150
PPM-5	411.24	3.45	3.30	-0.20	0.15	0	0.15	150
PPM-6	421.56	3.15	3.00	-0.20	0.15	0	0.05	165
PPM-7	396.96	3.75	3.45	-0.20	0.15	0	0	165
PPM-8	424.32	3.75	3.75	-0.25	0.10	0.40	0.10	0

Table 6 – Parameter sets for the PPMM Lagrangian density ((86)). The units of G_a are fm^2, and of χ_{ab} are fm^4. Λ and m_i are in MeV.

Set	Λ	G_s	G_v	G_ρ	χ_{sv}	$\chi_{s\rho}$	$\chi_{v\rho}$	$m_{p,n}$	m_Λ
PPMM-1	628.05	1.050	2.70	-3.00	0.03	0.13	0.15	135	286.25
PPMM-2	619.58	1.05	3.00	-2.85	0.04	0.14	0	165	317.69
PPMM-3	606.89	1.35	2.85	-2.85	0.01	0.14	0.14	0	148.64

and ((112)), as usual. It also was convenient to define the quantities $\rho_3 = n_p - n_n$ and $\rho_8 = n_p + n_n - 2n_\Lambda$.

The constituent mass and the renormalized chemical potential were introduced during the deduction, in the same fashion of the previous ways, and reads

$$M_i = m_i - 4G_s\rho_{s_i} - \frac{8}{3}G_{sv}\rho_{s_i}n_B^2 + 4G_{s\rho}\rho_{s_i}\left(\rho_3^2 + \frac{1}{3}\rho_8^2\right), \tag{92}$$

for $i = \{p,n,\Lambda\}$,

$$\begin{aligned}\tilde{\mu}_i = \mu_i &- \frac{4}{3}G_v n_B \pm 2G_\rho\left(\rho_3 \pm \frac{1}{3}\rho_8\right)\\ &+ \frac{4}{3}G_{sv}(\rho_{s_p}^2 + \rho_{s_n}^2 + \rho_{s_\Lambda}^2)\rho \mp 4G_{s\rho}(\rho_{s_p}^2 + \rho_{s_n}^2 + \rho_{s_\Lambda}^2)\left(\rho_3 \pm \frac{1}{3}\rho_8\right)\\ &\mp \frac{4}{3}G_{v\rho}n_B\left[\left(\rho_3^2 + \frac{1}{3}\rho_8^2\right) \mp n_B\left(\rho_3 + \frac{1}{3}\rho_8\right)\right],\end{aligned} \tag{93}$$

with the upper (lower) signs taken for $i = p$ ($i = n$), and

$$\begin{aligned}\tilde{\mu}_\Lambda = \mu_\Lambda &- \frac{4}{3}G_v n_B - \frac{4}{3}G_\rho\rho_8 + \frac{4}{3}G_{sv}(\rho_{s_p}^2 + \rho_{s_n}^2 + \rho_{s_\Lambda}^2)n_B\\ &+ \frac{8}{3}G_{s\rho}(\rho_{s_p}^2 + \rho_{s_n}^2 + \rho_{s_\Lambda}^2)\rho_8 + \frac{4}{3}G_{v\rho}n_B\left[\left(\rho_3^2 + \frac{1}{3}\rho_8^2\right) - \frac{2}{3}n_B\rho_8\right].\end{aligned} \tag{94}$$

The suitable sets found for the PPMM NJL Lagrangian ((90)) are shown in Table 6.

The application of the equations of state of hadronic matter obtained above to the description of bulk nuclear matter quantities starts from taking the expressions of P and ε in the zero-temperature limit (as presented in Appendix A) and for symmetric matter, see Eqs. (184), (188), (185) and (189). So, the coupling parameters of the PPM

Table 7 – Symmetric nuclear matter properties at saturation density n_0 (in fm^{-3}). The other quantities are in MeV.

Set	n_0	$\mathcal{E}_0$	K_0	Q_0	$\mathcal{S}_0$	L_0
PPM-1	0.147	-16.50	360.87	-453.85	30.02	75.31
PPM-2	0.147	-16.50	360.87	-453.85	30.08	75.89
PPM-3	0.155	-16.43	374.64	-532.25	30.45	75.87
PPM-4	0.148	-15.60	360.84	-502.12	30.01	75.12
PPM-5	0.148	-15.60	360.84	-502.12	30.07	75.69
PPM-6	0.157	-15.56	375.66	-326.77	30.75	75.71
PPM-7	0.148	-15.78	278.84	-374.25	30.18	75.69
PPM-8	0.159	-16.42	332.25	-423.31	34.93	99.80

Table 8 – Symmetric nuclear matter properties at saturation density n_0. The units are the same as in Table 7.

Set	n_0	$\mathcal{E}_0$	$\mathcal{S}_0$
PPMM-1	0.169	-15.74	31.61
PPMM-2	0.167	-15.41	32.12
PPMM-3	0.169	-16.21	31.74

(Eq. (86)) and PPMM (Eq. (90)) models were fitted from symmetric nuclear matter properties at saturation density presented in Chapter 1. The cutoff Λ is determined from a given choice of G_s and $m_{p,n}$ by imposing the effective mass observed in vacuum to be the nucleon mass, i.e., M = 939 MeV. This procedure is redone for the PPMM model, where the G_s and cutoff previously obtained is applied to set the bare mass of the Λ hyperon (m_Λ) to reproduce M_Λ = 1115 MeV. In this work, the parameter sets were investigated through a brute-force search in order to find parameterizations that reproduce nuclear matter theoretical/experimental constraints. The acceptable range of bulk nuclear matter quantities values used in this first investigation was slightly broader than the suggested by [53, 52], and are explicitly given by $-17 \leq \mathcal{E}_0 \leq -15$, $200 \leq K_0 \leq 380$, $-1200 \leq Q_0 \leq -200$, $30 \leq \mathcal{S}_0 \leq 35$ and $40 \leq L_0 \leq 76$ (all quantities given in MeV).

Table 5 shows all approved parameter sets found to the PPM model, the set PPM-8 do not satisfy the constraint of the symmetry energy slope L_0, but was included in order to allow comparisons with chirally symmetric (m = 0) models for quark matter. Table 7 gives the symmetric nuclear matter properties for these PPM model parameterizations. This first investigation failed to find parameter sets capable to fulfill all the desired constraints for the PPMM model, Table 6 shows some representative parameterizations that satisfy only the constraints in $\mathcal{E}_0$ and $\mathcal{S}_0$, whose respective values are given in Table 8. For this model, only very stiff EoS were found during the parameter search, with K_0 always exceeding 1500 MeV. Figures 34-36 show the behavior of the more important quantities discussed here, illustrating the effects of the parameter set choices or, in a given parameterization, taking different particle populations.

The symmetry energy curve given by equation ((27)) is illustrated in Figure 37, as well as two approximations of its value following equation ((32)), for the parameter set PPM-7. Notice that high order symmetry energies seem to be more significant in higher densities.

The symmetry energy curve given by equation ((27)) is illustrated in Figure 37, as well as two approximations of its value following equation ((32)), for the parameter set PPM-7. Notice that high order symmetry energies seem to be more significant in higher densities.

It is important to stress the results shown here are preliminary, and a more refined search of parameterizations must be performed in future works. In particular, we intend to understand better the consequences of the crossed coupling terms and the algebra $SU(3)$ in the PPMM model that, e.g., make the effective mass of the Λ hyperon dependent of the asymmetry between p and n, due to the term G_{sp} in ((92)). After that, a more refined search of parameterizations must be performed in future works, as well as the inclusion of temperature and eventually, magnetic field.

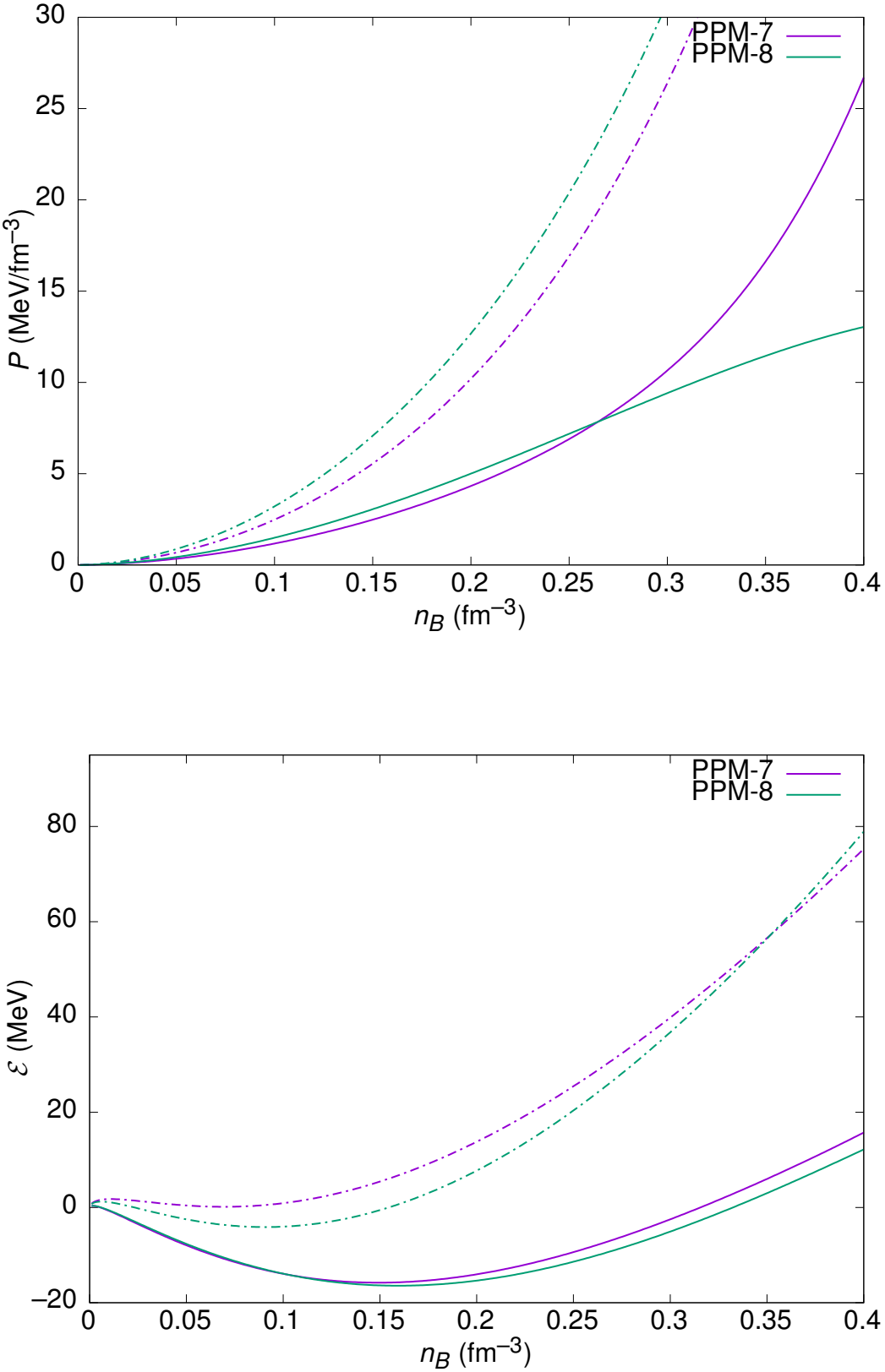

Figure 34 – Pressure (above) and binding energy (below) versus baryonic density for symmetric (solid line) and pure neutron (dashed line) matters in different PPM parameterizations, for $T = 0$.

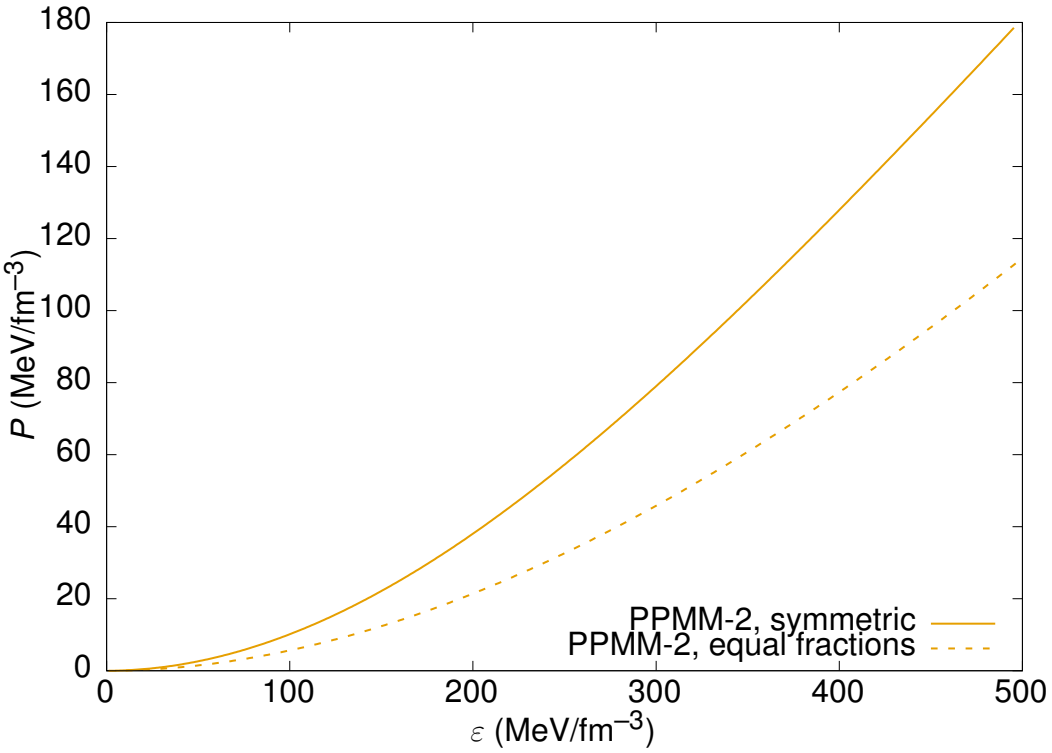

Figure 35 – Pressure versus energy density for symmetric ($n_p = n_n = n_B/2$, solid line) and equal particle fractions ($n_p = n_n = n_\Lambda = n_B/3$, dashed line) matters in PPMM, for $T = 0$.

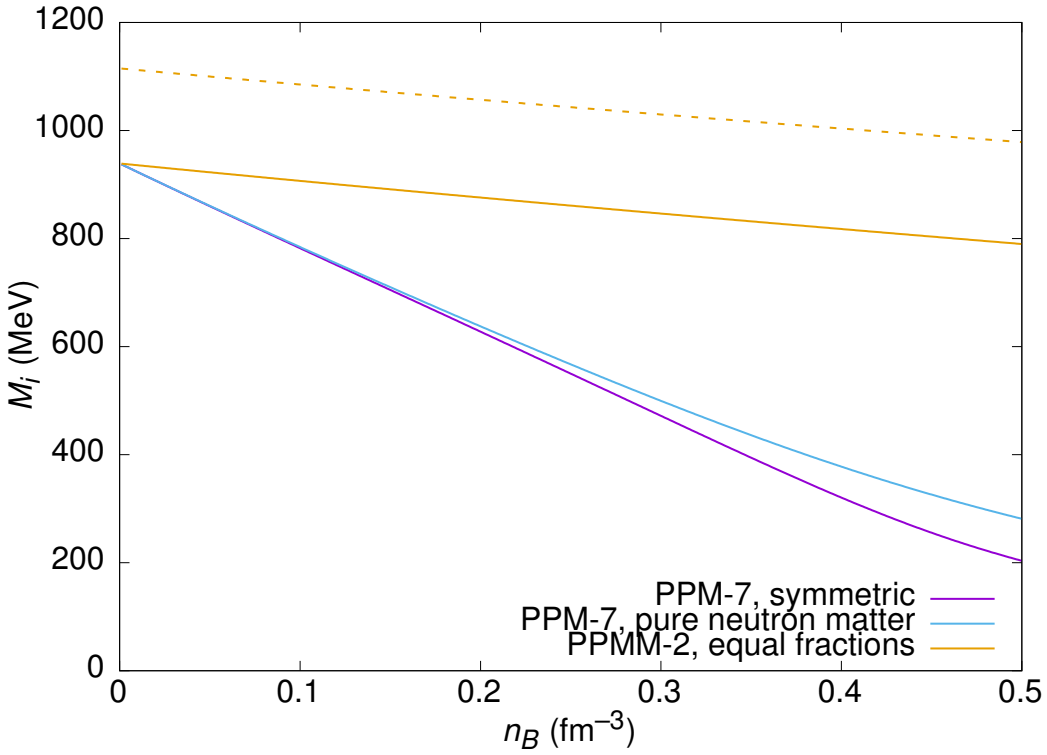

Figure 36 – Constituent hadron masses at $T = 0$ as a function of baryon number density in PPM and PPMM models, for symmetric ($n_p = n_n = n_B/2$), pure neutron ($n_n = n_B$) and equal particle fractions ($n_p = n_n = n_\Lambda = n_B/3$) matters. Solid and dashed lines represent nucleons and the Λ hyperon, respectively.

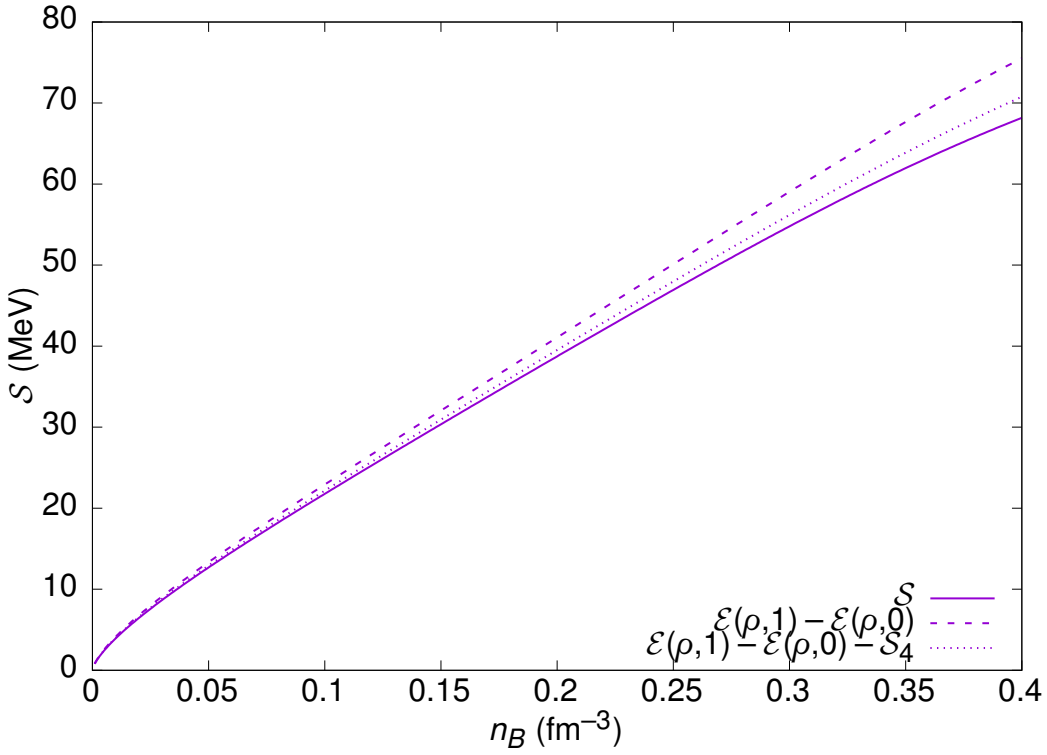

Figure 37 – Symmetry energy versus baryonic density, from its exact (Eq. (27)) and approximate expressions (Eq. (32)), for parameter set PPM-7 at $T = 0$.

5 QCD PHASE DIAGRAM IN THE NJL MODEL FRAMEWORK

This part of the work aims to study the QCD phase transition taking a two-model approach to describe hadron and free quark matters, but using, for the first time, chiral symmetric NJL-type models for both EoS. The two EoS formalism has been applied to the study of the hadron-quark phase transition in several studies of the QCD phase diagram. In [26] and [121], the hadron-quark phase transition was investigated with the help of two different models, namely, the non-linear Walecka model (NLWM) for the hadronic phase and the MIT bag model for the quark phase. A formalism understood as a more adequate one was used in [149, 150, 184] at zero temperature and by [103] for finite temperatures, all considering NJL-type models for the two phases. This formalism, which is also developed in this work, is arguably more adequate, because the effective models employed here allow to describe chiral symmetry in both hadronic and quark phases, which is demanded to take seriously the appearance of the quarkyonic phase. It is argued that the phase transition in QCD can take place in two different steps at low temperatures, first by the (partial) restoration of the chiral symmetry where chromodynamic matter is still confined, giving rise to the so-called quarkyonic phase [124], and only then by the deconfinement phase transition.

5.1 FORMALISM

The Nambu–Jona-Lasinio model does not reproduce the confinement of quarks expected from the quantum chromodynamics. There are models that emulate this feature, as the well-known *MIT bag model* (from Massachusetts Institute of Technology) [32], but versions of the NJL model can be interpreted as an schematic quark model for many situations where chiral symmetry breaking/restoration is the relevant feature of QCD, as in the aforementioned understanding of the pseudo-Goldstone nature of pions and in the description of interacting but deconfined quark matter (i.e., the QGP). In this section, the formalism that allows the thermodynamical description of free quark matter is obtained within the NJL model framework, for two and three quark flavors and in a mean-field (Hartree) level, following [20].

The NJL Lagrangian ((75)) can be extended by the inclusion of a vector-isoscalar interaction term, such that, considering two quark flavor fields $\psi = \begin{bmatrix}\psi_u & \psi_d\end{bmatrix}^T$, assumes the form

$$\mathcal{L} = \bar{\psi}(i\partial\!\!\!/ - \hat{m})\psi + G_S[(\bar{\psi}\psi)^2 + (\bar{\psi} i\gamma_5 \vec{\tau}\psi)^2] - G_V(\bar{\psi}\gamma^\mu\psi)^2, \tag{95}$$

where $\hat{m} = \mathrm{diag}(m_u, m_d)$ is the quark bare masses (here the isospin symmetry is assumed in the Lagrangian level, i.e., $m_u = m_d$), $\vec{\tau}$ is the Pauli isospin matrix, and G_S and G_V are the coupling constants. Both scalar and pseudoscalar (proportional to G_S), and vector-isoscalar (proportional to G_V) terms are symmetric in the chiral limit, meaning that Lagrangian ((95)) exhibits a $SU(2)$ flavor symmetry [159]. Other terms, e.g.

Table 9 – Parameter sets for the NJL Lagrangian density ((95)). M is the constituent mass at zero temperature and chemical potential [22, 20, 25].

Set	Λ (MeV)	G_S (fm^2)	G_V (fm^2)	m (MeV)	M (MeV)
Buballa$_1$	650	0.19721	0	0	313
Buballa$_2$	600	0.26498	0	0	400
Buballa$_{\text{R-2}}$	587.9	0.27449	$\propto G_S$	5.6	400
PCP$_{SU(2)}$	648	0.19565	$\propto G_S$	5.1	312.6

an isovector term, could be added as well, but they would not contribute at mean-field level with just one chemical potential for u and d quarks. As previously discussed, G_S, m and Λ are fitted by the pion mass m_π = 135.0 MeV and its decay constant f_π = 92.4 MeV. Table 9 shows four possible parameter sets usually considered in the literature.

The grand-canonical thermodynamic potential per volume V at temperature T can be obtained from the Lagrangian of the system through overall procedure discussed in the Appendix A, which essentially demands the knowledge of the quantity $\mathcal{L} + \mu\psi^\dagger\psi$. In the mean-field level, Lagrangian ((95)) can be rewritten again through the bosonization of the model, so it is straightforward to write

$$\begin{aligned}\mathcal{L} + \mu\psi^\dagger\psi &= \bar{\psi}\left(i\partial\!\!\!/ - m + 2G_S\rho_S\right)\psi + \left(\mu - 2G_V n_B\right)\psi^\dagger\psi - G_S\rho_S^2 - G_V n_B^2 \\ &= \bar{\psi}\left(i\partial\!\!\!/ - M\right)\psi + \tilde{\mu}\,\psi^\dagger\psi - \frac{(M-m)^2}{4G_S} - \frac{(\mu-\tilde{\mu})^2}{4G_V},\end{aligned} \tag{96}$$

where the constituent mass and renormalized chemical potential were introduced, respectively,

$$M = m - 2G_S\rho_S \quad \text{and} \quad \tilde{\mu} = \mu - 2G_V n_B. \tag{97}$$

Equation ((96)) shows that, in the mean-field level, particles governed by the Lagrangian ((95)) behave as non-interacting particles with mass M subject to a chemical potential $\tilde{\mu}$, apart field-independent terms that give trivial contributions to the thermodynamic potential. Thus, from the contribution of the displaced free fermion gas, given by equation ((167)), and the trivial terms arising from ((96)), the thermodynamic potential is

$$\Omega(T,\mu;M,\tilde{\mu}) = \Omega_M(T,\tilde{\mu}) + \frac{(M-m)^2}{4G_S} - \frac{(\mu-\tilde{\mu})^2}{4G_V}, \tag{98}$$

with

$$\begin{aligned}\Omega_M(T,\tilde{\mu}) = -2N_f N_c \int \frac{d^3p}{(2\pi)^3} \Big\{ E_p &+ T\ln\left[1 + e^{-(E_p-\tilde{\mu})/T}\right] \\ &+ T\ln\left[1 + e^{-(E_p+\tilde{\mu})/T}\right]\Big\},\end{aligned} \tag{99}$$

as presented in Appendix A, where now $E_p = \sqrt{p^2 + M^2}$, and $N_f = 2$ and $N_c = 3$ standing for the number of flavors and colors, respectively.

From equations ((81)), ((83)) and ((97)), the coupled set of self-consistent equations for M and $\tilde{\mu}$ that generalizes the gap equation for non-zero temperature and chemical potential can be written as

$$M = m + 4N_f N_c G_s \int \frac{d^3p}{(2\pi)^3} \frac{M}{\sqrt{p^2 + M^2}} \left[1 - n_p(T,\tilde{\mu}) - \bar{n}_p(T,\tilde{\mu})\right] \tag{100}$$

and

$$\mu = \tilde{\mu} + 4N_f N_c G_v \int \frac{d^3p}{(2\pi)^3} \left[n(T,\tilde{\mu}) - \bar{n}(T,\tilde{\mu})\right], \tag{101}$$

which can be inverted to define $\tilde{\mu}$ as a function of μ. The previous equations can also be obtained by requiring a thermodynamically consistent treatment, which demands the relations $\partial\Omega/\partial\tilde{\mu} = 0$ and $\partial\Omega/\partial M = 0$, that result in equations ((100))–((101)).

A constant term in the thermodynamic potential has no physical meaning, so an irrelevant constant can be chosen such that the thermodynamic potential is zero at $M = M_{\text{vac}}$, minimizing Ω at $T = \tilde{\mu} = 0$. This process may be represented by taking $\Omega_{\text{vac}} = \Omega(0,0; M_{\text{vac}}, 0)$ such that

$$\widetilde{\Omega}(T,\mu; M,\tilde{\mu}) = \Omega(T,\mu; M,\tilde{\mu}) - \Omega_{\text{vac}}. \tag{102}$$

The constituent mass at zero temperature and chemical potential M_{vac} can be obtained by taking the limits $T \to 0$ and $\mu \to 0$ in equation ((98)),

$$\Omega(0,0; M, 0) = -2N_f N_c \int \frac{d^3p}{(2\pi)^3} E_p + \frac{(M-m)^2}{4G_s}, \tag{103}$$

and solving for $\Omega(0,0; M_{\text{vac}}, 0) = 0$. From these results for the grand-canonical potential, other thermodynamic quantities can be obtained in the standard way (see Appendix A).

The importance of the vector channel G_v can be highlighted by some later considerations.The mathematical formalism of the vector interaction shows that it acts similarly to the ω meson in quantum hadrodynamical models [52], creating an additional repulsion between the particles, so stiffening the EoS. This effect is desirable once it has significant consequences to astrophysical applications of this results, such as allowing the description of more massive neutron stars. Also, the vector term weakens and delays the phase transition of the chiral restoration, and potentially makes the first order transition between the chiral and CFL phases become weaker, leading to the existence of the coexisting phase in which both the chiral and color-gauge symmetry are dynamically broken in a wider range of the density and temperature [92]. Also, as the additional term in ((98)) vanishes at zero chemical potential, there is no vacuum correction consequences due to the value of the coupling constant G_v. So, in principle, this parameter can be almost arbitrarily chosen, allowing to write it as $G_v = xG_s$. However, in order to obtain feasible physical results, it is desirable to constrain the values that the vector channel can take. From astrophysical considerations, [79] suggests that the free

parameter x can vary in the range $0 \leq x \leq 1$. Narrower ranges are proposed from direct comparisons with LQCD results in [92] and [91], the first establishing $0.2 \leq x \leq 0.3$ by studying the interplay between the chiral and color-gauge symmetry, and the latter setting $0.25 \leq x \leq 0.4$ through the fitting of LQCD pseudo-critical temperature. Yet, [176] suggests the very restrictive choice of $x = 0.33$. Furthermore, these constraints shall be taken into account during the discussion of results, and the parameterization choice will be written as, e.g., $\text{PCP}_{SU(2)}$-0.1, which reads as the $\text{PCP}_{SU(2)}$ parameter set taken with $x = 0.1$.

To consider asymmetric matter is important to properly describe many relevant situations found in nature. Up to this point, the isospin symmetry was assumed in the Lagrangian level and the same chemical potential was taken for both flavors of quarks. But, when generalizing the above results for the explicitly broken isospin symmetry ($m_u \neq m_d$) and different flavor fractions ($n_u \neq n_d$), the existence of two generally different quark condensates must be assumed, i.e., $\langle\bar{\psi}_u\psi_u\rangle \neq \langle\bar{\psi}_d\psi_d\rangle$ such that

$$\rho_{si} = \langle\bar{\psi}_i\psi_i\rangle \quad \text{and} \quad n_i = \langle\psi_i^\dagger\psi_i\rangle, \qquad i = u,d, \tag{104}$$

and the total scalar and number densities can be written as

$$\rho_s = \rho_{su} + \rho_{sd}, \tag{105}$$

$$n_B = n_u + n_d. \tag{106}$$

The mean-field thermodynamic potential can be straightforwardly obtained through the same arguments presented above, resulting in

$$\Omega(T,\{\mu_i\}) = \sum_{i=u,d} \Omega_{M_i}(T,\tilde{\mu}_i) + G_s\left(\rho_{su} + \rho_{sd}\right)^2 - G_v\left(n_u + n_d\right)^2, \tag{107}$$

where

$$\Omega_{M_i}(T,\tilde{\mu}_i) = -2N_c \int \frac{d^3p}{(2\pi)^3} \left\{ E_{p_i} + T\ln\left[1 + e^{-(E_{p_i}-\tilde{\mu}_i)/T}\right] + T\ln\left[1 + e^{-(E_{p_i}+\tilde{\mu}_i)/T}\right] \right\}, \tag{108}$$

with

$$M_i = m_i - 2G_s\left(\rho_{su} + \rho_{sd}\right), \tag{109}$$

$$\tilde{\mu}_i = \mu_i - 2G_v\left(n_u + n_d\right). \tag{110}$$

and $E_{p_i} = \sqrt{p^2 + M_i^2}$, for $i = u,d$. Setting a quark fraction $y_i = n_i/n_B$ allows to fix the chemical potentials during the solution of these equations for asymmetric matter, using

$$\rho_{si} = -2N_c \int \frac{d^3p}{(2\pi)^3} \frac{M_i}{\sqrt{p^2 + M_i^2}} \left[1 - n_p(T,\tilde{\mu}_i) - \bar{n}_p(T,\tilde{\mu}_i)\right] \tag{111}$$

and

$$n_i = 2N_c \int \frac{d^3p}{(2\pi)^3} \left[n_p(T,\tilde{\mu}_i) - \bar{n}_p(T,\tilde{\mu}_i) \right] . \tag{112}$$

It is relevant to notice that the *i*-flavor condensate, given by ((111)), depends only on the constituent mass of the same flavor, while the constituent mass for one flavor depends on both condensates, thus making both flavors coupled. Even so, in the isospin symmetric model ($m_u = m_d$), one has $M_u = M_d$ for any quark fractions considered.

The presence of the strange quark (s) in the description of free quark matter is relevant to many QCD phenomena taking place in the light quark sector. It is demanded when the Bodmer-Witten conjecture for the stability of quark matter [15, 196, 55] is considered, given that deconfined three-flavored quark matter (named *strange matter*) might be energetically favored as compared with the two-quark ordinary hadronic matter. It occurs because the inclusion of the *s* quark in the ordinary *u*-*d* matter represents a new degree of freedom for the Fermi seas of the particles, lowering the total binding energy of the system [192].

The NJL model version which incorporates the *s*-quark with the repulsive vector interaction is given by the Lagrangian density,

$$\begin{aligned} \mathcal{L}_{\mathrm{SU(3)}} = \bar{\psi} \left(i\partial\!\!\!/ - \hat{m} \right) \psi + G_S \sum_{a=0}^{8} [(\bar{\psi}\lambda_a\psi)^2 + (\bar{\psi} i\gamma_5 \lambda_a \psi)^2] - G_V (\bar{\psi}\gamma^\mu\psi)^2 \\ - K\{\det[\bar{\psi}(1+\gamma_5)\psi] + \det[\bar{\psi}(1-\gamma_5)\psi]\}, \end{aligned} \tag{113}$$

which is analogous to equation ((95)), where now ψ is the three-flavor quark field, $\psi = \begin{bmatrix} \psi_u & \psi_d & \psi_s \end{bmatrix}^T$, and $\hat{m} = \mathrm{diag}(m_u, m_d, m_s)$ is the quark bare masses, $\lambda_0 = \sqrt{2/3}\mathbb{1}$ and $\lambda_1, \ldots, \lambda_8$ are the $SU(3)$ flavor group generators (the so-called *Gell-Mann matrices*), and G_S, G_V and K are the coupling constants. Even assuming the isospin symmetry ($m_u = m_d$) in the Lagrangian level, m_s cannot be chosen equal to the non-strange quark mass in realistic calculations, thus making the $SU(3)$ symmetry explicitly broken.

The term proportional to K in ((113)) is known as *'t Hooft term*, and is a determinant in flavor space, i.e., for the $SU(3)$ case,

$$\det(\bar{\psi}\mathcal{O}\psi) = \sum_{i,j,k} \varepsilon_{ijk} (\bar{\psi}_u \mathcal{O} \psi_i)(\bar{\psi}_d \mathcal{O} \psi_j)(\bar{\psi}_s \mathcal{O} \psi_k), \tag{114}$$

where $i,j,k \in \{u,d,s\}$ and $\mathcal{O} = 1 \pm \gamma_5$. The 't Hooft interaction is chirally symmetric but breaks down the $U(1)_A$ symmetry otherwise left unbroken by the other interaction channels, thus emulating the relevant QCD feature of gluon-induced $U(1)_A$ anomalous symmetry breaking by employing a maximally flavor-mixing six-point interaction between quarks directly in the tree level of the NJL model. This term can be straightforwardly generalized to any number of flavors, and it is already included in the $SU(2)$ NJL Lagrangian ((95)) for a specific choice of K. As in the $SU(2)$ case, the free parameters

Table 10 – Parameter sets for the NJL Lagrangian density ((113)). m_i are the bare masses, and M_i are the constituent masses at zero temperature and chemical potential (in MeV) [80, 25].

Set	Λ (MeV)	G_S (fm^2)	G_V (fm^2)	K (fm^5)	$m_{u,d}$	m_s	$M_{u,d}$	M_s
RKH	602.3	0.19696	$\propto G_S$	0.04665	5.5	140.7	367.7	549.5
HK	631.4	0.17922	$\propto G_S$	0.02769	5.5	135.7	335.5	527
PCP$_{SU(3)}$	630.0	0.17472	$\propto G_S$	0.02800	5.5	135.7	312.2	508

of the model are fitted from properties of the pseudoscalar mesons, Table 10 shows four possible parameter sets usually considered in the literature, where again it is taken $G_V = xG_S$ as a free parameter.

The thermodynamic properties of the three-flavor NJL model given by Lagrangian ((113)) is obtained directly from the same procedure as the two-flavor case, just observing the inclusion of the six-point vertices the 't Hooft interaction, which means that there is an additional term involving two quark loops in the gap equation. The results of the previous section can then be generalized for this model, starting from three independent chemical potentials for the three flavors since the explicit breaking of the $SU(3)$ symmetry by the larger mass of the quark s. Then, the mean-field thermodynamic potential is given by

$$\Omega(T,\{\mu_i\}) = \sum_{i=u,d,s} \Omega_{M_i}(T,\tilde{\mu}_i) + 2G_S(\rho_{s_u}^2 + \rho_{s_d}^2 + \rho_{s_s}^2) - 2G_V\,(n_u + n_d + n_s)^2 - 4K\rho_{s_u}\rho_{s_d}\rho_{s_s}, \qquad (115)$$

where Ω_{M_i} is the same as given in equation ((108)), the densities ρ_{s_i} and n_i are still given by ((111)) and ((112)), respectively, and

$$M_i = m_i - 4G_S\rho_{s_i} + 2K\rho_{s_j}\rho_{s_k} \qquad (116)$$

$$\tilde{\mu}_i = \mu_i - 2G_V\,(n_u + n_d + n_s)\,, \qquad (117)$$

with $i \neq j \neq k$. Notice that there is a flavor mixing term in the mass gap equation, proportional to the coupling constant K, coupling explicitly the i-flavor quark constituent mass with all the other two condensates. However, that would not be true if the 't Hooft interaction were disregarded ($K = 0$), which would make the equation ((116)) no longer dependent of the other flavors, in contrast to the $SU(2)$ case (Eq. (109)). It is a consequence of the underlying algebra, reflected, e.g., in the shape of the scalar terms of the thermodynamic potentials ((107)) and ((115)). Also, since $m_s \approx 135$ MeV, the chiral limit might not be a good approximation to the model with realistic masses, so making the finite-mass effects much more pronounced here than in the two-flavor model.

A cautionary word about the absolute stability of free strange matter is, however, necessary. It is well known that the NJL model does not satisfy the Bodmer-Witten

Table 11 – Parameter sets for the eNJL thermodynamic potential ((120)). The units of G_a are fm^2, and of G_{ab} are fm^8. Λ and m are in MeV [142].

Set	G_s	G_v	G_{sv}	G_ρ	$G_{v\rho}$	$G_{s\rho}$	Λ	m
eNJL3$\sigma\rho$1	1.93	3.0	-1.8	0.0269	0	0.5	534.815	0
eNJL2m$\sigma\rho$1	1.078	1.955	-2.74	-0.1114	0	1	502.466	500

conjecture of absolutely stable deconfined quark matter [19]. However, the effects of a magnetic field or a small increase of temperature seem to be enough to guarantee that the strange matter acquires stability, as demonstrated by [44], and the Bodmer-Witten conjecture is considered here in this context.

The equations of state, i.e., pressure P and energy density ε, are easily obtained from the formalism discussed above in this chapter through the usual thermodynamic relations

$$P(T,\mu) = -\widetilde{\Omega}(T,\mu;M,\tilde{\mu}), \tag{118}$$

and

$$\varepsilon(T,\mu) = -P(T,\mu) + Ts(T,\mu) + \sum_i \mu_i n_i(T,\mu), \tag{119}$$

where $i = \{u,d\}$ or $i = \{u,d,s\}$ for the case of two or three quark flavors, respectively. The entropy density is $s = -\partial\Omega/\partial T$, given by the free fermion gas contribution alone (Eq. (170)), taken for particles of mass M_i subject to a chemical potential $\tilde{\mu}$. Employing the prescription of vacuum subtraction (Eq. (102)) also guarantees that P and ε vanish at zero temperature and density. The expressions to the zero temperature limit are derived in the Appendix A.

The model employed next to describe the hadronic matter, named here eNJL, is the original version proposed in [142], taken as a first version of the PPM model described in Chapter 4. The thermodynamic potential of the eNJL, at zero temperature, is given by

$$\Omega(0,\mu) = \varepsilon_{\rm kin} - \mu_p n_p - \mu_n n_n - G_s\rho_s^2 + G_v n_B^2 + G_\rho\rho_3^2 + G_{sv}\rho_s^2\rho^2 + G_{s\rho}\rho_s^2\rho_3^2 + G_{v\rho}n_B^2\rho_3^2, \tag{120}$$

and

$$M = m - 2G_s\rho_s + 2G_{sv}\rho_s n_B^2 + 2G_{s\rho}\rho_s\rho_3^2, \tag{121}$$

$$\mu_i = \tilde{\mu}_i + 2G_v n_B + 2G_{sv}n_B\rho_s^2 \pm 2G_\rho\rho_3 \pm 2G_{s\rho}\rho_3\rho_s^2 + 2G_{v\rho}(\rho_3^2 n_B \pm n_B^2\rho_3), \tag{122}$$

with the upper (lower) signs taken for $i = p$ ($i = n$) and all other variables are the same as presented in the PPM model discussion. Table 11, gives the eNJL model parameter sets obtained by [142] that are successful in describing all important nuclear and stellar constraints.

The vector contribution in the quark model has proved to make the quark EoS stiffer and may have important consequences on the structure of hybrid or pure quark

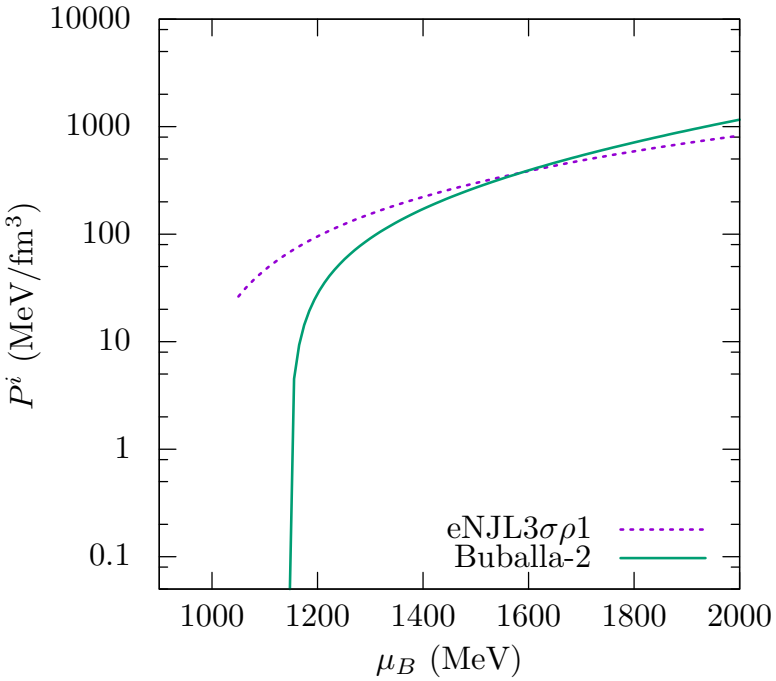

Figure 38 – Hadronic and quark matter pressures (i=H,Q) as functions of the baryonic chemical potential μ_B for symmetric matter.

Table 12 – Values of n_B and μ_B^i at the onset of chiral restoration for different NJL SU(2) and eNJL model parameterizations (i=H,Q).

Set	n_B (fm^{-3})	μ_B^i (MeV)
Buballa-1	0.27	941
Buballa-2	0.36	1035
PCP-0.0	0.29	1005
PCP-0.1	0.24	1011
PCP-0.2	0.20	1020
PCP-0.3	0.17	1032
PCP-0.4	0.17	1047
PCP-0.5	0.17	1059
eNJL3$\sigma\rho$1	1.0	1674
eNJL2$m\sigma\rho$1	1.0	1568

compact stars [94]. In particular, the inclusion of this term gives rise to larger star masses although with smaller quark cores in the case of hybrid stars.

5.2 HADRON-QUARK PHASE TRANSITION

Figure 38 displays the EoS of both phases for two specific choices of parameters. The discontinuities are related to the points where chiral symmetry is restored and the points where the pressure becomes negative are omitted. Table 12 shows, for each of the two flavor quark and hadronic parameterizations used in the present work, the density and chemical potential for which chiral symmetry is restored.

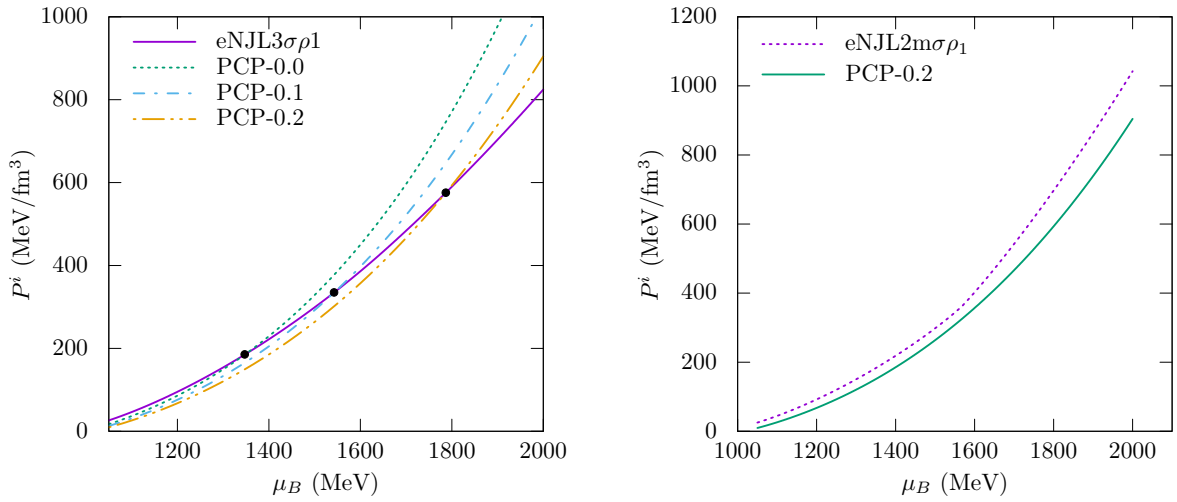

Figure 39 – Example of a combination of parameter sets for which hadron-quark phase transitions are (left) or are not (right) allowed to happen in symmetric matter.

The QCD phase diagram is characterized by potentially multiple phases, whose phase separation boundaries are referred as *binodals* [133]. Over those boundaries, the phases from the regions of either side of the boundary can coexist. The binodals may be determined using the Gibbs conditions [26],

$$\mu_B^Q = \mu_B^H, \qquad T^Q = T^H \qquad \text{and} \qquad P^Q = P^H, \tag{123}$$

where the indexes H and Q refer to the hadronic and quark phases. The chemical potentials are given by

$$\mu_B^H = \frac{\mu_p + \mu_n}{2} \qquad \text{and} \qquad \mu_B^Q = \frac{3}{2}(\mu_u + \mu_d) = 3\mu_q. \tag{124}$$

At a certain fixed temperature ($T = 0$ in the present context), the phase coexistence condition may be obtained by plotting $P^i \times \mu_B^i$, $i = Q, H$, and looking for the intersection of both curves. See the left panel of Figure 39 for an example, where the hadron pressure given by the eNJL3$\sigma\rho$1 parameterization is plotted together with the quark pressure given by the PCP parameterization of the NJL model for several choices of the vector interaction strength x such the coexistence of the hadron and the quark phases occurs, allowing the phase transition to happen. Otherwise, the absence of intersections imply that there are no phase transitions allowed between the phases considered within a specific pair of models, as shown in the right panel of Figure 39, where the hadronic matter is always more stable. The existence of a hadron-quark phase transition depends on both the quark matter and hadronic matter EoS: the same quark matter EoS, PCP-0.2, that predicts a phase coexistence with one hadronic EoS (eNJL3$\sigma\rho$1) ceases to predict with a different one.

The value of chemical potential μ_B^i for which the phase transition takes place for all combinations of parameter sets given in Tables 9 and 11 are determined, still

restricting the treatment of the hadron phase to symmetric matter due to the fact that here the quark phase is taken with equal fractions of u and d particles. This reflects the fact that both particles are assumed to have the same bare masses and the same chemical potentials. The results so obtained are displayed in Table 13. In particular one may note that no combinations involving the BuballaR-2 set with $G_V \neq 0$ give rise to a phase transition. It should be pointed out the large differences among the chemical potential and density at the hadron-quark transition predicted by the models considered. Compatibility constraints between the hadronic and quark model should be imposed when describing the hadron-quark phase transition within a two-model description, which may reduce the phase transition uncertainties. In the present study, chiral symmetry is present in both the hadron and quark model. Several compatibility constraints could be considered: i) the quark phase should not be in a chiral broken phase at deconfinement if the hadronic phase is already in a chiral symmetric phase. This condition is fulfilled for all cases discussed above. ii) a more restrictive constraint would be that at deconfinement the hadron and the quark phase have the same chiral symmetry. From Tables 12 and 13, one may conclude that for symmetric matter only quark models that predict a deconfinement chemical potential above 1674 (1568) MeV are compatible with eNJL3$\sigma\rho$1 (eNJL2m$\sigma\rho$1). i.e. Buballa-2, Buballa-R2, and PCP-0.2; iii) however, one may also interpret that the deconfinement coincides with chiral symmetry restoration. Moreover, in fact the eNJL2m$\sigma\rho$1 model has no chiral symmetric phase because this is a model with a term breaking explicitly the chiral symmetry, and the chemical potential indicated corresponds to half the vacuum mass. In this scenario the mixed phase between a pure hadronic and a pure quark matter phase would be constituted by clusters of non-chiral symmetric hadronic matter in a background of chiral symmetric quark matter, or the other way around; iv) for asymmetric matter the possible scenarios are much more complex because two or more conserved charges may be considered, and the restoration of chiral symmetry will occur at different baryonic densities or chemical potentials for different species. In the following, the discussion is based on interpretation iii).

As stated, the aim of this part of the work is to obtain the QCD phase diagram with both hadronic and quark models based on the same underlying formalism, i.e., within different versions of the NJL model. The study of the hadron-quark phase transition at zero temperature and for symmetric matter is the first step, but the inclusion of asymmetry, strangeness, temperature and eventually, magnetic field will be performed.

5.3 APPLICATION: METASTABLE STARS

In order to describe compact star matter, leptons are included and electric charge neutrality and chemical equilibrium must be taken enforced. Leptons are introduced in the system by adding them in the model Lagrangian density as a free fermionic

Table 13 – Chemical potential, pressure, and barionic density at the coexistence point for different parameterization combinations in symmetric matter. n_B refers to the hadronic phase. For BuballaR-2, in this table, $G_V = 0$ and eNJL2m$\sigma\rho$1 presents no chiral symmetric phase (see the text for details).

NJL SU(2)	eNJL	μ_B (MeV)	P (MeV/fm^3)	n_B (fm^{-3})
Buballa-2	eNJL2m$\sigma\rho$1	1674	504	1.420
	eNJL3$\sigma\rho$1	1567	356	0.812
BuballaR-2	eNJL2m$\sigma\rho$1	1729	586	1.497
	eNJL3$\sigma\rho$1	1585	373	0.839
PCP-0.0	eNJL2m$\sigma\rho$1	1312	158	0.506
	eNJL3$\sigma\rho$1	1348	185	0.553
PCP-0.1	eNJL3$\sigma\rho$1	1544	336	0.780
PCP-0.2	eNJL3$\sigma\rho$1	1787	576	1.088

Lagrangian, i.e.,

$$\mathcal{L} = \bar{\psi}_l(i\partial\!\!\!/ - m_l)\psi_l, \tag{125}$$

where l refers to the leptons, and unless stated otherwise, electrons and muons are considered, whose masses are, respectively, 0.511 MeV and 105.66 MeV. Thus, the following constraints on chemical potential and baryonic number density have to be imposed for hadronic star matter

$$\mu_n = \mu_p + \mu_e, \tag{126}$$

$$n_p = n_e + n_\mu, \tag{127}$$

and, similarly, for quark star matter,

$$\mu_s = \mu_d = \mu_u + \mu_e, \tag{128}$$

$$n_e + n_\mu = \frac{1}{3}(2n_u - n_d - n_s). \tag{129}$$

In both cases, $\mu_e = \mu_\mu$. This is the same discussion already made in the first part of the work, when stellar matter was discussed in the context of RMF models. The difference is that now there are no hyperons or deltas.

To study the possibility of a hadron-quark phase transition to take place in the interior of compact stars, it is considered in the description of hadronic stars the EoS obtained from the eNJL model, presented above, with β-equilibrium and electric charge neutrality enforced. As for the quark matter, the EoS discussed above are employed to describe deconfined quark star matter, also imposing β-equilibrium and electric charge neutrality. During the hadron-quark phase transition process, the composition of quark matter is not expected to be β-stable [21]. However, as the main interest here is the energetical content of the final quark or hybrid star, this intermediate stage is disregarded next.

Figure 40 shows the quark matter EoS for some parameter choices, from where one can see the hardening effect of the vector interaction in both situations, the same

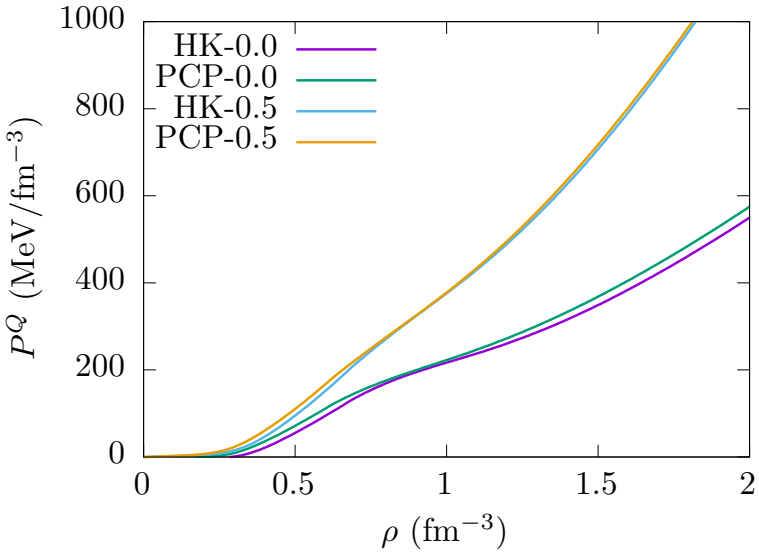

Figure 40 – Pressure versus baryonic density for NJL SU(3) parameterizations with different values of x. β-equilibrium and electric charge neutrality are enforced.

well known effect encountered in the SU(2) model for hadronic matter without equilibrium conditions [125]. The small bumps present in Figure 40 are a characteristic of the chiral symmetry restoration associated with the *s* quarks. Moreover, at large densities, after the total restoration of the chiral symmetry, the densities of the three quarks are the same (1/3 of the total baryonic number density each).

In the same way as previously shown, the transition pressure and chemical potential which satisfy the Gibbs conditions are obtained, now enforcing β-equilibrium and charge neutrality within both phases. In stellar matter, the baryonic and quark chemical potentials are usually defined in terms of the EoS variables as

$$\mu_B^H = \frac{\varepsilon_H + P_H}{n_B}, \qquad \mu_B^Q = \frac{\varepsilon_Q + P_Q}{n_B}, \tag{130}$$

taking $T = 0$. The results obtained for the coexistence points of hadron and quark stellar matter are displayed in Table 14. From it, one can see that the effect of the vector interaction on the phase transition is a displacement of the phase transition point towards higher pressures and higher chemical potentials.

Three diferent internal structures are next considered for the compact star families: (i) hadronic stars modeled by the eNJL equations of state; (ii) bare quark stars modeled by the NJL SU(3) EoS; and (iii) hybrid stars, constituted by hadronic matter in its outer region and deconfined quark matter in the center. The equation of state for hybrid stars is built from the hadronic and quark EoS by performing a Maxwell construction. This method might seem naive since charge neutrality is imposed only locally and results in the fact that the leptonic chemical potential suffers a discontinuity. But, as the aim is to study the macroscopic properties and the energetical content of the compact

Table 14 – Chemical potential and pressure at the coexistence point for different parameterization combinations for hadronic and three flavor quark stellar matter with equilibrium conditions enforced.

NJL SU(3)	eNJL	μ_0 (MeV)	P_0 (MeV/fm^3)
HK-0.0	eNJL2m$\sigma\rho$1	1399	196
HK-0.1	eNJL2m$\sigma\rho$1	1529	297
HK-0.2	eNJL2m$\sigma\rho$1	1710	482
HK-0.3	eNJL2m$\sigma\rho$1	2122	1144
HK-0.0	eNJL3$\sigma\rho$1	1349	154
HK-0.1	eNJL3$\sigma\rho$1	1462	227
HK-0.2	eNJL3$\sigma\rho$1	1579	313
HK-0.3	eNJL3$\sigma\rho$1	1709	422
HK-0.4	eNJL3$\sigma\rho$1	1863	571
PCP-0.0	eNJL2m$\sigma\rho$1	1209	83
PCP-0.1	eNJL2m$\sigma\rho$1	1420	211
PCP-0.2	eNJL2m$\sigma\rho$1	1594	356
PCP-0.0	eNJL3$\sigma\rho$1	1170	64
PCP-0.1	eNJL3$\sigma\rho$1	1328	143
PCP-0.2	eNJL3$\sigma\rho$1	1481	239
PCP-0.3	eNJL3$\sigma\rho$1	1617	344
PCP-0.4	eNJL3$\sigma\rho$1	1768	477
PCP-0.5	eNJL3$\sigma\rho$1	1949	663

stars, this construction suffices as shown in [145]. The BPS EoS [12] is also included to the hadronic matter results to account for the description of the low-density matter in the hadronic and hybrid stars outer crusts.

The family of possible compact stars are straightforwardly obtained by using the equations of state as input to the Tolman-Oppenheimer-Volkoff (TOV) equations for the relativistic hydrostatic equilibrium. To solve the TOV equations one needs to impose boundary conditions given by $P(R) = 0$ and $P(0) = P_c$, where R is the star radius and P_c is the central pressure. In the following, $M(R)$ and $M_B(R)$ are respectively the total gravitational and total baryonic masses.

In the following, the conversion mechanism of hadronic to hybrid stars is investigated. Similar analysis already exist in the literature [107, 145], but models based on the same underlying field theory class in both hadron and quark phases were never considered. If a compact star consisting only of hadrons and leptons in β-equilibrium, electrically neutral and with no fraction of deconfined quark matter, sustains a central pressure P_C larger than the coexistence pressure of the hadron and quark phases, i.e. P_0, the hadronic star is said to be metastable to conversion to a quark or hybrid star [121]. The possibility of the conversion depends on the values of the hadronic star central pressure, P_C, and the pressure that satisfies the condition of phase coexistence,

Table 15 – Stellar macroscopic properties obtained with the two eNJL parameterizations. The first set of values refers to the maximum mass star and the later to the canonical star.

	eNJL2m$\sigma\rho$1	eNJL3$\sigma\rho$1
M_{max} ($M_\odot$)	2.02	2.19
M_B ($M_\odot$)	2.33	2.56
R (km)	11.19	11.37
$C_{M_{\text{max}}}$ ($M_\odot$/km)	0.180	0.192
n_C (fm^{-3})	0.981	0.966
μ_C (MeV)	1623	1781
P_C (MeV/fm^3)	363	489
$R_{1.4M_\odot}$ (km)	12.20	12.94
$C_{1.4M_\odot}$ (km/$M_\odot$)	0.114	0.108

P_0, for a given pair of EoS obtained from the respective models.

Table 15 shows some basic properties of hadronic stars modeled with the parameterizations of the eNJL model discussed, for stars with the maximum mass and for canonical stars with $M = 1.4\ M_\odot$. Two of these results are of special relevance following recent observational and theoretical advances, namely the radius of the canonical neutron star ($R_{1.4M_\odot}$) and the compactness of the maximum mass and the canonical star ($C_{M_{\text{max}}}$ and $C_{1.4M_\odot}$), defined as the ratio between masses and radii of the respective compact stars. Both properties have been extensively discussed in the recent literature [108, 120]. Different hypotheses lead to predictions of the radii of the canonical neutron star varying from 9.7-13.9 km to 10.4-12.9 km [172] and from 10.1 to 11.1 km [141]. The results shown for the radii are not compatible with the predictions of very small radii of [141] but lie within the other two constraints, as also obtained in [120] for a very large number of models.

Similarly, properties of maximum mass configuration of quark and hybrid stars for some parameter choices are shown in Table 16. It is worth noticing that larger vector interaction parameters in the quark matter model result in more massive hybrid stars with smaller quark cores, reflecting the stiffening of the EoS discussed in [125]. Indeed, following the effect of the vector interaction in the displacement of the phase transition point to higher pressures, as P_0 approaches the maximum P_C of the metastable star family, the deconfined quark matter core is possible only inside the most massive stars. As a result, the TOV stable solutions for hadronic and hybrid EoS differ only for a narrow set of stars where the condition $P_C \geq P_0$ is fulfilled. The compactness of both pure hadronic and hybrid canonical star are close to the one recently measured for an isolated neutron star as being equal to 0.105 ± 0.002 [78].

Moreover, one can see that the central pressures P_C of the hadronic stars are

Table 16 – Stellar macroscopic properties of quark and hybrid stars, obtained with some different EoS parameterizations for the phases. The first set of values refers to the maximum mass star and the second to the canonical star. For the hybrid stars, n_H and n_Q denote the densities of the metastable and quark matter at the phase coexistence point, and $M_{H\text{-}Q}$ denotes the gravitational mass of the less massive star that sustains a deconfined quark core. The units are the same as the Table 15.

		Quark Star			Hybrid Star					
					eNJL2m$\sigma\rho$1		eNJL3$\sigma\rho$1			
	PCP-x:	0.0	0.2	0.5	0.0	0.2	0.0	0.1	0.2	0.4
Properties	M_{max}	1.63	1.79	1.97	1.80	2.02	1.63	1.97	2.18	2.19
	M_B	1.81	1.97	2.15	2.03	2.33	1.81	2.25	2.55	2.57
	R	9.90	10.19	10.79	11.60	11.23	12.02	12.25	12.13	11.39
	$C_{M_{\text{max}}}$	0.164	0.175	0.182	0.155	0.179	0.135	0.160	0.179	0.192
	n_C	1.035	0.995	0.915	0.910	1.084	1.021	0.834	0.820	1.118
	μ_C	1408	1527	1667	1380	1594	1408	1408	1481	1768
	P_C	230	283	332	202	356	227	205	239	477
	$R_{1.4M_\odot}$	10.00	10.43	11.05	12.20	12.20	12.94	12.94	12.94	12.94
	$C_{1.4M_\odot}$	0.140	0.134	0.126	0.114	0.114	0.108	0.108	0.108	0.108
	n_H				0.487	0.979	0.421	0.564	0.700	0.955
	n_Q				0.527	1.185	0.477	0.648	0.873	1.234
	$M_{H\text{-}Q}$				1.62	–	1.57	1.93	–	–

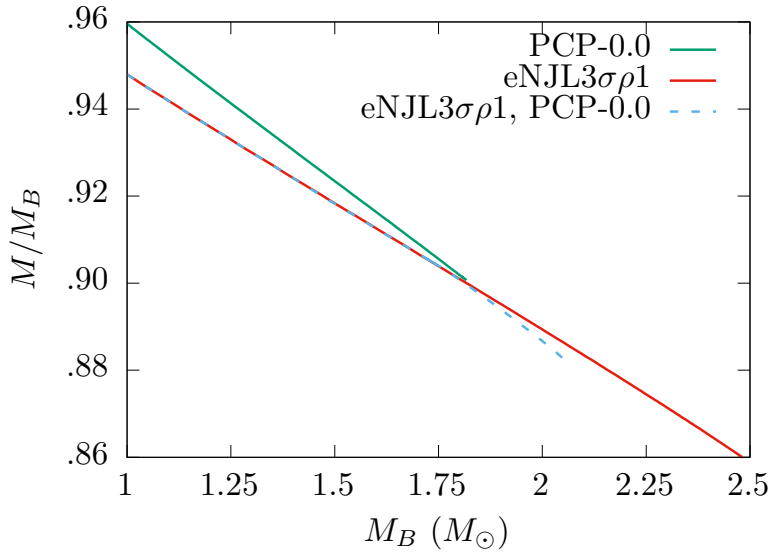

Figure 41 – Ratio between the gravitational and baryonic masses versus baryonic mass of hadronic, hybrid and quark stars, for diferent EoS parameterizations.

larger than some of the coexistence pressure values P_0, as shown in Table 14, notably for smaller values of the vector interaction parameter x in the quark matter modeling. This is the first condition that enables the conversion of a metastable neutron star into a quark or hybrid star. The other condition is that the gravitational mass of the initial metastable hadronic star must be bigger than the gravitational mass of the final star, either quark or hybrid star, for a given baryonic mass, so that the conversion can be exothermal in rest while respecting the baryonic number conservation [121]. Figure 41 illustrates the results by plotting the ratio between the gravitational and baryonic masses with respect to the baryonic mass, in a way that highlights the small differences between the curves while preserving the interpretation that the conversion is energetically allowed only if the final configuration is below the initial one for M_B fixed.

The gravitational masses of quark stars are bigger than the gravitational mass of the hadronic star with the same baryonic mass, which is already expected from previous results in literature, [e.g., 19]. Follows that the conversion of a hadronic star to a bare quark star is always energetically forbidden for the parameterizations considered in this work, even in cases where it would be allowed by the Gibbs thermodynamic condition. This feature can be better understood looking for some notable cases. For the PCP-0.5 case, which results in a quark star with P_C = 332 MeV/fm^3, one sees in Table 14 that the conversion is allowed by the Gibbs criteria only if the eNJL3$\sigma\rho$1 hadronic matter is used in the modeling of the metastable star. However, the coexistence pressure is much higher than the ones sustained by the compact stars described by each phase. This feature prevents the conversion to take place, since it would occur at constant P, i.e., both initial and final should sustain $P_C \geq P_0$. Taking the PCP-0.2 case, instead, the quark star sustains P_C = 283 MeV/fm^3, which allows a hadron-quark coexistence point with both hadronic matter parameterizations, as seen in Table 14. If the eNJL2m$\sigma\rho$1 hadronic matter is considered, one has P_C^H = 363 > P_0 = 356 > P_C^Q = 283 MeV/fm^3. It means that, despite the metastable hadronic star bulk is overpressured enough to allow the phase transition to the PCP-0.2 quark matter, there are not such final compact object constituted by the latter phase. The metastable star decays into a black hole or a hybrid star. In other words, this set fulfills the thermodynamic criteria but the astrophysical conditions do not allow the formation of a stable quark star. The last set to be analyzed is when the PCP-0.2 quark matter is compared with the eNJL3$\sigma\rho$1 hadronic matter. In this case P_C^H = 489 > P_0 = 239 MeV/fm^3 and P_C^Q = 283 > P_0 = 239 MeV/fm^3. The main imposition to the hadron-quark phase transition to take place inside metastable compact stars is to have $P_C \geq P_0$ for both stars, which is fulfilled by this choice of models. Nevertheless, a conversion process that preserves baryonic mass, requires that the final state has the same baryonic mass and a smaller gravitational mass. Since the quark star has a larger gravitational mass, the conversion is forbidden due to energy arguments.

A different situation occurs when hybrid stars are considered. In Figure 41, one can see the hybrid star family curve differs from the respective pure hadronic star family for stars with a central density above P_0, i.e., for hadronic metastable stars massive enough to sustain the conversion of their core from the hadronic matter to a deconfined quark matter bulk. It follows from previous results that the branches where the conversion is allowed are bigger for smaller values of the vector interaction parameter x in the quark matter modeling. In fact, one can only get a quark core for a low enough x value, which is 0.12 for nuclear matter model eNJL3$\sigma\rho$1 [143] and 0.1 for eNJL2m$\sigma\rho$1, as can be seen from table 16 by comparing the values of n_C with the values of n_Q. Stable stars are only possible if n_C is larger than n_Q and P_0 larger than P_C. Again, analysing the results shown in tables 14 and 16, one can see that in most cases these pressures are identical and a stable star with a quark core is not sustainable. Another feature worth noticing is that, even when the conversion from a hadronic to a hybrid star is allowed, the mass-energy difference of the initial and final objects are always small (a narrow gap of the order of 10^{-3}–10^{-2} $M_\odot$).

5.4 COMPARISON WITH THE VECTORIAL MIT MODEL

In this section we reproduce some results obtained with the Nambu–Jona-Lasinio (NJL) model to compare with the ones obtained in [111, 112] using the MIT bag model version on which both a vector field and a self-interacting term are introduced.

The MIT bag model considers that each baryon is composed of three non-interacting quarks inside a bag. The bag, in turn, corresponds to an infinity potential, which confines the quarks. In this simple model the quarks are free inside the bag and are forbidden to reach out. All the information about the strong force lies in the bag constant, also called the vacuum pressure. he MIT Lagrangian density reads

$$\mathcal{L} = \sum_{u,d,s} \{\bar{\psi}_q[i\gamma^\mu \partial_\mu - m_q]\psi_q - B\}\Theta(\bar{\psi}_q\psi_q), \tag{131}$$

where m_q is the q quark mass, ψ_q is the Dirac quark field, B is the constant vacuum pressure and $\Theta(\bar{\psi}_q\psi_q)$ is the Heaviside step function that is included to assure that the quarks exist only confined inside the bag.

A quark interaction described by a vector channel V_μ analogous to the ω meson in quantum hadrodynamics can be introduced via minimal coupling,

$$\mathcal{L}_V = \sum_{u,d,s} g_{qqV}\{\bar{\psi}_q[\gamma^\mu V_\mu]\psi_q\}\Theta(\bar{\psi}_q\psi_q), \tag{132}$$

as well as the mass term and a self-interaction on the vector field,

$$\mathcal{L}_V = \frac{1}{2}m_V^2 V_\mu V^\mu + b_4\frac{(g^2 V_\mu V^\mu)^2}{4} \tag{133}$$

where g_{qqV} is the coupling constant of the quark q with the vector field V^{μ}. There are two possibilities: an universal coupling with $g_{ssV} = g_{uuV} = g_{ddV}$, as well as a ratio that comes from symmetry group calculations [112]: $g_{ssV} = 2/5 \cdot g_{uuV} = 2/5 \cdot g_{ddV}$; m_V is the mass of the vector field, taken to be 780 MeV, b_4 is a dimensionless parameter to modulate the self-interaction of the vector field, and $g = g_{uuV}$ for short. As in our work g_{uuV} and g_{ddV} are always equal (and called only g for short), we define X_V as the ratio between g_{ssV} and g_{uuV}. Also, the strength of the vector channel is directly related to $(g/m_V)^2$, so we define G_V as this quantity:

$$X_V \doteq \frac{g_{ssV}}{g_{uuV}} \quad \text{and} \quad G_V \doteq \left(\frac{g}{m_V}\right)^2. \tag{134}$$

It is impossible to use a single bag pressure value to describe the whole energy spectrum with MIT-based models, so a possible prescription is to consider a temperature dependent bag model of the form

$$B(T) = B_0\left[1 + \left(\frac{T}{T_0}\right)^4\right]. \tag{135}$$

Although the simplest versions of the NJL model does not reproduce the asymptotic freedom behavior of QCD, and thus cannot describe the quark confinement/deconfinement transition, it can be interpreted as a schematic quark model for many situations where chiral symmetry breaking/restoration is one of the most relevant features of QCD [21]. Here the isospin symmetry is assumed in the Lagrangian level, i.e., $m_u = m_d = m$, and the situation of chemical equilibrium is considered, i.e., $\mu_u = \mu_d = \mu_q$, with $\mu_q = \mu/3$. The parameters G_S, m and Λ are fitted to reproduce the quark condensate value, the pion mass and its decay constant. In the following, we set $\Lambda = 590$ MeV, $G_S\Lambda^2 = 2.435$ and $m = 6.0$ MeV [21]. The parameter G_V is usually taken as a free parameter, whith some proposed constraints suggesting values between $0.25G_S$ and $0.5G_S$ [125]. We consider $0 \leq G_V/G_S \leq 0.5$.

The effective quark mass M is obtained solving the gap equations. This constituent mass is larger than the bare quark mass m at lower temperatures and/or densities, generating dynamically the larger particle mass expected in this region and breaking the chiral symmetry of the model. As the temperature or the density increase, M approaches the value of the current mass m, thus restorating the chiral symmetry. A chiral phase transiton $\mu - T$ diagram can be drawn determining the behavior of the thermodynamic potential minima with respect to M, for given chemical potentials. In the low temperature regime, several effective models predict a first order chiral phase transition to occur. Results from LQCD for the low chemical potential region, however, point to a crossover transition. These two seemingly contradictory pictures suggest that the first order transition line starting at $T = 0$ ends at a critical end point (CEP), from which it turns into a crossover [34, 35]. Figures 42 and 43 show that this behavior is reproduced

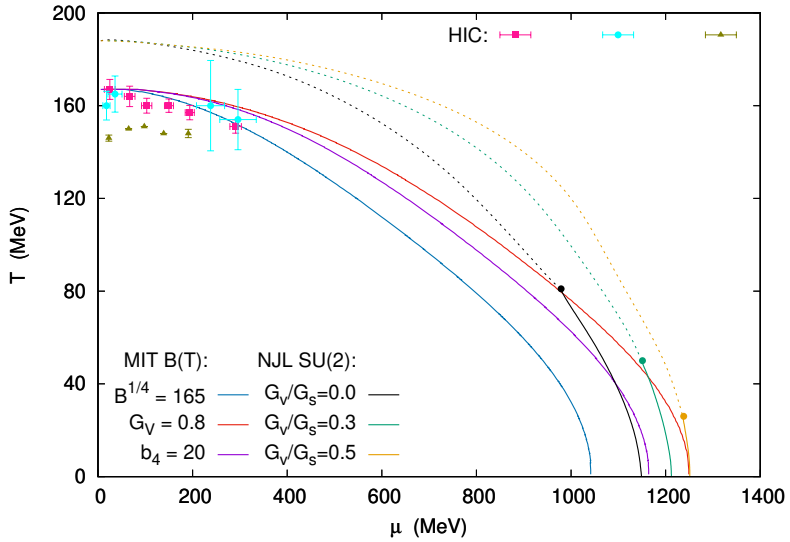

Figure 42 – QCD phase diagram for different values of G_V/G_S, from the SU(2) NJL model. A solid line represents a first order transition and a dashed line represents a crossover, the intersection is the CEP. Selected curves from the temperature dependent bag model are included for comparison, as well as some estimations of the chemical freeze-out parameters in heavy ion collisions [34, 109].

by the NJL model. Notice that, as the contribution associated to the vectorial coupling vanishes at zero chemical potential, there is no vacuum correction consequences due to the value of the coupling constant G_V. With the chosen parametrization, this model renders the crossover temperature at $\mu = 0$ being equal to 188 MeV, which is higher than the values obtained from previously discussed MIT-type model calculations, but also from the estimations of the chemical freeze-out parameters in heavy ion collisions and expected from LQCD results, as can be seen in Figs. 42 and 43. As stated above, the NJL model produces a first order phase transition for temperatures below the CEP, where it acquires a second order phase transition point, before the crossover region. Also, increasing the vector term weakens and delays the first order phase transition of the chiral restoration, favoring the crossover transition on the majority of the QCD phase diagram high temperature-low baryonic density part.

The purpose of the present section is to compare different model frameworks, and hence it is useful to display both two and three-flavored matter results obtained from the NJL-type models too. The extension of the NJL SU(2) to NJL SU(3) is not as straightforward as the inclusion of the *s* quark in the MIT-like models. Thus, we refer the interested reader to refs. [21]. The expressions for the grand-canonical potentials, the related gap equations and the chosen parametrizations are the same as in ref. [7], taking $\Lambda = 631.4$ MeV, $G_S\Lambda^2 = 1.835$, $K\Lambda^5 = 9.29$, $m_u = m_d = 5.5$ MeV and $m_s = 135.7$ MeV. The strange quark is largely responsible for shaping the phase diagram of QCD since its mass controls the nature of the chiral and deconfinement transitions.

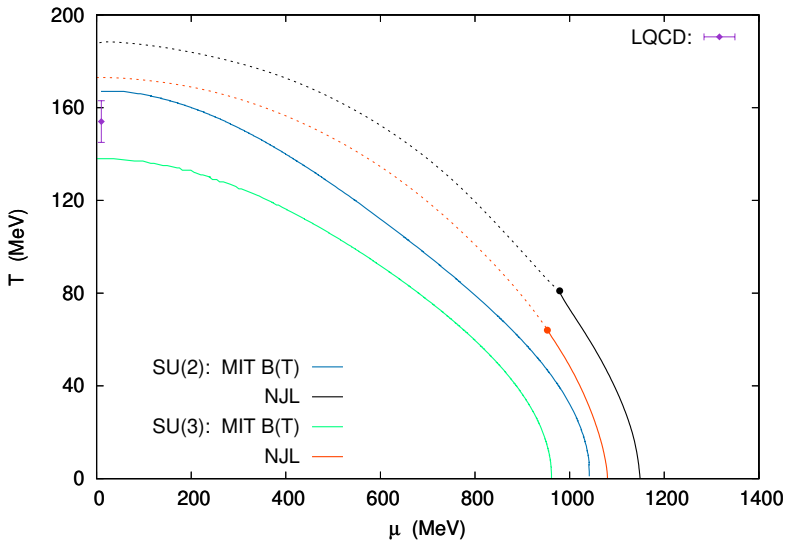

Figure 43 – QCD phase diagram for SU(2) and SU(3) NJL model (G_V/G_S = 0.0) [7] and temperature dependent bag model ($B^{1/4}$ = 165 MeV and G_V = 0). A solid line represents a first order transition and a dashed line represents a crossover, the intersection is the CEP. The LQCD predicted critical temperature for 2+1 quark flavors [13] is included for comparison.

Hence, to consider strangeness conservation without relying on the inclusion of β-stable matter, which, as discussed below, is justified only at the lower temperature range of the QCD phase transition diagram, we show the curves obtained with the same chemical potential for the three quarks, i.e., $\mu_u = \mu_d = \mu_s$ in Fig. 43, for the NJL and the MIT models. One can clearly see that within the SU(3) version of both models, the transition temperature at low chemical potential is lowered considerably in relation to the SU(2) curve and at low temperatures, the transition chemical potentials are also shifted towards lower values. Also, the effects of the vector interaction are the same as the ones just discussed for the SU(2) case, e.g. the transition point at $\mu = 0$ would be also kept fixed had different values of the vector interaction been plotted, as explained above.

Analyzing this framework and the results presented in [111, 112] together, it is possible to argue that the phase transition in QCD can take place either in one or two different steps, depending on the parameter choice adopted for the MIT-type model. From Figures 1 and 4 of Ref. [111], we can see that both MIT models allow the deconfinement phase transition to take place around μ = 1200 MeV in the low temperature region, at least for some sets. If this is the case considered, it suggests that both deconfinement and chiral transition occur simultaneously in the QCD phase diagram. It does happen at $T = 0$, e.g., when the parameters of the MIT model are taken to be $B^{1/4}$ = 165 MeV and G_V = 0.8 fm^2, while the vector coupling of the NJL is set as $G_V/G_S = 0.5$, at μ = 1250 MeV. However, even in such case, the MIT and NJL transition curves diverge rapidly for finite temperatures, as the dependence of the

transition temperature on the chemical potential is noticeably more intense in the MIT curves, specially for chemical potential greater than the μ at the CEP predicted for the NJL-type models.

The description of stellar matter cannot be done using the two-flavor formalism presented in this section, since strangeness is necessary to fulfill the Bodmer-Witten conjecture (but it is still a possibility in the framework of quark-meson models). Both hybrid and quark stars with vector NJL models have been described in several studies [113]. It is worth noting, however, that these models do not produce stable quark matter at zero temperature and/or magnetic field [22], but they can certainly describe the inner matter of a hybrid star, which is enough to justify the application of this type of model in theoretical studies, mainly the ones involving phase transitions. Increasing the vector term stiffens the equation of state, thus sustaining larger maximum stellar masses, but the macroscopic properties of the compact star depend strongly on the remaining parameter choice.

6 MAGNETIC FIELD EFFECTS ON THE DECONFINEMENT TRANSITION

The analysis of the QCD phase diagram points to a deconfined quark phase standing from the region of high temperatures and low densities down to the region of low temperatures and high densities. While lattice QCD (LQCD) can only describe a small part of the diagram with high temperatures and chemical potentials close to zero, effective models have been extensively used to investigate all other regions. From the LQCD perspective, the transition between hadronic matter and deconfined quark matter is a crossover. On the other hand, effective models foresee a first order phase transition. These two lines can only join if a critical end point (CEP), which should be a unique second order transition point, exists in between them. At low temperatures, the possibility that a quarkyonic phase [124] exists is not overruled. This phase would consist of matter with the chiral symmetry restored or partially restored but still confined.

But, what if matter is subject to strong magnetic fields, as in heavy ion collisions, for instance? What do we know about the QCD phase diagram? In [7], it is shown that the critical chemical potential oscillates around the zero magnetic field value for magnetic fields within 10^{17} to 10^{18} G range. It is also shown that the CEP position is affected. In this study, a unique model, the Nambu-Jona-Lasinio, with and without the Polyakov loop, was used to display the transition line between the hadronic and the quark phase.

Although many works have already investigated the hadron-quark phase transition at zero temperature [132, 182, 26, 121, 72] here we investigate the possible transition if matter is subject to strong magnetic fields. This is an interesting subject because of the existence of magnetars, which manifest themselves in quite different ways as compared to the traditional pulsars. Could these objects become magnetised quark stars? This is the question we try to answer in this part of the work. We use two different models, a relativistic hadronic model within a mean field approximation (RMF model) to describe hadronic matter [66], using the hyperon coupling scheme proposed in [68], and a density dependent model [197] to describe quark matter. The motivation behind the use of a density dependent quark model is two-fold: 1) such models were never utilised in previous works regarding the hadron-quark phase transition and 2) the description of quark stars could result in surface densities lower than the one of regular nuclear matter [197], which is a clear signal that the phase transition may occur. This suggests that the cases with low surface densities might be more appropriate to the description of hybrid stars instead of quark stars.

The study of hybrid stars gained more interest since a model-independent analysis based on the sound velocity in both hadronic and quark matter suggested that the cores of massive neutron stars should be composed of quark matter. In order to fully investigate this case, a proper study of the hadron-quark phase transition is in

order, further motivating the use of the density dependent model here considered. We restrict ourselves to the zero temperature regime and follow the prescription given in [17, 121], which assumes that flavor is conserved during the phase transition, but chemical equilibrium is not.

As we aim to observe how the phase transition point changes with the inclusion of magnetic field, specifically when considering a density dependent quark model, effects such as the inclusion of anomalous magnetic moments were neglected, since they would not substantially change the qualitative results. Similarly, we also restrain our study to isotropic matter and magnetisation is not taken into account.

In this work, the density dependent quark mass (DDQM) model is utilized to describe quark matter, and the GM1 model is used to describe the hadronic phase. Under this approach, the quark confinement is described by the density dependence introduced in the quark masses:

$$m_i = m_{i0} + \frac{D}{n_b^{1/3}} + C n_b^{1/3} = m_{i0} + m_I, \tag{136}$$

where m_{i0} ($i = u, d, s$) is the current mass of the ith quark, n_b is the baryon number density and m_I is the density dependent term that mimicks the interaction between quarks. The model has two free adjustable parameters: D, that dictates linear confinement; and C, that is responsible for leading-order perturbative interactions [197]. Whenever a density dependent term is introduced, the issue of thermodynamic consistency arises. To overcome this problem, we follow the formalism of [197], that presents a thermodynamically consistent DDQM model. The introduction of magnetic field is done in a similar way to [85], where the density dependent MIT Bag Model was thermodynamically treated. Under this approach, magnetised quark matter will be treated as being uniform and permeated by an external uniform magnetic field.

At zero temperature, the differential fundamental relation holds

$$\mathrm{d}\varepsilon_m = \sum_i \mu_i \mathrm{d}n_i, \tag{137}$$

where ε_m is the matter contribution to the energy density of the system, μ_i are the particles chemical potentials and n_i are the particle densities. One way of overcoming thermodynamic inconsistency is by the introduction of effective chemical potentials. Under this perspective, the energy density can be viewed as the one of a free system with particle masses $m_i(n_b)$ and effective chemical potentials μ_i^*,

$$\varepsilon_m = \Omega_m^0(\{\mu_i^*\}, m_i, B) + \sum_i \mu_i^* n_i, \tag{138}$$

where Ω_m^0 is the thermodynamic potential of a free system in the presence of an external magnetic field. At a fixed B, the differential form of Eq. (138) is

$$\mathrm{d}\varepsilon_m = \mathrm{d}\Omega_m^0 + \sum_i \mu_i^* \mathrm{d}n_i + \sum_i n_i \mathrm{d}\mu_i^*. \tag{139}$$

Explicitly, we can write $\mathrm{d}\Omega_m^0$ as

$$\mathrm{d}\Omega_m^0 = \sum_i \frac{\partial \Omega_m^0}{\partial \mu_i^*} \mathrm{d}\mu_i^* + \sum_i \frac{\partial \Omega_m^0}{\partial m_i} \mathrm{d}m_i \tag{140}$$

with

$$\mathrm{d}m_i = \sum_j \frac{\partial m_i}{\partial n_j} \mathrm{d}n_j, \tag{141}$$

where the densities are connected to the effective chemical potentials by

$$n_i = -\frac{\partial \Omega_m^0}{\partial \mu_i^*} \tag{142}$$

to ensure thermodynamic consistency.

Eq. (139) can then be rewritten as

$$\mathrm{d}\varepsilon_m = \sum_i \left(\mu_i^* + \sum_j \frac{\partial \Omega_m^0}{\partial m_j} \frac{\partial m_j}{\partial n_i} \right) \mathrm{d}n_i, \tag{143}$$

that should be consistent with the fundamental equation. Comparing eqs. (137) and (143), one gets the relation between the real and the effective chemical potentials

$$\mu_i = \mu_i^* + \sum_j \frac{\partial \Omega_m^0}{\partial m_j} \frac{\partial m_j}{\partial n_i}. \tag{144}$$

Considering magnetized quark matter to be an isotropic gas, the matter contribution to the pressure, P_m, is then given by

$$P_m = -\varepsilon_m + \sum_i \mu_i n_i. \tag{145}$$

The introduction of the effective chemical potentials through Eq. (138) gives

$$\begin{aligned} P_m &= -\Omega_m^0 + \sum_i (\mu_i - \mu_i^*) n_i \\ &= -\Omega_m^0 + \sum_{i,j} \frac{\partial \Omega_m^0}{\partial m_j} n_i \frac{\partial m_j}{\partial n_i}. \end{aligned} \tag{146}$$

One can note that, from basic thermodynamics, we can write the matter contribution to the thermodynamic potential, Ω_m, as

$$\Omega_m = \varepsilon_m - \sum_i \mu_i n_i, \tag{147}$$

and plugging Eq. (138) yields

$$\Omega_m = \Omega_m^0 - \sum_i (\mu_i - \mu_i^*) n_i, \tag{148}$$

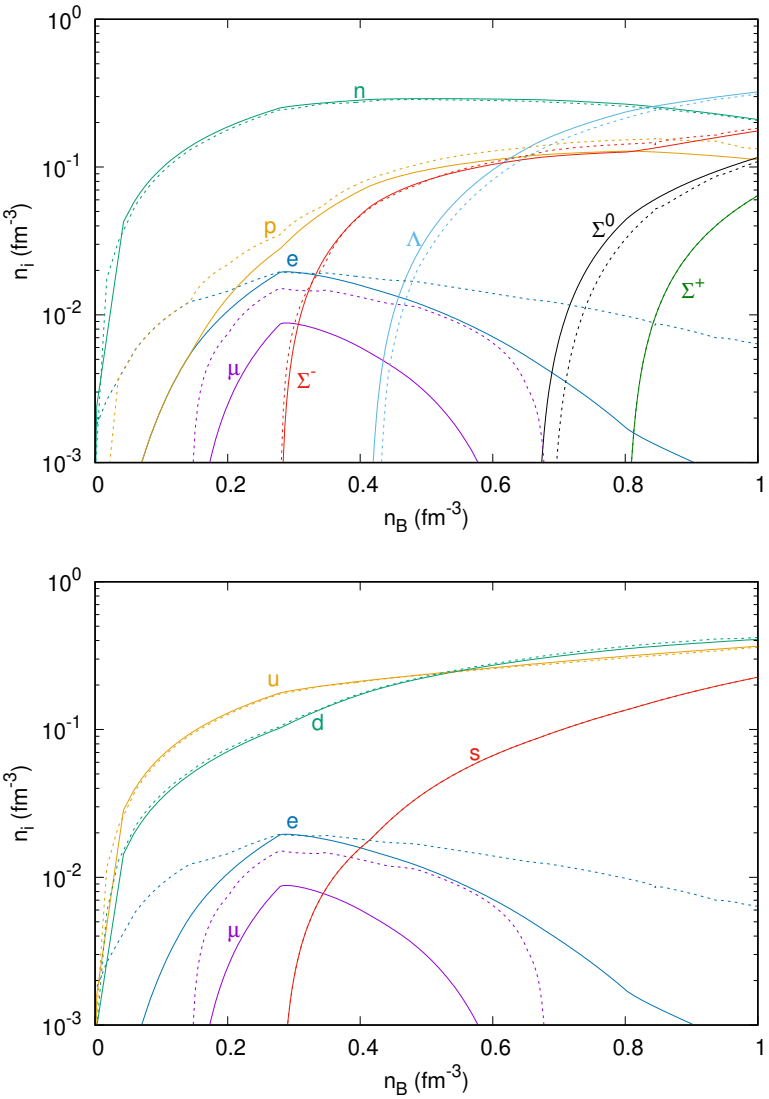

Figure 44 – Baryon species populations from the RMF model for GM1 parameterization (above) and the respective quark fractions (below). Full lines show results without magnetic fields, while dashed lines show results including a magnetic field of $B = 3 \times 10^{18}$ G.

so that the thermodynamic relation $\Omega_m = -P_m$ still holds.

It is worth noting that there are several different mass scaling relations for DDQM models, such as the inverse linear scaling and the simple cubic scaling. All of them remain thermodynamically consistent within this approach, and the main advantage of using the scaling relation of Eq. (136) is that the inclusion of the parameter C enables the attainment of more massive stars [8].

According to the Bodmer-Witten conjecture [15, 196], under certain circumstances, the electrically neutral and in chemical equilibrium hadronic matter is metastable and can be converted into an energetically favored, deconfined quark phase. The deconfinement of the hadronic matter into the quark phase must occur in the strong

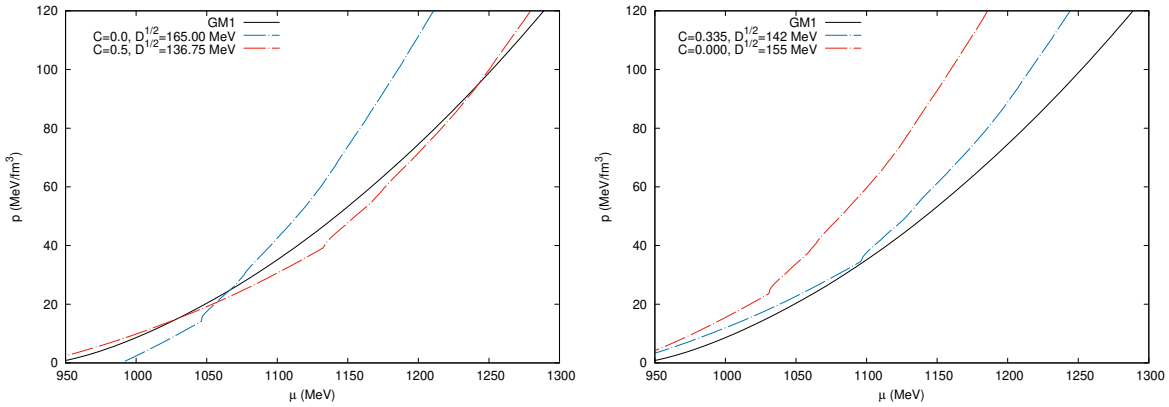

Figure 45 – Example of parameter sets that allow (left panel) and do not allow (right panel) the hadron-quark phase transition to occur at $B = 3 \times 10^{18}$ G.

interaction time scale, which is many orders of magnitude smaller than the weak interaction time scale [137, 18]. It implies that the relative flavor fractions must be conserved during the phase transition,

$$Y_q = \frac{1}{3}\sum_i n_{qi} Y_i, \tag{149}$$

where the baryonic number densities of each particle species $n_i = Y_i n_B$ are related by the number n_{qi} of q flavored quark constituents of baryon i [137, 121]. As we consider that the total baryonic mass and the lepton number are also conserved, Eq. (149) determines the composition of the resulting quark phase from the initial hadronic matter in chemical equilibrium. Quark matter will not be in β-equilibrium, but the process preserves charge neutrality, as explained in Ref. [121]. Figure 44 shows the particle population obtained from the RMF model, considering the equilibrium conditions, and the respective quark matter fractions associated with this hadronic distribution. Notice that the leptons are present in both configurations and are more affected by the magnetic field than the baryons and the quarks. In fact, the lepton contribution is defined in the hadronic phase, as stated above.

The deconfinement transition is assumed to be a first-order phase transition. The thermodynamic description of this kind of process can be obtained from the matching of the equations of state for the two phases. The transition can happen after the overpressured metastable matter reaches the phase coexistence point, defined according to the Gibbs criteria as,

$$\begin{aligned} P^{(i)} &= P^{(f)} = P_0, \\ \mu^{(i)}(P_0) &= \mu^{(f)}(P_0) = \mu_0, \end{aligned} \tag{150}$$

for the transition between the initial (i) and final (f) phases considered homogeneous, with

$$\mu^{(i,f)} = \frac{\varepsilon^{(i,f)} + P^{(i,f)}}{n_B^{(i,f)}}, \tag{151}$$

	B = 0	B = 3×10^{18} G	B-W
$C = 0$ $\sqrt{D} = 155$ MeV	no crossing	no crossing	yes
$C = 0$ $\sqrt{D} = 158.5$ MeV	$\mu_0 = 960$ $P_0 = 1.55$	$\mu_0 = 958$ $P_0 = 1.80$	yes
$C = 0$ $\sqrt{D} = 165$ MeV	$\mu_0 = 1062$ $P_0 = 21.98$	$\mu_0 = 1066$ $P_0 = 24.70$	no
$C = 0.23$ $\sqrt{D} = 155$ MeV	$\mu_0 = 1130$ $P_0 = 43.62$	$\mu_0 = 1145$ $P_0 = 51.32$	no
$C = 0.365$ $\sqrt{D} = 142$ MeV	$\mu_0 = 1105$ $P_0 = 34.98$	$\mu_0 = 1109$ $P_0 = 38.30$	yes
$C = 0.5$ $\sqrt{D} = 135.75$ MeV	$\mu_0 = 1202$ $P_0 = 72.66$	$\mu_0 = 1242$ $P_0 = 94.93$	yes
$C = 0.68$ $\sqrt{D} = 130$ MeV	$\mu_0 = 1440$ $P_0 = 215.50$	$\mu_0 = 1475$ $P_0 = 247.53$	yes

Table 17 – Values for μ_0 (in MeV) and P_0 (in MeV/fm^3) for which the conditions of phase coexistence are satisfied at $T = 0$. Results are shown for sets of parameters C and D within and outside of the stability window of SQM, for both magnetised and demagnetised matter. The latter column specifies whether or not the Bodmer-Witten conjecture is satisfied.

where $\varepsilon^{(i,f)}$, $p^{(i,f)}$ and $n_B^{(i,f)}$ are the total energy density, pressure and number density, obtained from the effective model EoS. [18]. These conditions leave the values of P_0 and μ_0 to be determined from the equations of state of both phases. Notice that in the results that follow, we neglect the $B^2/2$ term in the pressure of both models and verify only the crossing of the curves related to hadronic and quark matter, otherwise, it would be impossible to compare our results with the ones obtained with non-magnetised matter, since the contribution from the pure magnetic field (for a fixed value of B) is very large as compared with the contribution of magnetised matter.

Since we utilise only one parameterization to describe the hadronic phase, the condition of coexistence of phases may or may not be satisfied depending only on the DDQM model free parameters, C and D. The procedure for checking the Gibbs criteria is graphically shown in Figure 45, for sets of parameters that allow or do not allow the phase transition to occur. For some sets of parameters, such as $C = 0.5$ and $\sqrt{D} = 136.75$ MeV, the conditions of Eq. (150) are satisfied more than once. Whenever such double crossing occurs, only the hadron-quark phase transition is considered, since a quark-hadron phase transition is not expected to exist.

In regard to the DDQM models free parameters, the adequate stability window must be taken into account. We restrict our study to the sets of parameters that satisfy the Bodmer-Witten conjecture or are barely outside of the stability window of non magnetised strange quark matter [8], which is reasonable since the binding energy of magnetised matter is lower than the one of non magnetised matter [70, 194].

The results for μ_0 and P_0 are summarized in Table 17, where it can be seen that the inclusion of magnetic field shifts the coexistence point towards higher pressures and generally, also towards higher chemical potentials. The exception (second line on the table) may be due to numerical uncertainties implicit to these simple models. This shift tends to be higher when the perturbative parameter becomes larger. This result goes in line with the general notion that the EoS stiffens as the magnetic field increases. It was also observed that for a fixed value of D, the coexistence point occurs at higher pressures when C increases. Similarly, for a fixed value of C, the coexistence point occurs at higher pressures when D increases.

In Ref. [197], the same DDQM model used in this work is applied to the study of strange stars. It was shown that the surface density of stars described with high C parameters is even lower than nuclear saturation density, which points to the existence of a phase transition. By analysing the results of Table 17, it is noticeable that as C increases, the coexistence point indeed occurs at higher pressures. This result corroborates the previous findings, suggesting that whenever a large perturbative parameter is considered, the DDQM model could be more suitable for the description of hybrid stars instead of strange ones. Since the issue of hadron-quark phase transition with the DDQM model has already been addressed, we further analyse this possibility.

For large values of C, a double crossing can occur when one investigates the Gibbs criteria of phase coexistence, as shown in Figure 45. Whenever there is a double crossing, the first coexistence points (that predict a quark-hadron phase transition) are always at low enough densities, below the cusp that can be observed in the EoS at the point where strange quarks first appear, so that there are no strange quarks. Thus, not only such a transition is not expected to exist from a phenomenological point of view, but it is also not favorable since two flavor quark matter will always be unstable against nuclear matter, respecting the Bodmer-Witten hypothesis [15, 196] that was already considered for such quark model parameters [8]. Therefore, the first crossing point must be disregarded so that matter is confined at the low density regime.

An EoS that describes hybrid stars can be built by a Maxwell construction, interpolating the hadronic and the quark EoS at the coexistence point shown in Table 17. Figure 46 shows mass-radius curves produced from inserting some EoS obtained with a Maxwell construction into the Tolman–Oppenheimer–Volkoff (TOV) equations [180, 139] and adding the BPS EoS [12] for the low-density region of the crust. Our results here consider only stellar matter without magnetic field effects, since the use of the TOV-like equations for magnetised matter requires the solution of a more complicated system of equations in general relativity, which goes beyond the objectives of this part of the work. Pure strange stars would show maximum masses close to the ones of the respective hybrid star (the values for strange star are M = 1.63 M_{Sun} for the DDQM model parameters C = 0.0, $D^{1/2}$ = 158.5 MeV; M = 1.78 M_{Sun} for C = 0.23,

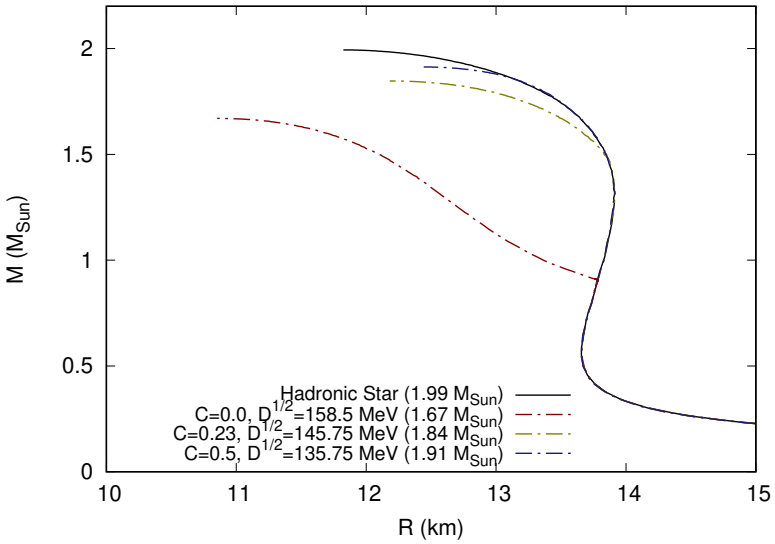

Figure 46 – Mass-radius diagram for hybrid EoS with chemical equilibrium in both phases, showing results without magnetic field effects. The maximum stellar masses are indicated for all cases.

$D^{1/2}$ = 145.75 MeV; and M = 1.92 M_{Sun} for C = 0.5, $D^{1/2}$ = 135.75 MeV), but the profile of the mass-radius curve would be different, as no crust is expected to remain in quark stars, although such possibility can also be considered.

Following the stellar evolution scenario proposed by Refs. [121, 72], we can assume the compact star as being initially a pure hadronic metastable star in the early stages after its emergence. In this stage, the equilibrium conditions are reached through the first deleptonization and cooling, and the resulting objects are the ones described by the black curve in Fig. 46. After a finite time interval, this metastable configuration can decay into an energetically more favorable one, and, according to the Bodmer-Witten conjecture, it can be reached by the quark deconfinement. So, the conversion of a metastable hadronic star into a hybrid (or strange) star can take place via a first order transition. The transition dynamics we consider in this work assumes flavor conservation in the first moment, as imposed by Eq. (149), and this condition is taken to determine the phase coexistence points. Finally, the quark matter would seek the chemical equilibrium soon after its formation, because this is the stable configuration of stellar matter, and it justifies the use of this configuration in Fig. 46.

Notice that a deconfined quark core starts appearing at a very low masses (M = 0.90 M_{Sun}) when the parameters C = 0.0, $D^{1/2}$ = 158.5 MeV are considered. On the other hand, the transition does not take place in the star matter density threshold for the parameters C = 0.68, $D^{1/2}$ = 130 MeV. In the stellar evolution scenario presented above, the conversion of a metastable hadronic star to a strange or hybrid star could take place if the initial object sustains a central pressure larger than the coexistence pressure of the hadron and quark phases (P_0). Yet, when the metastable hadronic

star matter is overpressured enough to allow the appearance of a quark core, there must exist a stable final compact object whose central density is that of the EoS latter phase, i.e., we must also have a final object whose central pressure (which is the higher pressure present in this object) is higher or equal P_0, or the metastable star will not have a stable compact star configuration to decay (if not a black hole). In the case of parameters $C = 0.68$, $D^{1/2} = 130$ MeV, this constraint is not fulfilled, and the maximum stable star would be a pure hadronic star of $M = 1.96$ M_{Sun} and $R = 12.42$ km, never sustaining a quark core beyond this point, following the trend of hybrid star maximum masses shown in Fig. 46. This set fulfills the thermodynamic criteria for the phase transition, but the astrophysical conditions do not allow the formation of a stable hybrid star.

7 FINAL REMARKS

We obtained a description of compact stars made up of dense matter from several relativistic models, with the purpose of analyzing pulsars as hadronic, hybrid and/or strange stars. In a first moment, the implications of including delta baryons in the stellar matter composition. In Chapter 2, results published in [123] are discussed. Analyzing the properties of nucleonic matter with delta baryons and nucleonic matter with hyperons and delta baryons, by applying a relativistic mean-field description of neutron star matter with density dependent couplings, it is verified that many models are excluded because the effective nucleon mass becomes zero before the maximum mass configuration is attained. Hyperon-free with delta-dominated composition compact stars are possible, the deltic stars. It is found that with a convenient choice of parameters the existence of deltic stars with 80% of delta baryons at the center of the star is possible. However, the presence of hyperons lowers the delta baryon fraction to values below 20% at the center and below 30% at 2-3 saturation densities. It is discussed that in the presence of delta baryons, the hyperon softening is not so drastic because deltas couple more strongly to the ω meson, and the stiffness of the equation of state is determined by the ω-dominance at high densities. The speed of sound reflects very well this behavior.

We then carefully investigated particle composition and spin polarization when delta baryons are included in neutron-star matter under the influence of strong magnetic fields with and without AMM corrections. Due to the effects of charge conservation and chemical equilibrium, there is no common behavior for all the particles (as predicted by their AMM signs and strengths). However, in general, while the population of charged particles increases with the inclusion of AMM, the population of neutral particles tends to decrease, as published in [47, 122].

In this work, different extensions of the NJL model, which are appropriate to describe systems where chiral symmetry is an important ingredient, were revisited. In special, one version of these NJL-type models, suitable to describe both nucleonic and hyperonic matter, was partially developed, but a better description of these models and more refined search of parameterizations must be performed in future works, as well as the inclusion of temperature and eventually, magnetic field. In an early exploratory study, NJL-type models were used to investigate a possible QCD hadron-quark phase transition at zero temperature. It was shown that the transition point is very sensitive to the model parameters and that both pressure and chemical potential increase drastically with the increase of the vector interaction strength in the quark sector. Within the same framework, the possibility of quark and hybrid star formation was analyzed. The same conclusions drawn before with respect to the coexistence pressure and chemical potentials are reinforced. One can concluded that even if a transition from a metastable

hadronic star to a quark star is thermodinamically possible, it is either energetically forbidden or gives rise to a blackhole. Nevertheless, conversions from metastable to hybrid stars are possible, but the mass difference between both compact objects is very small, as published in [72, 112].

Finally, we have analysed the conditions for a phase transition from a hadronic to a quark phase with the help of two different models at zero temperature and under the influence of a very strong magnetic field, possibly present in the core of magnetars. With the chosen models we have, in general, obtained an increase of pressure and chemical potential as compared with the transition point of non-magnetised matter. For the sake of completeness, whenever the phase transition is possible, we have checked whether stable hybrid stars would be allowed and if so, if their cores could indeed contain deconfined quarks, as published in [9].

Several interesting research possibilities follow from the results obtained here. The understanding of the meson-delta coupling parameters can be refined by symmetry group considerations, as it is made for the hyperon coupling schemes. The magnetic field effects on Δ-admixed matter can also be more robustly understood by having the complete solution of the spin-3/2 Rarita-Schwinger equation under a magnetic field. It would be a novel result, allowing us to calculate the parallel and perpendicular speeds of sound, as well as other quantities related to the equations of state for these anisotropic configurations. As the inclusion of deltas alter significantly the particle populations in stellar matter, it is also interesting to analyze how it would affect the hadron-quark deconfinement transition, considering that the conversion mechanism we explore in this work takes into account the quark flavor conservation.

Regarding the overall aim of obtaining the QCD phase diagram with both hadronic and quark models based on the same underlying formalism, i.e., within different versions of the NJL model, we need to improve the parameterizations of the two hadronic matter models deduced here, making a more refined search on the parameters in order to better satisfy nuclear matter constraints. If possible, find sets that also satisfy constraints of pure neutron matter, as it is intended to apply these models in contexts rich in neutrons, as in the description of stellar matter in chemical equilibrium.

BIBLIOGRAPHY

[1] Gert Aarts et al. “Light baryons below and above the deconfinement transition: medium effects and parity doubling”. In: *JHEP* 06 (2017), page 034. DOI: 10.1007/JHEP06(2017)034. arXiv: 1703.09246 [hep-lat].

[2] B. P. Abbott et al. “GW170817: Observation of Gravitational Waves from a Binary Neutron Star Inspiral”. In: *Phys. Rev. Lett.* 119 (16 October 2017), page 161101. DOI: 10.1103/PhysRevLett.119.161101. URL: https://link.aps.org/doi/10.1103/PhysRevLett.119.161101.

[3] Mark Alford. “Color superconductivity in ultra-dense quark matter”. In: *XXIVth International Symposium on Lattice Field Theory*. 2006.

[4] Mark G. Alford, Sophia Han, and Madappa Prakash. “Generic conditions for stable hybrid stars”. In: *Phys. Rev. D* 88.8 (2013), page 083013. DOI: 10.1103/PhysRevD.88.083013. arXiv: 1302.4732 [astro-ph.SR].

[5] Eemeli Annala et al. “Evidence for quark-matter cores in massive neutron stars”. In: *Nature Phys.* (2020). DOI: 10.1038/s41567-020-0914-9. arXiv: 1903.09121 [astro-ph.HE].

[6] S. S. Avancini, D. P. Menezes, and C. Providência. “Finite temperature quark matter under strong magnetic fields”. In: *Phys. Rev. C* 83 (6 June 2011), page 065805. DOI: 10.1103/PhysRevC.83.065805. URL: https://link.aps.org/doi/10.1103/PhysRevC.83.065805.

[7] Sidney S Avancini et al. “QCD critical end point under strong magnetic fields”. In: *Physical Review D* (2012).

[8] B. C. Backes et al. “Density dependent quark mass model revisited: Thermodynamic consistency, stability windows and stellar properties”. In: *Journal of Physics G: Nuclear and Particle Physics* (2020). URL: http://iopscience.iop.org/article/10.1088/1361-6471/abc6e9.

[9] Betânia CT Backes, Kauan D Marquez, and Débora P Menezes. “Effects of strong magnetic fields on the hadron-quark deconfinement transition”. In: *The European Physical Journal A* 57.7 (2021), pages 1–9.

[10] M. Baldo, G. F. Burgio, and H. J. Schulze. “Hyperon stars in the Brueckner-Bethe-Goldstone theory”. In: *Phys. Rev. C* 61 (2000), page 055801. DOI: 10.1103/PhysRevC.61.055801. arXiv: nucl-th/9912066.

[11] M. Baldo and G.F. Burgio. “The nuclear symmetry energy”. In: *Progress in Particle and Nuclear Physics* 91 (2016), pages 203–258.

[12] Gordon Baym, Christopher Pethick, and Peter Sutherland. “The Ground State of Matter at High Densities: equation of State and Stellar Models”. In: *The Astrophysical Journal* 170 (1971), page 299. DOI: 10.1086/151216.

[13] A. Bazavov et al. “Chiral and deconfinement aspects of the QCD transition”. In: *Physical Review D* 85.5 (March 2012), page 054503. DOI: 10.1103/physrevd.85.054503.

[14] Bipasha Bhowmick et al. “Massive neutron stars with a hyperonic core: A case study with the IUFSU relativistic effective interaction”. In: *Phys. Rev. C* 89.6 (2014), page 065806. DOI: 10.1103/PhysRevC.89.065806. arXiv: 1403.0341 [nucl-th].

[15] A. R. Bodmer. “Collapsed nuclei”. In: *Physical Review D* 4.6 (1971), pages 1601–1606.

[16] Ignazio Bombaci. “The Hyperon Puzzle in Neutron Stars”. In: *Proceedings of the 12th International Conference on Hypernuclear and Strange Particle Physics*. arXiv:1601.05339[nucl-th]. 2015. DOI: 10.7566/JPSCP.17.101002. URL: https://journals.jps.jp/doi/abs/10.7566/JPSCP.17.101002.

[17] Ignazio Bombaci and Domenico Logoteta. “Quark deconfinement in neutron stars and astrophysical implications”. In: *International Journal of Modern Physics D* 26.2 (2017), page 1730004.

[18] Ignazio Bombaci, Irene Parenti, and Isaac Vidaña. “Quark Deconfinement and Implications for the Radius and the Limiting Mass of Compact Stars”. In: *The Astrophysical Journal* 614.1 (2004), page 314. URL: http://stacks.iop.org/0004-637X/614/i=1/a=314.

[19] M. Buballa and M. Oertel. “Strange quark matter with dynamically generated quark masses”. In: *Physics Letters B* 457 (1999), page 261.

[20] Michael Buballa. “NJL-model analysis of dense quark matter”. In: *Physics Reports* 407.4 (2005), pages 205–376.

[21] Michael Buballa. “NJL-model analysis of dense quark matter”. In: *Physics Reports* 407.4–6 (2005), page 205. ISSN: 0370-1573. DOI: http://dx.doi.org/10.1016/j.physrep.2004.11.004. URL: http://www.sciencedirect.com/science/article/pii/S037015730400506X.

[22] Michael Buballa. “The problem of matter stability in the Nambu–Jona-Lasinio model”. In: *Nuclear Physics A* 611.4 (1996), page 393. ISSN: 0375-9474. DOI: http://dx.doi.org/10.1016/S0375-9474(96)00314-4. URL: http://www.sciencedirect.com/science/article/pii/S0375947496003144.

[23] N. Cabibbo and G. Parisi. “Exponential hadronic spectrum and quark liberation”. In: *Physics Letters B* 59.1 (1975), pages 67–69.

[24] Bao-Jun Cai and Lie-Wen Chen. “Nuclear matter fourth-order symmetry energy in the relativistic mean field models”. In: *Phys. Rev. C* 85 (2 February 2012), page 024302. DOI: 10.1103/PhysRevC.85.024302. URL: https://link.aps.org/doi/10.1103/PhysRevC.85.024302.

[25] Renan Câmara Pereira, Pedro Costa, and Constança Providência. “Two-solar-mass hybrid stars: a two model description with the Nambu-Jona-Lasinio quark model”. In: *Phys. Rev. D* 94.9 (2016), page 094001. DOI: 10.1103/PhysRevD.94.094001. arXiv: 1610.06435 [nucl-th].

[26] Rafael Cavagnoli, Constança Providência, and Debora P. Menezes. “Hadron-quark phase transition in asymmetric matter with boson condensation”. In: *Phys. Rev. C* 83 (4 April 2011), page 045201. DOI: 10.1103/PhysRevC.83.045201. URL: http://link.aps.org/doi/10.1103/PhysRevC.83.045201.

[27] N. Chamel et al. “On the Maximum Mass of Neutron Stars”. In: *Int. J. Mod. Phys. E* 22 (2013), page 1330018. DOI: 10.1142/S021830131330018X. arXiv: 1307.3995 [astro-ph.HE].

[28] Subrahmanyan Chandrasekhar. “The Maximum Mass of Ideal White Dwarfs”. In: *The Astrophysical Journal* 74 (1931). doi:10.1086/143324, page 81.

[29] Debarati Chatterjee, Jérôme Novak, and Micaela Oertel. “Structure of ultra-magnetised neutron stars”. In: *The European Physical Journal A* 57.8 (August 2021). ISSN: 1434-601X. DOI: 10.1140/epja/s10050-021-00525-5. URL: http://dx.doi.org/10.1140/epja/s10050-021-00525-5.

[30] Debarati Chatterjee and Isaac Vidaña. “Do hyperons exist in the interior of neutron stars?” In: *Eur. Phys. J. A* 52.2 (2016), page 29. DOI: 10.1140/epja/i2016-16029-x. arXiv: 1510.06306 [nucl-th].

[31] Lie-Wen Chen et al. “Density slope of the nuclear symmetry energy from the neutron skin thickness of heavy nuclei”. In: *Physical Review C* 82.2 (2010), page 024321.

[32] A. Chodos et al. “New extended model of hadrons”. In: *Physical Review D* 9.12 (1974), page 3471.

[33] I.C. Cloet, D.B. Leinweber, and A.W. Thomas. “Delta baryon magnetic moments from lattice QCD”. In: *Physics Letters B* 563.3 (2003), pages 157–164. ISSN: 0370-2693. DOI: https://doi.org/10.1016/S0370-2693(03)00418-0. URL: https://www.sciencedirect.com/science/article/pii/S0370269303004180.

[34] P. Costa, M. C. Ruivo, and C. A. de Sousa. “Thermodynamics and critical behavior in the Nambu–Jona-Lasinio model of QCD”. In: *Phys. Rev. D* 77 (9 May 2008), page 096001. DOI: 10.1103/PhysRevD.77.096001. URL: https://link.aps.org/doi/10.1103/PhysRevD.77.096001.

[35] Pedro Costa et al. “Phase Diagram and Critical Properties within an Effective Model of QCD: The Nambu–Jona-Lasinio Model Coupled to the Polyakov Loop”. In: *Symmetry* 2.3 (2010), page 1338. ISSN: 2073-8994. DOI: 10.3390/sym2031338. URL: http://www.mdpi.com/2073-8994/2/3/1338.

[36] M. D. Cozma and M. B. Tsang. “In-medium $\Delta(1232)$ potential, pion production in heavy-ion collisions and the symmetry energy”. In: *arXiv:2101.08679* (2021). arXiv: 2101.08679 [nucl-th].

[37] Tiago Custódio, Helena Pais, and Constança Providência. “Heavy baryons in hot stellar matter with light nuclei and hypernuclei”. In: (April 2022). arXiv: 2204.02260 [nucl-th].

[38] S Dall'Osso, L Stella, and C Palomba. "Neutron star bulk viscosity, 'spin-flip' and GW emission of newly born magnetars". In: *Monthly Notices of the Royal Astronomical Society* 480.1 (June 2018), pages 1353–1362. ISSN: 0035-8711. DOI: 10.1093/mnras/sty1706. eprint: https://academic.oup.com/mnras/article-pdf/480/1/1353/25405204/sty1706.pdf. URL: https://doi.org/10.1093/mnras/sty1706.

[39] Stanley Deser, A Waldron, and V Pascalutsa. "Massive spin 3/2 electrodynamics". In: *Physical Review D* 62.10 (2000), page 105031.

[40] V Dexheimer, D P Menezes, and M Strickland. "The influence of strong magnetic fields on proto-quark stars". In: *Journal of Physics G: Nuclear and Particle Physics* 41.1 (December 2013), page 015203. DOI: 10.1088/0954-3899/41/1/015203. URL: https://doi.org/10.1088/0954-3899/41/1/015203.

[41] V. Dexheimer, R. Negreiros, and S. Schramm. "Hybrid Stars in a Strong Magnetic Field". In: *Eur. Phys. J. A* 48 (2012), page 189. DOI: 10.1140/epja/i2012-12189-y. arXiv: 1108.4479 [astro-ph.HE].

[42] V. Dexheimer, R. Negreiros, and S. Schramm. "Reconciling Nuclear and Astrophysical Constraints". In: *Phys. Rev. C* 92.1 (2015), page 012801. DOI: 10.1103/PhysRevC.92.012801. arXiv: 1503.07785 [astro-ph.HE].

[43] V. Dexheimer and S. Schramm. "Proto-Neutron and Neutron Stars in a Chiral SU(3) Model". In: *Astrophys. J.* 683 (2008), pages 943–948. DOI: 10.1086/589735. arXiv: 0802.1999 [astro-ph].

[44] V. Dexheimer, J. R. Torres, and D. P. Menezes. "Stability windows for proto-quark stars". In: *European Physical Journal C* 73 (2013), page 2569. DOI: 10.1140/epjc/s10052-013-2569-5.

[45] V. Dexheimer et al. "GW190814 as a massive rapidly rotating neutron star with exotic degrees of freedom". In: *Phys. Rev. C* 103.2 (2021), page 025808. DOI: 10.1103/PhysRevC.103.025808. arXiv: 2007.08493 [astro-ph.HE].

[46] V. Dexheimer et al. "What is the magnetic field distribution for the equation of state of magnetized neutron stars?" In: *Phys. Lett. B* 773 (2017), pages 487–491. DOI: 10.1016/j.physletb.2017.09.008. arXiv: 1612.05795 [astro-ph.HE].

[47] Veronica Dexheimer, Kauan D. Marquez, and Débora P. Menezes. “Delta baryons in neutron-star matter under strong magnetic fields”. In: *The European Physical Journal A* 57.7 (July 2021). ISSN: 1434-601X. DOI: 10.1140/epja/s10050-021-00532-6. URL: http://dx.doi.org/10.1140/epja/s10050-021-00532-6.

[48] Alessandro Drago et al. “Early appearance of Δ isobars in neutron stars”. In: *Phys. Rev. C* 90.6 (2014), page 065809. DOI: 10.1103/PhysRevC.90.065809. arXiv: 1407.2843 [astro-ph.SR].

[49] Hans-Peter Duerr and Edward Teller. “Interaction of Antiprotons with Nuclear Fields”. In: *Physical Review* 101.1 (1956), page 494.

[50] M Dutra et al. “Relativistic mean-field hadronic models under nuclear matter constraints”. In: *Physical Review C* 90.5 (2014), page 055203.

[51] M. Dutra et al. In: *Phys. Rev. C* 90 (5 November 2014), page 055203. DOI: 10.1103/PhysRevC.90.055203. URL: https://link.aps.org/doi/10.1103/PhysRevC.90.055203.

[52] M. Dutra et al. “Relativistic mean-field hadronic models under nuclear matter constraints”. In: *Physical Review C* 90.5 (2014). arXiv:1405.3633, page 55203.

[53] M. Dutra et al. “Skyrme interaction and nuclear matter constraints”. In: *Physical Review C* 85.3 (2012), page 35201.

[54] Mariana Dutra, Odilon Lourenço, and Debora P. Menezes. “Stellar properties and nuclear matter constraints”. In: *Physical Review C* 93.2 (2016), page 25806.

[55] Edward Farhi and R. L. Jaffe. “Strange matter”. In: *Physical Review D* 30.11 (1984), pages 2379–2391.

[56] Márcio Ferreira, Renan Câmara Pereira, and Constança Providência. “Hybrid stars with large strange quark cores constrained by GW170817”. In: *Phys. Rev. D* 103.12 (2021), page 123020. DOI: 10.1103/PhysRevD.103.123020. arXiv: 2105.06239 [nucl-th].

[57] Efrain J. Ferrer et al. “Equation of state of a dense and magnetized fermion system”. In: *Phys. Rev. C* 82 (6 December 2010), page 065802. DOI: 10.1103/

PhysRevC.82.065802. URL: https://link.aps.org/doi/10.1103/PhysRevC.82.065802.

[58] E. Fonseca et al. “Refined Mass and Geometric Measurements of the High-mass PSR J0740+6620”. In: *Astrophys. J. Lett.* 915.1 (2021), page L12. DOI: 10.3847/2041-8213/ac03b8. arXiv: 2104.00880 [astro-ph.HE].

[59] M. Fortin et al. “Hypernuclei and massive neutron stars”. In: *Phys. Rev. C* 95.6 (2017), page 065803. DOI: 10.1103/PhysRevC.95.065803. arXiv: 1701.06373 [nucl-th].

[60] M. Fortin et al. “Relativistic hypernuclear compact stars with calibrated equations of state”. In: *Phys. Rev. D* 101.3 (2020), page 034017. DOI: 10.1103/PhysRevD.101.034017. arXiv: 2001.08036 [hep-ph].

[61] B. Franzon, V. Dexheimer, and S. Schramm. “A self-consistent study of magnetic field effects on hybrid stars”. In: *Mon. Not. Roy. Astron. Soc.* 456.3 (2016), pages 2937–2945. DOI: 10.1093/mnras/stv2606. arXiv: 1508.04431 [astro-ph.HE].

[62] Joachim Frieben and Luciano Rezzolla. “Equilibrium models of relativistic stars with a toroidal magnetic field”. In: *Mon. Not. Roy. Astron. Soc.* 427 (2012), pages 3406–3426. DOI: 10.1111/j.1365-2966.2012.22027.x. arXiv: 1207.4035 [gr-qc].

[63] John L. Friedman, James R. Ipser, and Rafael D. Sorkin. “Turning point method for axisymmetric stability of rotating relativistic stars”. In: *Astrophys. J.* 325 (1988), pages 722–724. DOI: 10.1086/166043.

[64] A. Gal, E. V. Hungerford, and D. J. Millener. “Strangeness in nuclear physics”. In: *Rev. Mod. Phys.* 88.3 (2016), page 035004. DOI: 10.1103/RevModPhys.88.035004. arXiv: 1605.00557 [nucl-th].

[65] N. K. Glendenning. “Neutron Stars Are Giant Hypernuclei?” In: *Astrophys. J.* 293 (1985), pages 470–493. DOI: 10.1086/163253.

[66] N. K. Glendenning and S. A. Moszkowski. “Reconciliation of neutron-star masses and binding of the Λ in hypernuclei”. In: *Physical Review Letters* 67 (18 1991), pages 2414–2417.

[67] N.K. Glendenning. “The Hyperon Composition of Neutron Stars”. In: *Phys. Lett. B* 114 (1982), pages 392–396. DOI: 10.1016/0370-2693(82)90078-8.

[68] Norman K. Glendenning. *Compact Stars: Nuclear Physics, Particle Physics, and General Relativity*. 2nd. New York: Springer, 2000.

[69] R. O. Gomes et al. “Limiting magnetic field for minimal deformation of a magnetized neutron star”. In: *Astron. Astrophys.* 627 (2019), A61. DOI: 10.1051/0004-6361/201935310. arXiv: 1902.08146 [nucl-th].

[70] F. R. González and A. M. Pérez. “Stability window and mass–radius relation for magnetized strange quark stars”. In: *Journal of Physics G: Nuclear and Particle Physics* 36.7 (May 2009), page 075202. DOI: 10.1088/0954-3899/36/7/075202. URL: https://doi.org/10.1088/0954-3899/36/7/075202.

[71] Eric Gourgoulhon. *3+1 Formalism in General Relativity*. Springer Verlag, 2012. ISBN: 978-3-642-24525-1.

[72] Clebson A. Graeff et al. “Hadron-quark phase transition: the QCD phase diagram and stellar conversion”. In: *Journal of Cosmology and Astroparticle Physics* 2019.01 (January 2019), pages 024–024. DOI: 10.1088/1475-7516/2019/01/024. URL: https://doi.org/10.1088%2F1475-7516%2F2019%2F01%2F024.

[73] Walter Greiner, Stefan Schramm, and Eckart Stein. *Quantum Chromodynamics*. 2nd. New York: Springer, 2002.

[74] David Griffiths. *Introduction to Elementary Particles*. 2nd. Weinheim, Germany: Wiley-VCH, 2008.

[75] David J. Gross. “The discovery of assymptotic freedom and the emergence of QCD”. In: *Nobel Prize lecture* (2004). [Disponível em https://www.nobelprize.org/nobel_prizes/physics/laureates/2004/gross-lecture.pdf].

[76] W.J. de Haas and P.M. van Alphen. “Magnetic Oscillations in Metals”. In: *Proc. Am. Acad. Arts Sci* 33 (1936), page 1106.

[77] P. Haensel, A.Y. Potekhin, and D.G. Yakovlev. *Neutron Stars 1: Equation of State and Structure*. Astrophysics and Space Science Library. Springer New

York, 2006. ISBN: 9780387335438. URL: https://books.google.fr/books?id=iIrj9nfHnesC.

[78] V. Hambaryan et al. “The compactness of the isolated neutron star RX J0720.4-3125”. In: *Astronomy & Astrophysics* 601, A108 (2017), A108. DOI: 10.1051/0004-6361/201630368.

[79] M. Hanauske et al. “Strange quark stars within the NambuJona-Lasinio model”. In: *Phys. Rev. D* 64 (4 July 2001), page 043005. DOI: 10.1103/PhysRevD.64.043005. arXiv: astro-ph/0101267 [astro-ph]. URL: http://link.aps.org/doi/10.1103/PhysRevD.64.043005.

[80] Tetsuo Hatsuda and Teiji Kunihiro. “QCD phenomenology based on a chiral effective Lagrangian”. In: *Physics Reports* 247.5 (1994), page 221. ISSN: 0370-1573. DOI: https://doi.org/10.1016/0370-1573(94)90022-1. URL: http://www.sciencedirect.com/science/article/pii/0370157394900221.

[81] K. Hebeler et al. “Equation of State and Neutron Star Properties Constrained by Nuclear Physics and Observation”. In: *The Astrophysical Journal* 773.1, 11 (August 2013), page 11. DOI: 10.1088/0004-637X/773/1/11. arXiv: 1303.4662 [astro-ph.SR].

[82] D. W. Hertzog et al. “Exotic Atom Measurement of the Magnetic Dipole Moment of the Σ^- Hyperon”. In: *Phys. Rev. D* 37 (1988), pages 1142–1152. DOI: 10.1103/PhysRevD.37.1142.

[83] Antony Hewish et al. “Observation of a Rapidly Pulsating Radio Source”. In: *Nature* 217 (February 1968). doi:10.1038/217709a0, pages 709–713.

[84] Kunihito Ioka and Misao Sasaki. “Relativistic Stars with Poloidal and Toroidal Magnetic Fields and Meridional Flow”. In: *The Astrophysical Journal* 600.1 (January 2004), pages 296–316. ISSN: 1538-4357. DOI: 10.1086/379650. URL: http://dx.doi.org/10.1086/379650.

[85] A. A. Isayev. “Stability of magnetized strange quark matter in the MIT bag model with a density dependent bag pressure”. In: *Phys. Rev. C* 91 (1 January 2015), page 015208. DOI: 10.1103/PhysRevC.91.015208. URL: https://link.aps.org/doi/10.1103/PhysRevC.91.015208.

[86] D. D. Ivanenko and D. F. Kurdgelaidze. “Hypothesis concerning quark stars”. In: *Astrophysics* 1.4 (1965). doi:10.1007/BF01042830, pages 251–252.

[87] D. D. Ivanenko and D. F. Kurdgelaidze. “Remarks on quark stars”. In: *Lettere al Nuovo Cimento* 2.1 (1969). doi:10.1007/BF02753988, pages 13–16.

[88] M. H. Johnson and Edward Teller. “Classical Field Theory of Nuclear Forces”. In: *Physical Review* 98.3 (1955), page 783.

[89] Joseph I. Kapusta and Charles Gale. *Finite-Temperature Field Theory: Principles and Applications*. 2nd edition. Cambridge Monographs on Mathematical Physics. Cambridge University Press, 2006. DOI: 10.1017/CBO9780511535130.

[90] F. Karsch. “The phase transition to the quark gluon plasma: Recent results from lattice calculations”. In: *Nuclear Physics A* 590.1 (1995), pages 367–381.

[91] Kouji Kashiwa, Thomas Hell, and Wolfram Weise. “Nonlocal Polyakov–Nambu–Jona-Lasinio model and imaginary chemical potential”. In: *Phys. Rev. D* 84 (5 September 2011), page 056010. DOI: 10.1103/PhysRevD.84.056010. URL: https://link.aps.org/doi/10.1103/PhysRevD.84.056010.

[92] Masakiyo Kitazawa et al. “Chiral and Color-Superconducting Phase Transitions with Vector Interaction in a Simple Model”. In: *Progress of Theoretical Physics* 108.5 (November 2002), pages 929–951. URL: https://doi.org/10.1143/PTP.108.929.

[93] Kenta Kiuchi and Shijun Yoshida. “Relativistic stars with purely toroidal magnetic fields”. In: *Phys. Rev. D* 78 (4 August 2008), page 044045. DOI: 10.1103/PhysRevD.78.044045. URL: https://link.aps.org/doi/10.1103/PhysRevD.78.044045.

[94] T. Klahn et al. “Modern compact star observations and the quark matter equation of state”. In: *Phys. Lett.* B654 (2007), page 170. DOI: 10.1016/j.physletb.2007.08.048. arXiv: nucl-th/0609067 [nucl-th].

[95] T. Klähn, R. Łastowiecki, and D. Blaschke. “Implications of the measurement of pulsars with two solar masses for quark matter in compact stars and heavy-ion collisions: A Nambu–Jona-Lasinio model case study”. In: *Phys. Rev. D* 88

(8 October 2013), page 085001. DOI: 10.1103/PhysRevD.88.085001. URL: https://link.aps.org/doi/10.1103/PhysRevD.88.085001.

[96] Hagen Kleinert. “Hadronization of Quark Theories”. In: *Understanding the Fundamental Constituents of Matter*. Edited by Antonino Zichichi. Boston, MA: Springer, 1978, pages 289–389. DOI: 10.1007/978-1-4684-0931-4_7.

[97] S. Klimt et al. “Generalized SU(3) Nambu-Jona-Lasinio model: (I). Mesonic modes”. In: *Nuclear Physics A* 516.3 (1990), pages 429–468. ISSN: 0375-9474. DOI: https://doi.org/10.1016/0375-9474(90)90123-4. URL: http://www.sciencedirect.com/science/article/pii/0375947490901234.

[98] Volker Koch et al. “A chirally invariant fermionic field theory for nuclear matter”. In: *Physics Letters B* 185.1 (1987), page 1. ISSN: 0370-2693. DOI: http://dx.doi.org/10.1016/0370-2693(87)91517-6. URL: http://www.sciencedirect.com/science/article/pii/0370269387915176.

[99] E.E. Kolomeitsev, K.A. Maslov, and D.N. Voskresensky. “Delta isobars in relativistic mean-field models with σ -scaled hadron masses and couplings”. In: *Nucl. Phys. A* 961 (2017), pages 106–141. DOI: 10.1016/j.nuclphysa.2017.02.004. arXiv: 1610.09746 [nucl-th].

[100] Dong Lai and Stuart L. Shapiro. “Cold Equation of State in a Strong Magnetic Field: Effects of Inverse beta-Decay”. In: *APJ* 383 (December 1991), page 745. DOI: 10.1086/170831.

[101] G. A. Lalazissis et al. “New relativistic mean-field interaction with density-dependent meson-nucleon couplings”. In: *Phys. Rev. C* 71 (2005), page 024312. DOI: 10.1103/PhysRevC.71.024312.

[102] C. M. G. Lattes et al. “Processes involving charged mesons”. In: *Nature* 159 (1947). doi:10.1038/159694a0, pages 694–697.

[103] Tong-Gyu Lee et al. “Quark–hadron phase transition in an extended Nambu–Jona-Lasinio model with scalar–vector interaction: Finite temperature and baryon chemical potential case”. In: *Progress of Theoretical and Experimental Physics* 2013.1 (2013), page 013D02. DOI: 10.1093/ptep/pts055. URL: http://dx.doi.org/10.1093/ptep/pts055.

[104] Jia Jie Li, Wen Hui Long, and Armen Sedrakian. “Hypernuclear stars from relativistic Hartree-Fock density functional theory”. In: *Eur. Phys. J. A* 54.8 (2018), page 133. DOI: 10.1140/epja/i2018-12566-6. arXiv: 1801.07084 [nucl-th].

[105] Jia Jie Li and Armen Sedrakian. “Implications from GW170817 for Δ-isobar Admixed Hypernuclear Compact Stars”. In: *Astrophys. J. Lett.* 874.2 (2019), page L22. DOI: 10.3847/2041-8213/ab1090. arXiv: 1904.02006 [nucl-th].

[106] Jia Jie Li, Armen Sedrakian, and Fridolin Weber. “Rapidly rotating Δ-resonance-admixed hypernuclear compact stars”. In: *Phys. Lett. B* 810 (2020), page 135812. DOI: 10.1016/j.physletb.2020.135812. arXiv: 2010.02901 [astro-ph.HE].

[107] Domenico Logoteta et al. “A Chiral model approach to quark matter nucleation in neutron stars”. In: *Phys. Rev. D* 85 (2012), page 023003. DOI: 10.1103/PhysRevD.85.023003.

[108] L. L. Lopes and D. P. Menezes. “The Influence of Hyperons and Strong Magnetic Field in Neutron Star Properties”. In: *Brazilian Journal of Physics* 42.5–6 (August 2012), pages 428–436. ISSN: 1678-4448. DOI: 10.1007/s13538-012-0093-y. URL: http://dx.doi.org/10.1007/s13538-012-0093-y.

[109] Luiz L Lopes. “Hyperonic neutron stars: reconciliation between nuclear properties and NICER and LIGO/VIRGO results”. In: *Communications in Theoretical Physics* (2021).

[110] Luiz L Lopes. “The neutron star inner crust: An empirical essay”. In: *EPL (Europhysics Letters)* 134.5 (2021), page 52001.

[111] Luiz L Lopes, Carline Biesdorf, and Débora P Menezes. “Modified MIT bag Models—part I: Thermodynamic consistency, stability windows and symmetry group”. In: *Physica Scripta* 96.6 (March 2021), page 065303. DOI: 10.1088/1402-4896/abef34.

[112] Luiz L Lopes et al. “Modified MIT Bag Models—part II: QCD phase diagram and hot quark stars”. In: *Physica Scripta* 96.6 (March 2021), page 065302. DOI: 10.1088/1402-4896/abef35.

[113] Luiz L. Lopes and Debora P. Menezes. “Broken SU(6) symmetry and massive hybrid stars”. In: (April 2020). arXiv: 2004.07909 [astro-ph.HE].

[114] Luiz L. Lopes and Debora P. Menezes. “Hypernuclear matter in a complete SU(3) symmetry group”. In: *Physical Review C* 89.2 (2014). arXiv:1309.4173, page 25805.

[115] G. López Castro and A. Mariano. “Determination of the ++ magnetic dipole moment”. In: *Physics Letters B* 517.3 (2001), pages 339–344. ISSN: 0370-2693. DOI: https://doi.org/10.1016/S0370-2693(01)00980-7. URL: https://www.sciencedirect.com/science/article/pii/S0370269301009807.

[116] G. López Castro and A. Mariano. “Elastic and radiative +p scattering and properties of the ++ resonance”. In: *Nuclear Physics A* 697.1 (2002), pages 440–468. ISSN: 0375-9474. DOI: https://doi.org/10.1016/S0375-9474(01)01246-5. URL: https://www.sciencedirect.com/science/article/pii/S0375947401012465.

[117] Odilon Lourenço et al. “Consistent relativistic mean-field models constrained by GW170817”. In: *Physical Review C* 99.4 (2019), page 045202.

[118] German Malfatti et al. “Delta baryons and diquark formation in the cores of neutron stars”. In: *Phys. Rev. D* 102.6 (2020), page 063008. DOI: 10.1103/PhysRevD.102.063008. arXiv: 2008.06459 [astro-ph.HE].

[119] Michał Marczenko, Krzysztof Redlich, and Chihiro Sasaki. “Chiral symmetry restoration and Δ matter formation in neutron stars”. In: *Phys. Rev. D* 105.10 (2022), page 103009. DOI: 10.1103/PhysRevD.105.103009. arXiv: 2203.00269 [nucl-th].

[120] Jérôme Margueron, Rudiney Hoffmann Casali, and Francesca Gulminelli. “Equation of state for dense nucleonic matter from metamodeling. II. Predictions for neutron star properties”. In: *Phys. Rev. C* 97 (2 2018), page 025806. DOI: 10.1103/PhysRevC.97.025806.

[121] K. D. Marquez and D. P. Menezes. “Phase transition in compact stars: nucleation mechanism and γ-ray bursts revisited”. In: *Journal of Cosmology of Astroparticle Physics* 12, 028 (December 2017), page 028. DOI: 10.1088/1475-7516/2017/12/028. arXiv: 1709.07040 [astro-ph.HE].

[122] K. D. Marquez et al. *Exploring the effects of Delta Baryons in magnetars*. 2022. DOI: 10.48550/ARXIV.2205.09827.

[123] Kauan D. Marquez et al. *Delta baryons in neutron stars*. 2022. DOI: 10.48550/ARXIV.2206.02935.

[124] Larry McLerran. "Inhomogeneous and Quarkyonic phases of High Density QCD". In: *PoS* CPOD2014 (2015), page 046. DOI: 10.22323/1.217.0046.

[125] Débora P. Menezes et al. "Repulsive vector interaction in three-flavor magnetized quark and stellar matter". In: *Phys. Rev. C* 89 (5 May 2014), page 055207. DOI: 10.1103/PhysRevC.89.055207. URL: https://link.aps.org/doi/10.1103/PhysRevC.89.055207.

[126] Débora Péres Menezes. *Introduçâo à física nuclear e de partículas elementares*. Florianópolis: Editora da UFSC, 2002.

[127] M.C. Miller et al. "PSR J0030+0451 Mass and Radius from *NICER* Data and Implications for the Properties of Neutron Star Matter". In: *Astrophys. J. Lett.* 887.1 (2019), page L24. DOI: 10.3847/2041-8213/ab50c5. arXiv: 1912.05705 [astro-ph.HE].

[128] C. W. Misner, K. S. Thorne, and J. A. Wheeler. *Gravitation*. San Francisco: W. H. Freeman & Co., 1973.

[129] T.F. Motta, A.W. Thomas, and Pierre A.M. Guichon. "Do Delta Baryons Play a Role in Neutron Stars?" In: *Phys. Lett. B* 802 (2020), page 135266. DOI: 10.1016/j.physletb.2020.135266. arXiv: 1906.05459 [nucl-th].

[130] Theo F. Motta and Anthony W. Thomas. "The role of baryon structure in neutron stars". In: *Mod. Phys. Lett. A* 37.01 (2022), page 2230001. DOI: 10.1142/S0217732322300014. arXiv: 2201.11549 [nucl-th].

[131] Ch. C. Moustakidis et al. "Bounds on the speed of sound in dense matter, and neutron star structure". In: *Phys. Rev. C* 95.4 (2017). [Erratum: Phys.Rev.C 95, 059904 (2017)], page 045801. DOI: 10.1103/PhysRevC.95.045801. arXiv: 1608.00344 [nucl-th].

[132] Horst Müller. "The deconfinement phase transition in asymmetric matter". In: *Nuclear Physics A* 618.3 (1997), page 349. ISSN: 0375-9474. DOI: https://doi.org/10.1016/S0375-9474(97)00018-3. URL: http://www.sciencedirect.com/science/article/pii/S0375947497000183.

[133] Horst Müller and Brian D. Serot. “Phase transitions in warm, asymmetric nuclear matter”. In: *Phys. Rev. C* 52 (4 October 1995), page 2072. DOI: 10.1103/PhysRevC.52.2072. URL: http://link.aps.org/doi/10.1103/PhysRevC.52.2072.

[134] Y. Nambu and G. Jona-Lasinio. “Dynamical Model of Elementary Particles Based on an Analogy with Superconductivity. I”. In: *Phys. Rev.* 122 (1 April 1961), page 345. DOI: 10.1103/PhysRev.122.345. URL: https://link.aps.org/doi/10.1103/PhysRev.122.345.

[135] M. Oertel et al. “Hyperons in neutron star matter within relativistic mean-field models”. In: *J. Phys. G* 42.7 (2015), page 075202. DOI: 10.1088/0954-3899/42/7/075202. arXiv: 1412.4545 [nucl-th].

[136] A. Ohnishi et al. “Possibility of s-wave pion condensates in neutron stars revisited”. In: *Phys. Rev. C* 80 (2009), page 038202. DOI: 10.1103/PhysRevC.80.038202. arXiv: 0810.3531 [nucl-th].

[137] Michael L. Olesen and Jes Madsen. “Nucleation of quark matter bubbles in neutron stars”. In: *Physical Review D* 49 (6 1994). arXiv:astro-ph/9401002, pages 2698–2702.

[138] Rosana de Oliveira Gomes. *Transições de fase hádron-quark em de estrelas de nêutrons*. (Dissertação de Mestrado). Porto Alegre: Universidade Federal do Rio Grande do Sul, 2011.

[139] Julius Robert Oppenheimer and George Michael Volkoff. “On Massive Neutron Cores”. In: *Physical Review* 55 (4 February 1939), page 374. DOI: 10.1103/PhysRev.55.374. URL: https://link.aps.org/doi/10.1103/PhysRev.55.374.

[140] Asaf Oron. “Relativistic magnetized star with poloidal and toroidal fields”. In: *Phys. Rev. D* 66 (2 July 2002), page 023006. DOI: 10.1103/PhysRevD.66.023006. URL: https://link.aps.org/doi/10.1103/PhysRevD.66.023006.

[141] F. Özel et al. “The Dense Matter Equation of State from Neutron Star Radius and Mass Measurements”. In: *The Astrophysical Journal* 820, 28 (March 2016), page 28. DOI: 10.3847/0004-637X/820/1/28. arXiv: 1505.05155 [astro-ph.HE].

[142] Helena Pais, Débora P. Menezes, and Constança Providência. “Neutron stars: from the inner crust to the core with the (extended) Nambu-Jona-Lasinio model”. In: *Physical Review C* 93.6 (2016), page 65805.

[143] Helena Pais and Constança Providência. “Vlasov formalism for extended relativistic mean field models: The crust-core transition and the stellar matter equation of state”. In: *Phys. Rev. C* 94.1 (2016), page 015808. DOI: 10.1103/PhysRevC.94.015808. arXiv: 1607.05899 [nucl-th].

[144] M. G. de Paoli et al. “The Rarita-Schwinger Particles Under de Influence of Strong Magnetic Fields”. In: *J. Phys. G* 40 (2013), page 055007. DOI: 10.1088/0954-3899/40/5/055007. arXiv: 1207.4063 [math-ph].

[145] M. G. Paoli and D. P. Menezes. “The importance of the mixed phase in hybrid stars built with the Nambu-Jona–Lasinio model”. In: *European Physical Journal A* 46 (2010), page 413. DOI: 10.1140/epja/i2010-11059-0.

[146] Michael E. Peskin and Daniel V. Schroeder. *An introduction to quantum field theory*. Boulder, CO: Westview, 1995.

[147] A. G. Pili, N. Bucciantini, and L. Del Zanna. “General relativistic models for rotating magnetized neutron stars in conformally flat space–time”. In: *Monthly Notices of the Royal Astronomical Society* 470.2 (May 2017), pages 2469–2493. ISSN: 0035-8711. DOI: 10.1093/mnras/stx1176. eprint: https://academic.oup.com/mnras/article-pdf/470/2/2469/18245433/stx1176.pdf. URL: https://doi.org/10.1093/mnras/stx1176.

[148] M. Prakash, J. R. Cooke, and J. M. Lattimer. “Quark - hadron phase transition in protoneutron stars”. In: *Phys. Rev. D* 52 (1995), pages 661–665. DOI: 10.1103/PhysRevD.52.661.

[149] C. Providência et al. “Nuclear matter mean field with extended NJL model”. In: *AIP Conf. Proc.* 660 (2003), page 231.

[150] Constança Providência, João Providência, and Steven A. Moszkowski. “EOS of nuclear matter within a generalised NJL model”. In: *Int. J. Mod. Phys.* B17 (2003). [Ser. Adv. Quant. Many Body Theor.6,242(2002)], page 5209. DOI: 10.1142/9789812777843_0030.

[151] A Rabhi et al. “Quark–hadron phase transition in a neutron star under strong magnetic fields”. In: *Journal of Physics G: Nuclear and Particle Physics* 36.11 (October 2009), page 115204. ISSN: 1361-6471. DOI: 10.1088/0954-3899/36/11/115204. URL: http://dx.doi.org/10.1088/0954-3899/36/11/115204.

[152] Adriana R. Raduta. “Δ-admixed neutron stars: spinodal instabilities and dUrca processes”. In: *Phys. Lett. B* 814 (2021), page 136070. DOI: 10.1016/j.physletb.2021.136070. arXiv: 2101.03718 [nucl-th].

[153] Adriana R. Raduta, Micaela Oertel, and Armen Sedrakian. “Proto-neutron stars with heavy baryons and universal relations”. In: *Mon. Not. Roy. Astron. Soc.* 499.1 (2020), pages 914–931. DOI: 10.1093/mnras/staa2491. arXiv: 2008.00213 [nucl-th].

[154] Brendan Reed and C. J. Horowitz. “Large sound speed in dense matter and the deformability of neutron stars”. In: *Phys. Rev. C* 101.4 (2020), page 045803. DOI: 10.1103/PhysRevC.101.045803. arXiv: 1910.05463 [astro-ph.HE].

[155] Brendan T. Reed et al. “Implications of PREX-2 on the Equation of State of Neutron-Rich Matter”. In: *Phys. Rev. Lett.* 126 (17 April 2021), page 172503. DOI: 10.1103/PhysRevLett.126.172503.

[156] Patricia Ribes et al. “Interplay between Delta Particles and Hyperons in Neutron Stars”. In: *The Astrophysical Journal* 883.2 (October 2019), page 168. DOI: 10.3847/1538-4357/ab3a93. URL: https://doi.org/10.3847/1538-4357/ab3a93.

[157] Thomas E. Riley et al. “A *NICER* View of PSR J0030+0451: Millisecond Pulsar Parameter Estimation”. In: *Astrophys. J. Lett.* 887.1 (2019), page L21. DOI: 10.3847/2041-8213/ab481c. arXiv: 1912.05702 [astro-ph.HE].

[158] Thomas E. Riley et al. “A NICER View of the Massive Pulsar PSR J0740+6620 Informed by Radio Timing and XMM-Newton Spectroscopy”. In: *Astrophys. J. Lett.* 918.2 (2021), page L27. DOI: 10.3847/2041-8213/ac0a81. arXiv: 2105.06980 [astro-ph.HE].

[159] Georges Ripka. *Quarks bound by chiral fields: the quark structure of the vacuum and of light mesons and baryons*. Oxford Stud. Nucl. Phys. Oxford: Clarendon Press, 1997.

[160] J. Roark and V. Dexheimer. “Deconfinement phase transition in proto-neutron-star matter”. In: *Phys. Rev. C* 98.5 (2018), page 055805. DOI: 10.1103/PhysRevC.98.055805. arXiv: 1803.02411 [nucl-th].

[161] J. Roark et al. “Hyperons and quarks in proto-neutron stars”. In: *Mon. Not. Roy. Astron. Soc.* 486.4 (2019), pages 5441–5447. DOI: 10.1093/mnras/stz1240. arXiv: 1812.08157 [astro-ph.HE].

[162] Himanshu S. Sahoo, Rabindranath Mishra, and Prafulla K. Panda. “Delta Matter in Neutron Stars in a Relativistic Quark Model”. In: *JPS Conf. Proc.* 32 (2020), page 010054. DOI: 10.7566/JPSCP.32.010054.

[163] B. M. Santos et al. “Correlations between the nuclear matter symmetry energy, its slope, and curvature from a nonrelativistic solvable approach and beyond”. In: *Phys. Rev. C* 90.3 (2014), page 035203.

[164] H. Sazdjian. “Introduction to chiral symmetry in QCD”. In: *European Physical Journal Web of Conferences*. Volume 137. 2017.

[165] Jurgen Schaffner and Igor N. Mishustin. “Hyperon rich matter in neutron stars”. In: *Phys. Rev. C* 53 (1996), pages 1416–1429. DOI: 10.1103/PhysRevC.53.1416. arXiv: nucl-th/9506011.

[166] Georg Schneider et al. “Double-trap measurement of the proton magnetic moment at 0.3 parts per billion precision”. In: *Science* 358.6366 (2017), pages 1081–1084. DOI: 10.1126/science.aan0207. eprint: https://www.science.org/doi/pdf/10.1126/science.aan0207. URL: https://www.science.org/doi/abs/10.1126/science.aan0207.

[167] Torsten Schürhoff, Stefan Schramm, and Veronica Dexheimer. “Neutron stars with small radii – the role of delta resonances”. In: *Astrophys. J. Lett.* 724 (2010), pages L74–L77. DOI: 10.1088/2041-8205/724/1/L74. arXiv: 1008.0957 [astro-ph.SR].

[168] Armen Sedrakian, Fridolin Weber, and Jia Jie Li. “Confronting GW190814 with hyperonization in dense matter and hypernuclear compact stars”. In: *Phys. Rev. D* 102.4 (2020), page 041301. DOI: 10.1103/PhysRevD.102.041301. arXiv: 2007.09683 [astro-ph.HE].

[169] Richard R. Silbar and Sanjay Reddy. “Neutron stars for undergraduates”. In: *American Journal of Physics* 72 (2004). arXiv:nucl-th/0309041, page 892.

[170] T. H. R. Skyrme. “The nuclear surface”. In: *Philosophical Magazine* 1.11 (1956). doi:10.1080/14786435608238186, pages 1043–1054.

[171] Patrick Steinbrecher. “The QCD crossover at zero and non-zero baryon densities from Lattice QCD”. In: *Nuclear Physics A* 982 (2019), pages 847–850. DOI: 10.1016/j.nuclphysa.2018.08.025.

[172] A. W. Steiner, J. M. Lattimer, and E. F. Brown. “The Neutron Star Mass-Radius Relation and the Equation of State of Dense Matter”. In: *Astrophysical Journal Letters* 765, L5 (March 2013), page L5. DOI: 10.1088/2041-8205/765/1/L5. arXiv: 1205.6871 [nucl-th].

[173] Misha Stephanov. “QCD phase diagram: an overview”. In: *XXIVth International Symposium on Lattice Field Theory*. 2006.

[174] J. R. Stone, N. J. Stone, and S. A. Moszkowski. “Incompressibility in finite nuclei and nuclear matter”. In: *Physical Review C* 89.4 (2014). arXiv:1404.0744, page 44316.

[175] J. R. Stone et al. “Equation of state of hot dense hyperonic matter in the Quark–Meson-Coupling (QMC-A) model”. In: *Mon. Not. Roy. Astron. Soc.* 502.3 (2021), pages 3476–3490. DOI: 10.1093/mnras/staa4006. arXiv: 1906.11100 [nucl-th].

[176] Junpei Sugano et al. “Determination of the strength of the vector-type four-quark interaction in the entanglement Polyakov-loop extended Nambu–Jona-Lasinio model”. In: *Phys. Rev. D* 90 (3 August 2014), page 037901. DOI: 10.1103/PhysRevD.90.037901. URL: https://link.aps.org/doi/10.1103/PhysRevD.90.037901.

[177] Ingo Tews et al. “Constraining the speed of sound inside neutron stars with chiral effective field theory interactions and observations”. In: *Astrophys. J.* 860.2 (2018), page 149. DOI: 10.3847/1538-4357/aac267. arXiv: 1801.01923 [nucl-th].

[178] Vivek Baruah Thapa et al. “Equation of State of Strongly Magnetized Matter with Hyperons and Δ-Resonances”. In: *Particles* 3.4 (2020). Edited by Armen Sedrakian, pages 660–675. DOI: 10.3390/particles3040043. arXiv: 2010.00981 [hep-ph].

[179] Vivek Baruah Thapa et al. “Massive Δ-resonance admixed hypernuclear stars with antikaon condensations”. In: *Phys. Rev. D* 103.6 (2021), page 063004. DOI: 10.1103/PhysRevD.103.063004. arXiv: 2102.08787 [astro-ph.HE].

[180] Richard Chace Tolman. “Static Solutions of Einstein’s Field Equations for Spheres of Fluid”. In: *Physical Review* 55 (4 February 1939), page 364. DOI: 10.1103/PhysRev.55.364.

[181] Laura Tolos, Mario Centelles, and Angels Ramos. “Equation of State for Nucleonic and Hyperonic Neutron Stars with Mass and Radius Constraints”. In: *The Astrophysical Journal* 834.1 (December 2016), page 3. DOI: 10.3847/1538-4357/834/1/3. URL: https://doi.org/10.3847/1538-4357/834/1/3.

[182] M. Di Toro et al. “Testing deconfinement at high isospin density”. In: *Nuclear Physics A* 775.1 (2006), page 102. ISSN: 0375-9474. DOI: https://doi.org/10.1016/j.nuclphysa.2006.04.007. URL: http://www.sciencedirect.com/science/article/pii/S0375947406001734.

[183] Antonios Tsokaros, Milton Ruiz, and Stuart L. Shapiro. “GW190814: Spin and equation of state of a neutron star companion”. In: (July 2020). arXiv: 2007.05526 [astro-ph.HE].

[184] Yasuhiko Tsue et al. “First-Order Quark-Hadron Phase-Transition in a NJL-Type Model for Nuclear and Quark Matter: — The Case of Symmetric Nuclear Matter —”. In: *Progress of Theoretical Physics* 123.6 (2010), page 1013. DOI: 10.1143/PTP.123.1013.

[185] S. Typel and H. H. Wolter. “Relativistic mean field calculations with density dependent meson nucleon coupling”. In: *Nucl. Phys. A* 656 (1999), pages 331–364. DOI: 10.1016/S0375-9474(99)00310-3.

[186] S. Typel et al. “Composition and thermodynamics of nuclear matter with light clusters”. In: *Phys. Rev. C* 81 (2010), page 015803. DOI: 10.1103/PhysRevC.81.015803. arXiv: 0908.2344 [nucl-th].

[187] Isaac Vidaña. “Hyperons in Neutron Stars”. In: *J. Phys. Conf. Ser.* 668.1 (2016). Edited by David Alvarez-Castillo et al., page 012031. DOI: 10.1088/1742-6596/668/1/012031. arXiv: 1509.03587 [nucl-th].

[188] U. Vogl and W. Weise. “The Nambu and Jona-Lasinio model: Its implications for Hadrons and Nuclei”. In: *Progress in Particle and Nuclear Physics* 27 (1991), pages 195–272.

[189] U. Vogl et al. “Generalized SU(3) Nambu-Jona-Lasinio model: (II). From current to constituent quarks”. In: *Nuclear Physics A* 516.3 (1990), pages 469–495. ISSN: 0375-9474. DOI: https://doi.org/10.1016/0375-9474(90)90124-5. URL: http://www.sciencedirect.com/science/article/pii/0375947490901245.

[190] John Dirk Walecka. “A theory of highly condensed matter”. In: *Annals of Physics* 83.2 (1974). doi:10.1016/0003-4916(74)90208-5, pages 491–529.

[191] John Dirk Walecka. *Theoretical Nuclear and Subnuclear Physics*. 2nd. London: World Scientific Publishing, 2004.

[192] F. Weber. “Strange quark matter and compact stars”. In: *Progress in Particle and Nuclear Physics* 54.1 (2005). arXiv:astro-ph/0407155, pages 193–288.

[193] K. Wehrberger, C. Bedau, and F. Beck. “Electromagnetic excitation of the delta-baryon in quantum hadrodynamics”. In: *Nuclear Physics A* 504.4 (1989), pages 797–817. ISSN: 0375-9474. DOI: https://doi.org/10.1016/0375-9474(89)90008-0. URL: https://www.sciencedirect.com/science/article/pii/0375947489900080.

[194] X. J. Wen et al. “Magnetized strange quark matter in a quasiparticle description”. In: *Phys. Rev. D* 86 (3 August 2012), page 034006. DOI: 10.1103/PhysRevD.86.034006. URL: https://link.aps.org/doi/10.1103/PhysRevD.86.034006.

[195] Frank A. Wilczek. “Assymptotic freedom: from paradox to paradigm”. In: *Nobel Prize lecture* (2004). [Disponível em https://www.nobelprize.org/nobel_prizes/physics/laureates/2004/wilczek-lecture.pdf].

[196] Edward Witten. “Cosmic separation of phases”. In: *Physical Review D* 30.2 (1984), pages 272–285.

[197] C. J. Xia et al. “Thermodynamic consistency, quark mass scaling, and properties of strange matter”. In: *Phys. Rev. D* 89 (10 May 2014), page 105027. DOI: 10.1103/PhysRevD.89.105027. URL: https://link.aps.org/doi/10.1103/PhysRevD.89.105027.

[198] Hu Xiang and Guo Hua. “Delta excitation and its influences on neutron stars in relativistic mean field theory”. In: *Phys. Rev. C* 67 (2003), page 038801. DOI: 10.1103/PhysRevC.67.038801.

[199] Dmitrii G. Yakovlev et al. “Lev Landau and the concept of neutron stars”. In: *Physics-Uspekhi* 56.3 (2013), page 289.

[200] Ghil-Seok Yang and Hyun-Chul Kim. “Meson–baryon coupling constants of the SU(3) baryons with flavor SU(3) symmetry breaking”. In: *Phys. Lett. B* 785 (2018), pages 434–440. DOI: 10.1016/j.physletb.2018.09.010. arXiv: 1807.09090 [hep-ph].

[201] Nobutoshi Yasutake, Kenta Kiuchi, and Kei Kotake. “Relativistic hybrid stars with super-strong toroidal magnetic fields: an evolutionary track with QCD phase transition”. In: *Monthly Notices of the Royal Astronomical Society* 401.3 (2010), pages 2101–2112.

[202] Hideki Yukawa. “Meson theory in its developments”. In: *Nobel Prize lecture* (1949). [Disponível em https://www.nobelprize.org/nobel_prizes/physics/laureates/1949/yukawa-lecture.pdf].

[203] Hideki Yukawa. “On the Interaction of Elementary Particles”. In: *Proceedings of the Physico-Mathematical Society of Japan* 17.48 (1935).

APPENDIX A – BASICS OF THERMAL FIELD THEORY

The derivation of the quantities of interest in this work, essentially the equations of state for dense matter, rely on quantum field theory methods and, in particular, on its relationship with the thermodynamics of those systems. Thus, one needs to introduce chemical potential and temperature in the QFT formalism that describes the vacuum properties of the model through its Lagrangian. The case of the free fermion gas at temperature T and chemical potential μ is specially relevant to the discussion of the Nambu–Jona-Lasinio model, and it is presented next, following [89].

A system of free spin-1/2 fermions ψ of mass m is described by the Lagrangian density

$$\mathcal{L} = \bar{\psi}\left(i\partial\!\!\!/ - m\right)\psi. \tag{152}$$

The inclusion of the chemical potential in the Lagrangian must be associated with a conserved charge. From the *Noether's theorem*, it is known that a conserved current is related to the symmetries of the Lagrangian, i.e., the global symmetry $\psi \to e^{-i\theta}\psi$. Hence, the conserved current is

$$j^{\mu} = \frac{\partial\mathcal{L}}{\partial(\partial_{\mu}\psi)}\frac{\delta\psi}{\delta\theta} = \bar{\psi}\gamma^{\mu}\psi, \tag{153}$$

which, since $\bar{\psi} = \psi^{\dagger}\gamma^{0}$, yields the conserved charge $j^{0} = \psi^{\dagger}\psi$, identified as the barionic number density. Then, the Lagrangian with chemical potential simply is

$$\mathcal{L} = \bar{\psi}\left(i\partial\!\!\!/ + \gamma^{0}\mu - m\right)\psi. \tag{154}$$

The conjugate momentum is

$$\pi = \frac{\partial\mathcal{L}}{\partial(\partial_{\mu}\psi)} = i\psi^{\dagger}, \tag{155}$$

which means ψ and $\psi^{\dagger}$ must be taken as independent variables and allows to write the Hamiltonian as

$$H = \int_{0}^{\beta} d\tau \int d^{3}x\, \bar{\psi}\left(-\gamma^{0}\partial_{\tau} - i\vec{\gamma}\cdot\nabla + \gamma^{0}\mu - m\right)\psi, \tag{156}$$

where the temperature is introduced in replacement of the temporal degree of freedom via the *imaginary time formalism*, with $\tau = it$ and $\beta = 1/T$.

The partition function $Z = \mathrm{Tr}\exp(-\beta H)$ can then be written, taking the the path integral representation of the trace, as

$$Z = \int \mathcal{D}\psi^{\dagger}\mathcal{D}\psi \exp\left[\int_{0}^{\beta} d\tau \int d^{3}x\, \bar{\psi}\left(-\gamma^{0}\partial_{\tau} - i\vec{\gamma}\cdot\nabla + \gamma^{0}\mu - m\right)\psi\right]. \tag{157}$$

In the path integral formalism, the partition function can be derived from a transition amplitude with identical initial and final states. In the case of fermions, the fields integral are *Grassmann variables*, as a consequence of the anticommutation relations

of creation and annihilation operators. So, the trace involves a transition amplitude where initial and final states differ by a sign, imposing the functional integration to be performed over antiperiodic fields $\psi(0,\vec{x}) = -\psi^\dagger(\beta,\vec{x})$ and $\psi(0,\vec{x}) = -\psi^\dagger(\beta,\vec{x})$. Introducing the dimensionless Fourier-transformed fields

$$\psi(x) = \frac{1}{\sqrt{V}}\sum_k e^{-ik\cdot x}\psi(k) \quad \text{and} \quad \psi^\dagger(x) = \frac{1}{\sqrt{V}}\sum_k e^{ik\cdot x}\psi^\dagger(k), \tag{158}$$

from where the *Matsubara frequencies* ω_n were defined from the zeroth component of the four-momentum k, i.e., $k_0 = -i\omega_n$. To fulfill the antiperiodicity requirement, one must have $e^{i\beta\omega_n} = -1$ which implies that the fermionic Matsubara frequencies are

$$\omega_n = (2n+1)\pi T, \qquad n \in \mathbb{Z}. \tag{159}$$

With the Fourier decomposition, ((157)) can be rewritten as

$$Z = \int \mathcal{D}\psi^\dagger \mathcal{D}\psi \exp\left[\sum_k \psi^\dagger(k)\frac{G^{-1}(k)}{T}\psi(k)\right], \tag{160}$$

with the free fermion inverse propagator in momentum space being

$$G^{-1}(k) = \not{k} + \gamma^0\mu - m. \tag{161}$$

The functional integration over Grassmann variables can be done using the relation

$$\int \prod_a^N d\eta_a^\dagger d\eta \exp\left(-\sum_{i,j}^N \eta_i^\dagger M_{ij}\eta_j\right) = \det M, \tag{162}$$

allowing to get the partition function

$$Z = \det\left(-\frac{G^{-1}(k)}{T}\right) = \det\frac{1}{T}\begin{pmatrix} -(k_0+\mu)+m & -\vec{\sigma}\cdot\vec{k} \\ \vec{\sigma}\cdot\vec{k} & (k_0+\mu)+m \end{pmatrix}, \tag{163}$$

where the determinant is taken over Dirac and momentum spaces and $\vec{\sigma}$ is the Pauli vector. With $k_0 = -i\omega_n$ and using $(\vec{\sigma}\cdot\vec{k})^2 = k^2$, one can work out

$$\ln Z = \sum_k\sum_n \ln\left[\frac{E_k^2 + (\omega_n + i\mu)^2}{T^2}\right]^2 \tag{164}$$

$$= \sum_k\sum_n \left\{\ln\left[\frac{\omega_n^2 + (E_k-\mu)^2}{T^2}\right] + \ln\left[\frac{\omega_n^2 + (E_k+\mu)^2}{T^2}\right]\right\}, \tag{165}$$

where it was defined $E_k = \sqrt{k^2+m^2}$. The sum over fermionic Matsubara frequencies is performed via contour integration in the complex plane, the details of the calculation are discussed in most textbooks that deal with thermal field theory and are not presented here, c.f., [89]. For the free fermion case, this sum reads

$$\sum_n \ln\left[\frac{\omega_n^2 + (E_k \pm \mu)^2}{T^2}\right] = \frac{E_k \pm \mu}{T^2} + 2\ln\left[1 + \exp\left(-\frac{E_k \pm \mu}{T}\right)\right] + \text{const.}, \tag{166}$$

which, taking the thermodynamic limit, allows to get the grand-canonical thermodynamic potential per volume for the free fermion gas at temperature T, from $\Omega = -T \ln Z$, as

$$\Omega = -2 \int \frac{d^3k}{(2\pi)^3} \left\{ E_k + T \ln \left[1 + \exp\left(-\frac{E_k - \mu}{T} \right) \right] + T \ln \left[1 + \exp\left(-\frac{E_k + \mu}{T} \right) \right] \right\}, \tag{167}$$

where overall factor 2 accounts for the two spin states of the spin-1/2 fermion.

From these results for the grand-canonical potential, other thermodynamic quantities can be obtained in the standard way. Since the system is uniform, pressure P and energy density ε are obtained through

$$P(T,\mu) = -\Omega(T,\mu), \tag{168}$$

and

$$\varepsilon(T,\mu) = -P(T,\mu) + Ts(T,\mu) + \mu\rho(T,\mu), \tag{169}$$

where $s = -\partial\Omega/\partial T$ is the entropy density, given by

$$s(T,\mu) = 2 \int \frac{d^3k}{(2\pi)^3} \left[\frac{E_k - \mu}{T} n_k(T,\mu) + \frac{E_k - \mu}{T} \bar{n}_k(T,\mu) - \ln\left(1 - n_k(T,\mu)\right) - \ln\left(1 - \bar{n}_k(T,\mu)\right) \right]. \tag{170}$$

Many applications of effective models of QCD are performed in the $T = 0$ limit. It is a reasonable approximation in situations where the thermal energy is smaller than the average kinetic energy of the particles of the system, i.e., when $k_B T \ll E_p$. For the gases of light quarks or hadrons considered in this work, it remains true until temperatures of the order of 10^{10} K, making the so-called *degenerate case* suitable to the description of cold stellar remnants, as neutron stars some time after their formation in supernovae, as well as to deal with nuclear matter.

In the Nambu–Jona-Lasinio model, the temperature dependence is embedded in the scalar and number densities, ρ_{si} and ρ_i, and in the displaced free fermion gas contribution Ω_{M_i}, given by equations ((111)), ((112)) and ((108)), respectively. In the equations for the densities, the temperature is included via the Fermi-Dirac distribution functions ((82)), remembering that they are here taken for particles of mass M_i subject to a chemical potential $\tilde{\mu}_i$, from where is easy to verify that, for each species of fermion i,

$$\lim_{T\to 0} n_p(T) = \begin{cases} 0 & \text{if } E_{p_i} - \tilde{\mu}_i > 0 \\ 1 & \text{if } E_{p_i} - \tilde{\mu}_i < 0 \end{cases}, \tag{171}$$

as illustrated in Figure 47. So, in the degenerate case, the particle distribution behaves as the step function $\theta(\tilde{\mu}_i - E_{p_i})$, which implies that all states down to the state of eigenvalue $E_{p_i} = \tilde{\mu}_i$, are occupied and the remaining are empty. It is a direct consequence

of the Pauli exclusion principle, since that, in the $T = 0$ limit, the fermions have to be in the energy level with the lowest energy that are still unoccupied. The most energetic level occupied is known as *Fermi level*, associated to the Fermi energy

$$E_{Fi} = \tilde{\mu}_i = \sqrt{p_{Fi}^2 + M_i^2}, \tag{172}$$

where p_{Fi} is the momentum associated to the most energetic particle, called Fermi momentum, which allows to redefine the step function as $\theta(p_{Fi}-p)$. It is also straightforward to see that

$$\lim_{T\to 0} \bar{n}_p(T) = 0, \tag{173}$$

which means that there are no antiparticles present in the degenerate matter, as already expected.

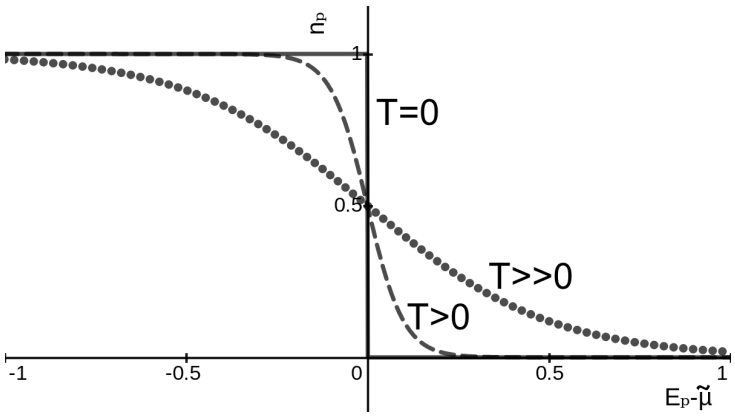

Figure 47 – Fermi-Dirac distribution functions for particles as a function of $E_p - \tilde{\mu}$.

Hence, it is direct to obtain the density of a degenerate Fermi gas,

$$\rho_i = 2N_c \int_0^{\Lambda} \frac{d^3p}{(2\pi)^3}\theta(p_{Fi}-p) = \frac{N_c}{3\pi^2}p_{Fi}^3, \tag{174}$$

where N_c is the color degeneracy factor ($N_c = 3$ for quarks and $N_c = 1$ for hadrons), and $p_{Fi} = \sqrt{\tilde{\mu}_i^2 - M_i^2}$, always demanding $p_{Fi} \leq \Lambda$. Also, the scalar density at $T = 0$ can be written as

$$\rho_{si} = -2N_c \int_0^{\Lambda} \frac{d^3p}{(2\pi)^3} \frac{M_i}{\sqrt{p^2+M_i^2}} \left[1-\theta(p_{Fi}-p)\right] = N_c M_i [F_0(p_{Fi}) - F_0(\Lambda)], \tag{175}$$

where it was defined the function

$$F_0(x) = \int_0^x \frac{dp}{\pi^2} \frac{p^2}{\sqrt{p^2+M_i^2}}. \tag{176}$$

To evaluate the zero-temperature limit of the displaced free fermion gas contribution, it is useful to define

$$f_{\pm}(T) = T \ln\left[1 + e^{-(E_{p_i} \pm \tilde{\mu}_i)/T}\right], \tag{177}$$

such that

$$\lim_{T\to 0} f_+(T) = 0, \tag{178}$$

and

$$\lim_{T\to 0} f_-(T) = \begin{cases} 0 & \text{if } E_{p_i} - \tilde{\mu}_i > 0 \\ \tilde{\mu}_i - E_{p_i} & \text{if } E_{p_i} - \tilde{\mu}_i < 0 \end{cases}, \tag{179}$$

where the $E_{p_i} - \tilde{\mu}_i < 0$ case was evaluated through the *generalized Puiseux series expansion* of $\ln(1+x)$ around $x = \infty$, i.e.,

$$\ln(1+x) = -\ln x + \frac{1}{x} - \frac{1}{2x^2} + \frac{1}{3x^3} + \cdots \tag{180}$$

and taking advantage that the terms of the type $(nx^n)^{-1}$ vanish for $x \to \infty$. Again, both possible outcomes can be written as a step function such that, taking $\theta(\tilde{\mu}_i - E_{p_i})$ in the momentum space, the degenerate displaced free fermion gas contribution is given by

$$\begin{aligned} \Omega_{M_i}(0,\tilde{\mu}) &= -2N_c \int_0^{\Lambda} \frac{d^3p}{(2\pi)^3} \left[E_{p_i} + (\tilde{\mu}_i - E_{p_i})\theta(p_{F\,i} - p) \right] \\ &= N_c[F_1(p_{F\,i}) - F_1(\Lambda)] - \tilde{\mu}_i \rho_i, \end{aligned} \tag{181}$$

where it was defined

$$F_1(x) = \int_0^x \frac{dp}{\pi^2} p^2 \sqrt{p^2 + M_i^2}, \tag{182}$$

and the result ((174)) was identified. It is convenient to define

$$\varepsilon_{\text{kin}} = \sum N_c[F_1(p_{F\,i}) - F_1(\Lambda)], \tag{183}$$

with the summation over all particles species.

Using the results presented above, it is straightforward to write the equations of state for free quark and hadronic matter at $T = 0$ from the thermodynamic potentials. Below, the expressions for degenerate matter that follow from the eNJL models considered in this work are shown. The same procedure allows us to get the equations for quark matter, changing the hadronic parameters to the quark model one and disregarding the extra terms of the generalized case. From ((87)), one gets for the PPM NJL model,

$$\begin{aligned} P_{\text{PPM}} = &\sum_{i=p,n} \tilde{\mu}_i \rho_i - \varepsilon_{\text{kin}} - G_s \rho_s^2 + G_v \rho^2 - G_\rho \rho_3^2 \\ &- G_{sv} \rho_s^2 \rho^2 + G_{s\rho} \rho_s^2 \rho_3^2 - G_{v\rho} \rho^2 \rho_3^2 + \Omega_{\text{vac}}, \end{aligned} \tag{184}$$

and

$$\begin{aligned} \varepsilon_{\text{PPM}} = &\sum_{i=p,n} (\mu_i - \tilde{\mu}_i)\rho_i + \varepsilon_{\text{kin}} + G_s \rho_s^2 - G_v \rho^2 + G_\rho \rho_3^2 \\ &+ G_{sv} \rho_s^2 \rho^2 - G_{s\rho} \rho_s^2 \rho_3^2 + G_{v\rho} \rho^2 \rho_3^2 - \Omega_{\text{vac}}, \end{aligned} \tag{185}$$

with

$$M = m - 2G_s\rho_s - 2G_{sv}\rho_s\rho^2 + 2G_{s\rho}\rho_s\rho_3^2 \tag{186}$$

$$\mu_i = \sqrt{p_{F_i}^2 + M_i^2} + 2G_v\rho \mp 2G_\rho\rho_3 - 2G_{sv}\rho\rho_s^2 \pm 2G_{s\rho}\rho_3\rho_s^2 - 2G_{v\rho}\rho\rho_3(\rho_3 \pm \rho). \tag{187}$$

Also, from ((91)), one gets for the PPMM NJL model,

$$\begin{aligned} P_{\text{PPMM}} = & \sum_{i=p,n,\Lambda} \tilde{\mu}_i\rho_i - \varepsilon_{\text{kin}} - 2G_s(\rho_{s_p}^2 + \rho_{s_n}^2 + \rho_{s_\Lambda}^2) + \frac{2}{3}G_v\rho^2 - G_\rho\left(\rho_3^2 + \frac{1}{3}\rho_8^2\right) \\ & - \frac{4}{3}G_{sv}(\rho_{s_p}^2 + \rho_{s_n}^2 + \rho_{s_\Lambda}^2)\rho^2 + 2G_{s\rho}(\rho_{s_p}^2 + \rho_{s_n}^2 + \rho_{s_\Lambda}^2)\left(\rho_3^2 + \frac{1}{3}\rho_8^2\right) \\ & - \frac{2}{3}G_{v\rho}\rho^2\left(\rho_3^2 + \frac{1}{3}\rho_8^2\right) + \Omega_{\text{vac}}, \end{aligned} \tag{188}$$

and

$$\begin{aligned} \varepsilon_{\text{PPMM}} = & \sum_{i=p,n,\Lambda} (\mu_i - \tilde{\mu}_i)\rho_i + \varepsilon_{\text{kin}} + 2G_s(\rho_{s_p}^2 + \rho_{s_n}^2 + \rho_{s_\Lambda}^2) - \frac{2}{3}G_v\rho^2 + G_\rho\left(\rho_3^2 + \frac{1}{3}\rho_8^2\right) \\ & + \frac{4}{3}G_{sv}(\rho_{s_p}^2 + \rho_{s_n}^2 + \rho_{s_\Lambda}^2)\rho^2 - 2G_{s\rho}(\rho_{s_p}^2 + \rho_{s_n}^2 + \rho_{s_\Lambda}^2)\left(\rho_3^2 + \frac{1}{3}\rho_8^2\right) \\ & + \frac{2}{3}G_{v\rho}\rho^2\left(\rho_3^2 + \frac{1}{3}\rho_8^2\right) - \Omega_{\text{vac}}, \end{aligned} \tag{189}$$

with

$$M_i = m_i - 4G_s\rho_{s_i} - \frac{8}{3}G_{sv}\rho_{s_i}\rho^2 + 4G_{s\rho}\rho_{s_i}\left(\rho_3^2 + \frac{1}{3}\rho_8^2\right), \tag{190}$$

for $i = \{p,n,\Lambda\}$,

$$\begin{aligned} \mu_i = & \sqrt{p_{F_i}^2 + M_i^2} + \frac{4}{3}G_v\rho \mp 2G_\rho\left(\rho_3 \pm \frac{1}{3}\rho_8\right) \\ & - \frac{4}{3}G_{sv}(\rho_{s_p}^2 + \rho_{s_n}^2 + \rho_{s_\Lambda}^2)\rho \pm 4G_{s\rho}(\rho_{s_p}^2 + \rho_{s_n}^2 + \rho_{s_\Lambda}^2)\left(\rho_3 \pm \frac{1}{3}\rho_8\right) \\ & \pm \frac{4}{3}G_{v\rho}\rho\left[\left(\rho_3^2 + \frac{1}{3}\rho_8^2\right) \mp \rho\left(\rho_3 + \frac{1}{3}\rho_8\right)\right], \end{aligned} \tag{191}$$

with the upper (lower) signs taken for $i = p$ ($i = n$), and

$$\begin{aligned} \mu_\Lambda = & \sqrt{p_{F_i}^2 + M_i^2} + \frac{4}{3}G_v\rho + \frac{4}{3}G_\rho\rho_8 - \frac{4}{3}G_{sv}(\rho_{s_p}^2 + \rho_{s_n}^2 + \rho_{s_\Lambda}^2)\rho \\ & - \frac{8}{3}G_{s\rho}(\rho_{s_p}^2 + \rho_{s_n}^2 + \rho_{s_\Lambda}^2)\rho_8 - \frac{4}{3}G_{v\rho}\rho\left[\left(\rho_3^2 + \frac{1}{3}\rho_8^2\right) - \frac{2}{3}\rho\rho_8\right], \end{aligned} \tag{192}$$

where, for both models, the upper (lower) signs taken for $i = p$ ($i = n$) in the equations of the chemical potential, and the number and scalar densities are given by ((174)) and ((175)).

Yet, the vacuum constant contribution Ω_{vac} can be obtained noticing that, in the $T = 0$ case, taking the limit $\mu \to 0$ implies $\tilde{\mu} \to 0$, making $p_{F\,i} = 0$ and, consequently, $\rho_i = 0$.

APPENDIX B – PUBLICATIONS

1. Graeff, C. A., Alloy, M. D., Marquez, K. D., Providência, C., Menezes, D. P. (2019). *Hadron-quark phase transition: the QCD phase diagram and stellar conversion*. **Journal of Cosmology and Astroparticle Physics**, 2019(01), 024 [72].
2. Lopes, L. L., Biesdorf, C., Marquez, K. D., Menezes, D. P. (2021). *Modified MIT Bag Models—part II: QCD phase diagram and hot quark stars*. **Physica Scripta**, 96(6), 065302 [112].
3. Backes, B. C., Marquez, K. D., Menezes, D. P. (2021). *Effects of strong magnetic fields on the hadron-quark deconfinement transition*. **The European Physical Journal A**, 57(7), 1-9 [9].
4. Dexheimer, V., Marquez, K. D., Menezes, D. P. (2021). *Delta baryons in neutron-star matter under strong magnetic fields*. **The European Physical Journal A**, 57(7), 1-9 [47].
5. Marquez, K. D., Pais, H., Menezes, D. P., Providência, C. (2022). *Delta baryons in neutron stars*. **arXiv:2206.02935** [123].
6. Marquez, K. D., Pelicer, M. R., Ghosh, S., Peterson, J., Chatterjee, D., Dexheimer, V., Menezes, D. P. (2022). *Exploring the effects of Delta Baryons in magnetars*. **arXiv:2205.09827** [122].

Journal of Cosmology and Astroparticle Physics
An IOP and SISSA journal

Hadron-quark phase transition: the QCD phase diagram and stellar conversion

Clebson A. Graeff,[a] **Marcelo D. Alloy,**[b] **Kauan D. Marquez,**[c] **Constança Providência**[d] **and Débora P. Menezes**[c]

[a]Universidade Tecnológica Federal do Paraná, Campus Pato Branco, Via do Conhecimento, Km 1 CEP 85503-390 Pato Branco PR, Brazil
[b]Departamento de Ciências Exatas e Educação, Universidade Federal de Santa Catarina, Blumenau, SC, CEP 89.065-300, Brazil
[c]Departamento de Física, Universidade Federal de Santa Catarina, Florianópolis, SC, CP 476, CEP 88.040-900, Brazil
[d]Departamento de Física, Universidade de Coimbra, 3004-516 Coimbra, Portugal

E-mail: cgraeff@utfpr.edu.br, marcelo.alloy@ufsc.br, kmarkez@hotmail.com, cp@uc.pt, debora.p.m@ufsc.br

Received November 23, 2018
Revised December 13, 2018
Accepted December 31, 2018
Published January 11, 2019

Abstract. Different extensions of the Nambu-Jona-Lasinio model, known to satisfy expected QCD chiral symmetry aspects, are used to investigate a possible hadron-quark phase transition at zero temperature and to build the corresponding binodal sections. We have shown that the transition point is very sensitive to the model parameters and that both pressure and chemical potential increase drastically with the increase of the vector interaction strength in the quark sector. Within the same framework, the possibility of quark and hybrid star formation is analyzed. The same conclusions drawn before with respect to the coexistence pressure and chemical potentials are reinforced. We conclude that even if a transition from a metastable hadronic star to a quark star is thermodinamically possible, it is either energetically forbidden or gives rise to a blackhole. Nevertheless, conversions from metastable to hybrid stars are possible, but the mass difference between both compact objects is very small, never larger than 0.2 $M_{\odot}$.

Keywords: baryon asymmetry, massive stars, neutron stars

ArXiv ePrint: 1806.04170

https://doi.org/10.1088/1475-7516/2019/01/024

JCAP01(2019)024

Modified MIT Bag Models - part II: QCD phase diagram and hot quark stars

Luiz L. Lopes,[1,*] Carline Biesdorf,[2] K. D. Marquez,[2] and Débora P. Menezes[2]

[1] *Centro Federal de Educação Tecnológica de Minas Gerais Campus VIII, CEP 37.022-560, Varginha, MG, Brasil*
[2] *Departamento de Fisica, CFM - Universidade Federal de Santa Catarina; C.P. 476, CEP 88.040-900, Florianópolis, SC, Brasil*

In the present work we use the modified versions of the MIT bag model, on which both a vector field and a self-interacting term are introduced, to obtain hot quark matter and to investigate the QCD phase diagram. We first analyze two-flavored quark matter constrained to both the freeze-out and the liquid-gas phase transition at the hadronic phase. Later, three-flavored quark matter subject to β equilibrium and charge neutrality is used to compute quark star macroscopic properties, which are confronted with recent observational massive and canonical star radius results. Finally, a comparison with QCD phase diagrams obtained from the Nambu-Jona-Lasinio model is performed.

PACS numbers: 21.65.Qr, 12.39.Ki

I. INTRODUCTION

One of the most important features of the quantum chromodynamics (QCD) is the asymptotic freedom, which predicts that strongly interacting matter undergoes a phase transition from hadrons (constituted of confined quarks) to deconfined quarks and gluons - the quark gluon plasma (QGP) - at some high temperature as well as high density [1, 2]. Therefore, the correlation between two external parameters arises: for a fixed temperature, what is the density (or equivalently, the baryon chemical potential), at which the phase transition occurs in equilibrium QCD?

To study the QGP as well as the hadron-quark phase transition several experiments have been proposed and performed in recent years at LHC, RICH and others [3–6]. Studying Au+Au and Pb+Pb collisions, Cleymans [7] was able to trace the chemical freeze-out line, obtained when inelastic collisions between particles cease such that the abundance ratios do not change anymore [8]. Although the chemical freeze-out is not directly related to the hadron-quark phase transition, the hadron multiplicities in central high energy nucleus-nucleus collisions are established very close to the phase boundary between hadronic and quark matter [9], especially at very low baryon chemical potential, when the chemical freeze-out temperature and the critical temperature are expected to lie at the same error bar [9, 10]. Moreover, the chemical freeze-out is expected to be a pure hadronic process, therefore, its trace needs to be in the hadron phase. This feature acts as a constraint for hadron-quark phase transition modeling.

In the standard model, the tool to describe strong interacting matter is the QCD. For low chemical potential and high temperature, the lattice QCD (LQCD) can be employed yielding satisfactory results. For instance, LQCD predicts the existence of a smooth crossover around a temperature of 160 MeV at low chemical potentials, while at higher densities a first order phase transition [11–13] is generally obtained from effective models. Furthermore, the first order phase transition must end at an unique point where a second order phase transition takes place, the critical end point (CEP), although its existence and exact location are not well-established [14, 15]. Another important region in the QCD phase diagram is the liquid-gas instability region related to nuclear fragmentation [16–18]. For low temperatures and chemical potential, the nucleons are confined into the nuclei [19], which can be regarded as a liquid phase. As the temperature increases, the nuclei start to dissolve into a diluted interacting gas of nucleons. A critical temperature, above which only the gas phase survives, is expected [20]. Like the chemical freeze-out, the liquid-gas phase transition is a pure hadronic process, where the contribution from the quark degrees of freedom can be neglected. Nevertheless, the region expected to undergo this phase transition can also be used as a constraint.

In this work we use the modified versions of the MIT bag model, as originally introduced in ref. [21] - on which a vector field is added in a minimal coupling scheme, as well as a self-interacting term that mimics the contribution from the quark Dirac sea [22] - to study the QCD phase diagram and hot quark matter. We start considering symmetric two-flavored quark matter, $\mu_d = \mu_u$, and check if we can fit both the freeze-out and the liquid-gas phase transition at the hadronic phase. Then, we verify if it is possible to fulfill these constraints alongside the existence of stable strange quark matter (SQM) as proposed by the Bodmer-Witten conjecture [23, 24]. If this is true, therefore, the nuclear matter as we know, made of protons and neutrons is only meta-stable, and the true ground state of all matter are not the baryons but three-flavored deconfined quark matter ($\mu_d = \mu_u = \mu_s$).

The next step is to construct a QCD phase diagram for three-flavored quark matter in β equilibrium and zero electrical charge using the modified versions of the MIT bag model. At $T = 0$, this study is important if one

* luiz_kiske@yahoo.com.br

EPJ manuscript No.
(will be inserted by the editor)

Effects of Strong Magnetic Fields on the Hadron-Quark Deconfinement Transition

Betânia C. T. Backes, Kauan D. Marquez, and Débora P. Menezes

Departamento de Física, CFM - Universidade Federal de Santa Catarina; C.P. 476, CEP 88.040-900, Florianópolis, SC, Brasil

Received: date / Revised version: date

Abstract. The aim of the present work is to investigate the effects of strong magnetic fields on the hadron-quark phase transition point at zero temperature. To describe the hadronic phase, a relativistic mean field (RMF) model is used and to describe the quark phase a density dependent quark mass model (DDQM) is employed. As compared with the results obtained with non-magnetised matter, we observe a shift of the transition point towards higher pressures and, generally also towards higher chemical potentials. An investigation of the phase transitions that could sustain hybrid stars is also performed.

PACS. XX.XX.XX No PACS code given

1 Introduction

The analysis of the QCD phase diagram points to a deconfined quark phase standing from the region of high temperatures and low densities down to the region of low temperatures and high densities. While lattice QCD (LQCD) can only describe a small part of the diagram with high temperatures and chemical potentials close to zero, effective models have been extensively used to investigate all other regions [1]. From the LQCD perspective, the transition between hadronic matter and deconfined quark matter is a crossover. On the other hand, effective models foresee a first order phase transition. These two lines can only join if a critical end point (CEP), which should be a unique second order transition point, exists in between them. At low temperatures, the possibility that a quarkyonic phase [2] exists, is not overruled. This phase would consist of matter with the chiral symmetry restored or partially restored but still confined.

But, what if matter is subject to strong magnetic fields, as in heavy ion collisions, for instance? What do we know about the QCD phase diagram? In [3], it is shown that the critical chemical potential oscillates around the zero magnetic field value for magnetic fields within 10^{17} to 10^{18} G range. It is also shown that the CEP position is affected, a result corroborated in [4]. In both studies, a unique model, the Nambu-Jona-Lasinio, with and without the Polyakov loop, was used to display the transition line between the hadronic and the quark phase.

Although many works have already investigated the hadron-quark phase transition at zero temperature [5, 6, 7, 8, 9] with two different models, there are no works investigating the possible transition if matter is subject to strong magnetic fields. This is an interesting subject because of the existence of magnetars [10, 11, 12, 13, 14], which manifest themselves in quite different ways as compared to the traditional pulsars. Could these objects become magnetised quark stars? This is the question we try to answer in the present work. We use two different models, a relativistic hadronic model within a mean field approximation (RMF model) to describe hadronic matter [15] and a density dependent model [16] to describe quark matter. The motivation behind the use of a density dependent quark model is two-fold: 1) such models were never utilised in previous works regarding the hadron-quark phase transition and 2) the description of quark stars could result in surface densities lower than the one of regular nuclear matter [16], which is a clear signal that the phase transition may occur. This suggests that the cases with low surface densities might be more appropriate to the description of hybrid stars instead of quark stars. The study of hybrid stars gained more interest since a model-independent analysis based on the sound velocity in both hadronic and quark matter suggested that the cores of massive neutron stars should be composed of quark matter [17]. In order to fully investigate this case, a proper study of the hadron-quark phase transition is in order, further motivating the use of the density dependent model here considered. In this paper, we restrict ourselves to the zero temperature regime and follow the prescription given in [18, 8], which assumes that flavor is conserved during the phase transition, but chemical equilibrium is not. We first present the main aspects of the formalism used and then show the results for both the effects of strong magnetic fields on the phase transition and for hybrid stars in chemical equilibrium, followed by a discussion.

EPJ manuscript No.
(will be inserted by the editor)

Delta Baryons in Neutron-Star Matter under Strong Magnetic Fields

Veronica Dexheimer[1], Kauan D. Marquez[2] and Débora P. Menezes[2]

[1] Department of Physics, Kent State University, Kent, OH 44243 USA
[2] Depto de Física - CFM - Universidade Federal de Santa Catarina Florianópolis - SC - CP. 476 - CEP 88.040 - 900 - Brazil

Received: date / Revised version: date

Abstract. In this work, we study magnetic field effects on neutron star matter containing the baryon octet and additional heavier spin 3/2 baryons (the Δ's). We make use of two different relativistic hadronic models that contain an additional vector-isovector self interaction for the mesons: one version of a relativistic mean field (RMF) model and the Chiral Mean Field (CMF) model. We find that both the additional interaction and a strong magnetic field enhance the Δ baryon population in dense matter, while decreasing the relative density of hyperons. At the same time that the vector-isovector meson interaction modifies neutron-star masses very little (< 0.1 M_{Sun}), it decreases their radii considerably, allowing both models to be in better agreement with observations. Together, these features indicate that magnetic neutron stars are likely to contain Δ baryons in their interior.

PACS. PACS-key discribing text of that key – PACS-key discribing text of that key

1 Introduction

The role of the baryon decuplet has been studied in neutron stars in several works, since first investigated by Glendenning in 1982 [1]. More recently, it has appeared in several publications [2–9]. The energies involved in the core of neutron stars is more than sufficient to create these heavier baryons, the lightest one, Δ, being only 292 MeV heavier than a neutron (see Fig. 1 in Ref. [3]). Considering charge neutrality, negatively charged spin 3/2 baryons are favored, while the positively charged ones are suppressed, in the same way as the hyperons. In this way, the only mechanism that could prevent Δ's from appearing in neutron stars would be a very repulsive coupling. The interested reader can see Ref. [10] for a discussion on the stability of Δ-rich matter. Currently, there is very little known about how these particles couple in dense matter, including some potentials extracted from heavy-ion collisions and scattering experiments, resulting in a range for the Δ potential for symmetric matter at saturation (with respect to the nucleon potential) of $U_N - 30$ MeV $\rightarrow$ $2/3\ U_N$. See discussions in Refs. [11, 12] and references therein for more details. Note that recent transport model calculations suggest, on the other hand, that the Δ potential is different from that of the nucleon [13].

The fact that Δ-baryons have spin 3/2 immediately raises the question about how they are affected by the presence of strong external magnetic fields. This was first discussed in Ref. [14], but only investigated in the context of neutron stars recently in Ref. [15], where the authors used the so-called universal magnetic field profile [16] in the Tolman-Oppenheimer-Volkoff equations. They found that the magnetic field affects the particle population, enhancing strangeness in neutron stars.

In the present work, we introduce for the first time a non-trivial (in the sense that is not yet commonly used in the literature) self vector-isovector interaction to describe matter found in the core of neutron stars under the influence of strong magnetic fields. This interaction was shown to improve the agreement of mean-field models with neutron-skin data [17], neutron-star radii [18–20], symmetry energy slope [21, 22], tidal deformability, and low-density constraints from chiral effective field theory [23].

In order to generalize our results, we repeat our analysis for two different relativistic hadronic models. The first one is a modified version of the Walecka model within a relativistic mean field (RMF) approximation and the second one, the CMF model, includes chiral symmetry restoration in the expected regime of high energy.

2 Basic formalism and Results

2.1 Magnetic Field

In order to study modifications introduced by an external magnetic field B on fermions, we modify the calculation of thermodynamical quantities of each hadronic and leptonic particle species with non-zero electric charge q according to the general procedure of taking

$$\sum_{\rm spin} \int d^3k \rightarrow \frac{|q|B}{(2\pi)^2} \sum_{\rm spin} \sum_n \int dk_z, \qquad (1)$$

Delta baryons in neutron stars

Kauan D. Marquez and Débora P. Menezes
Departamento de Física - CFM, Universidade Federal de Santa Catarina, Florianópolis, SC CEP 88.040-900, CP. 476, Brazil

Helena Pais and Constança Providência
CFisUC, Department of Physics, University of Coimbra, 3004-516 Coimbra, Portugal

By applying a relativistic mean-field description of neutron star matter with density dependent couplings, we analyse the properties of two different matter compositions: nucleonic matter with Δ baryons and nucleonic matter with hyperons and Δ baryons. The delta-meson couplings are allowed to vary within a wide range of values obtained by experimental data, while the hyperon-meson couplings are fitted to hypernuclear properties. Neutron star properties with no deconfinement phase transition are studied. It is verified that many models are excluded because the effective nucleon mass becomes zero before the maximum mass configuration is attained. Hyperon-free with Δ-dominated composition compact stars are possible, the *deltic stars*. It is found that with a convenient choice of parameters the existence of deltic stars with 80% of Δ baryons at the center of the star is possible. However, the presence of hyperons lowers the Δ baryon fraction to values below 20% at the center and below 30% at 2-3 saturation densities. It is discussed that in the presence of Δ baryons, the hyperon softening is not so drastic because Δs couple more strongly to the ω meson, and the stiffness of the equation of state is determined by the ω-dominance at high densities. The speed of sound reflects very well this behavior. The compactness of the pulsar RX J0720.4-3125 imposes $x_{\sigma\Delta} > x_{\omega\Delta} > 1$ and favors $x_{\rho\Delta} > 1$.

I. INTRODUCTION

Although the class of stellar remnants that are neither white dwarves nor black holes is traditionally named *neutron stars* (NS), these objects are not composed solely of neutrons. Even the more naïve description of such objects must include some amount of protons in order to guarantee the stability of the nuclear matter, and this fact was already pointed out in the first proposals of the existence of NS by Landau, Baade and Zwicky in the early 1930s. Almost forty years ago, Glendenning [1] discussed in his seminal paper different scenarios considering non-nucleonic degrees of freedom in NS matter, including hyperons, Δ baryons, pions and kaons, within a relativistic mean field approach. In this work, Glendenning found that the Δ baryons do not nucleate inside the NS core. This result was due to the coupling parameters chosen, as it was shown later that, with a convenient choice of the couplings minimally constrained by the existing experimental measurements, Δ baryons may indeed occur inside neutron stars [2–11].

The knowledge of the NS composition and the signatures of this composition is presently a field of intense investigation. To consider the entire spin-1/2 baryon octet as part of the NS matter composition is almost the standard in the nuclear astrophysics community [12–22] but, more recently, there is a strong interest in understanding how the presence of the Δ baryons specifically may influence the properties of NS and their evolution [23–31]. The lightest spin-3/2 baryons are just $\sim 30\%$ heavier than the nucleons, and are even lighter than the heaviest spin-1/2 baryons of the octet, what makes very reasonable to expect them to appear at the same density range as the hyperons (about 2-3 times the nuclear saturation density). One thing that could forbid the Δ onset would be if they were subject to a very repulsive coupling, but that is not the case, since their coupling potential for isospin-symmetric matter at saturation density is expected to be attractive and in a range of to 2/3 to 1 times the potential of the nucleons [6, 8, 11].

In [32], the authors have studied the effect of heavy baryons on the constitution of hot non-homogeneous matter, in particular their effects on the light clusters abundance and dissolution, using two relativistic mean-field nuclear models (FSU2H [33], a model with non-linear mesonic terms, and DD2 [34], a model with density-dependent couplings). For the Δ baryon, the couplings were restricted to values compatible with experimental observations as discussed in [6, 10]. It was found that the model FSU2H was much more restrictive, because most of the couplings would not be acceptable to describe neutron stars since the effective nucleon mass would become zero at densities below the maximum mass configuration. On the other hand, the DD2 model seemed to show much more flexibility and allowed a wider range of acceptable couplings. In [10], the FSU2H model has been fully investigated, but there was no reference to the implications of the fact that the effective nucleon mass may become null at still low densities. In [8], this problem was also encountered, but the authors have modified their model in order to avoid this issue.

In the present work, we will explore in depth the effects of the Δ baryon couplings considering a model that describes adequately nuclear matter properties and NS observations, considering the Δ admixture, in both pure nucleonic and hyperonic NS matters. We will study the behavior of the nucleon effective mass, that was not addressed in Ref. [23], the speed of sound, the Δ and hy-

Exploring the effects of Delta Baryons in magnetars

K. D. Marquez,[1,*] M. R. Pelicer,[1] S. Ghosh,[2] J. Peterson,[3] D. Chatterjee,[2] V. Dexheimer,[3] and D. P. Menezes[1]

[1]*Depto de Física - CFM - Universidade Federal de Santa Catarina Florianópolis - SC - CP. 476 - CEP 88.040 - 900 - Brazil*
[2]*Inter-University Centre for Astronomy and Astrophysics, Post Bag 4, Ganeshkhind, Pune University Campus, Pune, 411007, India*
[3]*Department of Physics, Kent State University, Kent, OH 44243, USA*

Strong magnetic fields can modify the microscopic composition of matter with consequences on stellar macroscopic properties. Within this context, we study, for the first time, the possibility of the appearance of spin-3/2 Δ baryons in magnetars. We make use of two different relativistic models for the equation of state of dense matter under the influence of strong magnetic fields considering the effects of Landau levels and the anomalous magnetic moment (AMM) proportional to the spin of all baryons and leptons. In particular, we analyze the effects of the AMM of Δ baryons in dense matter for the first time. We also obtain global properties corresponding to the EoS models numerically and study the corresponding role of the Δ baryons. We find that they are favored over hyperons, which causes an increase in isopin asymmetry and a decrease in spin polarization. We also find that, contrary to what generally occurs when new degrees of freedom are introduced, the Δs do not make the EoS significantly softer and magnetars less massive. Finally, the magnetic field distribution inside a given star is not affected by the presence of Δs.

I. INTRODUCTION

Magnetars are a class of compact objects that possess the largest stable magnetic fields observed in nature, with surface magnitudes inferred for the poloidal component in the range of $10^{11} - 10^{15}$ G at the surface [1] and values more than one order of magnitude larger in the interior [2, 3]. Although the strength of the magnetic field in the central region of these stars remains unknown, they could reach $\sim 10^{18}$ G according to the scalar virial theorem [4, 5], and simultaneous solutions of Einstein and Maxwells equations for poloidal [6, 7] and also toroidal configurations [8, 9]. Such extreme conditions certainly play a considerable role when determining the internal composition and structure of magnetars.

The starting point for determining the macroscopic structure of compact stars is the assumption of a specific microscopic model, which leads to the calculation of an equation of state (EoS) for dense matter. The EoS encodes the particle population of baryons and leptons and how they interact through the strong interactions, constrained by equilibrium conditions, such as β-stability and charge neutrality. The extremely high energies estimated in the core of neutron stars are more than sufficient to create heavier particle species, beyond the traditional proton-neutron-electron admixture. It has become common in the literature to consider the entire spin-1/2 baryon octet [e.g. 10–26] but, recently, the role of the spin-3/2 decuplet has been slowly gaining attention, not just for its influence on the microscopic aspects of dense matter but also for the astrophysical implications, since its presence may reduce the radius and tidal deformability in intermediate mass neutron stars [27–38]. The lightest spin-3/2 baryons (the Δs) are only $\sim 30\%$ heavier than the nucleons (protons and neutrons) and are even lighter than the heaviest spin-1/2 baryons of the octet (the Ξs). Thus, unless the Δs are subject to a very repulsive coupling, they are expected to appear at the same density range as the hyperons (around 2 or 3 times the nuclear saturation density). Not much is known about how Δ baryons couple in dense matter, but their potential for isospin-symmetric matter at saturation density is expected to be attractive and in a range of 2/3 to 1 times the potential of the nucleons, which is of order -80 MeV [39–41].

Additionally, it is of special interest to investigate how spin-3/2 baryons are affected by the presence of strong magnetic fields due to the possibility of them having large electric charge and additional spin and isospin projections. The effects of Landau levels in dense stellar matter containing Δ baryons was first discussed in the context of neutron-star matter by Thapa et al. [42] and later by Dexheimer et al. [37]. In this work we study for the first time the effects of strong magnetic fields in Δ-admixed hypernuclear stellar matter, accounting for effects due to their anomalous magnetic moments (AMMs).

For magnetic fields larger than $\sim 10^{16}$ G, the deformation of the stellar geometry away from spherical symmetry is above 2% [43]. Therefore, the usual relativistic hydrostatic equations usually employed when describing non-magnetised stars, i.e., the Tolman-Oppenheimer-Volkoff equations [44, 45], which assume spherical symmetry as part of their derivation from the general relativity equations, cease to be adequate. For this reason, we make use of anisotropic solutions from the Einstein and Maxwell equations to explore for the first time the macroscopic structure of magnetars with strong internal magnetic fields and containing Δ-admixed hypernuclear matter. Beyond accounting for the non-spherical configurations of stars and anisotropies introduced by magnetic fields, this approach allows us to obtain an *ab initio* magnetic field profile in the interior of a given star [46, 47].

*marquezkauan@gmail.com